

# **IMPROVED INTERMITTENT CLUTTER FILTERING FOR WIND PROFILER RADAR**

A dissertation submitted to the  
FACULTY OF BIOLOGY, CHEMISTRY AND GEOSCIENCES  
OF THE UNIVERSITY OF BAYREUTH, GERMANY

to attain the academic degree of  
DR.RER.NAT.

presented by  
VOLKER LEHMANN  
Diplom-Meteorologe

born December 31, 1965  
in Leipzig

Bayreuth, December 2009



# Improved Intermittent Clutter Filtering for Wind Profiler Radar

This doctoral thesis was prepared at the UNIVERSITY OF BAYREUTH, FACULTY  
OF BIOLOGY, CHEMISTRY AND GEOSCIENCES, DEPARTMENT OF  
MICROMETEOROLOGY under the supervision of

PROF. DR. THOMAS FOKEN

Die vorliegende Arbeit wurde unter der Betreuung von Prof. Dr. Thomas Foken in  
der Zeit vom 01. September 2008 bis 31. Dezember 2009 angefertigt.

Vollständiger Abdruck der von der Fakultät Biologie, Chemie und Geowissenschaften  
der Universität Bayreuth genehmigten Dissertation zur Erlangung des akademischen  
Grades Doktor der Naturwissenschaften (Dr. rer.nat.).

Erster Prüfer:	Prof. Dr. Thomas Foken
Zweiter Prüfer:	Prof. Dr. Peter Maaß
Dritter Prüfer:	Prof. Dr. Hans Josef Pesch
Vierter Prüfer:	Prof. Dr. Andreas Held
Prüfungsvorsitz:	Prof. Dr. Michael Hauhs

Einreichung der Dissertation:	08.01.2010
Zulassung zur Promotion:	17.02.2010
Annahme der Dissertation:	21.04.2010
Auslage der Arbeit:	21.04. 2010 - 04.05.2010
Kolloquium:	21.05.2010

# Contents

<b>Summary</b>	<b>I</b>
<b>Zusammenfassung</b>	<b>II</b>
<b>Acknowledgements</b>	<b>III</b>
<b>List of publications and manuscripts</b>	<b>IV</b>
<b>List of additional publications</b>	<b>V</b>
<b>1 Introduction</b>	<b>1</b>
<b>2 RWP instrument theory and signal processing</b>	<b>5</b>
2.1 Measurement physics . . . . .	5
2.2 Radar hardware . . . . .	12
2.3 Standard RWP signal processing . . . . .	17
2.4 Clutter effects: Signal processing revisited . . . . .	28
<b>3 Non-stationary clutter and its filtering</b>	<b>31</b>
3.1 A first clutter filtering approach using Wavelets . . . . .	33
3.2 The potential of time-frequency analysis . . . . .	36
3.3 Gabor frame expansion and its statistics . . . . .	38
3.4 Optimal Gabor frame expansions . . . . .	39
<b>4 Conclusions</b>	<b>42</b>
<b>References</b>	<b>44</b>
<b>Individual contributions to joint publications</b>	<b>65</b>
<b>A Wavelet based methods for improved wind profiler signal processing</b>	<b>67</b>
<b>B Advanced Radar Wind Profiling</b>	<b>80</b>
<b>C Advanced intermittent clutter filtering for radar wind profiler: signal separation through a Gabor frame expansion and its statistics</b>	<b>98</b>
<b>D Optimal Gabor frame expansion based intermittent clutter filtering method for wind profiler radar</b>	<b>124</b>

## Summary

Ground-based remote measurements of the vertical profile of the horizontal wind vector in the atmosphere by radar wind profiler (RWP) is a technique that has been significantly developed since the first demonstration with the Jicamarca radar by Woodman and Guillen in the early 1970s. Currently, there exist several operational networks of those instruments in the USA, Europe and Japan which provide continuous wind measurements in real-time and most of the data are successfully assimilated in numerical weather prediction models. Although this is an obvious indication of maturity, practical experience has shown that further improvements are both possible and necessary. While the high sensitivity of these clear-air radars is required for receiving the weak atmospheric echoes, it makes them also particularly vulnerable to unwanted radar returns and in-band radio frequency interference. Signal processing must therefore especially deal with the problem of filtering of these unwanted contributions, to avoid associated measurement errors.

A specific difficulty are clutter echoes from various airborne objects, such as aircraft or birds, which generate strong, intermittent contributions to the received signal. The standard RWP signal processing is not able to deal with these signals in an efficient way, because the model assumption on which the processing is based is violated. With the development of sophisticated mathematical tools for the analysis of non-stationary signals in the last two decades and a better understanding of the practically relevant RWP clutter issues, a number of efforts have been made to tackle especially the challenging problem of intermittent clutter returns from migrating birds.

In this dissertation it is shown that the signal structure of RWP raw data contaminated by intermittent clutter is much clearer revealed by a joint time-frequency analysis based on the windowed Fourier transform than by other possible signal descriptions, in particular pure time or frequency representations. An effective intermittent clutter reduction algorithm, called the Gabor filter, is obtained by a combination of a numerically feasible discrete Gabor frame expansion with the statistical test for a stationary Gaussian random signal. This approach is optimized by using near-tight frames and selecting a time-frequency resolution that provides a jointly sparse representation of both atmospheric and clutter signal components. A first evaluation of this approach has shown a superior performance in comparison with hitherto existing methods, but it was also found that additional quality-control of the derived Doppler spectra is still required during extreme bird migration events. The latter is in all likelihood indicative of a principal limit of radar wind profiling during such conditions. However, an effective quality control of the measurement is possible through a combination of a stationarity estimate provided by the Gabor algorithm with a-priori information about typical atmospheric echoes.

## Zusammenfassung

Die bodengebundene Fernmessung des Vertikalprofils des horizontalen Windvektors in der Atmosphäre mittels Radar-Windprofiler (RWP) ist eine Technik, die sich seit der ersten Demonstration mit dem Jicamarca Radar durch Woodman und Guillen im Jahre 1974 erheblich weiterentwickelt hat. Derzeit existieren mehrere operationelle Netze dieser Instrumente in den USA, Europa und Japan, die kontinuierliche Windmessungen in Echtzeit bereitstellen, wobei ein Großteil dieser Daten erfolgreich in numerischen Wettervorhersagemodellen assimiliert wird. Obwohl diese Tatsache einen Hinweis auf den Reifegrad des Verfahrens gibt, zeigt die praktische Erfahrung jedoch, dass weitere Verbesserungen sowohl nötig als auch möglich sind. Die hohe Empfindlichkeit dieser "Klarluftdargeräte" ist dabei einerseits eine notwendige Voraussetzung, um die schwachen Echos aus der Atmosphäre überhaupt empfangen zu können, macht die Systeme aber andererseits auch sehr störanfällig in Bezug auf unerwünschte Rückstreuungssignale und externe Hochfrequenzeinstreuung. Die Signalverarbeitung muss daher vor allem das Problem der Filterung dieser Störungen behandeln, um entsprechende Messfehler zu vermeiden.

Ein spezielle Schwierigkeit sind dabei Fehlechos von fliegenden Objekten, z.B. Flugzeugen und Vögeln, die starke intermittierende Beiträge zum Empfangssignal generieren. Die RWP-Standard-Signalverarbeitung ist aufgrund unzutreffender Annahmen nicht in der Lage, derartige Signale adäquat zu behandeln. Mit der Entwicklung komplexer mathematischer Werkzeuge zur Analyse instationärer Signale in den letzten zwei Jahrzehnten und einem besseren Verständnis der in der Praxis relevanten Störechos sind eine Reihe von Anstrengungen unternommen worden, um speziell das anspruchsvolle Problem der von Zugvögeln verursachten Fehlechos zu bewältigen.

In dieser Dissertation wird gezeigt, dass im Falle vorhandener instationärer Fehlechos eine simultane Zeit-Frequenzdarstellung von RWP-Rohdaten auf Basis der gefensternten Fourier-Transformation im Vergleich zu anderen Signalrepräsentationen, insbesondere reinen Zeit- oder Frequenzdarstellungen, ein wesentlich deutlicheres Bild der Signalstruktur vermittelt. Durch Kombination einer numerisch realisierbaren diskreten Gabor-Framezerlegung mit einem statistischen Test für ein stationäres Gaußsches Zufallsignal konnte ein vielversprechender Clutterreduktionsalgorithmus entwickelt werden. Dieser wird durch die Wahl von quasi-festen Frames und eine die dünne Darstellung von Atmosphären- und Cluttersignal begünstigenden Zeit-Frequenzauflösung optimiert. In ersten Vergleichen haben die Ergebnisse dieser Methode die Leistung der bisher verwendeten Verfahren übertroffen, obwohl bei Extremereignissen weiterhin eine zusätzliche Qualitätskontrolle notwendig ist. Mit hoher Wahrscheinlichkeit stößt man hier an prinzipielle Grenzen der radarbasierten Windmessung. Allerdings lässt sich eine solche Qualitätskontrolle der Messungen mittels Kombination eines durch den Gabor-Algorithmus geliefertes Stationaritätsmaßes mit weiteren a-priori Informationen über typische Atmosphärenechos realisieren.

## Acknowledgments

This work is the result of 15 years of continuous involvement in nearly all aspects of radar wind profiling. During this time, I had the privilege of working with a large number of colleagues. First of all, I am grateful to my colleagues in the Remote Sensing Group of the Lindenberg Meteorological Observatory of the Deutscher Wetterdienst (DWD), in particular to Hans Steinhagen and Dirk Engelbart, for giving me some freedom beyond daily routine duties to follow my research interests. The dedication of Sven Volland in maintaining the profiler hardware was very important and is gratefully acknowledged. Many thanks are due to Frank Beyrich and Ulrich Görtsdorf for proof-reading the manuscript and many valuable suggestions.

The co-operation with many European colleagues during the COST Action 76 and the EUMETNET Project WINPROF has largely affected this work. I am especially thankful to John Nash, Hans Richner, Thomas Griesser, Dominique Ruffieux, Tim Oakley and Myles Turp. During several research stays between 1996 and 2001 at NCAR and NOAA in Boulder, Colorado, I had the pleasure of meeting renowned experts in the field. In particular, I benefitted from discussions with Earl E. Gossard, Richard G. Strauch, Russel B. Chadwick, Douglas W. van de Kamp, Kenneth S. Gage, David A. Carter, Bob L. Weber, David A. Merritt, David B. Wuertz, Timothy L. Wilfong, Daniel C. Law, Scott A. McLaughlin, James R. Jordan, Richard J. Latatits, Larry B. Cornman and Corinne S. Morse.

I am particularly indebted to Andreas Muschinski, who guided me with uncountable stimulating conversations, where I benefitted from his deep theoretical understanding of clear-air radars. Furthermore, he provided useful suggestions to the final version of this thesis. Invaluable was the long-standing cooperation with my co-author Gerd Teschke, who put all my ideas on a solid mathematical ground. I am grateful to Lutz Justen, who first suggested a joint time-frequency approach for clutter filtering. Unforgettable is a one-week secluded working stay of Andreas, Gerd, Lutz and myself in a cottage up in the Rocky Mountains in March of 2004, where we worked on a joint paper (Muschinski et al., 2005) undistracted by email and the trouble of daily life.

Many thanks are due to John W. Neuschaefer and Raisa Lehtinen of Vaisala. While John taught me many details about the radar hardware, Raisa was instrumental in writing the first online implementation of the algorithm. Her programming tricks led to a significant speed-up of the processing and her questions were instrumental for its further development.

Last, but not least, I would like to thank my thesis advisor Prof. Dr. Thomas Foken for his initiative to compile many years of research into this dissertation. His interest in this topic had already started while he was working as the head of the Boundary Layer Processes Group at the Lindenberg Observatory and it has continued ever since. His support and encouragement was essential for completing this work.

## **List of publications and manuscripts**

This dissertation in cumulative form consists of a synopsis and three individual publications or manuscripts. For the sake of completeness, a fourth, peer-reviewed research paper that precedes the current work is given in Appendix A. The main publications are given in Appendices B-D, two of them were published in peer-reviewed, international scientific journals and one manuscript is prepared for subsequent submission.

### **Peer-reviewed research papers**

Lehmann, V. and Teschke, G.: Wavelet Based Methods for Improved Wind Profiler Signal Processing, *Ann. Geophys.*,19,825-836, 2001.

Muschinski, A., Lehmann, V., Justen, L., and Teschke, G.: Advanced Radar Wind Profiling, *Meteor. Z.*, 14, 609-626, 2005.

Lehmann, V. and Teschke, G.: Advanced Intermittent Clutter Filtering for Radar Wind Profiler: Signal Separation through a Gabor Frame Expansion and its Statistics, *Ann. Geophys.*,26, 759-783, 2008.

### **Submitted manuscript**

Lehmann, V.: Optimal Gabor Frame Expansion based Intermittent Clutter Filtering Method for Radar Wind Profiler, submitted to *J. Atmos. Oceanic Technol.*, 2009.

## List of additional publications

Additional research papers which are no integral part of this dissertation are listed here for completeness.

### Peer-reviewed research papers

Steinhagen, H., Dibbern, J., Engelbart, D., Görsdorf, U., Lehmann, V., Neisser, J. and Neuschaefer, J. W.: Performance of the First European 482 MHz Wind Profiler Radar with RASS under Operational Conditions, *Meteor. Z.*, N.F.7, 248-261, 1998.

Görsdorf, U. and Lehmann, V.: Enhanced Accuracy of RASS Measured Temperatures Due to an Improved Range Correction, *J. Atmos. Oceanic Technol.*, 17, 406-416, 2000.

Dahlke, S., Teschke, G. and Lehmann, V. Applications of wavelet methods to the analysis of meteorological radar data - an overview, *The Arabian Journal for Science and Engineering (AJSE)*, 28, 3-44, 2003.

Böhme, T., Hauf, T. and Lehmann, V. Investigation of short-period gravity waves with the Lindenberg 482 MHz tropospheric wind profiler, *Quart. J. Roy. Meteor. Soc.*, 130, 2933-2952, 2004.

Serafimovich, A., Hoffmann, P., Peters, D. and Lehmann, V. Investigation of inertia-gravity waves in the upper troposphere / lower stratosphere over Northern Germany with collocated VHF/UHF radars, *Atmos. Chem. Phys.* 5, 295-310, 2005.

### Selection of non peer-reviewed research papers

Hirsch, L., Klaus, V., Klein Baltink, H., Lehmann, V. and Peters, G.: Fundamentals of wind profiler operations, in: COST Action 76 - Final Report: Development of VHF/UHF Wind Profilers and Vertical Sounders for use in European Observing Systems, European Commission, Rue de la Loi/Wetstraat 200, Brussels, 68-132, 2003.

Justen, L. and Lehmann, V.: Radar wind profiler signal processing using redundant windowed Fourier and Wavelet transforms, 6th Int. Symposium of Tropospheric Profiling, Leipzig, 91-93, 2003.

Lehmann, V.: Intermittent clutter echoes in Radar Wind Profilers: Signal Characteristics and Filtering (invited paper), 12th International Workshop on Mesosphere, Stratosphere, Troposphere Radars, London, Ontario, 2009.



# 1 Introduction

Environmental information is becoming increasingly more important in our complex society. This includes in particular data about the state of the atmosphere which are needed for both weather prediction and climate monitoring (Hollingsworth et al., 2005). The current global observational system for the atmosphere consists of a mix of ground and space based systems, with a large part of them being remote sensing instruments (Dow, 2004).

For ground based remote sensing systems, radar wind profilers (RWP) are among the most thoroughly developed and widely used sensors. As the name implies, they are special Doppler radars designed for measuring the vertical profile of the wind vector in the lowest 5 - 20 km of the atmosphere (depending on the operating frequency) on timescales ranging from seconds to years. RWP's are also able to provide additional information about the atmospheric state through the profiles of backscattered signal intensity and frequency spread (spectral width) of the echo signal. In contrast to the automated wind measurement, however, such data need to be carefully analyzed by instrument experts due to the complexity of the measurement process. Reviews of the technical and scientific aspects of RWP have been provided by Gage (1990); Röttger and Larsen (1990); Doviak and Zrnić (1993); Ackley et al. (1998); Muschinski (2004) and recently Fukao (2007). If the RWP system is equipped with an additional Radio-Acoustic Sounding System (RASS) component, then measurements of the vertical profile of the virtual temperature are also possible. More information on RASS can be found in Peters et al. (1993); Lataitis (1993); Görzdorf and Lehmann (2000). A photograph of a 482 MHz RWP/RASS system is shown in Fig. 1.

After the first successful demonstration of clear-air wind measurements by Woodman and Guillen (1974), the potential capabilities of this technique for meteorological applications became suddenly apparent (Larsen and Röttger, 1982) and dedicated meteorological profiler systems were suggested (Hogg et al., 1983). It took not long until the installation of a small experimental wind profiler network in Colorado (Strauch et al., 1984). The first truly operational network, called the Wind Profiler Demonstration Network (WPDN), was completed in May 1992, later it became known as the NOAA National Profiler Network (Weber et al., 1990; Barth et al., 1994; Schlatter and (Editors), 1994). While the first systems used mostly operating frequencies in the VHF or lower UHF range, higher frequency (so-called boundary layer) profilers were also developed and later commercialized by a technology transfer from NOAA to the private sector (Ecklund et al., 1988; Carter et al., 1995). In Europe, a first demonstration of wind profiler networking was organized during the COST-76 action in early 1997 as the CWINDE<sup>1</sup>-97 project (Nash and Oakley, 2001).

At present, RWP's are used in operational meteorology and atmospheric research,

---

<sup>1</sup>COST WIND initiative for a network demonstration in Europe

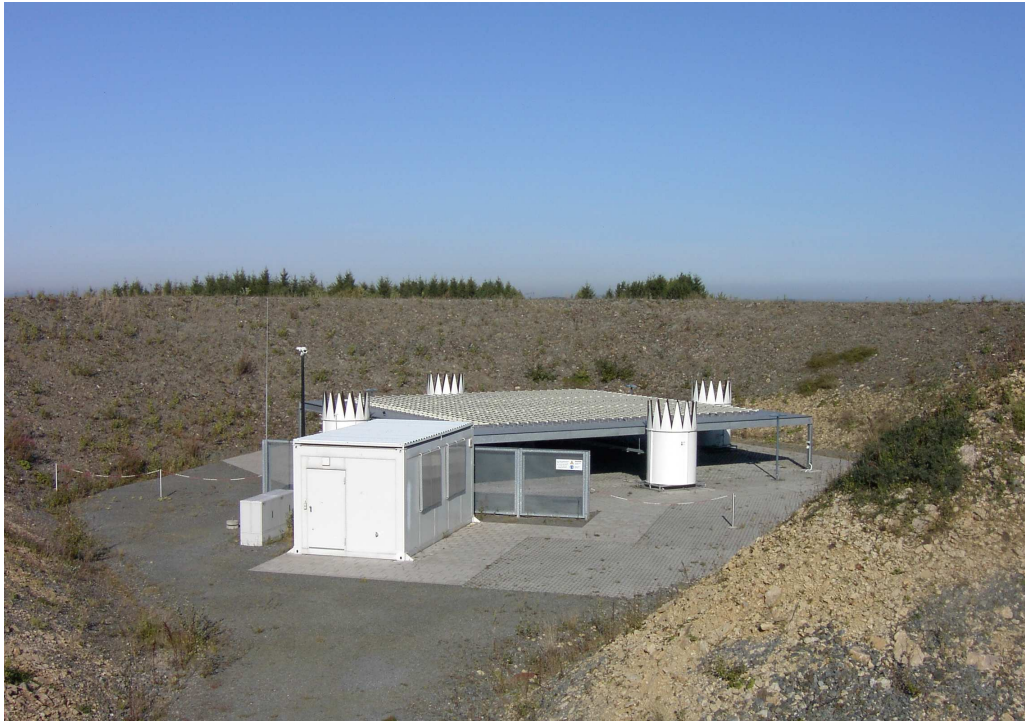


Figure 1: Photograph of the 482 MHz RWP installation at Bayreuth (Oschenberg), showing the antenna array platform surrounded by four acoustic sources for RASS and the shelter containing the radar electronics.

like atmospheric boundary layer studies (Gossard et al., 1982; Angevine et al., 1994; Wilczak et al., 1996; Angevine et al., 1998b; Pollard et al., 2000; Bianco and Wilczak, 2002; Grimsdell and Angevine, 2002; Heo et al., 2003; Bianco et al., 2008; Scipion et al., 2009a), turbulence research (Ecklund et al., 1979; Balsley and Peterson, 1981; Gossard et al., 1998; VanZandt et al., 2000), investigation of atmospheric waves and tides (Ralph et al., 1992; Whiteman and Bian, 1996; Chilson et al., 1997; Browning et al., 2000; Röttger, 2000; Böhme et al., 2004, 2007; Vaughan and Worthington, 2007; Koch et al., 2008), cloud and precipitation physics (Fukao et al., 1985; Ralph et al., 1995; Orr and Martner, 1996; Rajopadhyaya et al., 1999; Gage et al., 2002; Atlas and Williams, 2003; Williams et al., 2007; Newman et al., 2009) as well as air quality investigations (Wolfe et al., 1995; Dabberdt et al., 2004). The listing of papers is far from being complete. For recent reviews see Fukao (2007) and Gage and Gossard (2003). Major meteorological field experiments make regular use of RWP as observation system, e.g. METCRAX (Whiteman et al., 2008), T-REX (Grubisic et al., 2008), NAME (Higgins et al., 2006), IHOP (Weckwerth et al., 2004), BAMEX (Davis et al., 2004), CASES (Poulos et al., 2002) and MCETEX (Keenan et al., 2000).

In a more operational setting, RWP measurements are used either directly in subjective

weather forecasting and case studies (Dunn, 1986; Kitzmiller and McGovern, 1990; Beckman, 1990; Edwards et al., 2002; Crook and Sun, 2004; Bond et al., 2006; Wagner et al., 2008), or automated in data assimilation for numerical weather prediction (Monna and Chadwick, 1998; Guo et al., 2000; De Pondeca and Zou, 2001; Bouttier, 2001; Andersson and Garcia-Mendez, 2002; Benjamin et al., 2004b; St-James and Laroche, 2005; Ishihara et al., 2006). Their particular advantages are a high temporal resolution and the capability to provide unambiguous profiles independently of the used assimilation system, the latter being in contrast to most passive remote sensing systems. Furthermore, measurements can be made under almost all weather conditions.

Due to the potential of RWP's to provide high-resolution observations, they are especially well suited to describe the atmospheric state at the mesoscale (Foken, 1989; Browning, 1989; Park and Zupanski, 2003; Browning, 2005). For a discussion of atmospheric scale-classification schemes see e.g. Thunis and Bornstein (1996). The dramatic rise in computational capabilities during the last decades has led to significant improvements in the discretization resolution of numerical weather prediction models (NWPM), see e.g. Lynch (2008). Global models are meanwhile using grid spacings of  $O(10\text{ km})$  (Satoh et al., 2008), while high-resolution limited area models already use grid sizes of  $O(1\text{ km})$  in an attempt to resolve small-scale meteorological processes (Bryan et al., 2003; Saito et al., 2007). Those are important because quite a number of high-impact weather systems, like severe thunderstorms, are small-scale phenomena. Of course, this brings along the need to initialize the models with adequate observations of small scale atmospheric features (Foken, 1989; Lilly, 1990; Daley, 1991; Gall and Shapiro, 2000; Roebber et al., 2004; Sun, 2005; de Lima Nascimento and Droege-meier, 2006; Weisman et al., 2008). However, the current observation coverage at those scales is quite incomplete in space, time and also state variables of the models. The current experience with high-resolution models has shown that even a 12-24 hour deterministic prediction of some intense convective precipitation systems can drastically fail. For example, Gallus et al. (2005) reported about an intense derecho event accompanied by a well-organized band of heavy rainfall that they were not able to simulate although a range of different models, different parameterizations and initial conditions was used. The authors conclude:

*Evidence suggests inadequacies in the initial and boundary conditions probably harmed the simulations.(..) It thus appears that useful forecasts of systems such as this one may require a much better observation network than what now exists.*

Mesoscale data assimilation in particular suffers from a penury of high-quality profile data, including wind (Roberts, 2007; Carbone et al., 2009; Fabry and Sun, 2009). Model spectra are known to be severely deficient in kinetic energy in the mesoscale in forecast initializations due to this lack of mesoscale observations (Skamarock, 2004). Furthermore, wind profile information, especially vertical shear, is critically needed

for the prediction of severe convective storms (Weisman and Klemp, 1982; Klemp, 1987; Markowski et al., 2003). Comparing model resolution and the density of available observations, the following statement made by Acheson et al. (1992) is obviously still valid:

*The need for better environmental information has overtaken the capabilities of our observing systems. Our ability to model has outrun our ability to observe. (...) Radiosonde operations are the lifeblood of numerical weather prediction (but) these observations are not capable of fully supporting the need to understand and predict atmospheric phenomena with lifetimes measured in a few hours and spatial extent less than a few hundred kilometers. (...) More frequent, higher density upper-air observations are essential.*

This need can, at least to some extent, be satisfied with data from RWP's. A necessary prerequisite is that the instruments are able to provide high-quality measurements in an operational, fully automated fashion. This seemingly trivial requirement is indeed difficult to achieve, for the required high sensitivity of the radars make them vulnerable to unwanted and potentially quality-degrading effects, like echoes from various clutter sources and radio-frequency interference. In particular, the automated data processing must be capable of sufficiently suppressing these clutter effects.

This dissertation deals with one specific clutter problem, namely intermittent echoes from airplanes and birds. The problem is relevant for all types of clear-air radars operating at UHF and L-band, but has not been adequately resolved yet, see e.g. Tanaka et al. (2007); Nielsen-Gammon et al. (2007) or Schmidli et al. (2009). The new approach presented in this thesis uses signal analysis methods for non-stationary data to achieve a clear separation of the atmospheric return from clutter echoes. This is a prerequisite for an efficient filtering method which is based on a statistical test for stationary Gaussian random signals. The first attempts tried to use wavelet transforms to achieve such a separation in the domain of the wavelet coefficients (Jordan et al., 1997; Boisse et al., 1999) and Lehmann and Teschke (2001, Paper A). During continued investigations, the advantages of a time-frequency analysis approach became obvious (Muschinski et al., 2005, Paper B). A practically applicable algorithm based on a Gabor frame expansion was developed and published in Lehmann and Teschke (2008a, Paper C) and questions of optimal settings were discussed in Lehmann (2009, Paper D). The method is meanwhile implemented in commercially available RWP systems (Shellhorn and Keskinen, 2009; Lehtinen et al., 2009), which is a prerequisite for comprehensive testing under operational conditions.

In the next section, the essential theoretical foundations of RWP instrument theory and signal processing will be summarized before the specific topic of intermittent clutter filtering is discussed.

## 2 RWP instrument theory and signal processing

Instrument theory, sometimes also called measurement physics, is the science of the interaction of a sensor with its environment (Wyngaard, 1984). It is particularly important for remote sensing instruments, where the physical parameter to be observed can only be inferred indirectly through its effects on the propagation of electromagnetic or acoustic waves. The main purpose is to get a sufficiently comprehensive but yet tractable functional relationship between the properties of the medium (the atmosphere) and the received signal (Woodman, 1991). For RWP, such a discussion must deal with the following four topics:

1. Generation and transmission of a well-defined electromagnetic wave or wave group into the atmosphere
2. Interaction of the electromagnetic wave with the atmosphere and generation of scattered waves containing atmospheric information
3. Reception of the scattered waves and transformation to a measurable function (Receiver voltage or current)
4. Extraction of the desired atmospheric information using adequate mathematical signal processing methods

This dissertation focuses on a particular problem of the last point. To put this into perspective, a high-level overview is given before delving into the specific problem of intermittent clutter filtering.

### 2.1 Measurement physics

RWP instrument theory is a specific problem within the theory of *Wave Propagation in Random Media*, which attempts to describe the interaction between electromagnetic waves and natural media. The fundamental physical process is the interaction of the electromagnetic wave with the discrete electric charges in matter, that is protons and electrons. Those charges are set in oscillatory (accelerated) motion by the wave which leads to secondary radiation that superposes with the incident field (Feynman et al., 1991). The macroscopic manifestation of this fundamental microscopic process are effects like diffraction, refraction, reflection, scattering, change of propagation speed and absorption (Gossard and Strauch, 1983), depending on the properties of the medium. It is impossible to describe those macroscopic effects for any practical problem at an elementary (microscopic) level, even with the aid of modern computers (Laughlin and Pines, 2000; Mishchenko et al., 2002). For this reason, macroscopic electrodynamics is used (Landau and Lifschitz, 1985; Fliessbach, 1994) and the electromagnetic properties of matter are described through bulk quantities like permittivity (Bohren and Huffman, 1983; Stephens, 1994). For RWP, the most interesting phenomenon is

backscattering, which needs to be theoretically described as completely and accurately as possible to obtain a link between the atmospheric properties of interest and the measurement.

The atmosphere below the thermosphere (below an altitude of about 85 km) can be assumed to be an electrically neutral continuum, i.e. a dielectric pure gas mixture (Salby, 1996), although short-lived ionization can occur in meteor trails or lightning channels. Furthermore, a suspension of a broad spectrum of liquid and solid particulates (aggregations of atoms or molecules) is embedded. This includes cloud and precipitation droplets, ice particles and aerosols. Last but not least, airborne objects like insects, birds and airplanes need to be considered in practical scattering problems as well.

To make the theoretical description tractable, various idealized scattering models can be formulated:

- Scattering at refractive index inhomogeneities in particle-free air
- Scattering at particle ensembles in an otherwise homogeneous medium
- Scattering at plasma in lightning channels
- Echoes from airborne objects
- Echoes from the ground surrounding the RWP (through antenna sidelobes)

Instrument theory for RWP is typically restricted to scattering at inhomogeneities of the refractive index of air. For the atmosphere is almost permanently in a turbulent state, the connection of electrodynamics and turbulence theory is the mainstay for an understanding of this problem. The synthesis of Maxwell's electromagnetic theory and statistical fluid mechanics (turbulence theory) was pioneered by Tatarskii (1961). For UHF RWP, the relevant model is that of **Bragg scattering**, see e.g. Ottersten (1969a,b); Gossard et al. (1982); Gossard and Strauch (1983); Chadwick and Gossard (1984). Bragg scattering is treated using a number of reasonable simplifications, like linear polarization of the transmitted wave and the neglect of multiple-scattering through the small fluctuation approximation (or Born approximation). Furthermore, an idealized radar system is assumed where the instrument function is characterized by a Gaussian beam with no sidelobes and where the emitted pulse also has a Gaussian shape. There exists a considerable amount of literature on that topic, including comprehensive review papers (Wheelon, 1972; Doviak and Zrnić, 1984; Gage, 1990; Woodman, 1991; Muschinski, 2004) as well as textbooks (Tatarskii, 1971; Ishimaru, 1978; Gossard and Strauch, 1983; Doviak and Zrnić, 1993; Monin and Yaglom, 2007). Nevertheless, it is still an area of active research, see Tatarskii and Muschinski (2001); Tatarskii (2003); Muschinski (2004); Muschinski et al. (2005).

The second major scattering process for UHF RWP is scattering at small particles, like droplets or ice crystals. The Rayleigh approximation can be used for simplification, because the particle diameter is always much smaller than the wavelength. Furthermore

it is usually assumed that small and randomly positioned particles give rise to incoherent scatter, and the whole process is often termed **Rayleigh scattering** (Gossard and Strauch, 1983; Oguchi, 1983; Kropfli, 1984; Doviak and Zrnić, 1993). However, there are open questions with regard to the possibility of coherent scattering effects from particles due to non-random position patterns (Gossard, 1979; Gossard and Strauch, 1983; Jameson and Kostinski, 1999; Kostinski and Jameson, 2000; Erkelens et al., 2001; Baker and Brenguier, 2007).

Bragg and Rayleigh scattering are the main atmospheric scattering processes for UHF RWP for most applications. Nevertheless, the practically relevant problem of separating simultaneous contributions of particulate scatter and clear-air scatter - the so-called Bragg/Rayleigh ambiguity, a term coined by Knight and Miller (1998) - has not been resolved in a satisfying manner so far (Fukao et al., 1985; Wuertz et al., 1988; Steiner and Richner, 1994; Ralph et al., 1995; Cohn et al., 1995; Ralph et al., 1996; Orr and Martner, 1996; Gage et al., 1999; Williams et al., 2000; McDonald et al., 2004).

The remaining scattering or echoing mechanisms are considered as clutter, that is unwanted echoes, for most applications. Scattering at the plasma in lightning channels is sometimes observed with UHF RWP (Petitdidier and Laroche, 2005). It is usually no issue for practical wind profiling due to the extremely short lifetime of the echoes which mostly contributes to a higher noise level, but it is surely a physically interesting phenomenon observable by radar and has therefore been treated to some extent (Rust and Doviak, 1982; Williams et al., 1989; Lee et al., 1998). Ground clutter echoes for RWP are also often observed due to ubiquitous sidelobes of finite aperture antennas and the high receiver sensitivity (Woodman and Guillen, 1974; Balsley et al., 1977; Farley et al., 1979; Ogura and Yoshida, 1981; Sato and Woodman, 1982; Woodman, 1985; Martner et al., 1993; May and Strauch, 1998). An example of a typical ground clutter signature in time series data of a 482 Mhz RWP and the corresponding Doppler spectrum is shown in Fig. 1-4 of Muschinski et al. (2005). Also, scattering at larger flying objects like airplanes (Hogg et al., 1983; Strauch et al., 1984; Farley, 1985; Hocking, 1997) or birds (Barth et al., 1994; Wilczak et al., 1995; Engelbart et al., 1998) is for obvious reasons not a part of RWP instrument theory, although it can hardly be denied that such effects can become very relevant in real-world applications. An example of an aircraft clutter signal is presented in Fig. 5 and 7 of Muschinski et al. (2005) and a number of different bird echoes are shown in Fig. 3 in Lehmann and Teschke (2008a) and Fig. 1 in Lehmann (2009). Most striking is the data set plotted in Fig. 10 of Lehmann (2009), which was obtained during a peak event of bird migration in spring of 2009. To avoid measurement errors due to misinterpretation of clutter echoes as atmospheric returns, all these effects need to be considered properly. The hope is that clutter signals have a quite distinct signal characteristic compared to atmospheric echoes, which would then allow for an identification and subsequent filtering during an early stage of signal processing.

To illustrate RWP measurement physics, the problem of clear-air scattering (e.g. a



$$N = c_1 \frac{p}{T} + c_2 \frac{e}{T} + c_3 \frac{e}{T^2} \quad (3)$$

with

$$c_1 = 0.776 \frac{K}{Pa}, \quad c_2 = 0.716 \frac{K}{Pa} \quad \text{and} \quad c_3 = 3.7 \cdot 10^3 \frac{K^2}{Pa} .$$

Obviously, the ubiquitous variations of temperature, humidity and pressure in the turbulent atmosphere cause subsequent variations of the refractive index (Tatarskii, 1971; Doviak and Zrnić, 1993), which are the very reason of macroscopic scattering effects of electromagnetic waves propagating through the atmosphere.

The analysis of the scattering problem starts with the macroscopic Maxwell's equations. It is convenient to consider only a harmonic time dependence of the fields by separating a factor  $e^{i\omega t}$  from the electric  $\mathbf{E}(\mathbf{r}, t)$  and magnetic field vector  $\mathbf{H}(\mathbf{r}, t)$  (Hoffman, 1964). This approach results in the following equation

$$\Delta \mathbf{E}(\mathbf{r}) + \varepsilon_0 \mu_0 \omega^2 \varepsilon(\mathbf{r}) \mathbf{E}(\mathbf{r}) = -\nabla[\mathbf{E}(\mathbf{r}) \cdot \nabla \ln \varepsilon(\mathbf{r})] , \quad (4)$$

which implicitly assumes that the phenomenon under consideration is essentially monochromatic. This is a good approximation whenever the time variation of the medium is much slower than the propagation time of the wave. The inhomogeneous vector Helmholtz equation (4) is the basic scattering equation. For the atmosphere, permittivity fluctuates around a value of one, so

$$\varepsilon(\mathbf{r}, t) = \langle \varepsilon(\mathbf{r}, t) \rangle + \varepsilon'(\mathbf{r}, t) = 1 + \varepsilon'(\mathbf{r}, t) . \quad (5)$$

The ansatz for the total electric field is written as  $\mathbf{E} = \mathbf{E}_0 + \mathbf{E}_s$ , where  $\mathbf{E}_0$  is the solution of the homogeneous version of equation (4), i.e. the field in the absence of permittivity fluctuations. For single scattering, all products of the two small quantities  $\mathbf{E}_s$  and  $\varepsilon'$  are neglected (Born approximation) and one obtains an equation for the scattered electric field  $\mathbf{E}_s$ :

$$\Delta \mathbf{E}_s(\mathbf{r}) + \varepsilon_0 \mu_0 \omega^2 \mathbf{E}_s(\mathbf{r}) = \varepsilon_0 \mu_0 \omega^2 \varepsilon'(\mathbf{r}) \mathbf{E}_0(\mathbf{r}) - \nabla[\mathbf{E}_0(\mathbf{r}) \cdot \nabla \ln \varepsilon'(\mathbf{r})] \quad (6)$$

The solution of this equation in the case of no additional boundary conditions (except the radiation condition) for  $\mathbf{E}_s$  in the far field is known to be (Tatarskii, 1971, 2003):

$$\mathbf{E}_s(\mathbf{r}) = \frac{k^2}{4\pi} \iiint_V \frac{e^{ik|\mathbf{r}-\mathbf{r}'|}}{|\mathbf{r}-\mathbf{r}'|} \boldsymbol{\varepsilon}'(\mathbf{r}') [\mathbf{o} \times [\mathbf{E}_0(\mathbf{r}') \times \mathbf{o}]] d^3\mathbf{r}' \quad (7)$$

The unit vector  $\mathbf{o} = \frac{\mathbf{r}-\mathbf{r}'}{|\mathbf{r}-\mathbf{r}'|}$  is directed from the variable scattering point to the observation point. Equation (7) is fairly general, because it only assumes that the observation point lies in the far-field of the scatterer.

For any concrete problem, the exact scattering geometry (e.g. location of transmitting and receiving antenna) as well as the incident field  $\mathbf{E}_0(\mathbf{r})$  needs to be specified. To obtain closed-form expressions it is customary to assume that the transmitted electromagnetic pulse has a Gaussian shape and that the antenna radiation pattern (beam geometry) is also Gaussian (Tatarskii, 2003; Muschinski, 2004). This model together with the term  $e^{ik|\mathbf{r}-\mathbf{r}'|}/|\mathbf{r}-\mathbf{r}'|$  essentially defines the instrument sampling functions. Muschinski (2004) has presented a comprehensive theoretical analysis of the measurement process for clear-air Doppler radars based on explicit formulations for the instrument sampling function. There are two levels of approximation to simplify this instrumental sampling function analytically which are obtained by expanding  $|\mathbf{r}-\mathbf{r}'|$  in a Taylor series and retaining terms up to linear (Fraunhofer approximation) or quadratic (Fresnel approximation) order.

The Fraunhofer diffraction or small volume scattering approximation assumes that the phase fronts of the incident wave can be considered as planar over the scattering volume, which implies that the maximum dimension of the scattering volume  $L$  satisfies  $L \ll \sqrt{\pi^{-1}\lambda r}$ . This condition is hardly ever met. If the longest correlation length of  $\boldsymbol{\varepsilon}'$  would be much smaller than  $L$ , then the full scattering volume could be divided into smaller subvolumes where the scattered signal from the subvolumes would add incoherently (Tatarskii, 1971; Doviak and Zrnić, 1993). Although this assumption is often not fulfilled (Doviak and Zrnić, 1984; Tatarskii, 2003), the traditional Fraunhofer approximation for the backscattering of a linear polarized plane wave provides already an important insight. In this case, equation (7) simplifies to

$$\mathbf{E}_s(\mathbf{r}, t) = \mathbf{E}_0 \frac{k^2}{4\pi r} \iiint_V \boldsymbol{\varepsilon}'(\mathbf{r}', t) e^{-i2\mathbf{k}\cdot\mathbf{r}'} d^3\mathbf{r}' , \quad (8)$$

where a slow temporal variation of the refractive index at a time scale much longer than the propagation time of the wave has been introduced again. It can be easily seen from (8) that the field of permittivity fluctuations is sampled at twice the wavenumber  $k$  of the incident electromagnetic wave. This makes it clear why the refractive-index fluctuations at half-wavelength scale play a prominent role in clear-air backscattering. It is

essentially a condition for constructive interference, which allows to obtain detectable backscattered signal levels. Current radar theory builds upon the Fresnel approximation, which is applicable under much weaker assumptions and includes additional relevant effects (Doviak and Zrnić, 1984; Tatarskii, 2003; Muschinski, 2004). A discussion of this comprehensive theory is beyond the scope of this overview. However, it was pointed out by Muschinski (2004, paragraph 54) that the Fresnel approximation leads to the same final radar equation as the traditional Fraunhofer approximation, if the refractive-index perturbations are statistically isotropic at the Bragg wavenumber.

The RWP antenna receives the backscattered electromagnetic wave and converts it into a measurable voltage or current signal at the antenna output port, which contains all the information regarding the measurement. This signal  $S$  is proportional to the integral of  $\mathbf{E}_s$  over the antenna aperture  $F$ .

$$S(\mathbf{r}, t) = \iint_F \mathbf{E}_s(\mathbf{r} + \boldsymbol{\rho}, t) d\mathbf{f} \quad (9)$$

$d\mathbf{f} = \mathbf{f}_A(\boldsymbol{\rho}) d^2\boldsymbol{\rho}$  includes the antenna radiation pattern (Herden, 1996; Kon and Tatarskii, 1980; Mailloux, 1994). Leaving the details aside, the received signal can be written as

$$S(\mathbf{r}, t) = \iiint_V G(\mathbf{r}', \mathbf{r}) n'(\mathbf{r}', t) d^3\mathbf{r}' . \quad (10)$$

$G(\mathbf{r}')$  is the instrument sampling function, which determines the mapping of the field of dielectric permittivity fluctuations, or with  $\epsilon' = 2n'$  due to  $n^2 = \epsilon$  the fluctuations of the refractive index, to the received signal.

The backscattered power can be obtained by squaring the voltage (or current) measured at the antenna output port. Equation (10) can be used to derive theoretical expressions for the Doppler velocity and higher order moments of the Doppler spectrum, as discussed in Muschinski et al. (2005), sections 2.4 and 2.5. It thus provides the basic mapping between the atmospheric properties of interest contained in the field of refractive-index fluctuations and the signal that is measured by the RWP. The instrument sampling function acts as an integral kernel and yields this an inverse problem with all associated challenges. The advantage of active remote sensing is the ability to tailor this kernel within the technical capabilities (e.g. the use of short pulses and a narrow antenna beam provide a small effective scattering volume and thus good resolution). Signal processing is used to convert  $S(t)$  into the typical radar measurables like reflected power, Doppler shift and spectral spread (e.g. the first three moments of the Doppler spectrum). Those values are then related to atmospheric properties like the structure constant of the refractive index  $C_n^2$  (Ottersten, 1969a; Tatarskii, 1971), radial

wind speed and radial velocity variance in the radar resolution volume. However, the exact meaning of the measurables in case of a non-homogeneous and nonstationary atmosphere is very difficult to ascertain (Muschinski, 2004). Beside such comprehensive attempts to establish analytical relations in RWP instrument theory, the very nature of turbulence makes this an extremely challenging effort, for the current understanding of turbulence and refractive-index structure at meter and submeter-scale in the free atmosphere is rather limited (Muschinski and Lenschow, 2001). However, such knowledge would be essential for the interpretation of RWP data. Numerical simulation techniques for realistic turbulent flows in the atmosphere like Large Eddy Simulation or even Direct Numerical Simulation (Davidson, 2004) have therefore recently been used in lieu of high-resolution in-situ measurements (Muschinski et al., 1999; Scipion et al., 2008, 2009a; Franke et al., 2009). Such tools allow a systematic investigation of nearly all aspects of RWP technology with unprecedented detail, for the simulation can generate a virtual 'in-situ truth' against which the results of the measurement process, including signal processing, can be tested.

## 2.2 Radar hardware

Depending on their particular hardware architecture, RWP can be classified into three main groups (Muschinski et al., 2005):

**Single signal systems** are the most frequently used wind profiler type (Law et al., 2002; Steinhagen et al., 1998; Engelbart et al., 1996; Carter et al., 1995; Ecklund et al., 1988; Strauch et al., 1984). They are monostatic<sup>2</sup> pulse radars using one single carrier frequency with the hardware architecture resembling that of a typical Doppler radar system, as described in Skolnik (2001). The term single signal refers to the characteristics of the instruments sampling function, which can be regarded as an integral kernel function that maps a field describing the physical properties of the atmosphere relevant for the actual scattering process to the received radar (voltage or current) signal. For clear-air scattering, this is the scalar field of the refractive index (or permittivity) irregularities.

**Two signal systems** are extensions of the single signal architecture, where basically two different sampling functions are realized to improve the retrieval of atmospheric properties of interest. The two techniques that have been used are the frequency-domain interferometry (FDI) using a monostatic radar with two different carrier frequencies (Kudeki and Stitt, 1987; Chilson et al., 1997) and the spaced-antenna technique using one carrier frequency and multiple receiving antennas (Lataitis et al., 1995; Doviak et al., 1996).

Recently, **multi-signal systems** have been developed and tested. They either use a bistatic combination of a single transmit and a multitude of receiving antennas to per-

---

<sup>2</sup>The same antenna is used for transmitting and receiving.

form digital beamforming (Mead et al., 1998; Pollard et al., 2000; Helal et al., 2001) or they transmit several carrier frequencies to achieve so-called range imaging (RIM) with a single (monostatic) antenna (Palmer et al., 1999; Luce et al., 2001; Smaïni et al., 2002; Chilson et al., 2003; Chilson, 2004). Much work remains to be done to further develop, understand and use this obviously most complex and demanding radar architecture.

In the following, the discussion will be restricted to single signal RWP systems, in particular to the 482 MHz instruments used in the operational network of the DWD (Lehmann et al., 2003) as shown in Fig. 1. A block diagram of the general hardware architecture is given in Fig. 5. The central unit is the radar controller, which uses a highly stable coherent oscillator as the single reference for all signals. It generates all control signals needed to operate the radar through Direct Digital Synthesis (DDS). The electromagnetic pulse to be transmitted is created by a waveform generator which acts essentially as an amplitude and phase modulator. After a frequency up-conversion and amplification (through a linear power amplifier), the transmit signal is delivered to the antenna and the resulting electromagnetic wave is radiated into free space. As the same antenna is also used for signal reception, a duplexer is necessary to protect the sensitive receiver electronics from the strong transmit signal. It is typically comprised of a ferrite circulator and additional receiver protecting limiters.

The antenna is a phased array comprised of coaxial-collinear (CoCo) elements (Law et al., 2003; Balsley and Ecklund, 1972). A relay-switched true-time delay phase shifting unit generates the necessary phasing of the individual elements required to steer the beam in three fixed directions for each CoCo sub-array, as shown on the right hand side of Fig. 3. For the five-beam pointing configuration indicated in Fig. 6, two such CoCo sub-arrays are combined. Due to the finite extent of the antenna array, the beam can not be made infinitely narrow. This results in unwanted radiation through so-called sidelobes in other than the boresight direction and can be visualized through the antenna radiation pattern, which shows the distribution of the total radiated power  $P$  as a function of spherical antenna coordinates  $\theta$  and  $\phi$ . Fig. 4 shows the ideal radiation pattern for the DWD 482 MHz network wind profiler calculated with the method of Law et al. (1997). Note that the sidelobe level will be somewhat more irregular and higher in reality because of stochastic excitation differences of array elements due to hardware imperfections (Mailloux, 1994).

The receiver is of the classical superheterodyne type (Tsui, 1989). A rather broadband low-noise amplifier with an excellent noise-figure is necessary to raise the signal level of the weak atmospheric return for further processing. After frequency down-conversion to an intermediate frequency (IF), the signal is bandpass-filtered, demodulated and A/D converted for further digital processing in the radar processor. To maximize the per-pulse signal-to-noise ratio (SNR) for optimal signal detection, the bandwidth of the bandpass filter is matched to the transmitted pulse (Zrnić and Doviak, 1978). Actual technical implementations differ, for example the received signal can be

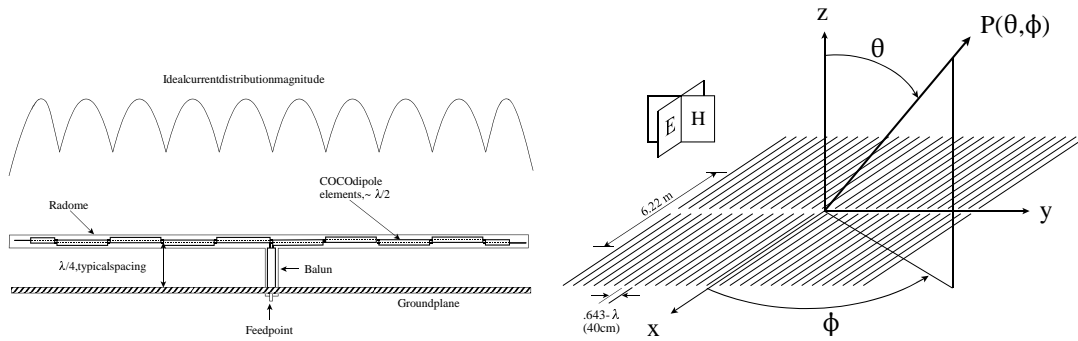


Figure 3: Single coaxial-collinear antennas with ideal current amplitude distribution (left) and array arrangement (right). A planar CoCo array generates a linear polarized electromagnetic wave, with the electric and magnetic field vector oscillating in the so-called E-plane or H-plane, respectively. The antenna beam is steerable in the H-plane through a different phasing of the CoCo lines. (Graphics courtesy of D.C. Law.)

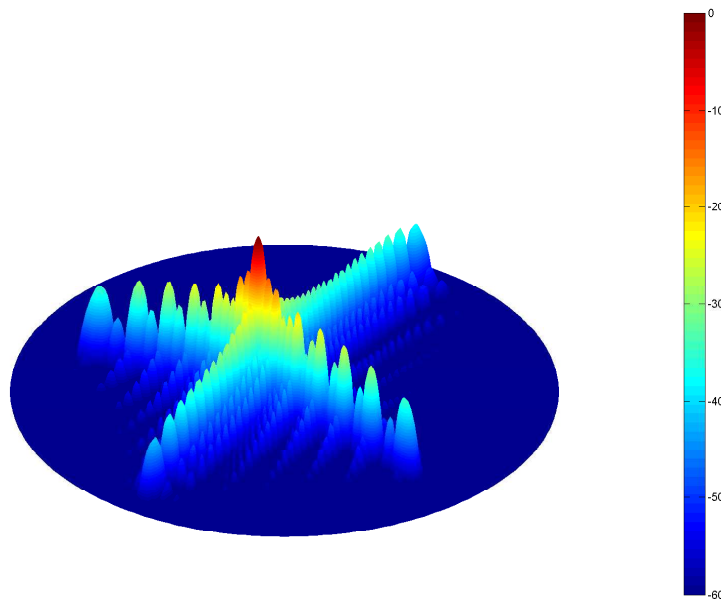


Figure 4: Surface plot of the ideal normalized antenna radiation pattern  $|P(\theta, \phi)|^2/P_0$  in logarithmic scaling (dB) for an oblique beam of the 482 MHz RWP at Bayreuth.

digitized either at IF (so called digital IF receivers) or at base-band, after further analog down-conversion by a quadrature detector (analog receiver).

Single signal RWP use the simple method of Doppler beam swinging (DBS) to determine the wind vector. At least three linear independent beam directions and some

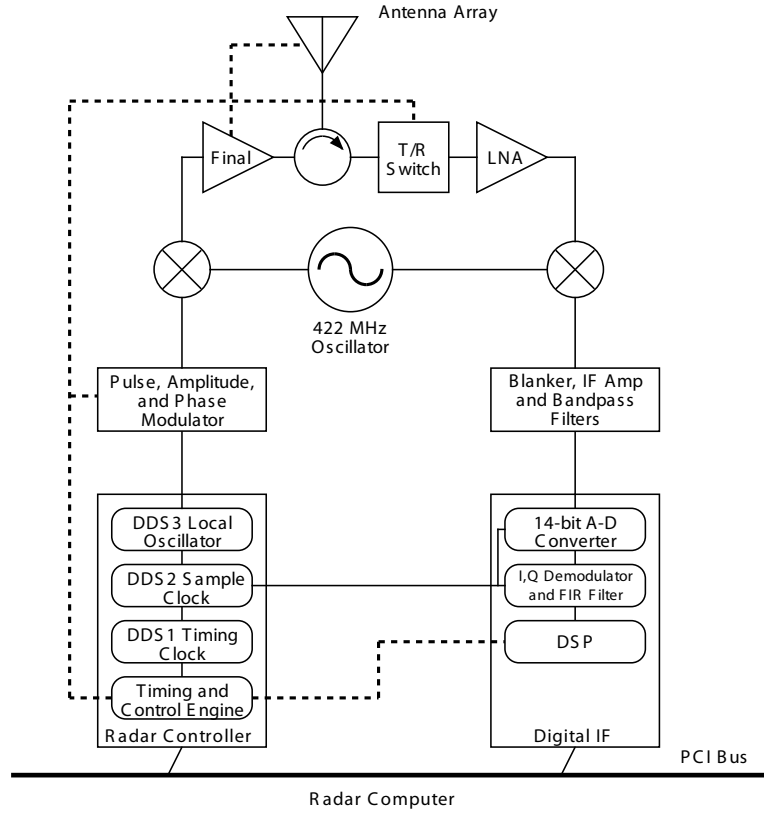


Figure 5: Simplified block diagram of the DWD 482 MHz radar wind profiler. (Graphics courtesy of J.W. Neuschaefer.)

assumptions concerning the wind field are required to transform the measured 'line-of-sight' radial velocities into the wind vector. This principle will be briefly shown for a five beam system as depicted in Fig. 6.

In the vicinity of the radar, the wind field  $\mathbf{v}$  with components  $(u, v, w)$  in a cartesian coordinate system can be approximated through a Taylor series expansion in the horizontal coordinates up to the linear term:

$$\mathbf{v}(x, y, z) \approx \mathbf{v}(x_0, y_0, z) + \nabla_h \mathbf{v}(x, y, z)|_{x_0, y_0} \cdot \Delta \mathbf{r}. \quad (11)$$

For simplicity it is further assumed (without loss of generality) that the antenna beam directions are aligned in parallel to the cartesian coordinate axes (i.e. x East, y North). If the radial velocity measured in the 'line-of-sight' of a radar beam described by unit directional vector  $\mathbf{n}$  is written as

$$v_r = \mathbf{v} \cdot \mathbf{n} \quad (12)$$

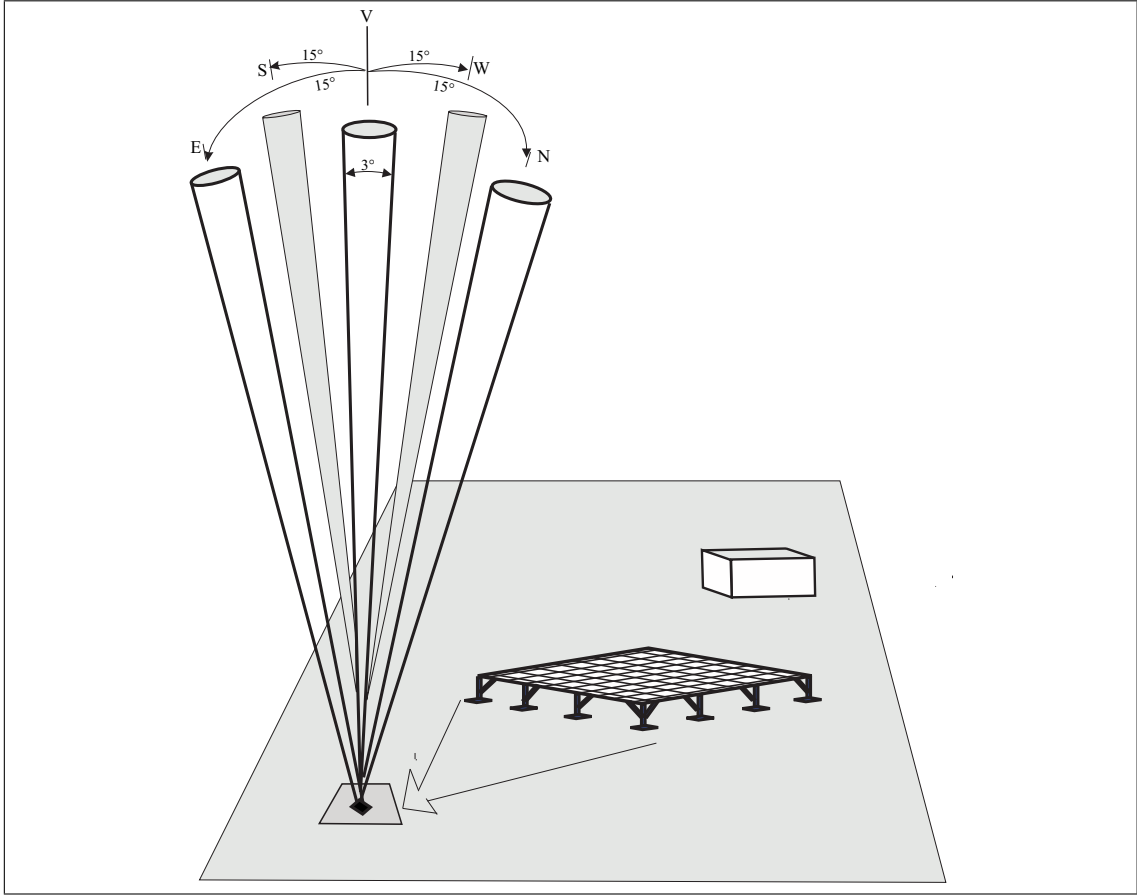


Figure 6: Beam pointing configuration of a five-beam DBS radar wind profiler

and with  $\delta x = \delta y = z \tan(\alpha_0) \cos(\alpha_0)$ , the differences of the radial winds of the four oblique beams at height  $z$  are obtained as

$$[v_{rE} - v_{rW}](z) = 2u_0(z) \sin(\alpha_0) + 2 \frac{\partial w}{\partial x}(z) \delta x(z) \quad (13)$$

$$[v_{rN} - v_{rS}](z) = 2v_0(z) \sin(\alpha_0) + 2 \frac{\partial w}{\partial y}(z) \delta y(z) . \quad (14)$$

Here,  $\alpha_0$  is the zenith distance of the oblique beams,  $z$  is the height above ground and the subscripts denote East, West, North and South, respectively. It is immediately obvious that one assumption is required to determine the (horizontal) wind components  $(u_0, v_0)$  above the radar, namely

$$\frac{\partial w}{\partial x} = \frac{\partial w}{\partial y} = 0 . \quad (15)$$

That is, the horizontal shear of the vertical wind must vanish to retrieve the horizontal wind without errors. A discussion of the problems associated with the DBS method can be found in Koscielny et al. (1984); Weber et al. (1992); Goodrich et al. (2002).

The condition (15) is of course not always fulfilled, in particular not in a convective boundary layer. The problem and the resulting measurement errors have recently been investigated by Scipion et al. (2008, 2009b), they are even noticeable in NWP data assimilation (Cardinali, 2009). However, the assumption is usually correct for mean winds averaged over a longer time interval. Cheong et al. (2008) have used data obtained with a volume-imaging multi-signal wind profiler in a convective boundary layer to show that for this particular case the assumptions inherent in the DBS method were valid for a wind field averaged over 10 minutes. More work is certainly required to obtain reliable estimates of this error under a variety of conditions.

### 2.3 Standard RWP signal processing

The mathematical definition of an analog signal is that of a function  $S: \mathbb{R} \mapsto \mathbb{R}$ , which assigns to every time  $t$  a signal value  $S(t)$  (Allen and Mills, 2004). For RWP, this signal is the voltage or current at the output port of the antenna:  $S(\mathbf{r}_0, t) = S(t)$ , which is the physical carrier of all information that is available about the atmosphere through the scattering process, see equation (10). The purpose of RWP signal processing is now to convert the measured electrical signal to meteorological parameters - this most concise definition is due to Zrnić (1990). The key aspects are (Keeler and Passarelli, 1990; Fabry and Keeler, 2003):

- To extract as much information as possible, with the specific purpose of obtaining accurate, unbiased estimates of the characteristics of the desired atmospheric echoes.
- To estimate the confidence/accuracy of the measurement.
- To mitigate effects of clutter or interfering signals.

In general, signal analysis aims at a full understanding of a signal. To achieve this it is necessary to first appreciate the nature of the signal itself, for its general properties obviously dictate the optimal mathematical analysis methods. In particular it is useful to find a problem adapted mathematical representation of the signal that facilitates an easier physical interpretation. The goal is to arrive at a simpler, structural description of the signal so that its information content can be interpreted by higher-level algorithms (Allen and Mills, 2004). For this purpose, the signal is usually transformed from its original form to another representation (e.g. from time domain to frequency domain) without the loss of information (through a one-to-one, or injective mapping) in order to obtain a clearer picture of its specific characteristics. In some sense, the intention is to look at the same piece of information from a different perspective (Flandrin, 1999).

The choice of this new representation is of course crucial for the following signal processing tasks, like detection, classification, and estimation. As long as there is little a-priori knowledge about the signal, the signal representation should require only few assumptions.

The quality of signal processing largely determines the accuracy and precision of the final data. RWP signal processing has evolved at a rather slow pace over the last three decades. Two factors might have contributed to this fact: The original algorithms were mainly developed for an idealized profiler setting where the receiver signal is assumed to consist of only two components: The atmospheric signal and the ubiquitous thermal noise of the receiver electronics. Other contributions, especially clutter components or interference are neglected. Furthermore, hardware constraints were a limiting factor with regard to technically feasible implementations, thus preventing the use of more sophisticated methods. The majority of RWP's today uses the same standard signal processing which consists of the following steps (Strauch et al., 1984; Tsuda, 1989; Barth et al., 1994; Carter et al., 1995):

- Coherent integration of the digitized baseband signal, e.g. Schmidt et al. (1979)
- Estimation of the Doppler spectrum, e.g. Wilfong et al. (1999)
- Estimation of the noise level (Hildebrand and Sekhon, 1974)
- Determination of the first three moments of the maximum energy peak in the Doppler spectrum, e.g. Woodman (1985); May and Strauch (1989)
- Signal detection by consensus averaging (Fischler and Bolles, 1981)
- Computation of the horizontal wind, e.g. Adachi et al. (2005)

In the idealized setting, the general properties of the receiver signal at the antenna output port of a pulsed single-frequency RWP can be summarized as follows, see also Lehmann and Teschke (2008a):

**$S(t)$  is a continuous real-valued random voltage signal.** Every measurable physical quantity is real. The presence of electronic noise and the random nature of the scattering medium requires the application of the mathematical concept of random functions.

**$S(t)$  is narrowband.** The transmitted radar signal is narrowband and concentrated around a carrier frequency. The bandwidth is restricted through frequency regulations constraints and the higher carrier frequency is needed to first obtain the necessary wave propagation and scattering properties (Bragg condition) and second, to ease the technical realization of such a radar, like the necessary antenna directivity with a feasible physical size of the antenna. Therefore, the receiver signal is band-limited ( $B \ll \omega_c$ ) as well, with a maximum bandwidth  $B$  that is largely determined by the bandwidth of the transmitted pulse. The signal information is contained in the slowly varying envelope of the signal, whereas the carrier frequency is irrelevant in that respect (Mc-

Donough and Whalen, 1995). Information extraction thus requires a demodulation of the measured signal.

$S(t)$  **exhibits a potentially large dynamic range.** This is due to the high sensitivity of RWP, the high efficiency of some clutter echoing and atmospheric scattering processes (e.g. precipitation) as well as geometric effects, and leads to signals whose intensity varies easily over many orders of magnitude. Whereas the sensitivity of a RWP receiver for a nearly monochromatic signal is about  $-150 \text{ dBm}^3$  or less, the range of backscatter signals from the atmosphere can easily exceed 10 orders of magnitude (White et al., 2000) and particularly strong clutter returns might extend this range even further. The large dynamic range must be considered for spectral estimation, especially in view of multi-component detection. Due to antenna geometry and the properties of volume scattering, the range dependence of the transmitted field strength is  $\propto 1/r$ , corresponding to a power reduction  $\propto 1/r^2$ . This naturally leads to very weak signals at upper range gates, which are often close to the detectability of the receiver. Detection of such weak signals in noise or, equivalently, an optimization of the SNR, requires a matched filter approach (Zrnić and Doviak, 1978; Tsuda, 1989; Doviak and Zrnić, 1993). In general, the variation of signal strength over many orders of magnitude is typical for radar systems.

### Demodulation, range gating and A/D conversion

The narrow-band RWP signal at the output port of the low noise amplifier can be written as

$$S_{rx}(t) = A(t) \cos [\omega_c t + \Phi(t)] . \quad (16)$$

All available information about the scattering process is contained in the amplitude and phase modulation of the received signal  $S_{rx}(t)$ . It is technically difficult to sample such a signal, therefore a demodulation step is performed first, which essentially removes the irrelevant carrier frequency  $\omega_c$  while the modulation information contained in the instantaneous amplitude  $A(t)$  and the instantaneous phase  $\Phi(t)$  remains unchanged.

The Fourier spectrum of such a narrowband signal is centered at both  $-f_c$  and  $+f_c$ , e.g. Randall (1987). Due to the modulation property of the Fourier transform (Mallat, 1999), a simple frequency down-shift operation by multiplication with  $e^{-i\omega_c t}$  is not helpful, because it would shift the negative part of the spectrum as well. Instead, a new signal  $S^+(t)$  with the following Fourier spectrum  $\hat{S}^+$  is created:

$$\hat{S}^+(\omega) = \hat{S}(\omega) + \text{sgn}[\omega] \hat{S}(\omega). \quad (17)$$

---

<sup>3</sup>1 dBm = 10 lg(P / 1 mW)

This operation clearly removes the negative part of the original signal spectrum. The signal  $S^+(t)$  is called the analytic signal or pre-envelope of  $S(t)$  (McDonough and Whalen, 1995). In the time domain, it is formed as

$$S^+(t) = S(t) + i\mathcal{H}[S(t)], \quad (18)$$

where the operator  $\mathcal{H}$  denotes the Hilbert transformation<sup>4</sup>

$$\mathcal{H}[S(t)] = \frac{1}{\pi} \int_{-\infty}^{+\infty} \frac{S(t')}{t-t'} dt'. \quad (19)$$

Obviously,  $S(t) = \Re[S^+(t)]$ . If a narrowband signal is going to be represented in terms of amplitude and phase as  $V(t) = A(t) \cos(\Phi(t))$ , then both amplitude and phase are not uniquely defined (Mallat, 1999). However, the signal extension defined by the Hilbert transform is unique and optimal in the sense that it minimizes the average rate of temporal variation of the envelope (Papoulis, 1991). The analytic narrowband signal can be written as

$$S^+(t) = [\tilde{S}(t)e^{i\omega_c t}], \quad (20)$$

where  $\tilde{S}(t)$  is the complex envelope of the original signal. Multiplication of  $S^+(t)$  with  $e^{-i\omega_c t}$  now clearly removes the carrier without loss of information and gives the complex envelope

$$\tilde{S}(t) = S^+(t)e^{-i\omega_c t} = (S(t) + i\mathcal{H}[S(t)])e^{-i\omega_c t} = I(t) + iQ(t), \quad (21)$$

where the real part of the complex envelope is the so-called in-phase  $I(t)$  and the imaginary part  $Q(t)$  the quadrature phase of the signal, see McDonough and Whalen (1995). For a stochastic narrowband signal, this representation is called Rice representation (Papoulis, 1991). The Hilbert transform is not easily implemented in real systems. Instead,  $I(t)$  and  $Q(t)$  are determined using a quadrature demodulator. Details depend on the receiver architecture of the RWP. Older analog systems use a hardware (mixer)-based quadrature detector to down-convert the signal to baseband and to obtain the complex envelope by determining the in-phase and quadrature-phase components, the

---

<sup>4</sup>The integral is understood in the sense of the Cauchy principal value.

so-called complex video signal. Matched filtering is also performed in hardware before the complex signal is sampled and digitized by two A/D converters. Modern digital systems start by first digitizing the signal at IF. Usually, the Nyquist criterion would require a high sampling rate to unambiguously represent the signal. However, if certain conditions (mainly signal bandwidth limitations) are fulfilled, a judiciously chosen subsampling can be used to both down-convert the signal and to determine the quadrature components digitally in one step, this is called quadrature sampling (McDonough and Whalen, 1995). Matched filtering is performed digitally in this case.

For a fixed beam direction, RWP transmit a series of short electromagnetic pulses, each one separated by a time interval  $\Delta T$ , in which the backscattered signal is sampled. For a single pulse, the sampling in time allows the determination of the radial distance of the measurement using the well-known propagation speed of the wave group. The maximum distance for unambiguously determining the measurement distance is limited by the pulse separation or inter-pulse-period  $\Delta T$  and  $h_{max} = c\Delta T/2$  is called the maximum unambiguous range.  $\Delta T$  has to be set sufficiently high to prevent range aliasing problems, that is arrival of backscattering signals from the preceding pulse after the next pulse is transmitted. For a typical wind profiler it is of the order of  $10^{-4}$ s.

Range gating is usually done in the A/D process using sample and hold circuitry. The sample strobe required for range gating and pulse repetition is provided by the radar controller. If the range sampling frequency is given by  $1/\Delta t$  and  $N_h$  is an integer denoting the number of range gates with  $\Delta T < N_h\Delta t$ , then signal  $\tilde{S}(t)$  is obtained at the discrete grid

$$\tilde{S}[j, n] = \tilde{S}(t_0 + j\Delta t + n\Delta T), \quad j = 0, \dots, N_h - 1, \quad n = 0, \dots, N_T - 1. \quad (22)$$

For each range gate  $j$ , that is for the height  $c/2 \cdot j \cdot \Delta t$ , a discrete time series of the complex envelope of the signal with a sampling interval of  $\Delta T$  is obtained<sup>5</sup>. In the following, only one range gate  $j$  will be considered, so the range gate index will be suppressed for convenience. Slightly abusing the notation, the tilde denoting the complex envelope will also no longer be used and the complex time series is written as

$$S[n] = S_I[n] + iS_Q[n], \quad n = 0, \dots, N_T - 1. \quad (23)$$

### The digitized raw signal

The standard model assumption of a RWP signal is that of a stationary Gaussian random process. Consider a zero-mean proper complex random sequence  $\mathbf{z} = \mathbf{x} + i\mathbf{y}$  with  $E\mathbf{z} = 0$  and a nonsingular covariance matrix  $\mathbf{C} = E[(\mathbf{z})(\mathbf{z}^T)]$ , where  $|\mathbf{C}|$  denotes the

---

<sup>5</sup>Hardware effects like the group delay of the pulse in the radar electronics are ignored for simplicity.

determinant. If the probability density function of the random sequence  $z_n = z(t_n)$  follows a multidimensional normal distribution (Miller, 1969; Neeser and Massey, 1993)

$$p(z_1, z_2, \dots, z_n) = p(\mathbf{z}) = \pi^{-n} |\mathbf{C}|^{-1} e^{-\mathbf{z}^H \mathbf{C}^{-1} \mathbf{z}} \quad (24)$$

it is said to be Gaussian and written as  $\mathcal{N}(0, \mathbf{C})$ . Obviously, the stochastic process is completely specified by its second order properties, namely the covariance matrix, and all higher order moments are zero by definition. If such a process is stationary, then  $E(z[p]\bar{z}[q]) = \text{Cov}(z[p], z[q]) = r[p - q]$ , where  $r[k]$  denotes the autocorrelation sequence.

The classical way to analyze such signals is based on spectral estimation. The concept of a power spectrum is motivated by Cramer's spectral representation theorem, which states that every stationary random process can be decomposed into a sum of sinusoidal components with uncorrelated random coefficients (Percival and Walden, 1993; Priestley, 1981). This is the analogue to the Fourier representation of deterministic functions. The model assumption for RWP signals is that the demodulated discrete voltage sequence at the receiver output can be written as

$$S[n] = I[n]e^{i\omega n \Delta T} + N[n], \quad (25)$$

where  $I[n] \sim \mathcal{N}(0, \mathbf{R}_I)$  and  $N[n] \sim \mathcal{N}(0, \mathbf{R}_N)$  are independent complex zero-mean Gaussian random vectors describing the atmospheric signal and the receiver noise, respectively (Zrnić, 1979),  $\Delta T$  is the sampling interval of the sequence and  $\omega$  the mean Doppler frequency. Furthermore,  $I[n]$  is narrowband compared to the receiver bandwidth and  $|\omega| \leq \pi/\Delta t$  (Nyquist criterion). Because  $S[n]$  is the result of the demodulation of a real valued zero-mean and stationary Gaussian random process, the resulting complex random process is also stationary, zero-mean and proper, that is the sequence has a vanishing pseudo-covariance  $E(S[p]S[q]) = 0$  (Neeser and Massey, 1993). The underlying random process of the realization  $S[n]$  is completely characterized through its covariance matrix  $\mathbf{R}$  with entries (Lehmann and Teschke, 2008a)

$$\begin{aligned} (\mathbf{R})_{p,q} &= \text{Cov}(S[p], S[q]) \\ &= \sigma_I^2 \rho[p - q] e^{i\omega(p-q)\Delta T} + \sigma_N^2 \delta_{p-q,0}, \end{aligned}$$

The autocorrelation sequence  $\rho$  is typically assumed to be Gaussian as well, which corresponds to a Gaussian signal peak in the power spectrum. If the spectral width of the signal is  $\sigma_v$ , then (Zrnić, 1979; Frehlich and Yadlowsky, 1994)

$$\rho[n] = e^{-2\pi^2 \sigma_v^2 n^2 \Delta T^2}. \quad (26)$$

Note that this Gaussian correlation model must not be confused with the characterization of the random process as Gaussian, which covers a much wider class of signals. To completely describe the random process it suffices to consider either the auto-covariance function, or, by the Wiener-Khintchine theorem, the power spectrum. In radar meteorology, the latter is usually referred to as the Doppler spectrum.

This signal model is the justification for the commonly employed restriction of further processing to estimate only the first three moments of the Doppler spectrum, which then contain the complete information. The assertions are often used in simulations of the radar signal (Zrnić, 1975; Frehlich and Yadlowsky, 1994; Muschinski et al., 1999). Furthermore, stationarity must be assumed over typical dwell-times of  $O(1 \text{ minute})$ . While this is a classical assumption in radar signal processing (Zrnić, 1975, 1979; Woodman, 1985; Frehlich and Yadlowsky, 1994; Lottman and Frehlich, 1997), the maximum time interval for which this assumption can be made safely is unknown. Somewhat surprisingly, this problem of selecting the dwell time  $T_d = N_T \cdot \Delta T$  is hardly ever mentioned explicitly in treatments of RWP signal processing, see the discussion in Lehmann (2009). For later convenience,  $N_T$  is defined as  $N_T = N_{ci} \cdot N_p \cdot N_s$ .

### Digital pre-filtering

Digital pre-filtering includes all operations on the signal  $\mathbf{S}$  before a Doppler spectrum is estimated. Most existing wind profiler systems still employ a simple digital filtering method called coherent integration. This method was previously implemented by hardware adder circuits which had to be used in the past because the sampling rate  $\Delta T$  was beyond the digital processing capabilities of the first wind profilers. This allows a reduction of the data rate at the expense of the analyzable Nyquist interval. Coherent integration through averaging of  $N_{ci}$  complex samples can be written as

$$S^{ci}[m] = \frac{1}{N_{ci}} \sum_{n=0}^{N_{ci}-1} S[m \cdot N_{ci} + n], \quad m = 0, \dots, (N_p \cdot N_s) - 1 \quad (27)$$

This can be regarded as a digital boxcar filter operation, followed by decimation (Farley, 1985). Its frequency response characteristics is often referred to as comb-filtering, with an amplitude transfer function depending on frequency as

$$|H(f)| = \frac{\sin(N_{ci}\pi f \Delta T)}{N_{ci} \sin(\pi f \Delta T)} = \mathcal{D}_{N_{ci}}(f \Delta T), \quad (28)$$

where  $\mathcal{D}_{N_{ci}}$  is the Dirichlet kernel (Schmidt et al., 1979; Percival and Walden, 1993). A plot of this function around baseband is shown in Fig. 7. Note that the function is periodic and only plotted over a finite interval. The time increment of the coherently

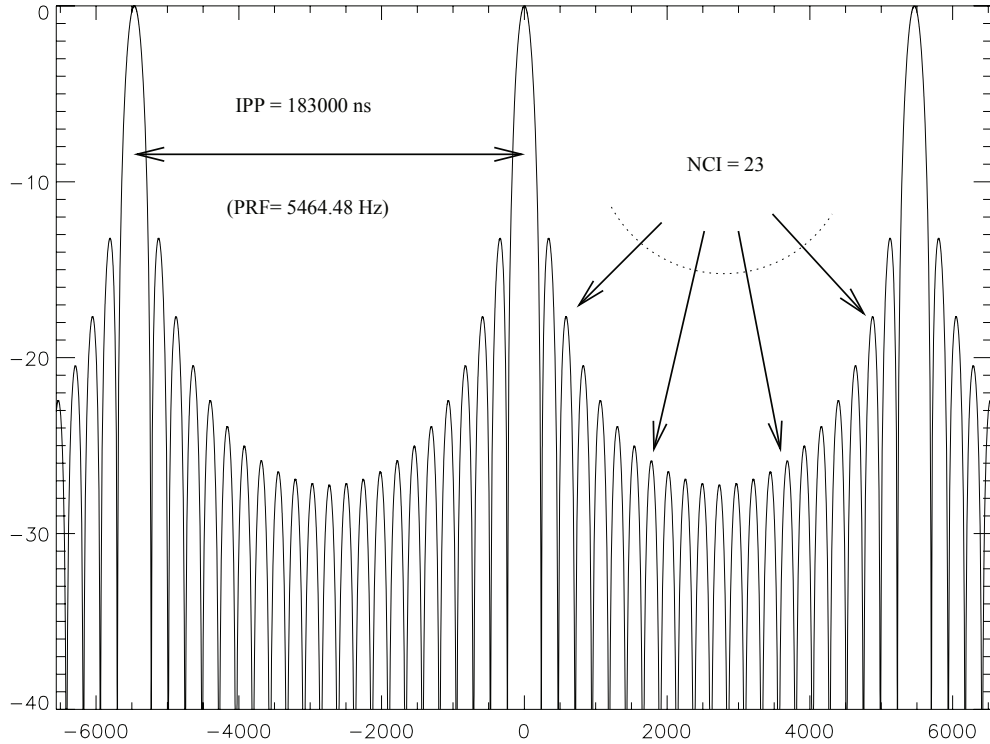


Figure 7: Example of the coherent filter response characteristics  $\left| \frac{H(f)}{H(0)} \right|$  for  $IPP=183\mu s$  and  $N_{ci} = 23$  for the limited frequency range given on the abscissa (Hz). The ordinate scaling is logarithmic (dB).

integrated series is now  $N_{ci} \cdot \Delta T$ . This method poses no problems if the number of coherent samples  $N_{ci}$  is chosen not to large.

### Spectral estimation

With the classical assumption that the coherently integrated time series  $S^{ci}[m]$  for atmospheric returns can be regarded as a stationary Gaussian random process, it suffices to estimate the power spectrum for a description of this process without loss of information. The latter is usually referred to as the Doppler spectrum. In wind profiler radars, a modified periodogram is used as a classical nonparametric estimator of the power spectrum (Kay and Marple, 1981; Percival and Walden, 1993). This method needs no further a-priori information and produces reasonable results for a large class of relevant processes, including ground clutter and some types of Radio Frequency Interference (RFI). Furthermore, it can be easily implemented using a Discrete Fourier Transform (DFT).

The (leakage) bias of the periodogram estimate is reduced through data tapering, e.g. the time series is multiplied with a window sequence  $w[n]$ . Traditionally, a Hanning

window is employed for it is conveniently implemented in the frequency domain, but in general a variety of windows is at disposal (Harris, 1978). For a reduction of the variance of the estimate, there are basically three options:

1. The whole time series is transformed through a DFT and the estimate is smoothed across frequencies (Muschinski et al., 2005). This is known as a lag window spectral estimator (Percival and Walden, 1993).
2. The time series is broken up into  $N_s$  segments of equal length, the direct spectral estimate is computed for each segment and the  $N_s$  estimates are averaged together. This method is called *Welch's overlapped segment averaging (WOSA) estimator* (Welch, 1967; Percival and Walden, 1993). It is popular due to its easy implementation and known as spectral or incoherent averaging in the RWP community (Strauch et al., 1984; Tsuda, 1989).
3. A series of estimates is calculated using a set of orthogonal data tapers, which are then averaged together. This *multitaper estimator* was proposed by Thomson (1982) and recently used for RWP by Anandan et al. (2004).

The most popular method in RWP signal processing is the WOSA approach. For  $N_s$  segments of length  $N_p$  without overlapping of the blocks, the individual estimates are obtained for  $N_s$  segments,  $l = 0, \dots, N_s - 1$ , and  $N_p$  discrete frequencies,  $k = 0, \dots, N_p - 1$  as

$$P[l, k] = \frac{1}{N_p} \left| \sum_{m=0}^{N_p-1} w[m] S^{ci}[l \cdot N_p + m] e^{-i \frac{2\pi km}{N_p}} \right|^2, \quad (29)$$

and simple averaging then yields the estimate:

$$P[k] = \frac{1}{N_s} \sum_{l=0}^{N_s-1} P[l, k]. \quad (30)$$

The Doppler spectrum is usually given as a function of velocity instead of frequency. The conversion between frequency shift  $f$  and radial velocity  $v_r$  uses the well-known relation  $f = 2v_r/\lambda$ , where  $\lambda$  denotes the radar wavelength.

### Signal detection, classification and moment estimation

An example of a typical Doppler spectrum is shown in Fig. 4 of Muschinski et al. (2005) where two spectral maxima are present that reside on white noise. To discriminate between noise and signals, an objective noise level is estimated using the method put forward by Hildebrand and Sekhon (1974). This method works well if white noise occupies a sufficient part of the spectrum. In the next step it is necessary to select the

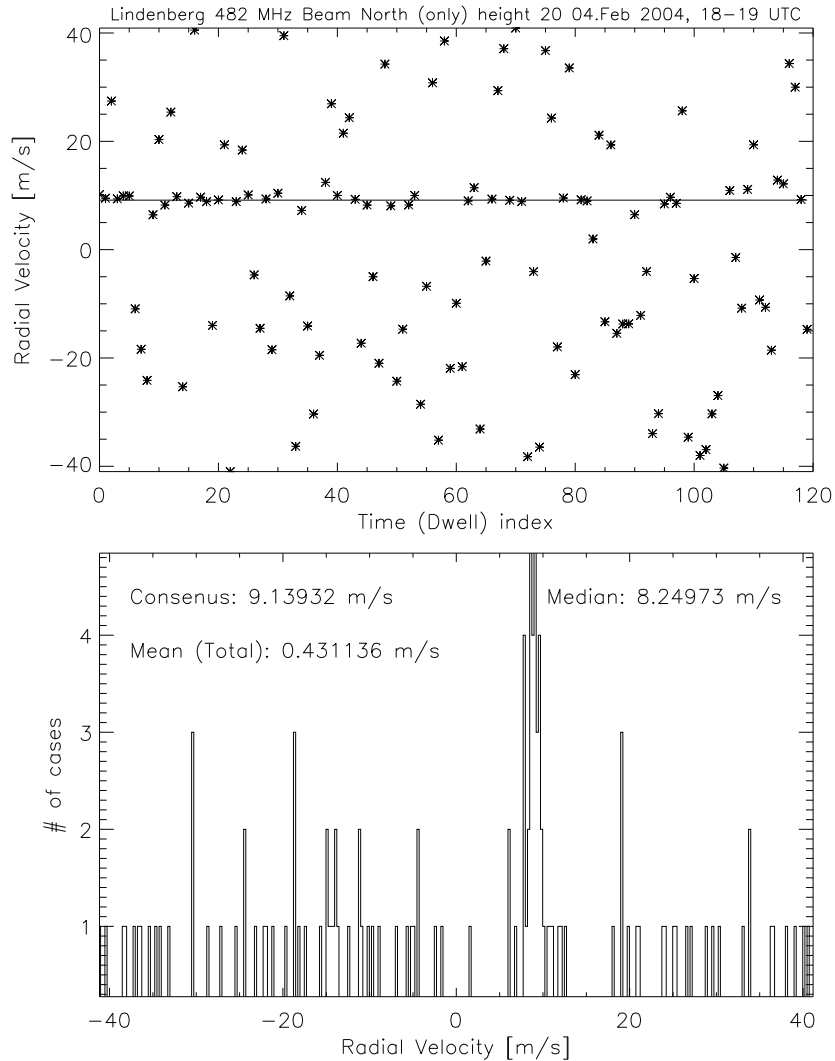


Figure 8: The consensus principle. The upper part shows the distribution of 120 individual estimates for the Doppler velocity at one range gate of a 482 MHz wind profiler measured over one hour. The line shows the consensus estimate. The lower part shows the histogram (distribution) of the individual estimates. Note that this resembles approximately the PDF of the velocity estimator. A distinct maximum of Doppler estimates can be seen near 9 m/s - this is in agreement with the value estimated by the CNS. Median values and arithmetic mean are given for comparison.

signal peak caused by the atmospheric return. A well-established method exists which is called the first moment algorithm (Strauch et al., 1984; May and Strauch, 1989), it essentially selects the signal peak with maximum power density as the atmospheric signal. The method works quite well for single peak spectra.

As already discussed, the power spectrum of the atmospheric signal is assumed to

have a Gaussian form though this can be violated for *certain radar returns* (Woodman, 1985). This has the advantage that the first three moments, namely power, mean frequency and frequency spread, are sufficient for a complete description of the signal (Woodman and Guillen, 1974). They are well-defined even if the Gaussian assumption of the form of the power spectrum is violated, see Appendix B in Lehmann (2009). For spectra with sufficient frequency resolution it might nevertheless be interesting to consider higher order moments. This is a topic for future work.

Small SNR values are typical for RWP, at least for the uppermost range gates. Consequently, one is faced with a statistical detection task, which leads to a binary decision problem with two hypotheses ( $H_0$  no atmospheric signal present,  $H_1$  atmospheric signal present). For known stationary signals, a matched filter approach (basically a correlation with the expected signal) optimizes the SNR in the detection process (Helstrom, 1968). Unlike classical radars, profilers operate with low detection thresholds which leads to the fact, that *for weak signals the probability of false alarm may be as high as the probability of detection* (Ferrat and Crochet, 1994). Of course one has to deal with an inevitably high number of bad estimates (Frehlich and Yadlowsky, 1994). The same problem occurs with other remote sensing systems, for instance with lidar (Smalikho, 2003).

To handle this situation, a rather simple but very powerful method is used which is called consensus averaging (a more appropriate name would perhaps be consensus filtering). The probability density function (PDF) of a maximum energy based estimate  $\hat{v}$  for the true mean Doppler velocity  $v$  in case of white noise (SNR parameterized by  $0 \leq b \leq 1$ ) is a Gaussian superposed on white noise (Frehlich and Yadlowsky, 1994):

$$p(\hat{v}) = \frac{b}{2v_N} + \frac{1-b}{\sqrt{2\pi}\sigma} e^{-\frac{(\hat{v}-v)^2}{2\sigma^2}} \quad (31)$$

Here,  $b$  determines the fraction of bad estimates and  $\sigma$  is the standard deviation of good estimates. This simple model makes the assumption that the Doppler frequency of the atmospheric echo is quasi-stationary over a time scale of up to 1 hour. The Gaussian is more pronounced for a higher SNR (a smaller value of  $b$ ) or less pronounced for a low SNR (a higher value of  $b$ ). In other words, a low SNR increases the chance that the estimated Doppler velocity estimate is drawn from the white noise part of the PDF. To minimize the influence of noise on the estimates, nonlinear digital filtering is performed by means of the so called consensus average (Fischler and Bolles, 1981; Strauch et al., 1984). The consensus has the following two purposes:

1. It acts as a decision statistics to discriminate between (false) Doppler estimates caused by random noise peaks and (correct) estimates which are due to stationary atmospheric returns.
2. It is a homogeneous, nonlinear estimator for the Doppler velocity that includes outlier suppression.

Other nonlinear filters are possible as well (for instance the Median), but consensus has proven its robustness and accuracy (Strauch et al., 1984). The principle is best illustrated graphically, see Fig. 8.

## 2.4 Clutter effects: Signal processing revisited

While instrument theory provides a first clue on the general properties of the measurable function at the antenna output port, this is necessarily a simplified one. In particular, the theory is not complete in the sense that it contains all real-world effects like clutter or radio interference. The simple model (25) for the demodulated voltage signal must therefore be extended and written as

$$S[n] = I[n]e^{i\omega n\Delta t} + N[n] + C[n], \quad (32)$$

where  $\mathbf{C}$  is a clutter component with possibly very diverse properties, depending on its origin. Taking the clutter component  $\mathbf{C}$  into account, the general properties of the RWP signal are modified as follows:

**$S(t)$  is multi-component.** This is caused by the possibility of different collectively acting scattering mechanisms, internal (electronic) noise and possibly also external (artificial) effects. In the strict sense, only the clear-air scattering mechanism is of interest for RWP. However, from a practical point of view it has become customary to also include scattering at hydrometeors as a non-clutter component, at least as long as the particles can be considered as passive tracers for wind measurements. As signal components from different scattering processes or other effects may be present simultaneously, they need to be separated and classified using available a-priori information. Electronic noise is ubiquitous in every receiver and external Radio Frequency Interference (RFI), e.g. digital television signals in UHF channel 22 (DVB-T) in Germany, may also be present (Wilfong et al., 1999).

**$S(t)$  may have nonstationary components.** While the receiver signal is intrinsically nonstationary due to the impulsive character of the transmitted signal (pulse) and the inhomogeneous vertical structure of the atmosphere, this property is significantly changed during range gate sampling. The assumption of stationarity is usually valid for atmospheric scattering, ground clutter and noise, provided the scattering medium at a fixed height does not change its properties significantly over the length of the time series (Woodman, 1991). This is one of the basic assumptions of signal processing for atmospheric radars (Keeler and Passarelli, 1990) and the main motivation for using spectral analysis. However, for bird, airplane and lightning echoes it is quite obvious that the clutter component can never be assumed to be stationary. The characteristic duration of these transient echoes varies: Lightning echoes are not longer than 100 ms (Röttger et al., 1995; Petitdidier and Laroche, 2005), aircraft echoes are typically

shorter than 10 s (Boisse et al., 1999) and echoes of a single bird can be estimated to extend 10-100 s (Merritt, 1995; Lehmann, 2009). This makes it necessary to apply mathematical methods for the analysis of nonstationary signals, which is the main focus of this thesis.

Ignoring the clutter term leads to errors in parameter estimation, the severity of which varies with the particular clutter type, strength and duration. Such problems were noted for horizontal wind profiling applications, (Angevine and MacPherson, 1995; Angevine et al., 1998b,a) as well as for measurements of other atmospheric parameters, like determination of refractive index gradients (Gossard et al., 1998, 1999), turbulence parameters (Angevine et al., 1994), vertical wind (Angevine, 1997), boundary layer properties (Grimsdell and Angevine, 2002; Bianco and Wilczak, 2002; Heo et al., 2003), tidal and gravity wave effects (Whiteman and Bian, 1996; Browning et al., 2000; Ralph, 2000) etc. This list of references is far from being complete. In research applications, a careful editing of data by trained experts can partly remedy the deficiencies of classical signal processing. In this case it is often stated that the quality of the measurements required careful *data cleaning* or even human *data editing*.

While a subjective data cleaning approach is at the very least unsatisfactory, it is truly impossible for continuously running operational wind profilers. This became soon obvious after installation of the NOAA-WPDN (Barth et al., 1994; Wilczak et al., 1995). Quality control postprocessing was therefore developed to address the observed problems at least partly (Wuertz and Weber, 1989; Weber and Wuertz, 1991; Barth et al., 1994), but the need for improved signal processing methods was also recognized. Consequently, work began to develop improved automatic signal processing algorithms (Riddle and Angevine, 1991; Clothiaux et al., 1994; Merritt, 1995; Hocking, 1997; Jordan et al., 1997; Griesser, 1998; Schumann et al., 1999; Boisse et al., 1999; Cornman et al., 1998; Cohn et al., 2001; Vogt and Sacher, 2001; Morse et al., 2002; Goodrich et al., 2002; Wilfong et al., 1999; Law et al., 2002; Bianco and Wilczak, 2002; Stankov et al., 2003; Weber et al., 2004). Unfortunately, most of these algorithms have only reached an experimental status. Long-term evaluations are often lacking as was in particular noted by Richner and Kretzschmar (2001) for intermittent clutter filtering methods. Also, it must be remarked that many of these advanced algorithms were developed using ad-hoc justifications. Some authors even noted explicitly that the algorithm was developed *to mimic the human expert* (Cornman et al., 1998), but this describes rather a goal than providing a clear guideline for algorithm development.

The need for improved and validated RWP signal processing is obvious to everyone working directly with these instruments. I can probably not do better than quoting Dr. Richard (Dick) Strauch, who installed the Colorado-Profiling network (Strauch et al., 1984) and developed much of the processing that is used until today (personal communication, September 2002):

*It is surprising (...) that we are now working with incredible compute power and memory but the processing is still about what it was with mini-*

*computers with 32k memory. However, I have always believed that when spectra are contaminated (as they almost always are at low altitude and more often these days at all altitudes with RFI) then it should be possible to do better.*

Not surprising, however, is the fact that methods of modern signal analysis have a tremendous potential for a deeper understanding of the nature of real-world signals, which consequently can lead to improved processing algorithms. Two important conclusions can be drawn from the discussion above:

1. The non-stationary character of  $\mathbf{C}$  makes it obvious that a sole spectral representation of the signal is inadequate to efficiently describe the clutter component. Methods of non-stationary signal analysis need to be used to find a decent (hopefully sparse) representation for such signals, which may then allow efficient filtering strategies with the purpose of removing  $\mathbf{C}$  (Jordan et al., 1997; Boisse et al., 1999; Lehmann and Teschke, 2001, 2008a).
2. Several independent stationary signal components will give rise to a Doppler spectrum with multiple signal peaks. Such a situation is not accounted for in standard processing, and a variety of so-called multi-peak algorithms have therefore been proposed. Among them are simple methods, like the ground clutter algorithm by Riddle and Angevine (1991) which is in widespread use, as well as other, more complex techniques (Griesser, 1998; Cornman et al., 1998; Wilfong et al., 1999; Morse et al., 2002). The number of existing algorithms is symptomatic for the many different approaches to tackle the multiple peak problem. Unfortunately, there are only few validation attempts (Cohn et al., 2001; Gaffard et al., 2006; Hooper et al., 2008) and operational experience is still indicative of problems with these methods. The most important issue is the excessive use of weakly justified a-priori assumptions, like vertical continuity constraints, for peak selection. More work is needed to refine multi-peak processing and a preceding intermittent clutter filtering will surely be beneficial in that respect.

### 3 Non-stationary clutter and its filtering

The focus of this thesis is on the problem of intermittent clutter, which includes echoes from lightning channels, aircraft and birds. The latter are by far the most problematic clutter source due to a relative long characteristic time scale of the echoes and a high frequency of occurrence during nocturnal migration in spring and fall. During such episodes, comparisons with independent reference data have shown errors in RWP wind speed measurements of up to about 10 m/s, which are furthermore correlated in vertical range over many hundred meters and in time over several hours. An example of the operational wind measurement obtained with the 482 MHz RWP at Lindenberg in spring 2002 illustrates the problem: Fig. 9 shows that the difference in wind speed between the two measurements in the height range between 1000 m and 2500 m msl is quite significant, with a maximum of about 10 m/s. Inspection of the Doppler spectra reveals the typical signature of bird echoes: Wide, irregular peaks, which are often discontinuous with respect to the overall vertical profile. An example is shown in Fig. 10 and more examples can be easily found.

It is mandatory to avoid the assimilation of bird-contaminated profiler wind data in numerical weather prediction models, as this can have significant effects on the quality of the forecasts (Semple, 2005; Cardinali, 2009). Such incorrect measurements, if not detected and excised, may be the cause of significant errors in data assimilation, in particular when several systems in a network are affected simultaneously and other measurements for a buddy-check based quality control (Nehrkorn, 2000; Guo et al., 2000; Benjamin et al., 2004a; Semple, 2005) are not available. The relative weighting assigned to the observation in the assimilation process is determined by its error characteristics, often expressed as an observation covariance (Talagrand, 1997; Rabier et al., 2008). This needs to be much smaller than what may be observed during bird migration for the observation to have any positive impact. In particular, it is important to avoid correlated errors, because most current data assimilation methods make the assumptions that measurement errors are uncorrelated (Stewart et al., 2008).

Birds are known to be effective targets for a wide range of radars, with frequencies ranging from X-band to UHF (Vaughn, 1985; Bruderer, 1997). The fact that migrating birds can drastically affect RWP measurements is known for more than a decade (Ecklund et al., 1990; Barth et al., 1994; Wilczak et al., 1995; Douglas and Stensrud, 1996; Engelbart et al., 1998). It was nicely summarized by Wilczak et al. (1996) as follows:

*It has only recently become widely appreciated that mean winds from operational wind profilers and scanning Doppler radars often have errors on the order of 5-10 m/s for heights up to several kilometers that result from nocturnal migrating birds. For wind profilers, signal processing techniques have been developed for periods of light and moderate contamination that remove the bird signal while leaving the true atmospheric signal. For times with severe contamination, the bird signal must be identified us-*

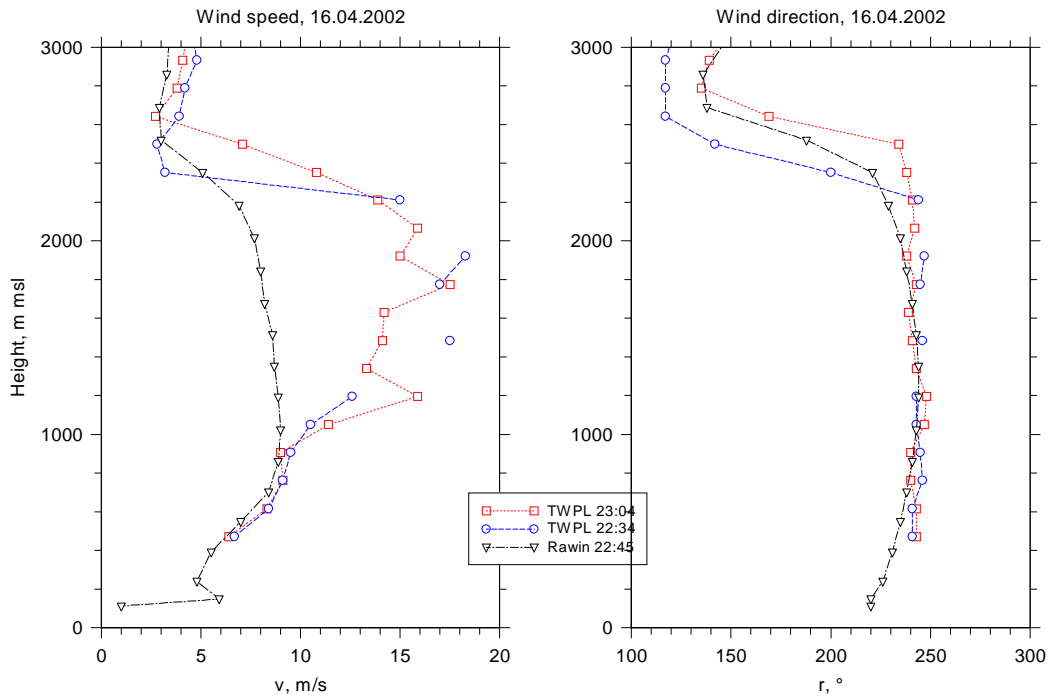


Figure 9: Measurement of the vertical profile of the horizontal wind on April 16, 2002, obtained with the Lindenberg 482 MHz RWP between 22:30 and 23:00 UTC (blue) and between 23:00 and 23:30 UTC (red). Additionally shown is the wind measurement of the co-located routine Radiosonde with launch time 22:45 UTC (black).

*ing combinations of the Doppler moments and then be excised from the data.*

This statement is in agreement with the operational experience at DWD. Depending on the actual weather conditions, significant bird echoes are observable from about mid-February until June for the spring migration period and between July and November for fall migration. Richner and Kretzschmar (2001) reported bird migration in more than 160 nights per year in Central Europe and consequently, about 10 percent of hourly wind data gathered with a 1290 MHz RWP in Payerne were found to be contaminated. They furthermore suggested to use bird migration data from a wind profiler network for ornithological purposes, much in line with Merritt (1995).

The susceptibility of RWP systems to bird echoes primarily depends on wavelength and antenna characteristics. It mostly affects L-band and UHF-radars, that is boundary layer and tropospheric profilers, as discussed in Wilczak et al. (1995). Intermittent clutter is an issue for both single-signal Doppler-beam swinging radars and multi-signal (imaging) radar systems (Cheong et al., 2006; Chen et al., 2007).

The occurrence of these intermittent clutter echoes makes it necessary to either use extensive quality control procedures to identify and excise contaminated data, or to

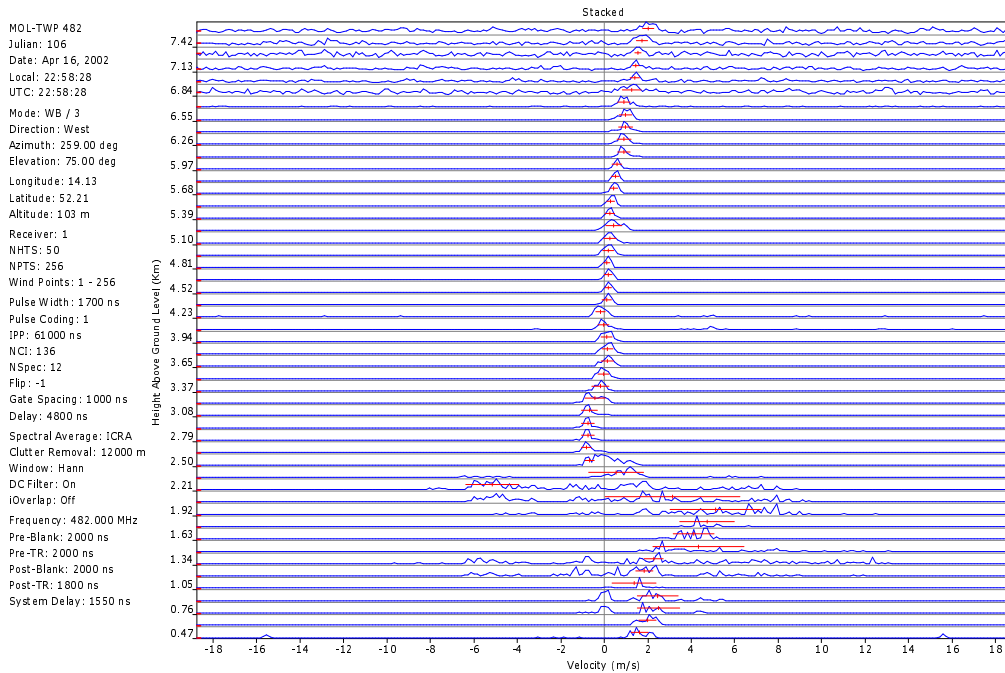


Figure 10: Stacked spectra during bird migration obtained with the Lindenberg RWP on April 16, 2001. The typical signature of intermittent clutter echoes is visible below 2.7 km.

limit the data use to time periods and heights where bird migration is negligible. While the need for an extensive manual data quality control and cleaning might be acceptable for research activities, it is surely not feasible in any operational setting. Current state-of-the-art profilers therefore already run specialized algorithms on site to reduce bird contamination (Merritt, 1995; Jordan et al., 1997; Ishihara et al., 2006), but practical experience supports the statement that the problem has not been fully resolved. In fact, the data shown in Figs. 9 and 10 were obtained using an *Intermittent Clutter Reduction Algorithm* (ICRA) based on Merritt (1995). Similar problems exist with a commercially available implementation of the algorithm proposed by Jordan et al. (1997). Improvements are therefore imperative.

### 3.1 A first clutter filtering approach using Wavelets

Currently used operational intermittent clutter detection and filtering algorithms are based on spectral data (either before or after averaging) or even moments. This had mainly technical reasons, because technical limitations prevented any sophisticated

processing and storage of raw data. One notable exception is Jordan et al. (1997), who were the first to attempt a filtering of the (coherently integrated) time series of the demodulated receiver voltage using the technique of wavelet transforms. Their attempt was to filter both ground and intermittent clutter contributions. Notably, the *ability of the wavelet transform to isolate short-lived events* was mentioned as an argument in favor of the method, and the authors stated:

*Our technique is based on the observation that the clear-air and clutter components of the radar signal are more easily distinguished using wavelet transforms rather than Fourier transforms. In particular, we find that there is often a better match between the clutter signal and certain wavelet basis functions than can be obtained using the infinite sinusoids of Fourier analysis.*

Following this work, an attempt was started at Lindenberg to investigate and use this promising new method for an improvement of the data quality of the DWD profilers, which had also shown a variety of clutter problems during operation. In cooperation with the mathematical departments of the University Potsdam and the University of Bremen, a discrete wavelet transform (DWT) based clutter filtering algorithm was developed, implemented and tested on a small data set. This algorithm employed a combination of wavelet based multi-resolution analysis, see e.g. Burrus et al. (1998) and wavelet coefficient thresholding (Donoho, 1995). The results were published in Lehmann and Teschke (2001) and the main idea can be summarized as follows: The in-phase and quadrature phase of the time series is (independently) decomposed using an orthonormal wavelet basis (Daubechies family) up to a fixed, heuristically determined, number of decomposition scales. Filtering is achieved by a thresholding of the wavelet coefficients using two separate strategies: The first was borrowed from non-linear estimation theory, where a statistical scale-dependent threshold is estimated for the purpose of signal de-noising, i.e. a separation of random white noise from deterministic signals. In contrast to the usual strategy of *wavelet shrinkage* (Donoho, 1995; Donoho et al., 1995), the *de-noising* in Lehmann and Teschke (2001) is done in an opposite way, that is the small amplitude part of the signal is assumed to be due to the atmospheric echo, whereas the larger amplitude parts of the signal is thought to be due to (ground) clutter. The second method is based on the empirically determined distribution of wavelet coefficients, which shows differences between intermittent clutter and clear-air signal components. Using an ad-hoc decision strategy developed from reviewing the available data, a threshold was derived for the wavelet coefficients. The filtering itself is achieved by replacing the expansion coefficients associated with clutter with the thresholds, and a filtered version of the signal is finally obtained after inverting the transform.

Although the method worked reasonably well in a number of cases, it is now obvious in retrospect that this approach had a number of shortcomings:

- The selection of the wavelet was ad-hoc, due to the unknown general properties of the RWP signal components. The problem is discussed in sections 3 and 4 of the paper, but no satisfying answer could be given.
- The optimal number of decomposition scales was selected using a rule from approximation theory. As discussed in section 4 of the paper, this also depends on the unknown properties of the signal, like smoothness.
- The thresholding strategy for the wavelet coefficients was only based on empirical findings.

While the approach was by and large inspired by Jordan et al. (1997) and tried to extend the method on a more solid mathematical ground, a convincing justification of the algorithm based on signal theoretic considerations could not be given. Perhaps it has to be mentioned that only a small data basis was readily available before the year 2000. In fact, the time series data used in Lehmann and Teschke (2001) could only be obtained using undocumented features of the RWP software, whereby only a small fraction of the principally available data was accessible at all. A comment in Jordan et al. (1997) is indicative of similar problems:

*(The) choice of threshold ... seems reasonable but has not been verified because of a lack of supporting data. ... (The) paper presents initial results and examples of clutter removal utilizing wavelet transforms. The techniques have not been fine-tuned or extensively tested...*

For radar signals, the DWT now appears to be inferior to other methods, as expressed by a statement in Selesnick et al. (2005):

*The application of the DWT has proven somewhat disappointing (for applications) such as those involving complex or modulated signals.*

Nevertheless, the main ideas from this work are still relevant: The filtering is based on a linear expansion of the raw signal, or in other words, an atomic decomposition. The purpose of using this expansion is to get a better separation of atmospheric signal and clutter. Although the goal of striving for a sparse representation was not explicitly mentioned, it was indirectly formulated in Lehmann and Teschke (2001):

*The ultimate goal is obviously to find a wavelet basis, which would allow a separation of the desired and the unwanted parts of the signal, i.e. which would have the ability to approximate the unwanted signal components (ground clutter, intermittent clutter) with only a few non-zero wavelet coefficients.*

### 3.2 The potential of time-frequency analysis

From both theoretical considerations and practical experience, the general understanding of the clutter problem remained to be limited. Research therefore continued with an emphasis on finding a signal decomposition that was better adapted to the large variety of RWP signals encountered and on the development of a filtering approach that was better justified from a signal theoretic point of view. The main focus was directed toward the filtering of intermittent clutter signals, as it had turned out that ground clutter signals could quite effectively be suppressed by hardware improvements (better antennas having lower sidelobes), proper siting of the RWP's and processing methods for stationary signals.

In a continued collaboration between the author and the Centre for Technomathematics of the University of Bremen, some new ideas developed after the publication of Lehmann and Teschke (2001). In particular, it was found that other signal transforms than wavelets yielded quite clear and concise representations for a number of real-world RWP signals. Very helpful in that respect had been the development of a software tool that allowed a visualization of RWP signals as scalograms or spectrograms, using the continuous wavelet transform and the windowed Fourier transformation (Holschneider, 1995; Mallat, 1999).

Given a real symmetric and normalized window function  $g : \mathbb{R} \rightarrow \mathbb{R}$ , with  $\|g\|_2 = 1$  the windowed Fourier transform (WFT) of a signal  $f \in \mathbb{L}^2(\mathbb{R})$  is given by

$$Sf(u, \xi) := \int_{-\infty}^{\infty} f(t)g(t-u)e^{-i\xi t} dt. \quad (33)$$

This maps a one-dimensional signal to the two-dimensional time-frequency plane (or phase-space). The variances

$$\sigma_t^2 = \int_{-\infty}^{\infty} t^2 |g(t)|^2 dt \quad \text{and} \quad \sigma_w^2 = \frac{1}{2\pi} \int_{-\infty}^{\infty} \omega^2 |\hat{g}(\omega)|^2 d\omega \quad (34)$$

indicate the time and frequency localization capability of the WFT for a given window  $g$ , which is independent of time  $u$  and frequency  $\xi$ , but limited by Heisenberg's uncertainty principle (Mallat, 1999):

$$\sigma_t \cdot \sigma_w \geq \frac{1}{2}. \quad (35)$$

Equality is only achieved for a Gaussian window. The spectrogram

$$P_S f(u, \xi) := |Sf(u, \xi)|^2 \quad (36)$$

is a measure of how much energy the signal has at time  $u$  and frequency  $\xi$ , it provides an instructive visualization of the time-dependent energy content of the signal. Similarly, a normalized function  $\psi \in \mathbb{L}^2(\mathbb{R})$ ,  $\|\psi\|_2 = 1$ , is called a wavelet if its average  $\int \psi(t) dt = 0$  and the continuous wavelet transform (CWT) of  $f \in \mathbb{L}^2(\mathbb{R})$  is defined as (Mallat, 1999)

$$Wf(u, s) = \int_{-\infty}^{\infty} f(t) \frac{1}{\sqrt{s}} \bar{\psi} \left( \frac{t-u}{s} \right) dt. \quad (37)$$

Similar to the spectrogram, the scalogram is defined as

$$P_W f(u, s) := |Wf(u, s)|^2. \quad (38)$$

The scalogram is also a measure of energy at time  $u$  and frequency  $\frac{\eta}{s}$ , where  $\eta$  is some constant depending on  $\psi$  (Mallat, 1999). Time and frequency uncertainty is given by  $s^2 \sigma_t^2$  and  $\frac{\sigma_\omega^2}{s^2}$ , respectively, with  $\sigma_t$  and  $\sigma_\omega$  defined as in (34) with  $g$  replaced by  $\psi$ . Hence, in contrast to the WFT, time localization is best at high frequencies (i.e. small scale  $s$ ), whereas for low frequencies time localization is rather poor.

Spectrogram and scalogram visualizations of typical RWP signals were quite instructive and the work was reported at the ISTP conference in Leipzig 2003 (Justen and Lehmann, 2003). The response from international experts was very positive, probably because this method for visualizing RWP raw signals had not been used before, compare e.g. Jordan et al. (1997); Boisse et al. (1999), and the interpretation was quite easy and intuitive. From the examples shown in Fig. 11 it is immediately obvious that the spectrogram representation provides a clearer picture of the signal characteristics. This is due to the uniform time-frequency resolution of the WFT across the time-frequency plane, which turns out to be very appealing for RWP signals. In contrast, the time-frequency resolution in the scalogram varies as a function of frequency as indicated by the rectangles symbolizing the Heisenberg box. Especially near zero-frequency, the intermittent clutter signals are stretched along the time axis due to the much coarser time resolution.

WFT based time-frequency analysis was therefore identified as a potentially promising method for filtering intermittent clutter signals. This was reported in a tutorial overview on radar wind profiling (Muschinski et al., 2005), which attempted to provide a coherent conceptual framework of advanced radar wind profiling and to identify areas for future research and development. The paper reviewed the RWP signal standard processing method based on spectral estimation theory and tried to clearly define the terms clutter, noise and atmospheric signal, thus highlighting the multi-component nature of real-world RWP time series data. An example of a signal containing an aircraft echo is shown in Fig. 5 of the paper. Although quite simple, it showed how

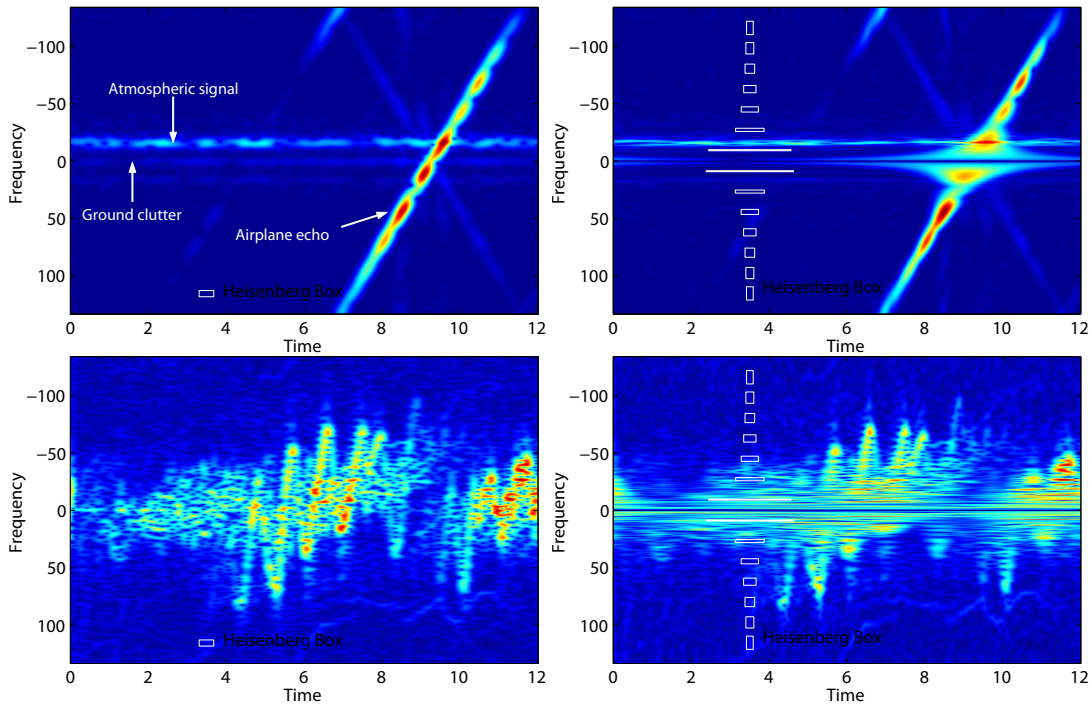


Figure 11: Examples of spectrogram (left) and scalogram (right) plots of two RWP signals containing intermittent clutter taken from Justen and Lehmann (2003). The upper part shows a clear air atmospheric echo together with a strong airplane echo. The lower part shows the typical signature of bird echoes, obtained during the migration season. Abscissa denotes time in seconds, the ordinate shows frequency in Hertz. For scalogram plots, a Gaussian wavelet (or Morlet wavelet) has been used (Holschneider, 1995). The Heisenberg box is indicated by white rectangles.

time-frequency methods could in principle be used to remove the intermittent clutter component, while leaving the desired atmospheric signal intact. The method performed well regardless of the very small signal-to-clutter ratio of the example. It was further concluded that it does not make sense to apply time-frequency methods to the problem of ground clutter removal, because this component is stationary over the observation interval (or dwell time) and the Doppler spectrum thus provides an adequate (sparse) signal representation.

### 3.3 Gabor frame expansion and its statistics

Building upon the ideas outlined in Muschinski et al. (2005), research continued regarding the question of how these time-frequency based signal analysis methods could be used to construct an efficient intermittent clutter filtering algorithm. Given the superior properties of the spectrogram in terms of its ability to visually separate stationary

and non-stationary signal components for a great variety of typical RWP data, it was quite natural to look for an equivalent discrete version, for the continuous representation is highly redundant and therefore computationally inefficient. A Gabor frame decomposition and synthesis algorithm, also called a discrete Gabor transform (DGT), was therefore implemented using the method described by Wexler and Raz (1990). It was found that sufficient speed could be achieved in both MATLAB and IDL, so the computational requirements should not be prohibitive for a later real-time use of this algorithm.

Signal filtering can be discussed using the idea of atomic decomposition, whereby a signal is decomposed into elementary functions as suggested by Gabor (1946). A related well-known concept is that of an orthonormal Hilbert space basis. Frames provide a generalization of this concept (Daubechies et al., 1986) and were found to be more flexible for time-frequency analysis than bases (Mallat, 1999). After the computation of a frame expansion (analysis step), a time and frequency dependent filtering of signals can simply be realized by a change of the series coefficients for a subset of atoms, thus modifying the corresponding signal components. A reconstruction through a frame synthesis then yields the modified or filtered signal. However, the question of how to separate the non-stationary clutter components from the stationary atmospheric signal part in Gabor phase space was quite difficult to answer. The breakthrough was obtained in November 2005 by employing the statistical test suggested by Merritt (1995), which uses a known relation between mean and variance for Gaussian random processes. The mapping of the Gaussian signal properties to the Gabor coefficients was investigated to adapt the statistical test accordingly and unbiased estimators to estimate expectation and variance of the process from Gabor coefficients were derived. The method was presented to the scientific community at the ISTP 2006 in Boulder, Colorado.

### **3.4 Optimal Gabor frame expansions**

After the paper Lehmann and Teschke (2008a) was published, efforts concentrated on the implementation of this new method in the online software of the RWP systems used by DWD. Two questions that were previously not addressed needed to be answered in that respect:

1. How should the parameters for the DGT be optimally selected ?
2. Is there an optimal data acquisition strategy for intermittent clutter filtering ?

The first question came up quite naturally: As there is more than one option for the selection of the lattice parameters, what would be an optimal discretization ? Also, what should be the length (or analyzing bandwidth) for the Gaussian window in the DGT ?

It turned out that the discrete Gabor frame expansion can be set-up in a way to resemble quite closely the properties of an orthogonal expansion, with primal and dual window being almost identical in shape but different in amplitude due to the redundancy of the frame. This can be achieved by a judicious choice of the lattice parameters and has the obvious advantage of providing a good simultaneous localization of the DGT in time and space during both analysis and synthesis. As a side effect, it also leads to stable numerical estimates of the dual window. Such a decent behavior is already observed for moderate oversampling rates. The optimal lattice constants can be obtained using a simple brute force approach by finding the minimum norm of the difference between primal and dual window (the latter corrected for the oversampling factor). The number of possible lattices is limited, so the method is technically feasible and sufficiently fast. Of course, redundancy should be limited to reasonable values.

With regard to the parameterized width of the Gaussian (primal) window, the selection needs to be made in such a way that signal component separation (atmospheric part vs. clutter part) is optimized. Borrowing ideas from Allen and Mills (2004) and Mallat (2009), it was found that such a separation is greatly facilitated by a sparse representation of the radar signal in Gabor phase space. In this case, only a minimum of Gabor coefficients have significant (non-noise) values. Such a situation is undoubtedly best suited for separation attempts.

The question of an optimal data acquisition strategy for intermittent clutter filtering was not so easy to answer. Data collection was tedious because the network prototype wind profiler at Lindenberg (Steinhagen et al., 1998) suffered from long hardware-related down times between 2006 and 2008, which prevented the collection of a contiguous time series data set during the bird migration period. In contrast, the more modern network wind profilers (Lehmann et al., 2003) were running flawlessly, but their network connection had insufficient bandwidth to transfer the time series data. Note that for the 482 MHz wind profiler of DWD, the daily file size of only the low mode data is about 3 Gigabyte. Testing of the algorithm thus concentrated on subjectively selected cases which showed intense clutter contamination.

One problem was already identified in Lehmann and Teschke (2008a), namely when the duration of the intermittent clutter signal component is on the order of the dwell time. As already mentioned in the paper, this observation raises the question of finding an optimal dwell time for the estimation of a Doppler spectrum and efficient intermittent clutter filtering. This problem is therefore discussed in Lehmann (2009) to some extent.

A first data set using a considerably longer dwell time of 166 s was obtained with the Lindenberg 482 Mhz RWP during the end of the bird migration season in fall on October 26, 2007. Results were reported in Lehmann and Teschke (2008b). It turned out that there is a great variability in the characteristics of intermittent clutter echoes, especially in the duration and number of transients. It was shown that the duration of bird transients can be up to 30 s, a value which is equal to typically used RWP dwell

times. However, it was only in spring 2009 that a contiguous data set with dwell time of 147 s could be collected, with a start time on February 26 and end time on June 26. This unique data set allowed to identify extreme situations of bird migration. An example case which occurred on April 03 is shown in Fig. 10 of the paper. This is probably the first measurement of this kind that clearly indicates the limits of radar wind profiling during extreme bird migration events.

As a consequence, it became necessary to add a quality control step to the Gabor filtering algorithm. The operational bird-algorithm currently used in the NOAA profiler network makes use of a-priori information about the characteristics of atmospheric signal peaks in the Doppler spectrum to identify bird contamination, with the signal peak being classified as clutter if its spectral width is larger than 2.37 m/s (van de Kamp, 1996). As precipitation also leads to signal peaks with large spectral widths, the test is only applied conditionally (depending on time of the year, time of day, height, wind direction, downward vertical velocity). After a comparison with radiosonde measurements, it was reported in van de Kamp (1996) that the algorithm had a high probability of detection ( $> 60\%$ ) while the false alarm rate was rather high (44 %). The Gabor filtering method now allows the definition of an indicator for signal nonstationarity. This provides a more appropriate condition for applying the spectral width test and the example shown in Lehmann (2009) yielded promising preliminary results.

## 4 Conclusions

The discrete Gabor frame expansion provides a method for analyzing wind profiler raw data simultaneously in time and frequency. This allows for a separation of stationary atmospheric signals (clear-air or continuous precipitation) and non-stationary (intermittent) clutter signals. A statistical method can then be employed to achieve an objective filtering of the intermittent signal components from the data.

The filtering results can be optimized using discrete near-tight frames, for which the dual window has an almost identical shape compared to the primal (Gaussian) window. This leads to superior localization properties in the time-frequency plane. The analysis bandwidth of the Gaussian window is adapted to the data by the requirement of a simultaneous sparse representation for both the atmospheric signal and clutter. Both optimizations improve the separation of signal components and make the filtering step more efficient. Comparisons with other intermittent clutter filtering methods show a consistent superiority of the Gabor filtering approach.

Unfortunately, there appears to be a critical bird density beyond which the clutter filtering fails and any retrieval of the clear-air atmospheric echo signals seems not possible at all. Such cases are observed during dense migration events. This can be remedied by an additional quality-control step, at the expense of data availability. Any improvements appear only feasible through radar hardware measures, like more narrow antenna beams, shorter pulses and larger dynamic range in the receiver.

Future research should be focussed on a comparison of the Gabor filtered winds with independent measurements for a large data set. Richner and Kretzschmar (2001) and Kretzschmar et al. (2003) have noted that there is little information on the performance of the intermittent clutter filtering algorithms, which is indicative of a lack of validation. A comprehensive and objective validation is therefore the most urgent topic for further investigation, regardless of the first successful demonstrations. It is hoped that new observing systems like Doppler lidar that apparently do not suffer from intermittent clutter problems can soon provide a suitable reference data base, at least for lower heights. The importance of such a validation is nicely summarized in the following quote from Fabry and Keeler (2003):

*Utilization of adaptive filters in processing of active meteorological sensors has only been marginally explored yet appears to have much to offer, especially in artifact identification and removal. These approaches consist of signal-processing algorithms that directly modify the I/Q samples from which the base data spectral moment estimates are made. Any attempt to improve data quality by this root level signal processing must be fully validated so as not to destroy the existing data so familiar to the research and operational communities.*

Further work should also test potential refinements of the quality control by consider-

ing moments of higher order in the Gaussianity test. Last, but not least, investigations on the potential use of this data for ornithological purposes as suggested by Merritt (1995) are certainly of interest.

## References

- Acheson, D., Beran, D., Bhumralkar, C., Blackmore, W., Clifford, S., MacDonald, A., Maddox, R., Facundo, J., Jalickee, J., Julian, P., Lavoie, R., McPherson, R., Telesetsky, W., Zbar, F., Hayden, C., Hussey, J., McMillin, L., Planet, W., Rao, K., and Schneider, S.: Strategic Plan for Upper-Air Observations, Tech. rep., NOAA - U.S. Department of Commerce, 1992.
- Ackley, M., Chadwick, R., Cogan, J., Crosiar, C., Eaton, F., Gage, K., Gossard, E., Lucci, R., Merceret, F., Neff, W., Ralph, M., Strauch, R., van de Kamp, D., and an Allen White, B. W.: U.S. Wind Profilers: A Review, Tech. Rep. FCM-R14-1998, U.S. DoC/ NOAA/OFCM, Washington, DC., 1998.
- Adachi, A., Kobayashi, T., Gage, K. S., Carter, D. A., Hartten, L. M., Clark, W. L., and Fukuda, M.: Evaluation of Three-Beam and Four-Beam Profiler Wind Measurement Techniques Using a Five-Beam Wind Profiler and Collocated Meteorological Tower, *J. Atmos. Oceanic Technol.*, 22, 1167–1180, 2005.
- Allen, R. L. and Mills, D. W.: *Signal Analysis: Time, Frequency, Scale and Structure*, IEEE Press and Wiley-Interscience, 2004, p. 937.
- Anandan, V. K., Pan, C., Rajalakshmi, T., and Reddy, G. R.: Multitaper spectral analysis of atmospheric radar signals, *Ann. Geophys.*, 22, 3995–4003, 2004.
- Andersson, E. and Garcia-Mendez, A.: Assessment of European Wind Profiler Data, in an NWP Context, Technical Memorandum 372, ECMWF, 2002.
- Angevine, W. M.: Errors in Mean Vertical Velocities Measured by Boundary Layer Wind Profilers, *J. Atmos. Oceanic Technol.*, 14, 565–569, 1997.
- Angevine, W. M. and MacPherson, J. I.: Comparison of Wind Profiler and Aircraft Wind Measurements at Chebogue Point, Nova Scotia, *J. Atmos. Oceanic Technol.*, 12, 421–426, 1995.
- Angevine, W. M., Doviak, R. J., and Sorbjan, Z.: Remote Sensing of Vertical Velocity Variance and Surface Heat Flux in a Convective Boundary Layer, *J. Appl. Meteor.*, 33, 977–983, 1994.
- Angevine, W. M., Bakwin, P. S., and Davis, K. J.: Wind Profiler and RASS Measurements Compared with Measurements from a 450-m-Tall Tower, *J. Atmos. Oceanic Technol.*, 15, 818 – 825, 1998a.
- Angevine, W. M., Grimsdell, A. W., Hartten, L. M., and Delany, A.: The Flatland Boundary Layer Experiments, *Bull. Amer. Meteor. Soc.*, 79, 419–431, 1998b.
- Atlas, D. and Williams, C. R.: The Anatomy of a Continental Tropical Convective Storm, *J. Atmos. Sci.*, 60, 3–15, 2003.

- Baker, B. and Brenguier, J.-L.: Radar and in situ observations of small cumulus: physical interpretations of radar Bragg scatter, *Quart. J. Roy. Meteor. Soc.*, 133, 1677–1692, 2007.
- Balsley, B. and Peterson, V. L.: Doppler-Radar Measurements of Clear Air Atmospheric Turbulence at 1290 MHz, *J. Appl. Meteor.*, 20, 266–274, 1981.
- Balsley, B., Cianos, N., Farley, D., and Baron, M.: Winds Derived from Radar Measurements in the Arctic Troposphere and Stratosphere, *J. Appl. Meteor.*, 16, 1235–1239, 1977.
- Balsley, B. B. and Ecklund, W. L.: A Portable Coaxial Colinear Antenna, *IEEE Trans. Antennas Propagation*, pp. 513–516, 1972.
- Barth, M., Chadwick, R., and van de Kamp, D.: Data Processing Algorithms Used by NOAA's Wind Profiler Demonstration Network, *Ann. Geophys.*, 12, 518–528, 1994.
- Beckman, S. K.: Operational use of Profiler Data and Satellite Imagery to Evaluate the NMC Numerical Model in Predicting Heavy Snow, *Wea. Forecasting*, 5, 259–277, 1990.
- Benjamin, S. G., Devenyi, D., Weygandt, S. S., Brundage, K. J., Brown, J. M., Grell, G. A., Kim, D., Schwartz, B. E., Smirnova, T. G., Smith, T. L., and Manikin, G. S.: An Hourly Assimilation - Forecast Cycle: The RUC, *Mon. Wea. Rev.*, 132, 495–518, 2004a.
- Benjamin, S. G., Schwartz, B. E., Szoke, E. J., and Koch, S. E.: The value of wind profiler data in U.S. weather forecasting, *Bull. Amer. Meteor. Soc.*, 85, 1871–1886, 2004b.
- Bianco, L. and Wilczak, J. M.: Convective Boundary Layer Depth: Improved Measurement by Doppler Radar Wind Profiler Using Fuzzy Logic Methods, *J. Atmos. Oceanic Technol.*, 19, 1745–1758, 2002.
- Bianco, L., Wilczak, J. M., and White, A. B.: Convective Boundary Layer Depth Estimation from Wind Profilers: Statistical Comparison between an Automated Algorithm and Expert Estimations, *J. Atmos. Oceanic Technol.*, 25, 1397–1413, 2008.
- Bohren, C. F. and Huffman, D. R.: *Absorption and Scattering of Light by Small Particles*, John Wiley & Sons, Inc., 1983, p. 530.
- Boisse, J.-C., Klaus, V., and Aubagnac, J.-P.: A Wavelet Transform Technique for Removing Airplane Echos from ST Radar Signals, *J. Atmos. Oceanic Technol.*, 16, 334–346, 1999.
- Bond, N. A., Dierking, C. F., and Doyle, J. D.: *Research Aircraft and Wind Profiler*

- Observations in Gastineau Channel during a Taku Wind Event:, *Wea. Forecasting*, 21, 489–501, 2006.
- Bouttier, F.: The use of profiler data at ECMWF, *Meteor. Z.*, 10, 497–510, 2001.
- Browning, G., Kreiss, H.-O., and van de Kamp, D.: Comments on "Observations of a Mesoscale Ducted Gravity Wave", *J. Atmos. Sci.*, 57, 595–598, 2000.
- Browning, K.: The mesoscale data base and its use in mesoscale forecasting, *Quart. J. Roy. Meteor. Soc.*, 115, 717–762, 1989.
- Browning, K.: Observational synthesis of mesoscale structures within an explosively developing cyclone, *Quart. J. Roy. Meteor. Soc.*, 131, 603–623, 2005.
- Bruderer, B.: The Study of Bird Migration by Radar Part 1: The Technical Basis, *Naturwiss.*, 84, 1–8, 1997.
- Bryan, G. H., Wyngaard, J. C., and Fritsch, J. M.: Resolution Requirements for the Simulation of Deep Moist Convection, *Mon. Wea. Rev.*, 131, 2394–2416, 2003.
- Burrus, C. S., Gopinath, R. A., and Guo, H.: Introduction to Wavelets and Wavelet Transforms, Prentice Hall, 1998, p. 268.
- Böhme, T., Hauf, T., and Lehmann, V.: Investigation of short -period gravity waves with the Lindenberg 482 MHz tropospheric wind profiler, *Quart. J. Roy. Meteor. Soc.*, 130, 2933–2952, 2004.
- Böhme, T., Lane, T., Hall, W. D., and Hauff, T.: Gravity waves above a convective boundary layer: A comparison between wind profiler observations and numerical simulations, *Quart. J. Roy. Meteor. Soc.*, 133, 1041–1055, 2007.
- Carbone, R. E., Block, J., Boselly, S. E., Carmichael, G. R., Carr, F. H., Chandrasekar, V., Hoff, R. M., Krajewski, W. F., LeMone, M. A., Purdom, J. F., Schlatter, T. W., Takle, E. S., and Tillow, J.: *Observing Weather and Climate from the Ground Up: A Nationwide Network of Networks*, The National Academies Press, 2009.
- Cardinali, C.: Monitoring the observation impact on the short-range forecast, *Quart. J. Roy. Meteor. Soc.*, 135, 239–250, 2009.
- Carter, D., K.S.Gage, W.L.Ecklund, W.M.Angvine, P.E.Johnston, A.C.Riddle, J.Wilson, and C.R.Williams: Developments in UHF Lower Tropospheric Wind Profiling at NOAA's Aeronomy Laboratory, *Radio Sci.*, 30, 977–1001, 1995.
- Chadwick, R. B. and Gossard, E. E.: Radar Probing and Measurement of the Boundary Layer: Part I Scattering from Refractive Index Irregularities, in: *Probing the Atmospheric Bondary Layer*, edited by Lenschow, D. H., pp. 163–182, Amer. Meteor. Soc., 1984.
- Chen, M.-Y., Yu, T.-Y., Chu, Y.-H., Brown, W. O., and Cohn, S. A.: Application of

- Capon technique to mitigate bird contamination on a spaced antenna wind profiler, *Radio Sci.*, 42, doi:10.1029/2006RS003604, 2007.
- Cheong, B., Hoffman, M., Palmer, R., Frasier, S. J., and Lopez-Dekker, F.: Phased-Array Design for Biological Clutter Rejection: Simulation and Experimental Validation, *J. Atmos. Oceanic Technol.*, 23, 585–598, 2006.
- Cheong, B. L., Yu, T.-Y., Palmer, R. D., Yang, K.-F., Hoffman, M. W., Frasier, S. J., and Lopez-Dekker, F. J.: Effects of Wind Field Inhomogeneities on Doppler Beam Swinging Revealed by an Imaging Radar, *J. Atmos. Oceanic Technol.*, 25, 1414–1422, 2008.
- Chilson, P. B.: The Retrieval and Validation of Doppler Velocity Estimates from Range Imaging, *J. Atmos. Oceanic Technol.*, 21, 1033–1043, 2004.
- Chilson, P. B., Muschinski, A., and Schmidt, G.: First observations of Kelvin-Helmholtz billows in an upper-level jet stream using VHF frequency domain interferometry, *Radio Sci.*, 32, 1149–1160, 1997.
- Chilson, P. B., Yu, T.-Y., Strauch, R. G., Muschinski, A., and Palmer, R. D.: Implementation and Validation of Range Imaging on a UHF Radar Wind Profiler, *J. Atmos. Oceanic Technol.*, 20, 987–996, 2003.
- Clothiaux, E., Penc, R., Thomson, D., Ackerman, T., and Williams, S.: A First-Guess Feature-Based Algorithm for Estimating Wind Speed in Clear-Air Doppler Radar Spectra, *J. Atmos. Oceanic Technol.*, 11, 888–908, 1994.
- Cohn, S. A., Rodgers, R. R., Jascourt, S., Ecklund, W. L., Carter, D. A., and Wilson, J. S.: Interactions between clear-air reflective layers and rain observed with a boundary-layer wind profiler, *Radio Sci.*, 30, 323–341, 1995.
- Cohn, S. A., Goodrich, R. K., Morse, C. S., Karplus, E., Mueller, S. W., Cornman, L. B., and Weekly, R. A.: Radial Velocity and Wind Measurement with NIMANWCA: Comparisons with Human Estimation and Aircraft Measurements, *J. Appl. Meteor.*, 40, 704–719., 2001.
- Cornman, L. B., Goodrich, R. K., Morse, C. S., and Ecklund, W. L.: A Fuzzy Logic Method for Improved Moment Estimation from Doppler Spectra, *J. Atmos. Oceanic Technol.*, 15, 1287–1305, 1998.
- Crook, N. A. and Sun, J.: Analysis and Forecasting of the Low-Level Wind during the Sydney 2000 Forecast Demonstration Project, *Wea. Forecasting*, 19, 151–167, 2004.
- Dabberdt, W. F., Frederick, G., Hardesty, R., Lee, W.-C., and Underwood, K.: Advances in meteorological instrumentation for air quality and emergency response, *Meteor. Atmos. Phys.*, 87, 57–88, 2004.
- Daley, R.: *Atmospheric Data Analysis*, Cambridge University Press, 1991, p. 457.

- Daubechies, I., Grossmann, A., and Meyer, Y.: Painless nonorthogonal expansions, *J. Math. Phys.*, 27, 1271–1283, 1986.
- Davidson, P. A.: *Turbulence*, Oxford Univ. Press., 2004, p. 657.
- Davis, C., Atkins, N., Bartels, D., Bosart, L., Coniglio, M., Bryan, G., Cotton, W., Dowell, D., Jewett, B., Johns, R., Jorgensen, D., Knievel, J., Knupp, K., Lee, W.-C., McFarquhar, G., Moore, J., Przybylinski, R., Rauber, R., Smull, B., Trapp, R., Trier, S., Wakimoto, R., Weisman, M., and Ziegler, C.: The Bow Echo and MCV Experiment, *Bull. Amer. Meteor. Soc.*, 85, 1075–1093, 2004.
- de Lima Nascimento, E. and Droegemeier, K. K.: Dynamic Adjustment in a Numerically Simulated Mesoscale Convective System: Impact of the Velocity Field, *J. Atmos. Sci.*, 63, 2246–2268, 2006.
- De Ponca, M. S. and Zou, X.: A Case Study of the Variational Assimilation of GPS Zenith Delay Observations Into a Mesoscale Model, *J. Appl. Meteor.*, 40, 1559–1576, 2001.
- Donoho, D., Johnstone, I., Kerkycharian, G., and Picard, D.: Wavelet shrinkage: asymptopia ?, *J. Royal Stat. Soc. B*, 57(2), 301–369, 1995.
- Donoho, D. L.: De-Noising by Soft-Thresholding, *IEEE Trans. Information Theory*, 41, 613–627, 1995.
- Douglas, M. W. and Stensrud, D. J.: Upgrading the North American Upper-Air Observing Network: What Are the Possibilities ?, *Bull. Amer. Meteor. Soc.*, 77, 907–928, authors are from the NOAA Severe Storms Lab, Norman, OK, 1996.
- Doviak, R., Latatits, R., and Holloway, C.: Cross correlations and cross spectra for spaced antenna wind profilers - 1. Theoretical analysis, *Radio Sci.*, 31, 157–180, 1996.
- Doviak, R. J. and Zrnić, D. S.: Reflection and Scatter Formula for Anisotropically Turbulent Air, *Radio Sci.*, 19, 325–336, 1984.
- Doviak, R. J. and Zrnić, D. S.: *Doppler Radar and Weather Observations*, Academic Press, 1993, p. 562.
- Dow, G.: *Developments in Observational Requirements for Global Numerical Weather Prediction*, Master's thesis, University of Reading, 2004.
- Dunn, L.: An Example of Subjective Interpretation of Network Profiler Data in Real-Time Forecasting, *Wea. Forecasting*, 1, 219–225, 1986.
- Ecklund, D., Carter, D. A., and Balsley, B. B.: Continuous measurement of upper-atmospheric winds and turbulence using VHF Doppler radar: preliminary results, *J. Atmos. Solar Terr. Phys.*, 41, 983–994, 1979.

- Ecklund, W., Carter, D., Balsley, B., Currier, P., Green, J., Weber, B., and Gage, K.: Field tests of a lower tropospheric wind profiler, *Radio Sci.*, 25, 899–906, 1990.
- Ecklund, W. L., Carter, D. A., and Balsley, B. B.: A UHF Wind Profiler for the Boundary Layer: Brief Description and Initial Results, *J. Atmos. Oceanic Technol.*, 5, 432–441, 1988.
- Edwards, R., Corfidi, S. F., Thompson, R. L., Evans, J. S., Craven, J. P., Racey, J. P., and McCarthy, D. W.: Storm Prediction Center Forecasting Issues Related to the 3 May 1999 Tornado Outbreak, *Wea. Forecasting*, 17, 544–558, 2002.
- Engelbart, D., Steinhagen, H., Görsdorf, U., Lippmann, J., and Neisser, J.: A 1290 MHz Profiler with RASS for Monitoring Wind and Temperature in the Boundary Layer, *Beitr. Phys. Atmos.*, 69, 63–80, 1996.
- Engelbart, D., Görsdorf, U., and Ruhe, W.: Effects and Observation of Migrating Birds on a Boundary-Layer Windprofiler in Eastern Germany, *Meteor. Z.*, NF 7, 280–287, 1998.
- Erkelens, J. S., Venema, V. K. C., Russchenberg, H. W. J., and Ligthart, L. P.: Coherent Scattering of Microwaves by Particles: Evidence from Clouds and Smoke, *J. Atmos. Sci.*, 58, 1091–1102, 2001.
- Fabry, F. and Keeler, R. J.: Innovative Signal Utilization and Processing, *Meteor. Monographs*, 30, 199–214, 2003.
- Fabry, F. and Sun, J.: For how long should what data be assimilated for Mesoscale forecasting of convection and why ? Part I: On the propagation of initial condition errors and its implications for data assimilation, *Mon. Wea. Rev.*, accepted for publication, 2009.
- Farley, D.: On-Line Data Processing Techniques for MST Radars, *Radio Sci.*, 20, 1177–1184, 1985.
- Farley, D., Balsley, B. B., Swartz, W., and La Hoz, C.: Tropical Winds Measured by the Arecibo Radar, *J. Appl. Meteor.*, 18, 227–230, 1979.
- Ferrat, S. and Crochet, M.: Methods of Detection and Estimation Errors in ST Radar Studies, *Ann. Geophys.*, 12, 489–496, 1994.
- Feynman, R. P., Leighton, R. B., and Sands, M.: Feynman Vorlesungen über Physik, R. Oldenbourg, 1991.
- Fischler, M. A. and Bolles, R. C.: Random Sample Consensus: A Paradigm for Model Fitting with Applications to Image Analysis and Automated Cartography, *Commun. Assoc. Comput. Mach.*, 24, 381–395, 1981.
- Flandrin, P.: Time-Frequency/Time-Scale Analysis, Academic Press, 1999, p. 386.
- Fliessbach, T.: Elektrodynamik, BI Wissenschaftsverlag, 1994, p. 383.

- Foken, T.: Erfordernisse der Datengewinnung, -übertragung und -bearbeitung für mesometeorologische Zwecke, *Abh. Meteorol. Dienst DDR*, Nr. 141, 9–17, 1989.
- Franke, P., Wan, K., Fritts, D., Werne, J., and T.Lund: Computation of radar backscatter from realistic turbulence volumes. I: Radar backscatter computations and measurement biases, submitted to *J. Geophys. Res.*, 2009.
- Frehlich, R. and Yadlowsky, M.: Performance of Mean-Frequency Estimators for Doppler Radar and Lidar, *J. Atmos. Oceanic Technol.*, 11, 1217–1230, 1994.
- Fukao, S.: Recent Advances in Atmospheric Radar Study, *J. Meteor. Soc. Japan*, 85B, 215–239, 2007.
- Fukao, S., Wakasugi, K., Sato, T., Morimoto, S., Tsuda, T., Hirota, I., Kimura, I., and Kato, S.: Direct measurement of air and precipitation particle motion by very high frequency Doppler radar, *Nature*, 316, 712–714, 1985.
- Gabor, D.: Theory of communication, *J. IEE (London)*, 93, 429–457, 1946.
- Gaffard, C., Bianco, L., Klaus, V., and Matabuena, M.: Evaluation of moments calculated from wind profiler spectra: A comparison between five different processing techniques, *Meteor. Z.*, 15, 73–85, 2006.
- Gage, K. S.: Radar observations of the free atmosphere: Structure and dynamics, in: *Radar in Meteorology*, edited by Atlas, D., pp. 534–565, Amer. Meteor. Soc., Boston, 1990.
- Gage, K. S. and Gossard, E. E.: Recent Developments in Observation, Model, and Understanding Atmospheric Turbulence and Waves, in: *Radar and Atmospheric Science: A Collection of Essays in Honor of David Atlas*, edited by Wakimoto, R. M. and Srivastava, R., pp. 139–174, Am. Meteorol. Soc., 2003.
- Gage, K. S., Williams, C. R., Ecklund, W. L., and Johnston, P. E.: Use of Two Profilers During MCTEX for Unambiguous Identification of Bragg Scattering and Rayleigh Scattering, *J. Atmos. Sci.*, 56, 3679–3691, 1999.
- Gage, K. S., Williams, C. R., Clark, W. L., Johnston, P. E., and Carter, D. A.: Profiler Contributions to Tropical Rainfall Measuring Mission (TRMM) Ground Validation Field Campaigns, *J. Atmos. Oceanic Technol.*, 19, 843–863, 2002.
- Gall, R. and Shapiro, M.: The Influence of Carl-Gustav Rossby on Mesoscale Weather Prediction and an Outlook for the Future, *Bull. Amer. Meteor. Soc.*, 81, 1507–1523, 2000.
- Gallus, W. A., Correia, J., and Jankov, I.: The 4 June 1999 Derecho Event: A Particularly Difficult Challenge for Numerical Weather Prediction, *Wea. Forecasting*, 20, 705–728, 2005.

- Goodrich, R. K., Morse, C. S., Cornman, L. B., and Cohn, S. A.: A Horizontal Wind and Wind Confidence Algorithm for Doppler Wind Profilers, *J. Atmos. Oceanic Technol.*, 19, 257–273, 2002.
- Görsdorf, U. and Lehmann, V.: Enhanced Accuracy of RASS Measured Temperatures Due to an Improved Range Correction, *J. Atmos. Oceanic Technol.*, 17, 406–416, 2000.
- Gossard, E., Wolfe, D., Moran, K., Paulus, R., Anderson, K., and Rodgers, L.: Measurement of Clear-Air Gradients and Turbulence Properties with Radar Wind Profilers, *J. Atmos. Oceanic Technol.*, 15, 321–342, 1998.
- Gossard, E. E.: A Fresh Look at the Radar Reflectivity of Clouds, *Radio Sci.*, 14, 1089–1097, 1979.
- Gossard, E. E. and Strauch, R. G.: *Radar Observations of Clear Air and Clouds*, Elsevier, 1983, p. 280.
- Gossard, E. E., Chadwick, R. B., Neff, W. D., and Moran, K. P.: Use of Ground-Based Doppler Radars to Measure Gradients, Fluxes and Structure Parameters in Elevated Layers, *J. Appl. Meteor.*, 21, 211–226, 1982.
- Gossard, E. E., Gutman, S., Stankov, B. B., and Wolfe, D. E.: Profiles of Radio Refractive Index and Humidity Derived from Radar Wind Profilers and the Global Positioning System, *Radio Sci.*, 34, 371–383, 1999.
- Griesser, T.: *Multipeakanalyse von Dopplerspektren aus Windprofiler-Radar-Messungen*, Ph.D. thesis, Eidgenössische Technische Hochschule Zürich, 1998.
- Grimsdell, A. W. and Angevine, W. M.: Observations of the Afternoon Transition of the Convective Boundary Layer, *J. Appl. Meteor.*, 41, 3–11, 2002.
- Grubisic, V., Doyle, J. D., Kuettner, J., Mobbs, S., Smith, R. B., Whiteman, C. C., Dirks, R., Czyzyk, S., Cohn, S. A., Vosper, S., Weissmann, M., Haimov, S., wekker, S. F. D., Pan, L. L., and Chow, F. K.: The Terrain-Induced Rotor Experiment, *Bull. Amer. Meteor. Soc.*, pp. 1513–1533, 2008.
- Guo, Y.-R., Kuo, Y.-H., Dudhia, J., and Parsons, D.: Four-Dimensional Variational Data Assimilation of Heterogenous Mesoscale Observations for a Strong Convective Case, *Mon. Wea. Rev.*, 128, 619–643, 2000.
- Harris, F. J.: On the Use of Windows for Harmonic Analysis with the Discrete Fourier Transform, *Proc. IEEE*, 66, 51–83, 1978.
- Helal, D., Crochet, M., Luce, H., and Spano, E.: Radar imaging and high-resolution array processing applied to a classical VHF-ST profiler, *J. Atmos. Solar Terr. Phys.*, 63, 263–274, 2001.

- Helstrom, C. W.: *Statistical Theory of Signal Detection*, Pergamon Press, 1968, p. 309.
- Heo, B.-H., Jacoby-Koaly, S., Kim, K.-E., Campistron, B., Benech, B., and Jung, E.-S.: Use of Doppler Spectral Width to Improve the Estimate of the Convective Boundary Layer Height from UHF Wind Profiler Observations, *J. Atmos. Oceanic Technol.*, 20, 408–424, 2003.
- Herden, S.: *Korrektur der Höhenzuordnung der Daten eines Wind-Temperatur-Radars*, Master's thesis, Institut für Meteorologie und Klimaforschung, Univ. Karlsruhe, 1996.
- Higgins, W., Ahijevych, D., Amador, J., Barros, A., Berbery, E. H., Caetano, E., Carbone, R., Ciesielski, P., Cifelli, R., Cortez-Vasquez, M., Douglas, A., Douglas, M., Emmanuel, G., Fairall, C., Gochis, D., Gutzler, D., Jackson, T., Johnson, R., King, C., Lang, T., Lee, M.-I., Lettenmaier, D., Lobato, R., Magana, V., Meiten, J., Mo, K., Nesbitt, S., Ocampo-Torres, F., Pytlak, E., Rodgers, P., Rutledge, S., Schemm, J., Schubert, S., White, A., Williams, C., Wood, A., Zamora, R., and Zhang, C.: The NAME 2004 Field Campaign and Model Strategy, *Bull. Amer. Meteor. Soc.*, pp. 79–94, 2006.
- Hildebrand, P. H. and Sekhon, R.: Objective Determination of the Noise Level in Doppler Spectra, *J. Appl. Meteor.*, 13, 808–811, 1974.
- Hirsch, L., Klaus, V., Klein Baltink, H., Lehmann, V., and Peters, G.: Fundamentals of wind profiler operations, in: *COST Action 76 - Final report: Development of VHF/UHF Wind Profilers and Vertical Sounders for use in European Observing Systems*, EUROPEAN COMMISSION Directorate-General for Research, Rue de la Loi/Wetstraat 200 (SDME 1/53), B - 1049 Brussels, 2003.
- Hocking, W.: System Design, Signal Processing Procedures, and Preliminary Results for the Canadian (London, Ontario) VHF Atmospheric Radar, *Radio Sci.*, 32, 687–706, 1997.
- Hoffman, W.: Electromagnetic Wave Propagation in a Random Medium, *Radio Sci.*, 68D, 455–459, 1964.
- Hogg, D., Decker, M., Guiraud, F., Earnshaw, K., Merritt, D., Moran, K., Sweezy, W., Strauch, R., Westwater, E., and Little, C.: An Automatic Profiler of the Temperature, Wind and Humidity in the Troposphere, *J. Climate Appl. Meteor.*, 22, 807–831, 1983.
- Hollingsworth, A., Uppala, S., Klinker, E., Burridge, D., Vitart, F., Onville, J., de Vries, J., de Roo, A., and Pfrang, C.: The transformation of earth-system observations into information of socio-economic value in GEOSS, *Quart. J. Roy. Meteor. Soc.*, 131, 3493–3512, 2005.
- Holschneider, M.: *Wavelets: An Analysis Tool*, Oxford University Press, 1995, p. 423.

- Hooper, D. A., Nash, J., Oakley, T., and Turp, M.: Validation of a new signal processing scheme for the MST radar at Aberystwyth, *Ann. Geophys.*, 26, 3253–3268, 2008.
- Ishihara, M., Kato, Y., Abo, T., Kobayashi, K., and Izumikawa, Y.: Characteristics and Performance of the Operational Wind Profiler Network of the Japan Meteorological Agency, *J. Meteor. Soc. Japan*, 84, 1085–1096, 2006.
- Ishimaru, A.: *Wave Propagation and Scattering in Random Media*, Academic Press, 1978, p. 600.
- Jameson, A. R. and Kostinski, A. B.: Non-Rayleigh Signal Statistics in Clustered Statistically Homogeneous Rain, *J. Atmos. Oceanic Technol.*, 16, 575–583, 1999.
- Jordan, J. R., Lataitis, R. J., and Carter, D. A.: Removing Ground and Intermittent Clutter Contamination from Wind Profiler Signals Using Wavelet Transforms, *J. Atmos. Oceanic Technol.*, 14, 1280–1297, 1997.
- Justen, L. and Lehmann, V.: Radar wind profiler signal processing using redundant windowed Fourier and wavelet transforms, in: 6th International Conference on Tropospheric Profiling - Extended Abstracts, 2003.
- Kay, S. M. and Marple, S. L.: Spectrum Analysis - A Modern Perspective, *Proc. IEEE*, 69, 1380–1491, 1981.
- Keeler, R. J. and Passarelli, R. E.: Signal Processing for Atmospheric Radars, in: *Radar in Meteorology*, edited by Atlas, D., chap. 20a, pp. 199–229, Amer. Meteor. Soc., Boston, 1990.
- Keenan, T., Rutledge, S., Carbone, R., Wilson, J., Takahasi, T., May, P., Tapper, N., Platt, M., Hacker, J., Sekelsky, S., Moncrieff, M., Saito, K., Holland, G., Crook, A., and Gage, K.: The Maritime Continent Thunderstorm Experiment (MCETEX): Overview and Some Results, *Bull. Amer. Meteor. Soc.*, 81, 2433–2455, 2000.
- Kitzmiller, D. H. and McGovern, W. E.: Wind Profiler Observations Preceding Outbreaks of Large hail over Northeastern Colorado, *Wea. Forecasting*, 5, 78–88, 1990.
- Klemp, J. B.: Dynamics of tornadic thunderstorms, *Ann. Rev. Fluid Mech.*, 19, 369–402, 1987.
- Knight, C. A. and Miller, L. J.: Early Radar Echoes from Small, Warm Cumulus: Bragg and Hydrometeor Scattering, *J. Atmos. Sci.*, 55, 2974–2992, 1998.
- Koch, S. E., Feltz, W., Fabry, F., Pagowski, M., Geerts, B., Bedka, K. M., Miller, D. O., and Wilson, J. W.: Turbulent Mixing Processes in Atmospheric Bores and Solitary Waves Deduced from Profiling Systems and Numerical Simulation, *Mon. Wea. Rev.*, 136, 1373–1400, 2008.

- Kon, A. and Tatarskii, V.: The Scattered Signal Frequency Spectrum for Radioacoustical Atmospheric Soundings, *Bull. (Izv.) Acad. Sci. USSR, Atmospheric and Oceanic Physics*, 16, 142–148, 1980.
- Koscielny, A. J., Doviak, R. J., and Zrnic, D. S.: An Evaluation of the Accuracy of Some Radar Wind Profiling Techniques, *J. Atmos. Oceanic Technol.*, 1, 309–320, 1984.
- Kostinski, A. B. and Jameson, A. R.: On the Spatial Distributions of Cloud Particles, *J. Atmos. Sci.*, 57, 901–915, 2000.
- Kretzschmar, R., Karayiannis, N. B., and Richner, H.: Removal of bird-contaminated wind profiler data based on neural networks, *Pattern Recognit.*, 36, 2699–2712, 2003.
- Kropfli, R. A.: Radar Probing and Measurement of the Planetary Boundary Layer, in: *Probing the Atmospheric Boundary Layer*, edited by Lenschow, D. H., pp. 183–199, Amer. Meteor. Soc., 1984.
- Kudeki, E. and Stitt, G.: Frequency domain interferometry: A high resolution technique for studies of atmospheric turbulence, *Geophys. Res. Lett.*, 14, 198–201, 1987.
- Landau, L. and Lifschitz, E.: *Elektrodynamik der Kontinua*, Akademie-Verlag, 1985, p. 565.
- Larsen, M. and Röttger, J.: VHF and UHF Doppler Radars as Tools for Synoptic Research, *Bull. Amer. Meteor. Soc.*, 63, 996–1008, 1982.
- Lataitis, R., Clifford, S., and Holloway, C.: An alternative method of inferring winds from spaced-antenna radar measurements, *Radio Sci.*, 30, 463–474, 1995.
- Lataitis, R. J.: Theory of a radio-acoustic sounding system (RASS), Tech. Rep. NOAA Technical Memorandum ERL WPL-230, NOAA, 1993.
- Laughlin, R. B. and Pines, D.: The Theory of Everything, *PNAS*, 97, 28–31, 2000.
- Law, D., Khorrami, J., Sessions, W., and Shanahan, M.: Radiation Patterns of a Large UHF Phased-Array Antenna: A Comparison of Measurements Using Satellite Repeaters and Patterns Derived from Measurements of Antenna Current Distributions, *IEEE Ant. Propagation Mag.*, 39, 88–93, 1997.
- Law, D., McLaughlin, S., Post, M., Weber, B., Welsh, D., Wolfe, D., and Merritt, D.: An Electronically Stabilized Phased Array System for Shipborn Atmospheric Wind Profiling, *J. Atmos. Oceanic Technol.*, 19, 924–933, 2002.
- Law, D. C., Steinhagen, H., and Lehmann, V.: Improved Wind Profiler Antenna Radiation Pattern Measurements, in: *6th International Conference on Tropospheric Profiling - Extended Abstracts*, 2003.

- Lee, M. C., Dalkir, Y. R., and Williams, E. R.: Radar reflectivity of lightning-induced plasmas, *J. Atmos. Solar Terr. Phys.*, 60, 941–949, 1998.
- Lehmann, V.: Optimal Gabor Frame Expansion based Intermittent Clutter Filtering Method for Radar Wind Profiler, submitted to *J. Atmos. Oceanic Technol.*, pp. 1–22, 2009.
- Lehmann, V. and Teschke, G.: Wavelet Based Methods for Improved Wind Profiler Signal Processing, *Ann. Geophys.*, 19, 825–836, 2001.
- Lehmann, V. and Teschke, G.: Advanced Intermittent Clutter Filtering for Radar Wind Profiler: Signal Separation through a Gabor Frame Expansion and its Statistics, *Ann. Geophys.*, 26, 759–783, 2008a.
- Lehmann, V. and Teschke, G.: Radar wind profiler signal characteristics during bird migration episodes, in: *TECO-2008 -WMO Technical Conference on Meteorological and Environmental Instruments and Methods of Observation*, 2008b.
- Lehmann, V., Dibbern, J., Görsdorf, U., Neuschaefer, J. W., and Steinhagen, H.: The new operational UHF Wind Profiler Radars of the Deutscher Wetterdienst, in: *6th International Conference on Tropospheric Profiling - Extended Abstracts*, 2003.
- Lehtinen, R., Lilja, A., and Shellhorn, R.: New wind profiling algorithms from Vaisala, in: *Proceedings of the 8th International Symposium on Tropospheric Profiling*, ISBN 978-90-6960-233-2, 2009.
- Lilly, D. K.: Numerical prediction of thunderstorms - has its time come ?, *Quart. J. Roy. Meteor. Soc.*, 116, 779–798, 1990.
- Lottman, B. and Frehlich, R.: Evaluation of Doppler radar velocity estimators, *Radio Sci.*, 32, 677–686, 1997.
- Luce, H., Yamamoto, M., Fukao, S., Helal, D., and Crochet, M.: A frequency domain radar interferometric imaging (FII) technique based on high resolution methods, *J. Atmos. Solar. Terr. Phys.*, 63, 201–214, 2001.
- Lynch, P.: The origins of computer weather prediction and climate modeling, *J. Comput. Phys.*, 227, 3431–3444, 2008.
- Mailloux, R. J.: *Phased Array Antenna Handbook*, Artech House, 1994, p. 536.
- Mallat, S.: *A Wavelet Tour of Signal Processing*, Academic Press, 1999, p. 637.
- Mallat, S.: *A Wavelet Tour of Signal Processing - the Sparse Way*, Academic Press, 2009, p. 805.
- Markowski, P., Hannon, C., Frame, J., Lancaster, E., Pietrycha, A., Edwards, R., and Thompson, R. L.: Characteristics of Vertical Wind Profiles near Supercells Obtained from the Rapid Update Cycle:, *Wea. Forecasting*, 18, 1262–1272, 2003.

- Martner, B. E., Wurtz, D. B., Stankov, B. B., Strauch, R. G., Westwater, K., Gage, K. S., Ecklund, W. L., Martin, C. L., and Dabberdt, W. F.: An evaluation of wind profiler, RASS, and microwave radiometer performance, *Bull. Amer. Meteor. Soc.*, 74, 599–613, 1993.
- May, P. T. and Strauch, R. G.: An Examination of Wind Profiler Signal Processing Algorithms, *J. Atmos. Oceanic Technol.*, 6, 731–735, 1989.
- May, P. T. and Strauch, R. G.: Reducing the Effect of Ground Clutter on Wind Profiler Velocity Measurements, *J. Atmos. Oceanic Technol.*, 15, 579–586, 1998.
- McDonald, A. J., Carey-Smith, T. K., Hooper, D. A., Fraser, G. J., and Lublow, B. P.: The effect of precipitation on wind-profiler clear air returns, *Ann. Geophys.*, 22, 3959–3970, 2004.
- McDonough, R. N. and Whalen, A. D.: *Detection of Signals in Noise*, Academic Press, 1995, p. 495.
- Mead, J. B., Hopcraft, G., Frasier, S. J., Pollard, B. D., Cherry, C. D., Schaubert, D. H., and McIntosh, R. E.: A Volume-Imaging Radar Wind Profiler for Atmospheric Boundary Layer Turbulence Studies, *J. Atmos. Oceanic Technol.*, 15, 849–859, 1998.
- Merritt, D. A.: A Statistical Averaging Method for Wind Profiler Doppler Spectra, *J. Atmos. Oceanic Technol.*, 12, 985–995, 1995.
- Miller, K. S.: Complex Gaussian Processes, *SIAM Rev.*, 11, 544–567, 1969.
- Mishchenko, M. I., Travis, L. D., and Lacis, A. A.: *Scattering, Absorption and Emission of Light by Small Particles*, Cambridge University Press, 2002, p. 448.
- Monin, A. and Yaglom, A.: *Statistical Fluid Mechanics, Vol. II*, Dover Publications, 2007, p. 874.
- Monna, W. A. and Chadwick, R. B.: Remote-Sensing of Upper-Air Winds for Weather Forecasting: Wind-Profiler Radar, *B. World Meteorol. Organ.*, 47, 124–132, 1998.
- Morse, C. S., Goodrich, R. K., and Cornman, L. B.: The NIMA Method for Improved Moment Estimation from Doppler Spectra, *J. Atmos. Oceanic Technol.*, 19, 274–295, 2002.
- Muschinski, A.: Local and Global Statistics of Clear-Air Doppler Radar Signals, *Radio Sci.*, 39, doi:10.1029/2003RS002 908, 2004.
- Muschinski, A. and Lenschow, D. H.: Future Directions for Research on Meter- and Submeter-Scale Atmospheric Turbulence, *Bull. Amer. Meteor. Soc.*, 82, 2831–2843, 2001.
- Muschinski, A., Sullivan, P. P., Wuertz, D. B., Hill, R. J., Cohn, S. A., Lenschow,

- D. H., and Doviak, R. J.: First Synthesis of Wind-Profiler Signals on the Basis of Large-Eddy Simulation Data, *Radio Sci.*, 34, 1437–1459, 1999.
- Muschinski, A., Lehmann, V., Justen, L., and Teschke, G.: Advanced Radar Wind Profiling, *Meteor. Z.*, 14, 609–626, 2005.
- Nash, J. and Oakley, T. J.: Development of COST-76 Wind Profiler Network in Europe, *Phys. Chem. Earth (B)*, 26, 193–199, 2001.
- Neeser, F. D. and Massey, J. L.: Proper Complex Random Processes with Applications to Information Theory, *IEEE T. Inform. Theory*, 39, 1293–1302, 1993.
- Nehrkorn, T.: Analysis and Quality Control of Profiler Data Using Optimal Interpolation, *J. Atmos. Oceanic Technol.*, 17, 651–655, 2000.
- Newman, A. J., Kucera, P. A., Williams, C. R., and Bliven, L. F.: Snowflake Sice Spectra Retrieved From a UHF Vertical Profiler, *J. Atmos. Oceanic Technol.*, (submitted), 56 pp, 2009.
- Nielsen-Gammon, J. W., McNider, R. T., Angevine, W. M., White, A. B., and Knupp, K.: Mesoscale model performance with assimilation of wind profiler data: Sensitivity to assimilation parameters and network configuration, *J. Geophys. Res.*, 112, doi:10.1029/2006JD007 633, 2007.
- Oguchi, T.: Electromagnetic Wave Propagation and Scattering in Rain and Other Hydrometeors, *Proc. IEEE*, 71, 1029–1078, 1983.
- Ogura, H. and Yoshida, Y.: Spectral Analysis and Subtraction of Noise in Radar Signals, *IEEE Trans. Aerospace Electron. Sys.*, AES-17, 62–71, 1981.
- Orr, B. W. and Martner, B. E.: Detection of Weakly Precipitating Winter Clouds by a NOAA 404 MHz Wind Profiler, *J. Atmos. Oceanic Technol.*, 13, 570–580, 1996.
- Ottersten, H.: Atmospheric structure and radar backscattering in clear air, *Radio Sci.*, 4, 1179–1193, 1969a.
- Ottersten, H.: Radar backscattering from the turbulent clear atmosphere, *Radio Sci.*, 4, 1251–1255, 1969b.
- Owens, J. C.: Optical Refractive Index of Air: Dependence on Pressure, Temperature and Composition, *Appl. Optics*, 6, 51–59, 1967.
- Palmer, R. D., Yu, T.-Y., and Chilson, P. B.: Range imaging using frequency diversity, *Radio Sci.*, 34, 1485–1496, 1999.
- Papoulis, A.: *Probability, Random Variables and Stochastic Processes*, McGraw-Hill, 3 edn., 1991, p. 666.
- Park, S. and Zupanski, D.: Four-dimensional variational data assimilation for mesoscale and storm-scale applications, *Meteor. Atmos. Phys.*, 82, 173–208, 2003.

- Percival, D. B. and Walden, A. T.: Spectral Analysis for Physical Applications, Cambridge University Press, 1993, p. 583.
- Peters, G., Timmermann, H., and Hinzpeter, H.: Temperature sounding in the Planetary Boundary Layer by RASS-system, *Int. J. Remote Sens.*, 4, 49–63, 1993.
- Petitdidier, M. and Laroche, P.: Lightning observations with the Strato-Tropospheric UHF and VHF radars at Arecibo, Puerto Rico, *Atmos. Res.*, 76, 481–492, 2005.
- Pollard, B. D., Khanna, S., Frasier, S. J., Wyngaard, J. C., and Thomson, D. W.: Local Structure of the Convective Boundary Layer from a Volume-Imaging Radar, *J. Atmos. Sci.*, 57, 2281–2296, 2000.
- Poulos, G. S., Blumen, W., Fritts, D. C., Lundquist, J. K., Sun, J., Burns, S. P., Nappo, C., Banta, R., Newsom, R., Cuxart, J., Terradellas, E., Balsley, B., and Jensen, M.: CASES-99: A Comprehensive Investigation of the Stable Nocturnal Boundary Layer, *Bull. Amer. Meteor. Soc.*, pp. 555–581, 2002.
- Priestley, M.: Spectral Analysis and Time Series, Academic Press, 1981, p. 890.
- Rabier, F., Gauthier, P., Cardinali, C., Langland, R., Tsyrunikov, M., Lorenc, A., Steinle, P., Gelaro, R., and Koizumi, K.: An update on THORPEX-related research in data assimilation and observing strategies, *Nonlin. Processes Geophys.*, 15, 81–94, 2008.
- Rajopadhyaya, D. K., Avery, S. K., May, P. T., and Cifelli, R. C.: Comparison of Precipitation Estimation Using Single- and Dual-Frequency Wind Profilers: Simulations and Experimental Results, *J. Atmos. Oceanic Technol.*, 16, 165–173, 1999.
- Ralph, F., Crochet, M., and Venkateswaran, S.: A Study of Mountain Lee Waves Using Clear-Air Radar, *Quart. J. Roy. Meteor. Soc.*, 118, 597–627, 1992.
- Ralph, F. M.: Reply, *J. Atmos. Sci.*, 57, 599–608, 2000.
- Ralph, F. M., Neiman, P. J., van de Kamp, D. W., and Law, D. C.: Using Spectral Moment Data from NOAA's 404-MHz Radar Wind Profilers to Observe Precipitation, *Bull. Amer. Meteor. Soc.*, 76, 1717–1739, 1995.
- Ralph, F. M., Neiman, P. J., and Ruffieux, D.: Precipitation Identification from Radar Wind Profiler Spectral Data. Vertical Velocity Histograms, Velocity Variance, and Signal Power - Vertical Velocity Correlations, *J. Atmos. Oceanic Technol.*, 13, 545–559, 1996.
- Randall, R.: Frequency Analysis, Brüel & Kjaer, 1987, p. 344.
- Richner, H. and Kretzschmar, R.: Bird Identification on 1290-MHz Wind Profiler Data Applying Neural Networks and Neurofuzzy Systems, *Phys. Chem. Earth (B)*, 26, 181–185, 2001.

- Riddle, A. and Angevine, W.: Ground clutter removal from profiler spectra, in: Proceedings of the Fifth Workshop on Technical and Scientific Aspects of MST Radar, edited by Edwards, B., pp. 418–420, Scientific Committee on Solar Terrestrial Physics (SCOSTEP), SCOSTEP Secretariat, University of Illinois, 1406 W. Green Street, Urbana, IL 61801, USA, 1991.
- Roberts, N.: Meteorological components in forecasts of extreme convective rainfall using 12-km and 1-km NWP models: A tale of two storms, Tech. Rep. 520, UK MetOffice, 2007.
- Roebber, P. J., Schultz, D. M., Colle, B. A., and Stensrud, D. J.: Toward Improved Prediction: High-Resolution and Ensemble Model Systems in Operations, *Wea. Forecasting*, 19, 936–949, 2004.
- Röttger, J. and Larsen, M.: UHF/VHF Radar Techniques for Atmospheric Research and Wind Profiler Applications, in: *Radar in Meteorology*, chap. 21a, pp. 235–281, Amer. Meteor. Soc., 1990.
- Rust, W. D. and Doviak, R. J.: Radar research on thunderstorms and lightning, *Nature*, 297, 461–468, 1982.
- Röttger, J.: ST radar observations of atmospheric waves over mountainous areas: a review, *Ann. Geophys.*, 18, 750–765, 2000.
- Röttger, J., Liu, C. H., Pan, C. J., and Su, S. Y.: Characteristics of lightning echoes observed with VHF ST radar, *Radio Sci.*, 30, 1085–1097, 1995.
- Saito, K., Ichi Ishida, J., Aranami, K., Hara, T., Segawa, T., Narita, M., and Honda, Y.: Nonhydrostatic Atmospheric Models and Operational Development at JMA, *J. Meteor. Soc. Japan*, 85B, 271–304, 2007.
- Salby, M. L.: *Fundamentals of Atmospheric Physics*, International Geophysics Series, Academic Press, 1996, p. 624.
- Sato, T. and Woodman, R. F.: Spectral Parameter Estimation of CAT Radar Echoes in the Presence of Fading Clutter, *Radio Sci.*, 17, 817–826, 1982.
- Satoh, M., Matsuno, T., Tomita, H., Miura, H., Nasuno, T., and Iga, S.: Nonhydrostatic icosahedral atmospheric model (NICAM) for global cloud resolving simulations, *J. Comput. Phys.*, 227, 3486–3514, 2008.
- Schlatter, T. W. and (Editors), F. S. Z.: *Wind Profiler Assessment Report*, Tech. rep., NOAA, U.S. Dept. of Commerce, Silver Spring, MD, available from NOAA Forecast Systems Laboratory, 325 Broadway, Boulder, CO, 80303, 1994.
- Schmidli, J., Poulos, G. S., Daniels, M. H., and Chow, F. K.: External Influences on Nocturnal Thermally Driven Flows in a Deep Valley, *J. Appl. Meteor. Climatol.*, 48, 3–23, 2009.

- Schmidt, G., Ruster, R., and Czechowsky, P.: Complementary Code and Digital Filtering for Detection of Weak VHF Radar Signals from the Mesosphere, *IEEE Trans. Geosci. Electron.*, GE-17, 154–161, 1979.
- Schumann, R. S., Taylor, G. E., Merceret, F. J., and Wilfong, T. L.: Performance Characteristics of the Kennedy Space Center 50 MHz Doppler Radar Wind Profiler Using the Median Filter /First-Guess Data Reduction Algorithm, *J. Atmos. Oceanic Technol.*, 16, 532–549, 1999.
- Scipion, D., Palmer, R., Chilson, P., Fedorovich, E., and Botnick, A.: Retrieval of convective boundary layer wind field statistics from radar profiler measurements in conjunction with large eddy simulation, *Meteor. Z.*, 18, 175–187, 2009a.
- Scipion, D., Palmer, R., Chilson, P., Fedorovich, E., Doviak, R., Zhang, G., and Botnick, A.: Effects of horizontal shear of vertical velocity in DBS and SA mean wind estimates revealed by a combination of LES and virtual radar, in: 89th Annual Meeting of the AMS, Phoenix, AZ, Jan 11-15, 2009b.
- Scipion, D. E., Chilson, P. B., Fedorovich, E., and Palmer, R. D.: Evaluation of an LES-Based Wind Profiler Simulator for Observations of a Daytime Atmospheric Convective Boundary Layer, *J. Atmos. Oceanic Technol.*, 25, 1423–1436, 2008.
- Selesnick, I. W., Baraniuk, R. G., and Kingsbury, N. G.: The Dual-Tree Complex Wavelet Transform, *IEEE Signal Process. Mag.*, pp. 123–151, 2005.
- Semple, A.: Forecast Error Investigation 12th October 2003: Assimilation of Contaminated Wind Profiler Data into the Global Model (Forecasting Research Technical Report No. 465), Tech. rep., UK Met Office, 2005.
- Shellhorn, R. and Keskinen, M.: New advances in wind profiling from Vaisala, *Vaisala News* 179, 2009.
- Skamarock, W. C.: Evaluating Mesoscale NWP Model Using Kinetic Energy Spectra, *Mon. Wea. Rev.*, 132, 3019–3032, 2004.
- Skolnik, M. I.: *Introduction to Radar Systems*, McGraw-Hill, 2001, p. 772.
- Smaïni, L., Luce, H., Crochet, M., and Fukao, S.: An Improved High-resolution Processing Method for a Frequency Domain Interferometric Imaging (FII) Technique, *J. Atmos. Oceanic Technol.*, 19, 954–966, 2002.
- Smalikho, I.: Techniques of Wind Vector Estimation from Data Measured with a Scanning Coherent Doppler Lidar, *J. Atmos. Oceanic Technol.*, 20, 276–291, 2003.
- St-James, J. S. and Laroche, S.: Assimilation of Wind Profiler data in the Canadian Meteorological Centre’s Analysis System, *J. Atmos. Oceanic Technol.*, 22, 1181–1194, 2005.

- Stankov, B. B., Gossard, E. E., Weber, B. L., Lataitis, R. J., White, A. B., Wolfe, D. E., Welsh, D. C., and Strauch, R. G.: Humidity Gradient Profiles from Wind Profiling Radars Using the NOAA/ETL Advanced Signal Processing System (SPS), *J. Atmos. Oceanic Technol.*, 20, 3–22, 2003.
- Steiner, A. and Richner, H.: Separation of clear-air echoes from precipitation echoes in UHF wind profiler measurements, *Ann. Geophys.*, 12, 497–505, 1994.
- Steinhagen, H., Dibbern, J., Engelbart, D., Görsdorf, U., Lehmann, V., Neisser, J., and Neuschaefer, J. W.: Performance of the First European 482 MHz Wind Profiler Radar with RASS under Operational Conditions, *Meteor. Z.*, N.F.7, 248–261, 1998.
- Stephens, G. L.: *Remote Sensing of the Lower Atmosphere*, Oxford University Press, 1994, p. 523.
- Stewart, L., Dance, S., and Nichols, N.: Correlated observation errors in data assimilation, *Int. J. Num. Meth. Fluid*, 56, doi: 10.1002/flid.1636, 1521–1527, 2008.
- Strauch, R. G., Merritt, D. A., Moran, K. P., Earnshaw, K. B., and van de Kamp, D.: The Colorado wind profiling network, *J. Atmos. Oceanic Technol.*, 1, 37–49, 1984.
- Sun, J.: Convective-scale assimilation of radar data: Progress and challenges, *Quart. J. Roy. Meteor. Soc.*, 131, 3493–3463, 2005.
- Talagrand, O.: Assimilation of Observations, an Introduction, *J. Meteor. Soc. Japan*, 75, 191–209, 1997.
- Tanaka, H., Hiyama, T., Yamamoto, K., Fujinami, H., Shinoda, T., Higuchi, A., Endo, S., Ikeda, S., Li, W., and Nakamura, K.: Surface flux and atmospheric boundary layer observations from the LAPS project over the middle stream of the Huaihe River basin in China, *Hydrol. Processes*, 21, 1997–2008, 2007.
- Tatarskii, V.: *The Effects of the Turbulent Atmosphere on Wave Propagation*, Israel Program for Scientific Translations, 1971, p. 471.
- Tatarskii, V. I.: *Wave propagation in a turbulent medium*, McGraw-Hill, 1961, p. 285.
- Tatarskii, V. I.: Theory of Single Scattering by Random Distributed Scatterers, *IEEE Trans. Antennas Propagation*, 51, 2806–2813, 2003.
- Tatarskii, V. I. and Muschinski, A.: The Difference Between Doppler Velocity and Real Wind Velocity in Single Scattering from Refractive Index Fluctuations, *Radio Sci.*, 36, 1405–1423, 2001.
- Thomson, D. J.: Spectrum Estimation and Harmonic Analysis, *Proc. IEEE*, 70, 1055–1096, 1982.
- Thunis, P. and Bornstein, R.: Hierarchy of Mesoscale Flow Assumptions and Equations, *J. Atmos. Sci.*, 53, 380–397, 1996.

- Tsuda, T.: Middle Atmosphere Program - Handbook for MAP, vol. 30, chap. Data Acquisition and Processing, pp. 151–183, ICSU Scientific Committee on Solar-Terrestrial Physics (SCOSTEP), ISAR 24.-28. November 1988, Kyoto, 1989.
- Tsui, J. B.-y.: Digital Microwave Receivers: Theory and Concepts, Artech House, 1989, p. 389.
- van de Kamp, D.: A new algorithm to identify errors caused by migrating birds in profiler winds, Tech. Rep. SR/SSD 96-36, NOAA Forecasting Systems Laboratory, 1996.
- VanZandt, T. E., Clark, W. L., Gage, K. S., Williams, C. R., and Ecklund, W. L.: A dual-wavelength radar technique for measuring the turbulent energy dissipation rate  $\epsilon$ , *Geophys. Res. Lett.*, 27, 2537–2540, 2000.
- Vaughan, G. and Worthington, R. M.: Inertia-gravity waves observed by the UK MST radar, *Quart. J. Roy. Meteor. Soc.*, 133, 179–188, 2007.
- Vaughn, C. R.: Birds and Insects as Radar Targets: A Review, *P. IEEE*, 73, 205–227, 1985.
- Vogt, S. and Sacher, D.: A Neural Network Method for Wind Estimation Using Wind Profiler Data, *Meteor. Z.*, 10, 479–487, 2001.
- Wagner, T. J., Feltz, W. F., and Ackerman, S. A.: The Temporal Evolution of Convective Indices in Storm-Producing Environments, *Wea. Forecasting*, 23, 786–794, 2008.
- Weber, B., Wuertz, D., Law, D., Frisch, A., and Brown, J.: Effects of Small-Scale Vertical Motion on Radar Measurements of Wind and Temperature Profiles, *J. Atmos. Oceanic Technol.*, 9, 193–209, 1992.
- Weber, B., Welsh, D., Merritt, D., Wuertz, D., Wolfe, D., and Wilfong, T.: A new paradigm for Doppler radar wind profiler signal processing, Tech. Rep. OAR ETL-306, NOAA - Environmental Technology Laboratory, 2004.
- Weber, B. L. and Wuertz, D. C.: Quality control algorithm for profiler measurements of winds and temperatures, Tech. Rep. NOAA Technical Memorandum ERL WPL-212, U.S. Department of Commerce, National Oceanic and Atmospheric Administration, Boulder, CO., USA, 1991.
- Weber, B. L., Wuertz, D. B., Strauch, R. G., Merritt, D. A., Moran, K. P., Law, D. C., van de Kamp, D., Chadwick, R., Ackley, M., Barth, M., Abshire, N. L., Miller, P. A., and Schlatter, T. W.: Preliminary Evolution of the First NOAA Demonstration Network Wind Profiler, *J. Atmos. Oceanic Technol.*, 7, 909–918, 1990.
- Weckwerth, T. M., Parsons, D. B., Koch, S. E., Moore, J. A., LeMone, M. A., Demoz, B. B., Flamant, C., Geerts, B., Wang, J., and Feltz, W. F.: An Overview of the

- International  $H_2O$  Project (IHOP 2002) and some Preliminary Highlights, *Bull. Amer. Meteor. Soc.*, 85, 253–277, 2004.
- Weisman, M. L. and Klemp, J. B.: The Dependence of Numerically Simulated Convective Storms on Vertical Wind Shear and Buoyancy, *Mon. Wea. Rev.*, 110, 504–520, 1982.
- Weisman, M. L., Davies, C., Wang, W., Manning, K. W., and Klemp, J. B.: Experiences with 0-36-h Explicit Convective Forecasts with the WRF-ARW Model, *Wea. Forecasting*, 23, 407–437, 2008.
- Welch, P. D.: The Use of Fast Fourier Transform for the Estimation of Power Spectra: A Method Based on Time Averaging Over Short, Modified Periodograms, *IEEE Trans. Audio Electroacoustics*, AU-15, 70–73, 1967.
- Wexler, J. and Raz, S.: Discrete Gabor Expansions, *Signal Process.*, 21, 207–220, 1990.
- Wheelon, A. D.: Backscattering by Turbulent Irregularities: A New Analytical Description, *Proc. IEEE*, 60, 252–265, 1972.
- White, A. B., Jordan, J. R., Martner, B. E., Ralph, F. M., and Bartram, B. W.: Extending the Dynamic Range of an S-Band Radar for Cloud and Precipitation Studies, *J. Atmos. Oceanic Technol.*, 17, 1226–1234, 2000.
- Whiteman, C. D. and Bian, X.: Solar Semidiurnal Tides in the Troposphere: Detection by Radar Profilers, *Bull. Amer. Meteor. Soc.*, 77, 529–542, 1996.
- Whiteman, C. D., Muschinski, A., Zhong, S., Fritts, D., Hoch, S. W., Hahnenberger, M., Yao, W., Hohreiter, V., Behn, M., Cheon, Y., Clements, C. B., Horst, T. W., Brown, W. O., and Oncley, S. P.: METCRAX 2006 Meteorological Experiments in Arizona’s Meteor Crater, *Bull. Amer. Meteor. Soc.*, 89, 1665–1680, 2008.
- Wilczak, J., Strauch, R., Ralph, F., Weber, B., Merritt, D., Jordan, J., Wolfe, D., Lewis, L., Wuertz, D., Gaynor, J., McLaughlin, S., Rogers, R., Riddle, A., and Dye, T.: Contamination of Wind Profiler Data by Migrating Birds: Characteristics of Corrupted Data and Potential Solutions, *J. Atmos. Oceanic Technol.*, 12, 449–467, 1995.
- Wilczak, J., Gossard, E., Neff, W., and Eberhard, W.: Ground-Based Remote Sensing of the Atmospheric Boundary Layer: 25 Years of Progress, *Bound.-Layer Meteor.*, 78, 321–349, 1996.
- Wilfong, T. L., Merritt, D. A., Lataitis, R. J., Weber, B. L., Wuertz, D. B., and Strauch, R. G.: Optimal Generation of Radar Wind Profiler Spectra, *J. Atmos. Oceanic Technol.*, 16, 723–733, 1999.
- Williams, C. R., Ecklund, W. L., Johnston, P. E., and Gage, K. S.: Cluster Analysis

- Techniques to Separate Air Motion and Hydrometeors in Vertical Incident Profiler Observations, *J. Atmos. Oceanic Technol.*, 17, 949–962, 2000.
- Williams, C. R., White, A. B., Gage, K. S., and Ralph, F. M.: Vertical Structure of Precipitation and Related Microphysics Observed by NOAA Profilers and TRMM during NAME 2004, *J. Climate*, 20, 1693–1712, 2007.
- Williams, E. R., Geotis, S. G., and Bhattacharya, A. B.: A Radar Study of the Plasma and Geometry of Lightning, *J. Atmos. Sci.*, 46, 1173–1185, 1989.
- Wolfe, D., Weber, B., Wuertz, D., Welsh, D., Merritt, D., King, S., Fritz, R., Moran, K., Simon, M., Simon, A., Cogan, J., Littell, D., and Measure, E.: An Overview of the Mobile Profiler System: Preliminary Results from Field Tests during the Los Angeles Free-Radical Study, *Bull. Amer. Meteor. Soc.*, 76, 523–534, 1995.
- Woodman, R. F.: Spectral moment estimation in MST radars, *Radio Sci.*, 20, 1185–1195, 1985.
- Woodman, R. F.: A General Statistical Instrument Theory of Atmospheric and Ionospheric Radars, *J. Geophys. Res.*, 96, 7911–7928, 1991.
- Woodman, R. F. and Guillen, A.: Radar Observation of Winds and Turbulence in the Stratosphere and Mesosphere, *J. Atmos. Sci.*, 31, 493–505, 1974.
- Wuertz, D. B. and Weber, B. L.: Editing Wind Profiler Measurements, Tech. Rep. ERL 438-WPL 62, NOAA Wave Propagation Laboratory, 1989.
- Wuertz, D. B., Weber, B. L., Strauch, R. G., Frisch, A. S., Little, C. G., Merritt, D. A., Moran, K. P., and Welsh, D. C.: Effects of Precipitation on UHF Wind Profiler Measurements, *J. Atmos. Oceanic Technol.*, 5, 450–465, 1988.
- Wyngaard, J. C.: Measurement Physics, in: *Probing the Atmospheric Boundary Layer*, edited by Lenschow, D. H., pp. 5–18, Amer. Meteor. Soc., 1984.
- Zrnić, D. S.: Simulation of Weatherlike Doppler Spectra and Signals, *J. Appl. Meteor.*, 14, 619–620, 1975.
- Zrnić, D. S.: Estimation of Spectral Moments for Weather Echoes, *IEEE T. Geosci. Elect.*, GE-17, 113–128, 1979.
- Zrnić, D. S.: Signal Processing: Panel Report, in: *Radar in Meteorology*, edited by Atlas, D., chap. 20b, pp. 230–234, American Meteorol. Soc., 1990.
- Zrnić, D. S. and Doviak, R. J.: Matched Filter Criteria and Range Weighting for Weather Radar, *IEEE Transactions on Aerospace and Electronic Systems*, AES-14, 925–929, 1978.

## **Individual contribution to joint publications**

### **Appendix A - Lehmann and Teschke (2001)**

I have been the responsible scientist for all wind profiler radars at DWD since 1996, in particular for the 482 MHz RWP system at the Meteorologisches Observatorium Lindenberg used in this study. The configuration of the radar operating parameters as well as the preliminary analysis required for the identification of representative clutter cases was my first contribution to this paper. Furthermore, I had gained the idea of attempting a signal component separation through a wavelet analysis from several personal discussions with the main author of the paper Jordan et al. (1997). This led to the initiation of a meanwhile long-standing and fruitful co-operation with my co-author Prof. Gerd Teschke (now Director of the Institute for Computational Mathematics in Science and Technology at the University of Applied Sciences Neubrandenburg). The intention was to put the ideas of Jordan et al. (1997) on a more solid mathematical ground and to test this method with our own data. During this co-operation, I developed the software for converting the proprietary binary data format to an easy to import ASCII format. During the drafting of the paper, I tried to help adapting the mathematical theory of wavelet based multiresolution and wavelet shrinkage to the clutter problem at hand, based on my experience with the data. In particular, I suggested the idea for applying the wavelet thresholding based in the rather unconventional opposite way and suggested the testing of the method using the signal simulation by Zrnić (1975). My contributions as the lead author of this paper can be quantified as 100 % for Sections 1, 2 and 5 and about 25 % for Sections 3 and 4.

### **Appendix B - Muschinski et al. (2005)**

The paper was initiated by the lead author Prof. Andreas Muschinski (now at the University of Massachusetts at Amherst) with the intention of providing a tutorial overview of radar wind profiling, with an emphasis on physical and mathematical concepts. Most of the data used were obtained again with the Lindenberg 482 MHz RWP system. During paper drafting, my main contribution was to act as the main author for the signal processing section. In particular, I decided to put the main emphasis on intermittent clutter filtering, for this problem is both pertinent and relevant for single-signal and multi-signal radar wind profiling. The main new idea was to report about the emerging possibilities of joint time-frequency analysis methods, based on rather promising results published in Justen and Lehmann (2003). Based on my hardware knowledge of the RWP, I tried to establish the essential signal characteristics of the clutter components and we presented first ideas how to separate atmospheric returns from clutter. My contributions might be roughly quantified as 70 % for Sections 1, 2 and 5 and about 30 % for Sections 3 and 4.

## **Appendix C - Lehmann and Teschke (2008a)**

This paper was based on a continued co-operation with my co-author Prof. Dr. Gerd Teschke. In the meantime, DWD had installed three additional 482 MHz RWP systems at Ziegenderf (2003), Nordholz (2004) and Bayreuth (2005). Among the most useful capabilities of the new systems (Lehmann et al., 2003) was their ability to store complete time series of the demodulated receiver signals. This greatly helped expanding the available data base. While the main computational algorithm for the Gabor transform was derived by Gerd based on Wexler and Raz (1990), I implemented the method in an integrated software package (IDL). This allowed reading, processing and writing back of the data to the original format. The latter feature was essential for an easy integration of the new method into the usual (off-line) processing chain of the RWP, which allowed its evaluation for a multitude of long data sets. Furthermore, I can take credit in the suggestion of using the statistical method of Merritt (1995) for signal separation. The performance of this method was first surprising, but quite suddenly exciting to observe. Most satisfying, however, is the fact that the leading manufacturer of wind profiler radars has meanwhile implemented this method in its operational RWP software (Lehtinen et al., 2009). My contributions to the paper are estimated to be 100 % for Sections 1, 2, 5 and 6, about 70 % for Sections 3 and 4 and roughly 10 % for the Appendices A, B and C.

## **Appendix D - Lehmann (2009)**

This paper deals with the question of how to optimally set-up the DGT for getting the best results of the filtering approach. This is achieved by first selecting the discretization lattice constants in such a way, that the frame is nearly tight. This condition is also known as an orthogonal-like DGT. As a second condition, the analyzing bandwidth of the Gaussian window should be selected to provide a sparse representation of both the atmospheric and the clutter signal in Gabor phase space. If this requirement is satisfied, the best separation of signal and clutter in the Gabor representation is achieved. The paper also discusses limitations of the filtering method: Such situations occur during extreme bird migration events. An additional quality control method is suggested to prevent erroneous measurements in these cases.

# Wavelet based methods for improved wind profiler signal processing

V. Lehmann<sup>1</sup> and G. Teschke<sup>2</sup>

<sup>1</sup>Deutscher Wetterdienst, Meteorologisches Observatorium Lindenberg, D-15864 Lindenberg, Germany

<sup>2</sup>Zentrum für Technomathematik, Universität Bremen, D-28334 Bremen, Germany

Received: 8 August 2000 – Revised: 28 February 2001 – Accepted: 8 March 2001

**Abstract.** In this paper, we apply wavelet thresholding for removing automatically ground and intermittent clutter (air-plane echoes) from wind profiler radar data. Using the concept of discrete multi-resolution analysis and non-parametric estimation theory, we develop wavelet domain thresholding rules, which allow us to identify the coefficients relevant for clutter and to suppress them in order to obtain filtered reconstructions.

**Key words.** Meteorology and atmospheric dynamics (instruments and techniques) – Radio science (remote sensing; signal processing)

## 1 Introduction

Radar Wind Profilers (RWP) are versatile tools used to routinely probe the Earth's atmosphere. This technology originally developed for studying the dynamics of the middle atmosphere in the seventies (Hardy and Gage, 1990) is, meanwhile, very prominent in the meteorological research community. Meteorological services started using these systems operationally within the Global Observing System (GOS) (see Monna and Chadwick (1998)).

Most of these RWP employ the Doppler-beam swinging (DBS) method for the determination of the vertical profile of the horizontal wind and, under certain conditions, the vertical wind component. These radars transmit short electromagnetic pulses in a fixed beam direction and sample the small fraction of the electromagnetic field backscattered to the antenna. At least three linear independent beam directions are required to transform the measured 'line-of-sight' radial velocities into the wind vector. Due to the nature of the acting atmospheric scattering processes, the received signal is several orders of magnitude weaker than the transmitted signal. The received signal is Doppler shifted, which is used to determine the velocity component of "the atmosphere" projected onto the beam direction. As the bandwidth  $B$  of

a transmitted electromagnetic pulse of duration  $\tau$  is much larger ( $B \propto 1/\tau \approx 100 \dots 1000$  kHz) than the Doppler shift ( $f_d \approx 10 \dots 500$  Hz), the frequency shift cannot be determined from the processing of a single pulse. Instead, the return of many pulses is evaluated to compute the Doppler frequency from the slowly changing phase of the received signals (Burgess and Ray, 1986). Sampling is done after the receivers quadrature detector (for the in-phase and quadrature-phase components of the signal) using sample and hold circuits prior to the A/D conversion. The sampling rate is determined by the pulse repetition period  $T$ . The samples at each range gate form a discrete complex time series, which is the *raw data* of the measurement at this gate. The following digital signal processing has the purpose of extracting the desired atmospheric information from the radar echoes. More details about coherent radar technology and in particular, wind profilers, can be found in standard textbooks (Gossard and Strauch, 1983; Doviak and Zrnić, 1993) and in several review papers, e.g. Röttger and Larsen (1990).

In this paper, we propose a modified signal processing technique for RWPs. It must be noted that signal processing includes all operations that are performed on the radar signal, i.e. analog<sup>1</sup> as well as digital processing<sup>2</sup>. However, in the following, we will only concentrate on digital signal processing. The incredible development of fast digital processors opens up new opportunities to optimize this latter part of the signal processing chain. The goals of signal processing, as summarized by Keeler and Passarelli (1990), are:

- to provide accurate, unbiased estimates of the characteristics of the desired atmospheric echoes;
- to estimate the confidence/accuracy of the measurement;
- to mitigate effects of interfering signals;
- to reduce the data rate.

<sup>1</sup>amplification, mixing and matched filtering

<sup>2</sup>after A/D conversion

Correspondence to: V. Lehmann (volker.lehmann@dwd.de)

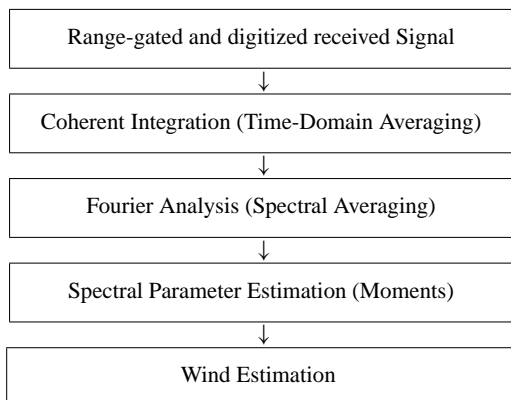


**Fig. 1.** The figure shows the flow diagram of 'classical' digital signal processing.

The fundamental base parameters of the atmospheric signal are the reflected power, the radial velocity and the velocity variance (e.g. the first three moments of the Doppler spectrum). Signal processing ends with the estimation of the moments of the Doppler spectrum and further data processing is then performed to finally determine the wind and other meteorological parameters using measurements from all radar beams. This distinction, which goes back originally to Keeler and Passarelli (1990), has become more and more blurred, since some modern algorithms make use of the moments of the Doppler spectrum with the help of continuity and other information (Wilfong et al., 1999b). However, we will refer here to the usually applied and well established "classical" signal processing, as described by Tsuda (1989), Röttger and Larsen (1990), among others.

## 2 Statement of the problem

Before we discuss the problems that are associated with the "classical" processing, let us briefly repeat the steps as visualized in Fig. 1. In particular, we refer to the signal processing as it is implemented in the RWP, whose data are used in this study.

Digital signal processing in a system using an analog receiver<sup>3</sup> starts with the sampling of the in- and quadrature-phase components of the received signal at a rate that is determined by the pulse repetition period  $T$ . To reduce the data rate for further processing, hardware adder circuits perform a so-called coherent integration (Barth et al., 1994; Carter et al., 1995; Wilfong et al., 1999a), adding some  $N$  (typically ten to hundred) complex samples together. Mathematically, this operation can be seen as a combination of a digital boxcar filtering, followed by an undersampling at a rate of  $NT$  (Schmidt et al., 1979; Farley, 1985). If the radar system uses pulse compression techniques (e.g. phase coding using

<sup>3</sup>For future systems, digital receivers will slightly change the signal processing but this has no consequence here.

complementary sequences), then the next step is decoding (Schmidt et al., 1979; Sulzer and Woodman, 1984; Farley, 1985; Ghebrehbrhan and Crochet, 1992; Spano and Ghebrehbrhan, 1996). The coherently averaged and decoded samples are then used to compute the Doppler spectrum using the Windowed Fourier Transform (FFT) and the Periodogram method (see Keeler and Passarelli, 1990). In our system, a Fourier transformed Hanning-window is convolved with the result of the FFT. A number (typically some ten) of individual Doppler spectra is then incoherently averaged to improve the detectability of the signal (Tsuda, 1989, see). Finally, the noise level is estimated with the method proposed by Hildebrand and Sekhon (1974), and the moments of the maximum signal in the spectrum are computed over the range where the signal is above the noise level (May and Strauch, 1989).

The problem with this type of signal processing is the underlying assumption that the signal consists of only two parts: the signal, that is produced by one atmospheric scattering process, and noise (different sources, mainly thermal electronic noise and cosmic noise). This is certainly not true, especially at UHF, where the desired atmospheric signal itself is often the result of two distinct scattering processes, namely scattering at inhomogeneities of the refractive index (Bragg scattering) and scattering at particles, such as droplets or ice crystals (Rayleigh scattering) (see, for instance, Gossard, 1979; Gossard and Strauch, 1981, 1983; Ralph et al., 1995, 1996; Gage et al., 1999). Therefore, even the desired atmospheric signal may have different characteristics. But, as experience shows us, the most serious problems are caused by the following contributions to the signal:

**Ground Clutter.** Echo returns from the ground surrounding the site, which emerge from antenna's sidelobes;

**Intermittent Clutter.** Returns from unwanted targets, such as airplanes or birds, from both the antenna's main lobe and the sidelobes;

**Radio Frequency Interference (RFI).** RFI can emerge from external radio-frequency transmissions within the passband of the receiver (matched filter), or it can be generated internally due to imperfections of the radar hardware.

Recently, much work has and continues to be done to develop frequency domain processing algorithms, i.e. to improve the process of moment estimation. The purpose of these methods is to select the "true" atmospheric signal in the Doppler spectrum even in the presence of severe contamination. Only this signal will then be used for the determination of the wind vector. Several criteria are used to make an "intelligent" selection of the signal (Clothiaux et al., 1994; Gossard, 1997; Griesser, 1998; Cornman et al., 1998; Schumann et al., 1999; Wilfong et al., 1999b; Morse et al., 2000). The emphasis on frequency domain processing was probably caused by the fact that it is much easier to handle spectral data, as the data volume is significantly reduced due to the data compression effect of the periodogram computation and the spectral integration. Some of these "multiple moment estimation" algorithms additionally assign a quality indicator

to the computed wind values, which does not only depend on the quality of the moment estimation, but also uses continuity criteria (Wilfong et al., 1999b) and the testing of assumptions that are inherent to the DBS method (Goodrich et al., 2000). First evaluations have indeed shown a very promising improvement of those new algorithms (Cohn et al., 2000), but no long-term evaluation against independent measurement systems, such as the Rawinsonde, has been performed so far.

Modified time domain processing has been proposed to reduce the problems caused by contaminating signals. One problem emerges from the fact that the receiver filter of the radar is matched to the transmitted pulse in order to optimize the single pulse signal-to-noise ratio for improved signal detection in the presence of noise (Tsuda, 1989; Papoulis, 1991; Doviak and Zrnić, 1993). This implies a receiver bandwidth of  $B \propto 1/\tau$ . Yet, the sampling is done at a rate of  $T$  (without coherent averaging) or even  $NT$  (with coherent averaging). Thus, the Nyquist frequency, after coherent averaging, is severely smaller than the frequency that a received signal might have. Of course, it is true that the desired atmospheric signal is band-limited by a sufficiently long coherence time of the scattering process, so that this undersampling has no consequences (aside from some modification due to the filtering characteristics of the coherent integration). If there is, however, some artificial signal, such as RFI present, whose spectrum falls into the receiver passband, the complex I/Q-timeseries then represents a process that is only band-limited by the receiver hardware. The consequence of undersampling is frequency aliasing of higher frequency components into the atmospheric band of interest. This problem is especially critical in the U.S., where profilers at 449 MHz operate simultaneously with amateur radios. Although the problem of principal undersampling cannot be solved due to the fact that  $1/\tau \gg 1/T$ , Wilfong et al. (1999a) achieved an improved time domain filtering using a four-term Blackman-Harris filter (Harris, 1978), instead of the usually applied boxcar filter of coherent averaging. While this kind of digital filtering helps to reject RFI, it is not helpful in the presence of ground and intermittent clutter. Those clutter signals fall well into the region of the desired atmospheric signal. May and Strauch (1998) proposed the use of linear convolution filters (digital FIR<sup>4</sup> filters) with a band rejection characteristic around zero Doppler shift (DC). This requires, however, a long filter sequence and also does not protect against intermittent clutter signals, which can occur at any frequency. Additionally, the transfer characteristic is fixed for a set of given filter coefficients. For that reason, wavelet domain filtering of ground and intermittent clutter (Jordan et al., 1997; Boisse et al., 1999) has been proposed. The main purpose of all these time domain operations is the filtering aspect, i.e. the intention is to “clean” the raw data from contaminating signals while leaving the desired atmospheric contribution ideally intact. In the following, we will concentrate on the clutter problem and investigate the properties of these

**Table 1.** Technical specification of RWP and radar operating parameters

Site name	Lindenberg 482 MHz Profiler
Latitude	52.21 N
Longitude	14.13 E
Altitude	101 m msl
Frequency	482.0078 MHz
One-way beamwidth	3 degrees
Number of beams	5
Zenith distance (oblique beams)	15 degrees
Effective antenna area	140 m <sup>2</sup>
Pulse peak power	16 kW
Altitude Range	0.5–8.0 km (Low Mode)
Beamdirection during raw data sampling	East (Azimuth: 79 Elev. 75)
InterPulsePeriod (T)	61 $\mu$ s
Pulsewidth ( $\tau$ )	1700 ns (Low Mode)
Delay to first gate	4800 ns
Gate Spacing	1700 ns
Number of gates	30
# of coherent integrations (N)	144
# of spectral integrations	1 (none)
# of points in online FFT	2048
System Delay (w/ 1700 ns pulse)	1550 ns

signals and the possibility of applying nonlinear wavelet filters. There are not many investigations about the properties of RWP raw data. Normally, using statistical arguments, one assumes simply a Gaussian signal characteristic for atmospheric and clutter signals, as well as for noise (Doviak and Zrnić, 1993; Petitdidier et al., 1997). Recently, Muschinski et al. (1999) used data from a large-eddy simulation to derive I/Q signals for clear air scattering, and Capsoni and D’Amico (1998) presented a software-based radar simulator for generating time series from a synthetic distribution of hydrometeors. For our purpose, we assume that the Gaussian model describes sufficiently well both the atmospheric scattering component and the ground clutter signal. Intermittent clutter returns can be described by the simple model given by Boisse et al. (1999), with their main property being the transient character.

The 482 MHz wind profiler, whose data are used in this study, was installed at the Meteorological Observatory Lindenberg during the summer of 1996. The system is the prototype for three additional profilers to be installed in Germany in the future to supplement the operational aerological network of the Deutscher Wetterdienst (DWD). A summary of the main characteristics of the system is given in Table 1. For a more detailed description, the reader is referred to Steinhagen et al. (1998). The system is operated quasi continuously using a five beam configuration. All the main system parameters can be freely programmed which eases special investigations, such as the investigation of the detrimental ground clutter signal that was present in the system’s

<sup>4</sup>Finite Impulse Response

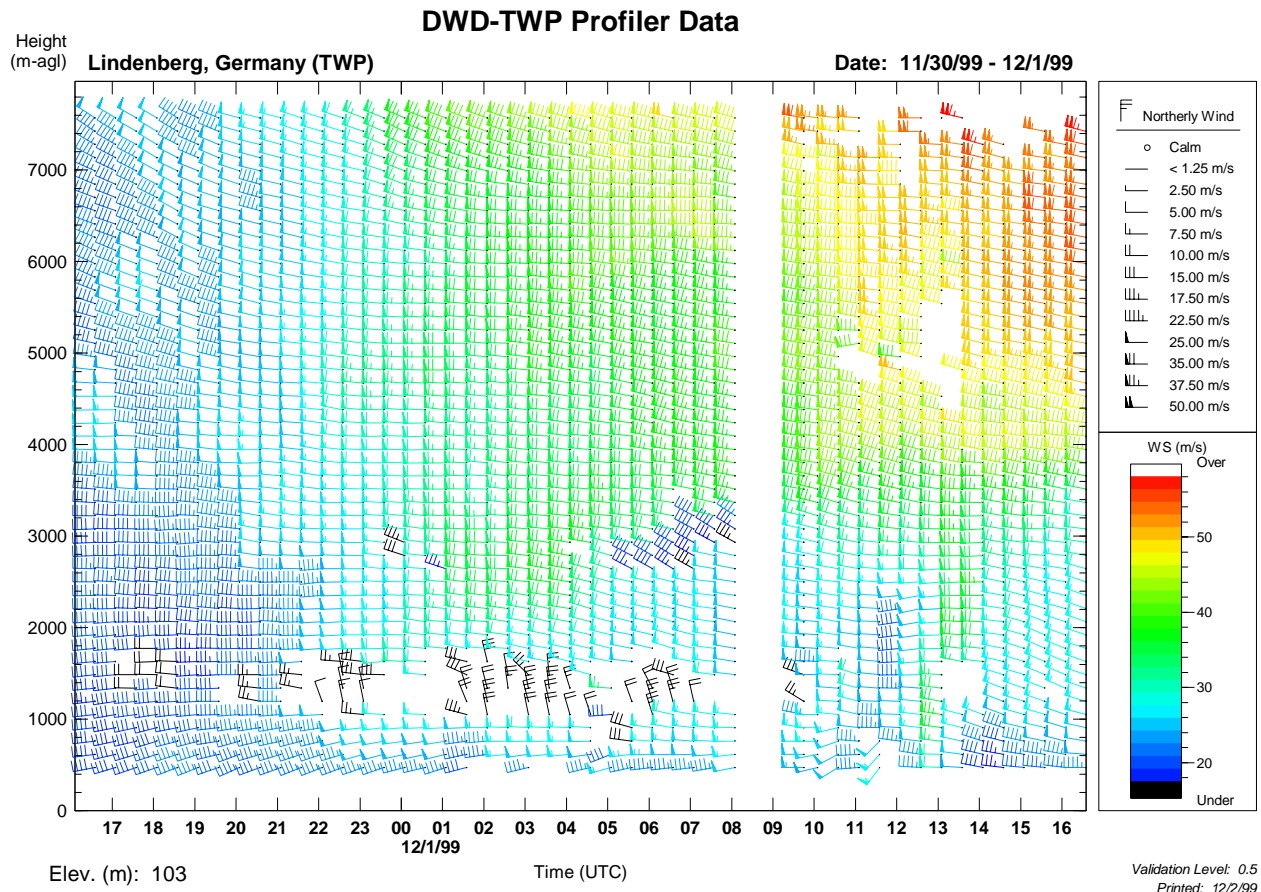


**Fig. 2.** The figure shows the final result of the measurement with the 482 MHz RWP at Lindenberg (Germany) on the 30 November and 1 December 1999. The wind barbs are color-coded according to the wind speed. Note the effects of the persistent ground clutter around the 1500 m and 3000 m heights. The gap in the data was caused by this detailed investigation, as the radar was programmed to store time series data for about 30 minutes, only in the East beam, thus, no wind computations were possible for that period of time.

East beam from the 30 November to the 1 December 1999. During this event, the profiler was operated for a short period using only this beam (and low mode), while the huge amount of time series data was stored for further investigation (namely, the wavelet filtering). We now substantiate the radar parameter settings that were used in collecting the radar raw data: from the table of the radar's parameter settings, we find that the spacing of the time series data is  $\Delta t = NT = 8.784$  ms. This corresponds to a Nyquist frequency of  $f_N = 1/2\Delta t = 56.92$  Hz, which gives, in turn, the maximum resolvable radial velocity  $v_R = \lambda f_d/2 = 17.6$  m/s. Clearly visible in Fig. 2 is the detrimental impact of ground clutter at the heights around 1400 m and 3000 m. The computed winds are obviously wrong and we will, therefore, look in detail into the problem. A more detailed, exemplary look into the raw data (coherently integrated I/Q-Time series) of gates 11 and 17, and the resulting power spectra (Fig. 3), immediately reveals that advanced signal processing for RWP is necessary to increase the accuracy of wind vector reconstruction. The time series at gate 11 shows the typical signature of a slowly fading, large amplitude ground clutter

signal component, which corresponds to the narrow spike centered around point 1024 (zero Doppler shift) in the resulting power spectrum (compare also May and Strauch, 1998). Additionally, the time series at gate 17 shows a strong transient component in the last quarter. Such a signature is quite typical for a flier echo, as was shown by Boisse et al. (1999). This transient almost completely covers up any atmospheric signal in the power spectrum.

### 3 Applying multiresolution analysis and statistical estimations

For the problem at hand, the goal of the signal processing should be signal component separation, i.e. an automatic, reliable and stable extraction of the different contributions to the signal (noise, clutter, interference). Motivated by Daubechies (1992); Vetterli and Kovačević (1995); Louis et al. (1998); Meyer (1993) and Holschneider (1995), our purpose was to embed the filtering procedure into the known mathematical theory of wavelets. In general, mathematical

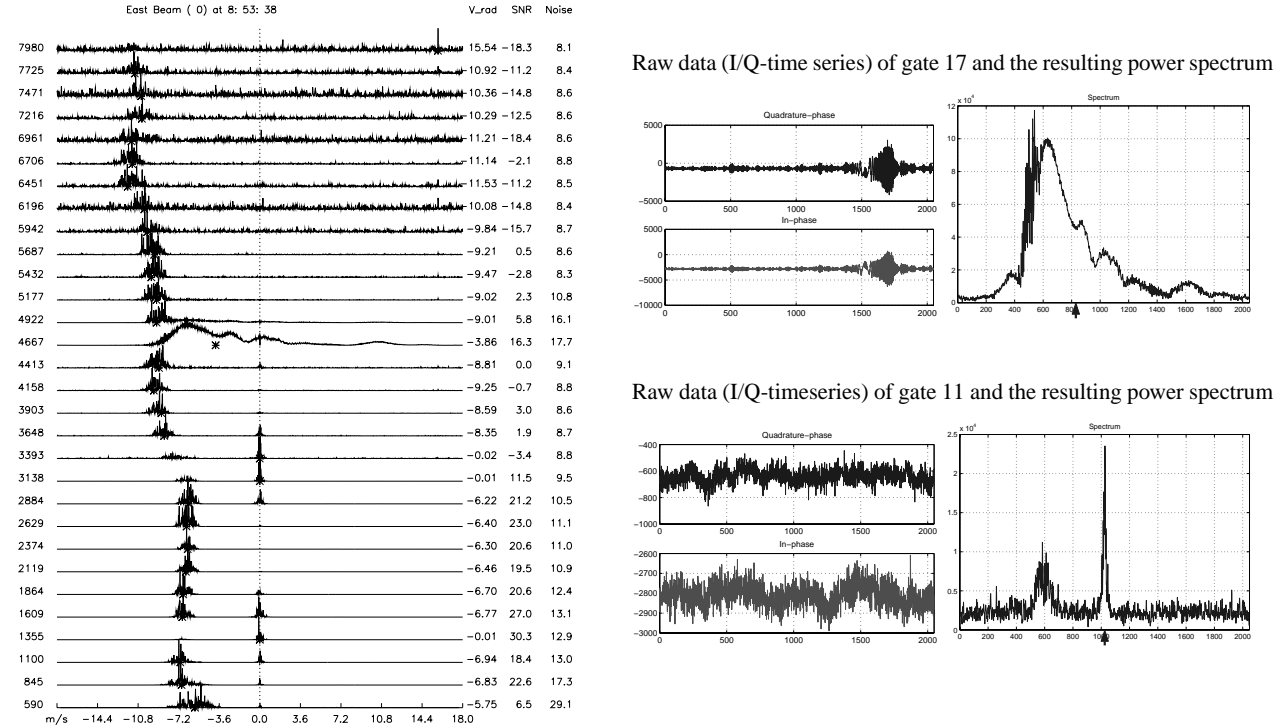


**Fig. 3.** The left part shows the “stacked spectrum” plot, i.e. the Doppler spectra for each range gate, for the radar dwell at 08:53:38 UTC on 1 December 1999. The right figures give a detailed look into the raw data (I/Q-timeseries) and the Doppler spectrum for the gates 11 and 17 (whose data will be wavelet processed). The black arrows indicate the estimated first moment (i.e. the radial velocity).

experience concerning problems related to contamination removal or denoising shows that usually more than time domain filtering and Fourier domain filtering techniques are required to obtain optimum results. Often, most of the existing and implemented methods are insufficient. The main reasons for the particular effectiveness of wavelet analysis can be summarized as follows:

- The fact that contamination appears often instationary or transient, and with a priori unknown scale structure, favors the superior localization properties of the wavelets. A wavelet expansion may allow the separation of signal components that overlap both in time and frequency (Burrus et al., 1998).
- In order to effectively localize clutter components, one can use a great variety of wavelet filters (Daubechies, 1992; Dahlke et al., 2000; Teschke, 1998; Stark, 1992; Dahlke and Maaß, 1995). To choose a certain wavelet that especially suits the desired signal component, one can determine the properties of the clutter signal; otherwise, one can select a wavelet empirically.
- The wavelet expansion coefficients,  $\beta_{jk}$ , drop off rapidly for a large class of signals, which makes the expansion very efficient (Burrus et al., 1998).
- The fast wavelet transform has a computationally complexity that is lesser than or equal to the fast Fourier

transform; the algorithm is recursive (Kaiser, 1994; Louis et al., 1998; Burrus et al., 1998). This allows for an efficient implementation on digital computers.

Thus, the application of wavelet techniques to our particular problem seems to be promising. Before we start, let us briefly repeat the basics of multi-resolution analysis.

Let  $L_2(\mathbb{R})$  be the space of functions of finite energy. Let  $\phi$  be some function in  $L_2(\mathbb{R})$ , such that the family of translates of  $\phi$  form an *orthonormal system*. We define

$$\phi_{jk}(x) := 2^{j/2} \phi(2^j x - k), \quad j \in \mathbb{Z}, \quad k \in \mathbb{Z}.$$

Further, we define linear spaces by

$$V_0 := \{f(x) = \sum_k c_k \phi(x - k) : \sum_k |c_k|^2 < \infty\}$$

⋮

$$V_j := \{h(x) = f(2^j x) : f \in V_0\}, \quad j \in \mathbb{Z}$$

Assuming that  $\phi$  is chosen in such a way that the spaces are nested:

$$V_j \subset V_{j+1}, \quad j \in \mathbb{Z} \quad \text{and that} \quad \bigcup_{j \geq 0} V_j \text{ is dense in } L_2(\mathbb{R})$$

then the sequence  $\{V_j, j \in \mathbb{Z}\}$  is called a multi-resolution analysis. This concept was introduced by Mallat (1989);

Meyer (1993).  $\phi$  is called the father wavelet. Furthermore, one may define subspaces  $W_j$  by

$$V_{j+1} := V_j \oplus W_j$$

and iterating this we have

$$\bigcup_j V_j = V_0 \oplus \bigoplus_j W_j \text{ and } L_2(\mathbb{R}) = V_0 \oplus \bigoplus_j W_j.$$

Assuming that our data may be described by some  $f \in L_2(\mathbb{R})$ , we can represent the signal as a series

$$f(x) = \sum_k \alpha_k \phi_{0k}(x) + \sum_j \sum_k \beta_{jk} \psi_{jk}(x),$$

where  $\{\psi_{jk}\}$ ,  $k \in \mathbb{Z}$  is an orthonormal basis in  $W_j$ . The function  $\psi$  is called mother wavelet.

This expansion is a special kind of orthogonal series. Hence, it would be useful to search in the framework of nonparametric statistical estimation theory for an applicable method to solve our problem (Donoho and Johnstone, 1992). In case of orthogonal series estimation, the idea of reconstructing the desired atmospheric signal is simple. Basically, we replace the unknown wavelet coefficients in the wavelet expansion by estimates which are based on observed data. For that, we need a selection procedure to choose relevant coefficients since the main emphasis of performing wavelet domain filtering is to create a suitable, i.e. problem matched, coefficient selecting procedure. To separate the atmospheric signal component, we apply statistical estimation theory. A side effect of using statistics is to obtain a measure of reconstruction quality. A typical quality measure is a loss function/estimation error. Minimizing the error function reveals an objective evaluation and a self-acting filter algorithm.

The following sub-section describes the construction of our atmospheric-signal-estimator. In advance, we briefly remark that in the following section, we assume that our signal belongs to some Besov space, i.e. a generalized mathematical function space. One special example is the previously introduced function space  $L_2(\mathbb{R})$ . But sometimes it makes more sense to suppose that the derivatives of our signal are of finite energy as well. In this and other situations, the framework of Besov spaces is an adequate mathematical tool for our application. A Besov space, denoted by  $B_{pq}^s$ , depends on three parameters:  $s$  smoothness, the number of bounded derivatives and  $p, q$  which describe the underlying function space  $L_q(l_p)$ . In the following, we make use of some well-known facts of estimation theory, which are valid for almost all Besov spaces (Donoho and Johnstone, 1992; Donoho et al., 1993; Johnstone and Silverman, 1995; v. Sachs and MacGibbon, 1998; Dahlhaus et al., 1998; Härdle et al., 1998). If our signal is an element of one of these spaces (which is true for all practical signals), we can adapt wavelet threshold estimators. The main advantage of this framework is that we can use existing rules for evaluating bounds and rates of convergence for our loss function, which describes the quality of our reconstructed atmospheric signal component. By optimizing bounds and rates of convergence, we obtain self acting algorithms.

For our purpose, we only need the following characterization of Besov spaces: A function  $f$  belongs to  $B_{pq}^s$  if

$$J_{pq}^s(f) = \|\alpha\|_{l_p} + \left( \sum_{j \geq 0} (2^{j(s+1/2-1/p)} \|\beta_j\|_{l_p})^q \right)^{1/q} < \infty.$$

We are looking for optimal reconstructions of functions belonging to some subset  $F_{pq}^s(M) = \{f \in B_{pq}^s : J_{pq}^s(f) < M\}$ . For our calculations, we assume that the function is in  $L_2(\mathbb{R})$  and  $s$  is small.

From given measurements  $(Y_1, \dots, Y_n)$ , we want to estimate the function  $f$  in the simple model

$$Y_i = f(X_i) + \varepsilon_i.$$

We assume that we have the  $X_i$  on a regular grid and  $\varepsilon$  is a random variable (a stochastic process which describes all non-atmospheric components). The basic idea is to replace the wavelet coefficients in the series expansion by empirical estimates

$$\hat{\alpha}_k = \frac{1}{n} \sum_{i=1}^n Y_i \cdot \varphi_{0k}(X_i) \text{ and } \hat{\beta}_{jk} = \frac{1}{n} \sum_{i=1}^n Y_i \cdot \psi_{jk}(X_i),$$

where the  $X_i$  are time stamps and the  $Y_i$  are observations. A straightforward linear estimation is given by the projection onto a subspace  $V_{j_1}$

$$\hat{f}_{j_1}(x) = \sum_k \hat{\alpha}_k \varphi_{0k}(x) + \sum_{j=0}^{j_1} \sum_k \hat{\beta}_{jk} \psi_{jk}(x).$$

To appraise this estimator, it is known that one may measure the expected loss or the risk (in  $L_2$  sense)  $E \|\hat{f}_{j_1} - f\|_2^2$ . This measure is the so-called MISE (mean integrated squared error). To determine the MISE, one may decompose it into  $E \|\hat{f}_{j_1} - E \hat{f}_{j_1}\|_2^2$  (stochastic contribution) and  $E \|E \hat{f}_{j_1} - f\|_2^2$  (deterministic contribution). Under certain conditions, one may find bounds for MISE:

$$\sup_{F_{22}^s(M)} \|E \hat{f}_{j_1} - f\|_2 \leq C_1 2^{-j_1 s}$$

and

$$E \|\hat{f}_{j_1} - E \hat{f}_{j_1}\|_2^2 \leq C_2 \frac{2^{j_1+1}}{n}$$

and hence,

$$\sup_{f \in F_{22}^s(M)} E \|\hat{f}_{j_1} - f\|_2^2 \leq C_3 \frac{2^{j_1}}{n} + C_4 2^{-j_1 s}.$$

A minimum of the sum is given by

$$\sup_{f \in F_{22}^s(M)} E \|\hat{f}_{j_1} - f\|_2^2 \leq C_5 n^{-2s/(2s+1)},$$

furthermore, one can generalize this result for  $p > 2$

$$\sup_{f \in F_{pq}^s(M)} E \|\hat{f}_{j_1} - f\|_p^p \leq C_5 n^{-ps/(2s+1)}.$$

This gives us an upper bound for the maximum risk. This bound becomes small if the number of observation increases and if  $j_1(n)$  is determined in such a way that the bias and stochastic bound are balanced (for detailed computations of bounds, see v. Sachs and MacGibbon, 1998; Donoho et al., 1993; Donoho and Johnstone, 1992; Dahlhaus et al., 1998).

Obviously, this kind of linear estimation includes oscillating components, in particular, the clutter components. This phenomenon occurs because we have taken the whole set of wavelet coefficients up to scale  $j_1$ , i.e. we have not performed any filtering step thus far. In the following, we need a suitable selection procedure for the coefficients in order to perform the necessary filtering step. We apply a so-called hard thresholding and soft thresholding, respectively. This methodology was introduced and adapted to several problems by Donoho and Johnstone (1992); Donoho et al. (1993). It is based on taking the discrete wavelet transform (using a multiresolution analysis), passing the transform through a threshold (actually, the expansion coefficients are thresholded) and then taking the inverse DWT to obtain a filtered reconstruction. Note that this type of thresholding is usually applied in a different way, by removing coefficients *below* a certain threshold in order to “de-noise” the data (Burrus et al., 1998, see Fig. 4). The functions for hard and soft thresholding are defined by

$$\theta^h(u) := \begin{cases} u, & |u| \geq \lambda \\ 0, & |u| < \lambda \end{cases}, \quad \theta^s(u) := \begin{cases} (u - \frac{\lambda u}{|u|}), & |u| \geq \lambda \\ 0, & |u| < \lambda \end{cases}$$

and the modified functions used here for hard and soft thresholding are given by the rule  $\eta^*(u) = u - \theta^*(u)$ :

$$\eta^h(u) = \begin{cases} u, & |u| < \lambda \\ 0, & |u| \geq \lambda \end{cases}, \quad \eta^s(u) = \begin{cases} u, & |u| < \lambda \\ \lambda \frac{u}{|u|}, & |u| \geq \lambda \end{cases}.$$

Here,  $\lambda$  is an adequate threshold. Applying this rule to our linear wavelet estimator, we obtain a nonlinear estimator

$$\hat{f}^*(x) = \sum_k \eta^*(\hat{\alpha}_k) \varphi_{0k}(x) + \sum_{j=j_0}^{j_1} \sum_k \eta^*(\hat{\beta}_{jk}) \psi_{jk}(x),$$

where  $\eta^*$  is  $\eta^s$  or  $\eta^h$ , respectively.

If the threshold  $\lambda$  is specified according to the asymptotic distribution of the empirical coefficients, then only those coefficients remain which are supposed to carry significant signal information. These are finally used for the reconstruction by the inverse wavelet transform. For the correct level of significance, an appropriate choice of the threshold  $\lambda$  is needed. In general, this does not only depend on the sample size  $n$ , but also on the resolution scale  $j$ , and location  $k$  of the coefficients. In the case of regression with non-stationary errors, we have to use both a level and location dependent threshold rule (v. Sachs and MacGibbon, 1998). The resulting non-linear estimator does not only provide local smoothers, but, in many situations, achieves the near-minimax  $L_2$ -rate for the risk of estimation, i.e. v. Sachs and MacGibbon (1998) for (random) thresholds  $\lambda_{jk}$  satisfying

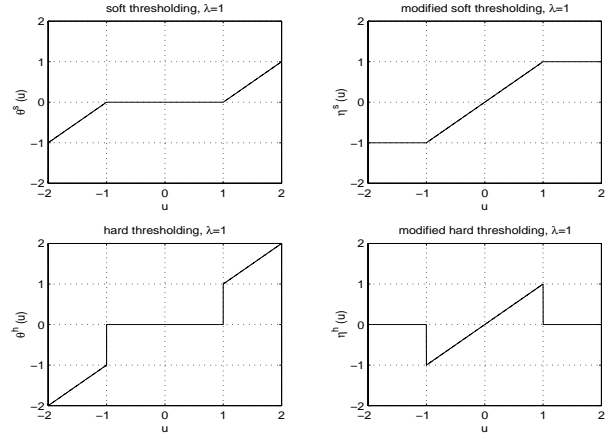


**Fig. 4.** This figure shows hard and soft thresholding.

$\sigma_{jk} \sqrt{2 \log M_j} \leq \lambda_{jk} \leq C \sqrt{\frac{\log n}{n}}$  for any positive constant  $C$ :

$$\sup_{f \in F_{22}^s(M)} E \|\hat{f}^* - f\|_2^2 = O\left(\frac{\log(n)}{n}\right)^{2s/(2s+1)},$$

where  $\sigma_{jk}$  is the variance and  $M_j$  denotes the number of the coefficients used in the nonlinear estimator. The optimal threshold rate  $(1/n)^{2s/(2s+1)}$  is attained only for the ideal threshold. However, in practice, this is unknown. Therefore, we have to replace  $\sigma_{jk}$  by some estimation  $\hat{\sigma}_{jk}$ , which results in random thresholds  $\hat{\lambda}_{jk} = \hat{\sigma}_{jk} \sqrt{2 \log M_j}$ . Hence, the log-term has to be understood as the price for some data-driven threshold rule, and it originates due to the estimation of the unknown variance  $\sigma_{jk}^2 = \text{Var}(\hat{\beta}_{jk})$ .

We conclude that we may adapt an estimation rule for our desired atmospheric signal component where the quality is measurable in the sense of  $L_2$ -risk. This means the procedure used displays bounds for our reconstruction, and we may easily determine the rate of convergence. The calculation of the wavelet coefficients can be done by using the fast wavelet algorithm which is easily implemented.

#### 4 Removing clutter

In this section, we will demonstrate the performance of nonlinear wavelet filtering. This is done both with simulated and with real data. For a better understanding, we particularize Fig. 1 to see where we have inserted the wavelet tool. To apply our procedure, a more substantiated algorithm flow diagram is shown in Fig. 5.

Following the first box in the algorithm flow diagram, one has first to determine the analyzing wavelet (high and low pass filter coefficients). Usually, the decomposition of a signal in a basis (i.e. a wavelet series) has the goal of highlighting particular properties of the signal (Mallat, 1999). In the problem of wind profiler signal filtering, the desired atmospheric signal component can be contaminated with spurious signal components. The ultimate goal is obviously to find a

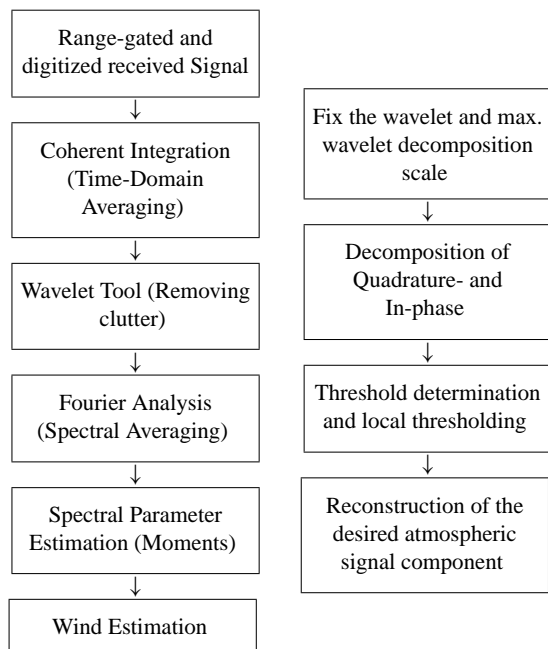


**Fig. 5.** Left: The flow diagram extended by the wavelet tool. Right: The wavelet algorithm flow diagram.

wavelet basis, which would allow a separation of the desired and the unwanted parts of the signal, i.e. which would have the ability to approximate the unwanted signal components (ground clutter, intermittent clutter) with only a few non-zero wavelet coefficients. In other words, the wavelet  $\psi$  has to be chosen in such a way that a maximum number of wavelet coefficients,  $\beta_{jk}$ , are close to zero. This depends primarily on the regularity of the (contaminating) signal  $f$ , the number of vanishing moments of the wavelet  $\psi$ , and the size of the wavelets support. If  $f$  is regular and  $\psi$  has enough vanishing moments, then the coefficients  $\beta_{jk}$  are guaranteed to be small for small scales. If, however, the signal  $f$  contains isolated singularities, the strategy to have a maximum number of small wavelet coefficients would be to reduce the support size of the wavelet. Unfortunately, there is a tradeoff between both properties for orthogonal wavelets: if  $\psi$  has  $p$  vanishing moments, then its support size is at least  $2p - 1$ . The best compromise between those two requirements are Daubechies wavelets, which are optimal in the sense that they have minimum support for a given number of vanishing moments.

There have been no detailed investigations thus far about the regularity properties of contaminating wind profiler signals, but there is evidence that these can be both “quite regular” (ground clutter) or “not so regular” (intermittent clutter). Thus, the Daubechies family was selected. The order of the Daubechies wavelet was chosen according to the regularity condition, which we have conservatively chosen to be rather small ( $s \leq 1$ ). To approximate correctly a function of  $B_{pq}^s$ , we need to select an analyzing wavelet of regularity  $[s] + 1$ . A wavelet with regularity of the order of  $s = 2$  and minimal compact support is the Daubechies-2-wavelet; hence, we

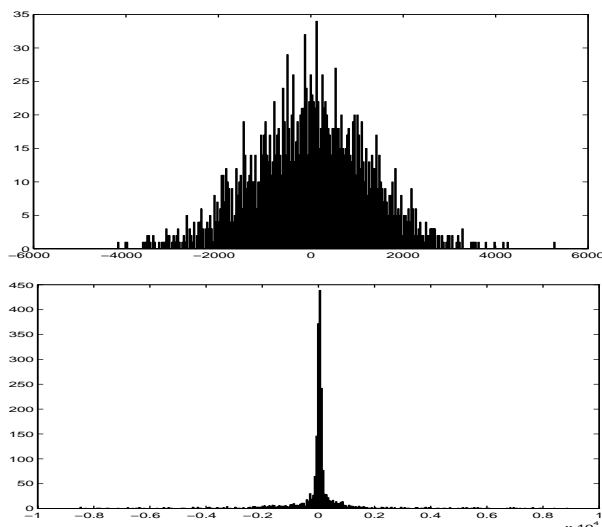


**Fig. 6.** This figure shows typical histograms of the wavelet coefficients (see text). The upper histogram represents an in-phase series without an airplane echo and the lower histogram represents an in-phase series with an airplane reflection.

have chosen this one for our calculations. Mathematically, it is no problem to increase the wavelet order (regularity), but the wavelet support size and the number of filter coefficients also increases, and this will decelerate the algorithm. Finally, we note, in passing, that we have concentrated on the fast wavelet transform (multiresolution analysis), which is a special case of the discrete wavelet transform. Obviously, for an online algorithm, the number of operations per data point is limited. The fast wavelet transform is, therefore, the best choice, since it has the highest numerical efficiency (i.e. it is faster than the fast Fourier transform). This, of course, restricts the possible choices of the underlying basis wavelet.

The number of decomposition scales is determined by balancing the stochastic and the deterministic part of the MISE. Thus, the optimal scale may be evaluated automatically by the rule  $2^{j_1(n)} \simeq n^{1/(2s+1)}$ . After fixing the main parameters, one may start the wavelet decomposition of the in-phase and the quadrature-phase time series. To separate the atmospheric component, the algorithm calculates for each decomposition level the local thresholds  $\hat{\lambda}_{jk}$ .

Additionally, one may use histogram information, which displays the empirical distribution of the coefficients  $\hat{\alpha}_k$  and  $\hat{\beta}_{jk}$ . In particular, if the signal was contaminated by an airplane echo, the main part of the observations is concentrated in a small neighborhood around zero. If there is no airplane echo, the coefficients are exponentially distributed (see Fig. 6).

The histogram methods acts as follows: we denote by  $h_j(k)$ , the histogram function of the coefficient sequence of scale  $j$ , and by  $H_j(z)$ , the connected empirical distribution function. We know that  $H_j$  is monotonic increasing, continuous from the right and a step function. If  $H_j(z)$  is given then all values  $z_i$  may be recognized completely; this means that

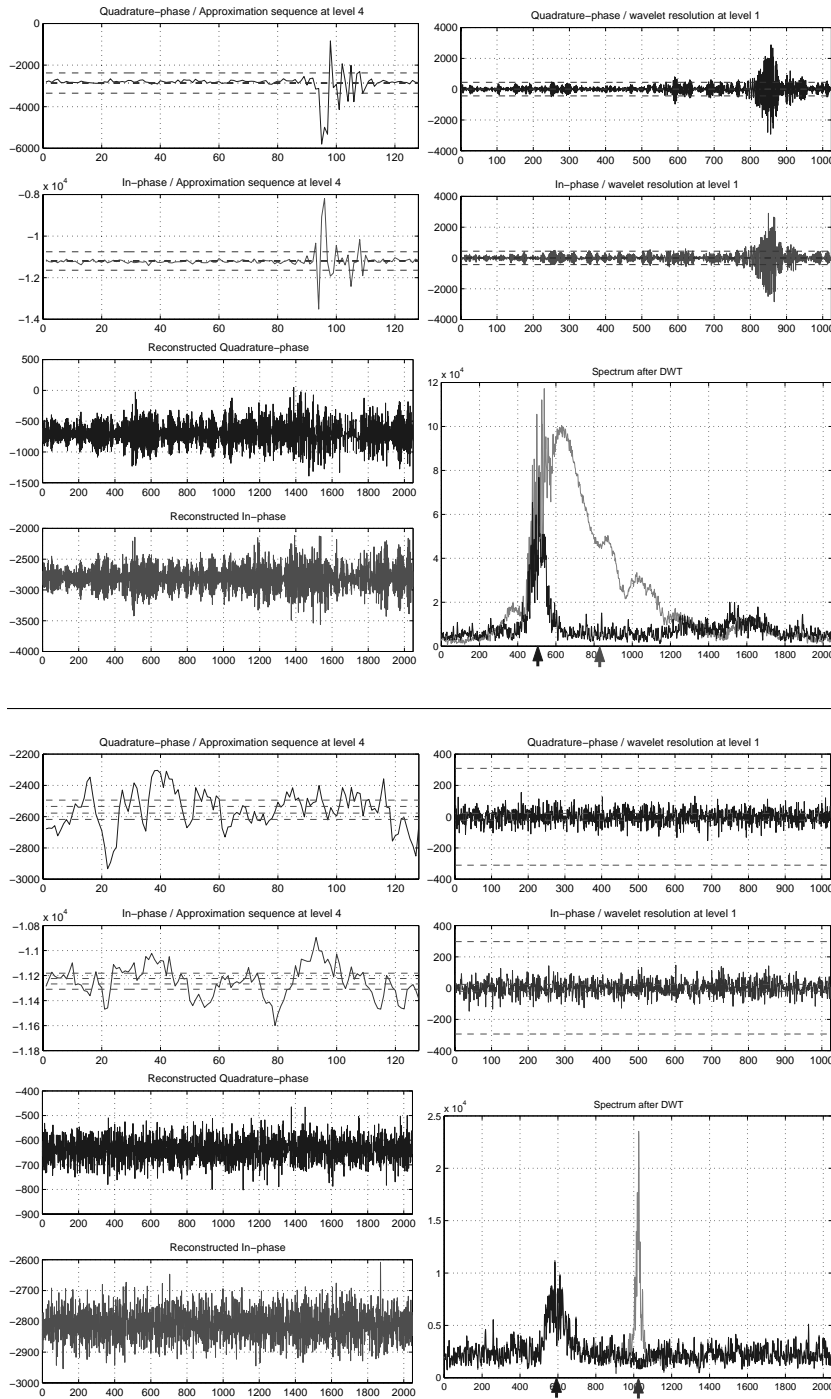


**Fig. 7.** Decomposition ( $\alpha_k$  und  $\beta_{1k}$ ), reconstruction and Fourier power spectrum of gate 17 (top) and gate 11 (below). The black curves in the power spectra representations display the decontaminated spectra. One clearly recognizes are the differences of moment estimations; see the computed first moment before (gray arrow) and after (black arrow) the filtering step.

one can detect the smallest value  $q_0$  with  $H_j(q_0) \leq c_{j,\alpha}$  (so-called empirical  $\alpha$ -quantile). If we now determine a lower bound for the number of coefficients we want to have available for reconstructing, we may easily evaluate  $q_{j,\alpha}$  by solving

$$\int_{-q_{j,\alpha}}^{q_{j,\alpha}} h_j(k) dk = c_{j,\alpha}.$$

We define the histogram-based threshold by  $\lambda_{jk}^{hist} := q_{j,\alpha}$ .

Since there is only empirically information and no model about the characteristics of intermittent clutter echoes, we assume that the histogram method should remove a maximum of 15 percent of the observations and hence, we have chosen  $c_{j,\alpha} = 0.85$ . This is, of course, just a heuristic value. For our dataset, this value has given the best results for the loss function. We are quite confident that the rule is robust if a larger percentage of the dwell time is contaminated with flier echos. However, more research about the properties of

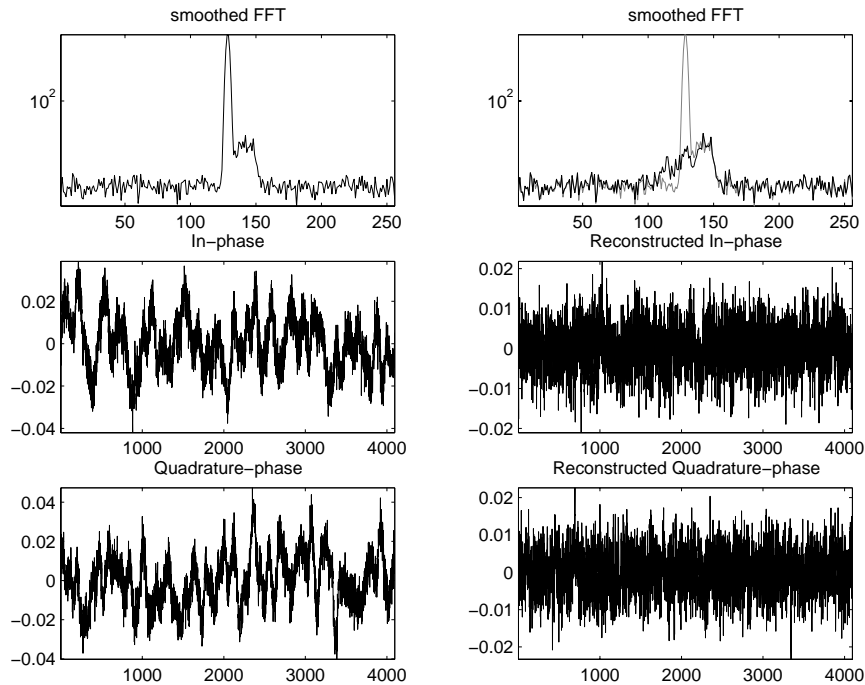


**Fig. 8.** Top left: Simulated Fourier-power-spectrum with strong ground clutter influence and with an atmospheric signal overlapping the ground clutter peak. Lower left: I/Q time series derived from the simulated Fourier-power-spectrum using the Zrnić (1975) method. Lower right: I/Q time series after applying the nonlinear wavelet filter. Top right: Resulting Fourier-power-spectrum based on the reconstructed (filtered) signal.

the contaminating signals and the distribution of the wavelet coefficients is certainly needed.

In the case of having only ground clutter,  $\hat{\lambda}_{jk}$  and  $\lambda_{jk}^{hist}$  are almost equal. In the case of intermittent clutter, we choose our data driven threshold,  $\hat{\lambda}_{jk}$ , by taking the minimum of  $\hat{\lambda}_{jk}$  and  $\lambda_{jk}^{hist}$ . Hence, in case of having bird or airplane echoes, it may occur that the resulting threshold underestimates the threshold evaluated by minimizing the MISE. Yet from extensive test calculations, we know that no problems accrue. In addition, by using this simple histogram rule, the accuracy of the thresholding step increases. But the price of applying the rule is an enlargement of the number of calculations per data point.

To observe how this algorithm works, we start by simulating one easy test sample. Using the statistical-stochastic approach of Zrnić (1975) to generate I/Q-timeseries, we first generate an atmospheric signal with Gaussian characteristics in the frequency domain. We choose the Doppler frequency of the atmospheric signal close to zero to force the separation problem. Now we add a noise variable and a ground clutter peak, which is generated by a narrow Gaussian. The order of the ground clutter amplitude is much higher than the atmospheric signal amplitude. Since the algorithm removes the ground clutter completely, the reconstructed signal consists only of the atmospheric part (and some noise). This demonstrates impressively the difference between the nonlinear wavelet filtering method and the Fourier methods and digital filtering: the spectra of clutter and atmospheric signal can overlap as much as they want; nonetheless, we can still separate the two components. The different amplitude of both signals allows for the discrimination.

For intermittent clutter, one of the advantages of wavelet-based techniques is certainly the ability to describe a transient signal with only a few wavelet coefficients. This is caused by the finite support of the wavelet basis, in contrast to the basis functions (the so-called windowed Fourier atoms)  $e^{i\omega t} g(t-u)$  of the windowed Fourier transform. It is the localizing properties of wavelets (Burrus et al., 1998) that makes the wavelet transform especially suited for filtering of transient signals (e.g. intermittent clutter).

To expose how the routine is acting on measured RWP time series, we eventually go back to the presented “real life” problem (example Fig. 3) in order to demonstrate the robustness of the method. The problem was that the signal at gate 17 was contaminated by intermittent clutter (aircraft echo) and the signal at gate 11 was contaminated by persistent ground clutter. The spectra obtained with the standard signal processing were severely affected by clutter contributions to the received signal and thus, the moment estimation and finally the wind vector determination were significantly biased. Figure 7 shows exemplarily how wavelet thresholding was realized in decomposition sequences  $\alpha_k$  and  $\beta_{1k}$  of gates 11 and 17. The dotted lines may be identified with the threshold. It can be observed that in both cases, the clutter components could be completely removed.

## 5 Conclusions

This paper discusses an algorithm that employs discrete multi-resolution analysis and nonlinear estimation theory to separate the atmospheric Doppler signal in RWP measurements in the presence of contaminating signals. Using simulated and

real wind profiler data, we have demonstrated that wavelet thresholding is effective in removing ground and intermittent clutter (airplane echoes) from the RWP raw data (I/Q time-series). The presented wavelet based filtering technique is self-acting and, therewith, a step toward an automatic algorithm for clutter removal in Doppler spectra. Real time implementation in profiler systems is required to test the new method with a substantially longer dataset, preferably in parallel with the standard processing (comparison), and to demonstrate its use for operational applications.

*Acknowledgements.* This work was supported by the Bundesministerium für Bildung und Forschung through grant BMBF 01 LA 9905/9. The authors wish to thank Prof. P. Maaß and Dr. H. Steinhagen for their continuous support regarding this paper. We are also grateful to J. R. Jordan of NOAA's Environmental Technology Laboratory, for sharing his expertise about RWP raw data and interesting discussions about wavelet filtering methods. Finally, the valuable comments of two reviewers helped to improve this paper.

Topical Editor J.-P. Duvel thanks T. Shimomai and J. Jordan for their help in evaluating this paper.

## References

- Barth, M., Chadwick, R., and van de Kamp, D., Data processing algorithms used by NOAA's wind profiler demonstration network, *Ann. Geophysicae*, 12, 518–528, 1994.
- Boisse, J.-C., Klaus, V., and Aubagnac, J.-P., A wavelet transform technique for removing airplane echos from ST radar signals, *J. Atmos. Oceanic Technol.*, 16, 334–346, 1999.
- Burgess, D. and Ray, P. S., *Mesoscale Meteorology and Forecasting*, chap. Principles of radar, pp. 85–117, AMS, 1986.
- Burrus, C. S., Gopinath, R. A., and Guo, H., *Introduction to Wavelets and Wavelet Transforms*, Prentice Hall, 1998.
- Capsoni, C. and D'Amico, M., A physically based radar simulator, *J. Atmos. Oceanic Technol.*, 15, 593–598, 1998.
- Carter, D., Gage, K. S., Ecklund, W. L., Angevine, W. M., Johnston, P. E., Riddle, A. C., Wilson, J., and Williams, C. R., Developments in UHF lower tropospheric wind profiling at NOAA's Aeronomy Laboratory, *Radio Sci.*, 30, 977–1001, 1995.
- Clothiaux, E., Penc, R., Thomson, D., Ackerman, T., and Williams, S., A first-guess feature-based algorithm for estimating wind speed in clear-air doppler radar spectra, *J. Atmos. Oceanic Technol.*, 11, 888–908, 1994.
- Cohn, S. A., Goodrich, R. K., Morse, C. S., Karplus, E., Mueller, S. W., Cornman, L. B., and Weekly, R. A., Radial velocity and wind measurement with NIMA: Comparisons with human estimation and aircraft measurements, submitted to *J. Appl. Meteor.*, 1–25, 2000.
- Comman, L. B., Goodrich, R. K., Morse, C. S., and Ecklund, W. L., A fuzzy logic method for improved moment estimation from Doppler spectra, *J. Atmos. Oceanic Technol.*, 15, 1287–1305, 1998.
- Dahlhaus, R., Neumann, M. H., and v. Sachs, R., Nonlinear wavelet estimation of time-varying autoregressive processes, preprint, 1998.
- Dahlke, S. and Maaß, P., The affine uncertainty principle in one and two dimensions, *Comp. Math. Appl.*, 30, 293–305, 1995.
- Dahlke, S., Maaß, P., and Teschke, G., Interpolating scaling functions with duals, Tech. Rep. 00-08, Zentrum für Technomathematik, Universität Bremen, 2000.
- Daubechies, I., *Ten Lectures on Wavelets*, SIAM, Philadelphia, 1992.
- Donoho, D. L. and Johnstone, I. M., Minimax estimation via wavelet shrinkage, Tech. Rep. 402, Department of Statistics, Stanford University, 1992.
- Donoho, D. L., Johnstone, I. M., Kerkyacharian, G., and Picard, D., Density estimation by wavelet thresholding, Preprint, Dept. of Statistics, Stanford University, 1993.
- Doviak, R. J. and Zrnić, D. S., *Doppler radar and weather observation*, Academic Press, 1993.
- Farley, D., On-line data processing techniques for MST radars, *Radio Sci.*, 20, 1177–1184, 1985.
- Gage, K. S., Williams, C. R., Ecklund, W. L., and Johnston, P. E., Use of two profilers during MCTEX for unambiguous identification of Bragg scattering and Rayleigh scattering, *J. Atmos. Sci.*, 56, 3679–3691, 1999.
- Ghebrehrehan, O. and Crochet, M., On full decoding of truncated ranges for ST/MST radar applications, *IEEE Trans. Geosci. Electron.*, 30, 38–45, 1992.
- Goodrich, R. K., Morse, C. S., Cornman, L. B., and Cohn, S. A., A horizontal wind and wind confidence algorithm for Doppler wind profilers, submitted to *J. Atmos. Oceanic Technol.*, pp. 1–22, 2000.
- Gossard, E. E., A fresh look at the radar reflectivity of clouds, *Radio Sci.*, 14, 1089–1097, 1979.
- Gossard, E. E., Automated editing of spectra from wind profilers, Tech. Rep. ERL-ETL 286, NOAA Environmental Technology Laboratory, 1997.
- Gossard, E. E. and Strauch, R. G., The refractive index spectra within clouds from forward-scatter radar observations, *J. Appl. Meteor.*, 20, 170–183, 1981.
- Gossard, E. E. and Strauch, R. G., *Radar Observations of Clear Air and Clouds*, Elsevier, 1983.
- Griesser, T., *Multipleanalyse von Dopplerspektren aus Windprofiler-Radar-Messungen*, Ph.D. thesis, Eidgenössische Technische Hochschule Zürich, 1998.
- Härdle, W., Kerkyacharian, G., Picard, D., and Tsybakov, A., *Wavelets, Approximation, and Statistical Applications*, Springer, New York, 1998.
- Hardy, K. R. and Gage, K. S., The history of radar studies of the clear atmosphere, in *Radar in Meteorology*, chap. 17, 130–142, American Meteorological Society, Boston, 1990.
- Harris, F. J., On the use of windows for harmonic analysis with the discrete Fourier transform, *Proc. IEEE*, 66, 51–83, 1978.
- Hildebrand, P. H. and Sekhon, R., Objective determination of the noise level in Doppler spectra, *J. Appl. Meteor.*, 13, 808–811, 1974.
- Holschneider, M., *Wavelets: An Analysis Tool*, Clarendon Press, Oxford, 1995.
- Johnstone, I. M. and Silverman, B. W., Wavelet threshold estimators for data with correlated noise, Tech. Rep. Dept. of Statistics, Stanford University, 1995.
- Jordan, J. R., Lataitis, R. J., and Carter, D. A., Removing ground and intermittent clutter contamination from wind profiler signals using wavelet transforms, *J. Atmos. Oceanic Technol.*, 14, 1280–1297, 1997.
- Kaiser, G., *A Friendly Guide to Wavelets*, Birkhäuser, Basel, 1994.
- Keeler, R. J. and Passarelli, R. E., Signal processing for atmospheric radars, in *Radar in Meteorology*, edited by D. Atlas, chap. 20a, 199–229, American Meteorological Society, Boston, 1990.
- Louis, A. K., Maaß, P., and Rieder, A., *Wavelets*, Teubner, Stuttgart, 1998.

- Mallat, S., Multiresolution approximations and wavelet orthonormal bases of  $L^2(R)$ , *Trans. Amer. Math. Soc.*, 69–87, 1989.
- Mallat, S., *A Wavelet Tour of Signal Processing*, Academic Press, 1999.
- May, P. T. and Strauch, R. G., An examination of wind profiler signal processing algorithms, *J. Atmos. Oceanic Technol.*, 6, 731–735, 1989.
- May, P. T. and Strauch, R. G., Reducing the effect of ground clutter on wind profiler velocity measurements, *J. Atmos. Oceanic Technol.*, 15, 579–586, 1998.
- Meyer, Y., *Wavelets: Algorithms and Applications*, SIAM, Philadelphia, 1993.
- Monna, W. A. and Chadwick, R. B., Remote-sensing of upper-air winds for weather forecasting: Wind-profiler radar, *Bull. WMO*, 47, 124–132, 1998.
- Morse, C. S., Goodrich, R. K., and Cornman, L. B., The NIMA method for improved moment estimation from Doppler spectra, submitted to *J. Atmos. Oceanic Technol.*, 1–24, 2000.
- Muschinski, A., Sullivan, P. P., Wuertz, D. B., Hill, R. J., Cohn, S. A., Lenschow, D. H., and Doviak, R. J., First synthesis of wind-profiler signals on the basis of large-eddy simulation data, *Radio Sci.*, 34, 1437–1459, 1999.
- Papoulis, A., *Probability, Random Variables and Stochastic Processes*, McGraw-Hill, 3 edn., 1991.
- Petitdidier, M., Sy, A., Garrouste, A., and Delcourt, J., Statistical characteristics of the noise power spectral density in UHF and VHF wind profilers, *Radio Sci.*, 32, 1229–1247, 1997.
- Ralph, F. M., Neiman, P. J., van de Kamp, D. W., and Law, D. C., Using spectral moment data from NOAA's 404-MHz radar wind profilers to observe precipitation, *Bull. Amer. Meteorol. Soc.*, 76, 1717–1739, 1995.
- Ralph, F. M., Neiman, P. L., and Ruffieux, D., Precipitation identification from radar wind profiler spectral moment data: Vertical velocity histograms, velocity variance, and signal power – vertical velocity correlation, *J. Atmos. Oceanic Technol.*, 13, 545–559, 1996.
- Röttger, J. and Larsen, M., UHF/VHF radar techniques for atmospheric research and wind profiler applications, in *Radar in Meteorology*, chap. 21a, 235–281, American Meteorological Society, Boston, 1990.
- Schmidt, G., Rüster, R., and Czechowsky, P., Complementary code and digital filtering for detection of weak VHF radar signals from the Mesosphere, *IEEE Trans. Geosci. Electron.*, GE-17, 154–161, 1979.
- Schumann, R. S., Taylor, G. E., Merceret, F. J., and Wilfong, T. L., Performance characteristics of the Kennedy Space Center 50 MHz Doppler Radar wind profiler using the median filter /first-guess data reduction algorithm, *J. Atmos. Oceanic Technol.*, 16, 532–549, 1999.
- Spano, E. and Ghebrehbrhan, O., Pulse coding techniques for ST/MST radar systems: A general approach based on a matrix formulation, *IEEE Trans. Geosci. Remote Sensing*, 34, 304–316, 1996.
- Stark, H.-G., Continuous wavelet transform and continuous multiscale analysis, *Math. Anal. and Appl.*, 169, 179–196, 1992.
- Steinhagen, H., Dibbern, J., Engelbart, D., Görsdorf, U., Lehmann, V., Neisser, J., and Neuschaefer, J. W., Performance of the first European 482 MHz wind profiler radar with RASS under operational conditions, *Meteorol. Z.*, N.F.7, 248–261, 1998.
- Sulzer, M. and Woodman, R., Quasi-complementary codes: A new technique for MST radar sounding, *Radio Sci.*, 19, 337–344, 1984.
- Teschke, G., *Komplexwertige Wavelets und Phaseninformation, Anwendungen in der Signalverarbeitung*, Diplomarbeit, Institut für Mathematik, Universität Potsdam, 1998.
- Tsuda, T., *Middle Atmosphere Program – Handbook for MAP*, vol. 30, chap. Data Acquisition and Processing, pp. 151–183, ICSU Scientific Committee on Solar-Terrestrial Physics (SCOSTEP), ISAR 24–28 November 1988, Kyoto, 1989.
- v. Sachs, R. and MacGibbon, B., Nonparametric curve estimation by wavelet thresholding with locally stationary errors, preprint, 1998.
- Vetterli, M. and Kovačević, J., *Wavelets and Subband Coding*, Prentice Hall PTR, New Jersey, 1995.
- Wilfong, T. L., Merritt, D. A., Lataitis, R. J., Weber, B. L., Wuertz, D. B., and Strauch, R. G., Optimal generation of radar wind profiler spectra, *J. Atmos. Oceanic Technol.*, 16, 723–733, 1999a.
- Wilfong, T. L., Merritt, D. A., Weber, B. L., and Wuertz, D. B., Multiple signal detection and moment estimation in radar wind profiler spectral data, submitted to *J. Atmos. Oceanic Technol.*, 1999b.
- Zrnić, D. S., Simulation of weatherlike Doppler spectra and signals, *J. Appl. Meteor.*, 14, 619–620, 1975.



# Advanced radar wind profiling

ANDREAS MUSCHINSKI<sup>1</sup>, VOLKER LEHMANN<sup>2</sup>, LUTZ JUSTEN<sup>3</sup> and GERD TESCHKE<sup>3</sup>

<sup>1</sup>Department of Electrical and Computer Engineering, University of Massachusetts, Amherst, Massachusetts, USA

<sup>2</sup>Meteorologisches Observatorium Lindenberg, Deutscher Wetterdienst, Lindenberg, Germany

<sup>3</sup>Zentrum für Technomathematik, Universität Bremen, Bremen, Germany

(Manuscript received May 10, 2005; in revised form July 11, 2005; accepted July 11, 2005)

## Abstract

During the last three decades, radar wind profiling (RWP) has evolved into a key technology for atmospheric science and operational meteorology. In this tutorial status report, RWP is divided into three distinct areas: single-signal RWP, two-signal RWP, and multi-signal RWP. While single-signal RWP, or standard RWP, is a mature technology in many respects, there is still much room for improvement, particularly in the interpretation of signals that are severely contaminated by radio interference or by clutter from aircraft, birds, hydrometeors, etc. Two-signal RWP, the best known examples of which are the spaced-antenna (SA) and frequency-domain interferometry (FDI) techniques, have been used to overcome some of the limitations inherent to standard RWP. Multi-signal RWP is, to a large extent, still unexplored territory. This paper attempts to provide a coherent conceptual framework of advanced RWP and to identify areas of future research and development.

## Zusammenfassung

Im Laufe der letzten drei Jahrzehnte hat sich Radar-Windprofilung (RWP) zu einer Schlüsseltechnologie in der Atmosphärenforschung und der operationellen Meteorologie entwickelt. Im Rahmen einer einführenden Bestandsaufnahme wird RWP in drei Kategorien eingeteilt: Einzel-Signal-RWP, Zwei-Signal-RWP und Multi-Signal-RWP. Obwohl Einzel-Signal-RWP, d.h. Standard-RWP, in vielerlei Hinsicht eine ausgereifte Technologie ist, gibt es dennoch Verbesserungsmöglichkeiten, insbesondere hinsichtlich der Auswertung von Messungen, die durch Radio-Einstreuung oder Störschos von Flugzeugen, Vögeln, Hydrometeoren usw. stark beeinträchtigt sind. Zwei-Signal-RWP, als deren Hauptvertreter die Technik der versetzten Antennen und die Frequenzbereich-Interferometrie gelten können, haben sich als hilfreich zur Überwindung einiger Limitierungen der Standard-RWP erwiesen. Multi-Signal-RWP hingegen ist im wesentlichen noch unbekanntes Territorium. Dieser Beitrag versucht, einen einheitlichen begrifflichen Rahmen der fortgeschrittenen RWP-Technologie zu liefern. Zudem werden mögliche Bereiche zukünftiger Forschung und Entwicklung aufgezeigt.

## 1 Introduction

The era of radar wind profiling (RWP) began with the pioneering paper by WOODMAN and GUILLÉN (1974), who were the first to demonstrate that the extremely weak VHF radio-wave echoes from clear-air refractive-index perturbations in the troposphere and stratosphere are indeed measurable and that the temporal changes of these echoes can be used to retrieve wind velocities.

Within one decade, the first RWP network, called the Colorado wind-profiling network (STRAUCH et al., 1984), was implemented and provided quasi-operational wind data. The network consisted of four VHF profilers operating at 50 MHz (wavelength 6 m) and one UHF profiler operating at 915 MHz (wavelength 33 cm). According to STRAUCH et al. (1984, p. 37), one objective of that program was “to develop tropospheric wind-

profiling radars that will provide vertical profiles of the horizontal wind throughout the troposphere, operate in nearly all weather conditions, provide wind data automatically and continuously with unattended operation, be suitable for widespread use in networks, provide data for mesoscale and synoptic scale applications.” The design goal was “to provide vertical profiles of the horizontal wind with accuracy of orthogonal components to better than  $1 \text{ m s}^{-1}$ ; height resolution of 100 m below 600 mb, 300 m to 300 mb, and 1 km to 100 mb; temporal resolution of 15 min for profiles to 600 mb, 30 min for profiles to 300 mb, and 60 min for profiles to 100 mb.” The design goals for operational RWPs have barely changed during the last twenty years, which in hindsight may be seen as an indication that the problems encountered in RWP are more serious and complicated than originally anticipated.

The Colorado network was the precursor of the National Oceanic and Atmospheric Administration’s (NOAA) National Profiler Network (BARTH et al., 1994), which has been operating continuously since

\*Corresponding author: Andreas Muschinski, Dept. of Electrical and Computer Engineering, University of Massachusetts at Amherst, 151 Holdsworth Way, Amherst, MA 01003-9284, USA, e-mail: muschinski@ecs.umass.edu

1992, and by the end of 2004 consisted of 35 RWP sites across the United States. Similar RWP networks are now operating in Europe and Japan.

Today, there are hundreds of research and operational RWPs worldwide, measuring wind velocities in the atmospheric boundary layer, the free troposphere, and in the lower stratosphere. Overviews of the technical and scientific aspects of RWP have been provided, among others, by Gage (1990), RÖTTGER and LARSEN (1990), DOVIK and ZRNIC (1993), and MUSCHINSKI (2004). Based on the overall success of RWPs, many consider RWP a mature technology. A closer look at the underlying physical and mathematical principles, however, reveals that there is still room for substantial improvement and further development. Major progress can be anticipated in two directions. First, traditional RWP, or single-signal RWP, can be made more efficient by taking advantage of new methods in mathematical signal analysis. Second, two-signal and multi-signal RWP techniques, which have been studied by researchers for many years but have not yet entered the operational arena, offer a wide range of options to overcome limitations that are inherent to single-signal RWP.

The purpose of this paper is to give a tutorial overview of single-signal, two-signal, and multi-signal radar wind profiling. Emphasis is placed on the physical and mathematical concepts. Examples of RWP measurements are presented in order to give an impression of the wide variety of problems that arise from non-atmospheric signal contributions, i.e., clutter and noise.

The paper is organized as follows. Section 2 gives an overview of the physical nature of a single RWP signal. The RWP signal is divided into a clear-air component, a clutter component, and a noise component. Basic single-signal statistics are introduced and explained, among them the so-called Doppler spectrum and its first three moments. A number of the difficulties to retrieve clear-air statistics from contaminated RWP signals are explained. Limitations inherent to single-signal RWP are discussed. Section 3 reviews two-signal RWP techniques, mainly the spaced-antenna technique and the frequency-domain interferometry technique. Section 4 gives an introduction to multi-signal RWP, which is mathematically much more demanding than single-signal and two-signal RWP. A wide variety of forward problems can be formulated, and the associated inverse problems will remain a fertile research area in the foreseeable future. A summary and a brief outlook are given in Section 5.

## 2 Single-signal radar wind profiling

This section describes physical, technological, and mathematical aspects of single-signal RWP. Section 2.1 illustrates the nature of RWP signals on the basis of a

measurement example. Section 2.2 describes and discusses the various sources of clutter and noise, which often dominate the clear-air echo and make it difficult, sometimes impossible, to retrieve wind information from a measured RWP signal. Based on the measurement example of Section 2.1, Section 2.3 introduces the Doppler spectrum and explains why RWPs can measure wind velocities at signal-to-noise ratios as low as  $-35$  dB or even lower. Section 2.4 summarizes the theory that relates the intensity of the clear-air echo to the spatial spectrum of the refractive-index perturbations in the RWP's sampling volume. The relationship between Doppler shift and wind velocity has been analyzed only recently on the basis of first-principle theory, as summarized in Section 2.5. Of considerable practical importance for single-signal RWP are new mathematical time-frequency decomposition techniques. Section 2.6 illustrates the efficacy of these techniques by means of an RWP signal that is severely contaminated by an aircraft echo.

### 2.1 A measurement example

Figure 1 shows the time series of the real and imaginary parts of a single signal measured with the east beam of the 482-MHz profiler operated by the Deutscher Wetterdienst (DWD, German Weather Service) at its Meteorologisches Observatorium Lindenberg (MOL). The data were taken on Dec. 1, 1999, with the east beam ( $15^\circ$  off zenith) at a height of 3035 m MSL. The elevation of the MOL site is 103 m MSL.

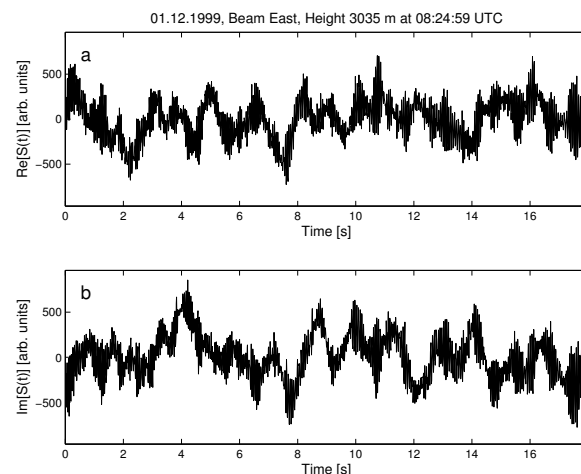


**Figure 1:** Time series of the in-phase (a) and quadrature (b) component of a signal measured on 1 December 1999 with the 482-MHz RWP at the Meteorologisches Observatorium Lindenberg, Germany. Each of the two time series contains 2048 samples. Each sample is the coherent sum of 144 echoes from subsequent pulses.

The real (in-phase) part and the imaginary (quadrature) part of the complex time series each contain 2048

samples. Each sample is the coherent average of the echoes from 144 subsequent pulses. That is, the data are the result of 294,912 subsequent pulses and their respective echoes. The pulse-repetition period was 61  $\mu$ s, such that the coherent-integration time was 8.8 ms, and the length of the entire time series (the “dwell time”) was 18.0 s. (Note that some authors use the term “dwell time” as the time during which the radar “dwells” in the same beam-pointing direction; that definition may or may not coincide with our definition.)

The coherent-integration time must be short compared to the time scales at which the signal’s phase and amplitude change significantly due to the mean and turbulent motion of the atmospheric refractive-index perturbations in the RWP’s resolution volume. For RWP operating in the lower UHF regime, where the radar wavelength is of order 1 m, a coherent-integration time of order 10 ms is usually a good choice.

Figure 2 shows the first second of the 18-s-long signal time series presented in Figure 1. The signal fluctuations at time scales of order 50 ms are due to echoes from atmospheric refractive-index perturbations while the fluctuations at one-second time scales, which dominate Figure 1, are caused by clutter from slowly moving objects on the ground.

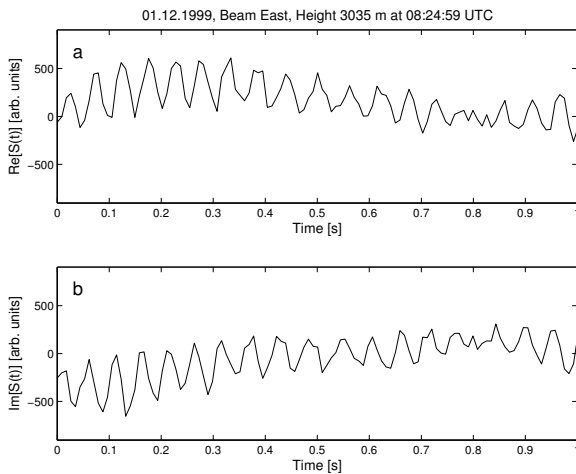


**Figure 2:** The first second of the signal time series shown in Figure 1.

## 2.2 Definitions: Clutter, noise, and clear-air signal

In Figure 2, the clear-air component can be clearly recognized as the nearly sinusoidal oscillations superposed on the slowly changing clutter component. Uncorrelated noise has been substantially suppressed because of the coherent averaging. If the single echoes were shown instead of the coherently added echoes, then Figure 2 would have been noise-dominated, as we will show in

the next subsection. (For the data shown in Figure 2 the coherent adding, or averaging, had been done with hardware, and because of hardware limitations the single-echo samples could not be saved; therefore, the single-echo samples cannot be shown here.) The clutter, however, which dominates Figure 1 and in this case is much stronger than the atmospheric echo, cannot be reduced by coherent averaging.

At this point, it is helpful to define the terms clutter, noise, and signal more clearly. Unfortunately, the term “signal” is used in the literature with two different meanings. In the context of “signal processing,” “signal” stands for “measured receiver output,” which is the sum of clutter, noise, and atmospheric echo. Often, however, “signal” is used synonymously with “atmospheric echo.” In the following, we avoid this ambiguity by using the terms “total signal”  $S(t)$ , “clear-air signal”  $I(t)$ , clutter  $C(t)$ , and noise  $N(t)$ :

$$S(t) = I(t) + C(t) + N(t), \quad (2.1)$$

where all terms are complex-valued “base-band” currents measured at the receiver output. Our definition of  $I(t)$  is identical to the one in DOVIAK and ZRNIC (1984), DOVIAK and ZRNIC (1993, eq. 11.115 on p. 456), and MUSCHINSKI (2004).

Clutter is the totality of undesired echoes. In the case of RWP, clutter includes echoes from airborne objects such as aircraft, birds, bats, insects, atmospheric plankton, airborne debris, hydrometeors, and moving or nonmoving objects on the ground like buildings, power lines, trees, cars, or wind turbines. Whether or not clutter is easily distinguishable from clear-air signals depends on the distribution of the echoing objects in space and time, and on their radial velocities. Insect echoes, for example, are difficult to distinguish from clear-air echoes because insects constitute a “distributed target” (there are often many insects in the same sampling volume), and often they are passively advected with the local wind velocity. The same is true for small rain droplets or small snowflakes. From a purely practical point of view, particularly if one is interested only in wind measurements, there is no need to distinguish between the clear-air component and the clutter component if one can safely assume that the sources of airborne clutter are passively advected with the wind.

We define noise as the sum of all contributions to  $S(t)$  that are not the result of an echoing mechanism. From this definition it follows that noise is independent of the strength, the shape, or the transmit time of the transmitted pulses. Noise includes thermal noise in the RWP system, electromagnetic radiation from the sun or other astronomical objects (cosmic noise), and radio signals transmitted from satellites, mobile phones, electrical machinery, etc. (radio interference). It is usually assumed that system noise and cosmic noise are well ap-

proximated by a flat “noise floor” (white noise) in the spectrum.

Because clear-air signal, clutter, and noise are uncorrelated from each other, such that  $\langle I^*C \rangle = 0$ ,  $\langle I^*N \rangle = 0$ , and  $\langle C^*N \rangle = 0$  (the angle brackets mean “expectation value of”), the “total Doppler spectrum,” i.e., the frequency spectrum of  $S(t)$ , is simply the sum of the frequency spectra of  $I(t)$ ,  $C(t)$ , and  $N(t)$ , respectively:

$$\phi_S(\omega) = \phi(\omega) + \phi_C(\omega) + \phi_N(\omega), \quad (2.2)$$

where  $\phi(\omega)$  is the spectrum of the clear-air signal,  $\phi_C(\omega)$  is the clutter spectrum, and  $\phi_N(\omega)$  is the noise spectrum. We have suppressed the subscript “ $T$ ” in  $\phi(\omega)$  in order to keep the notation in the analytical Sections 2.5 and 3.1 simple.

### 2.3 Measurement example: Periodogram, Doppler spectrum, and signal-to-noise ratio

Figure 3 shows the periodogram of the signal time series presented in Figure 1. The periodogram was computed by means of a Fast Fourier Transform (FFT) algorithm. As is customary in the RWP community, we present the periodogram as a function of frequency  $f = \omega/2\pi$  and not of cycle frequency  $\omega$ . Three features can be clearly distinguished from each other: a peak centered at  $f = -18$  Hz, a second peak at  $f = 0$ , and noise spread over the entire resolvable frequency interval. The resolvable frequencies range from  $-f_{Ny}$  to  $+f_{Ny}$ , where

$$f_{Ny} = \frac{1}{2T_c} \quad (2.3)$$

is the Nyquist frequency and  $T_c$  the coherent-integration time. In our case,  $T_c = 8.8$  ms, which leads to  $f_{Ny} = 56.9$  Hz, in agreement with the frequency range depicted in Figure 3. The frequency increment in a periodogram is

$$\Delta f = \frac{1}{T_d}, \quad (2.4)$$

where  $T_d$  is the dwell time, in our example  $T_d = 18$  s, such that  $\Delta f = 0.056$  Hz. That is, in Figure 3 a frequency interval of width 10 Hz (like the width of the peak centered at  $-18$  Hz) is represented by 180 points in the periodogram.

A clear distinction has to be made between the periodogram, which can be *calculated* from a finite time series, and the power spectrum, which can only be *estimated* from a finite time series. Definitions of the power spectrum and the cross-spectrum of complex-valued, random variables can be found, e.g., in MUSCHINSKI (2004). Sometimes, the power spectrum is referred to as the auto-spectrum (as opposed to the cross-spectrum), the variance spectrum (because integration over all frequencies gives the variance), or simply as the spectrum.

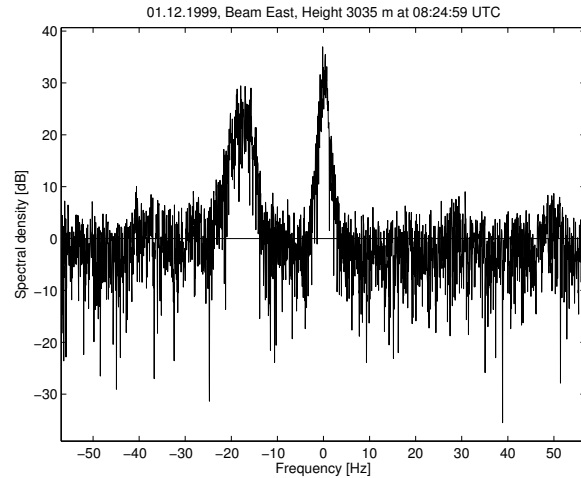


Figure 3: Periodogram of the RWP signal shown in Fig. 1.

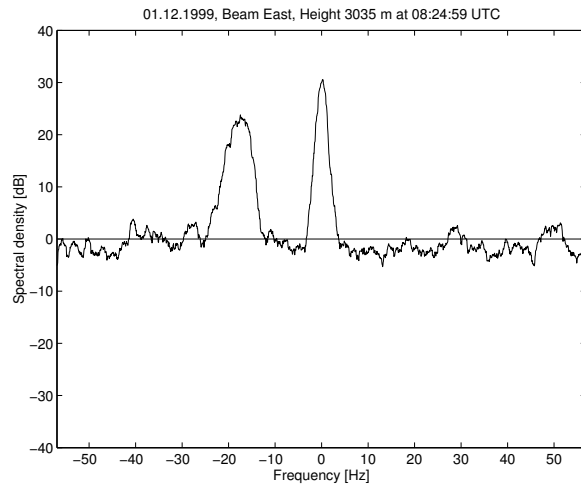


Figure 4: Doppler spectrum, estimated from the periodogram in Figure 3 after averaging in the frequency domain over 20 adjacent spectral points.

The most obvious difference between a periodogram and a spectrum is that in a periodogram the individual spectral points show a random behaviour, sometimes referred to as “speckle,” while a spectrum is usually smooth. Figure 4 shows the periodogram in Figure 3 after averaging over 20 adjacent spectral points, that is, over frequency intervals of 1.1 Hz. Obviously, smoothing reduces the speckle, such that a smoothed periodogram is a better approximation of the spectrum than the “raw” periodogram. It is important to note that the periodogram calculated from a finite data set is a *biased* estimator of the power spectrum (e.g., DOVIAK and ZRNIC, 1993, p. 99).

The noise spectral density,  $\phi_N$ , has been estimated with the HILDEBRAND and SEKHON (1974) algorithm and is depicted by the horizontal lines in Figures 3 and 4.

The algorithm does not require any *a priori* knowledge about which parts of the periodogram are pure white noise and which are not, as long as there are a sufficient number of periodogram points that represent pure white noise.

The peak at  $-18$  Hz (corresponding to an oscillation period of 56 ms, as visible in the time series in Figure 1) is the atmospheric signal while the peak at zero Doppler shift is ground clutter. The spectral densities in Figures 3 and 4 are given relative to the mean noise spectral density  $\phi_N$ , such that the actual noise spectral density (as a function of frequency) fluctuates around 0 dB. The peak spectral densities of the clear-air signal and the clutter are 23 dB and 30 dB, respectively, above the noise floor in this measurement example.

Let us estimate the single-pulse signal-to-noise ratio (SNR) of the clear-air signal:

$$SNR = \frac{\langle |I|^2 \rangle}{\langle |N|^2 \rangle}, \quad (2.5)$$

where  $I$  is the non-averaged clear-air component and  $N$  is the non-averaged noise. The width of the clear-air peak is about 10 Hz, while the Nyquist interval of the non-averaged echoes is  $1/(61 \mu s) = 16.4$  kHz, or  $2 \times 144$  times the Nyquist frequency of the coherently averaged samples, which we showed is 56.9 Hz. That is, the noise is spread over a frequency interval that is about 1600 times as wide as the bandwidth of the atmospheric signal. We found that the variance contained in the “wind peak” (the peak centered at  $-18$  Hz) is higher by 8.7 dB than the variance contained in the noise of the 144-pulse averages. Because the noise energy of single pulses is 144 times larger than the noise energy in the 144-pulse averages, the SNR is by a factor of 144, or by 21.6 dB, lower than 8.7 dB. That is, the SNR in our measurement example is  $-12.9$  dB.

As stated above, in our measurement example the peak spectral density of the clear-air signal is 23 dB above the noise floor, such that the clear-air peak were still 3 dB above the noise floor if the SNR were by 20 dB lower. In other words, the RWP could provide meaningful wind estimates for SNRs as low as  $-32.9$  dB. Moreover, if the bandwidth of the clear-air signal were only 1 Hz (instead of order 10 Hz, as in our example), which is not uncommon under low-turbulence conditions and for shorter dwell times, then the Lindenberg 482-MHz RWP could provide meaningful wind data even if the SNR were as small as  $-42.9$  dB.

The main reason why RWPs can provide meaningful data at extremely low SNRs is that the bandwidth of the clear-air signal is typically by three or more orders of magnitude smaller than the very wide Nyquist interval associated with the very short pulse-repetition period.

Ground clutter has a peak spectral density that often exceeds the clear-air peak spectral density. In that case,

ground clutter can be separated from the atmospheric signal only if, as in Figures 3 and 4, their spectra do not overlap.

## 2.4 Radio-wave propagation theory: Backscattered power from turbulent refractive-index perturbations in the optically clear air

RWP signals can be fully understood only on the basis of the theory of radio-wave propagation through the turbulent atmosphere. This theory, pioneered by TATARSKII (1961), is a synthesis of Maxwell’s electromagnetic theory and classical turbulence theory (KOLMOGOROV, 1941; BATCHELOR, 1953).

For single scatter, that is, under the assumption that the first-order Born approximation is valid, the instantaneous clear-air signal  $I(t)$  is unambiguously determined by the field of the instantaneous refractive-index perturbations,  $n(\mathbf{x}', t)$ , in the RWP’s resolution volume through an equation of the form

$$I(t) = \iiint G(\mathbf{x}') n(\mathbf{x}', t) d^3x' \quad (2.6)$$

(e.g., TATARSKII, 1961; DOVIAK and ZRNIC, 1984), where  $G(\mathbf{x}')$  is a complex-valued instrument function, or “sampling function” that does not vary with time. DOVIAK and ZRNIC (1984) put forward a closed-form model for  $G(\mathbf{x}')$  which is a good approximation for a wide range of RWP applications.

While DOVIAK and ZRNIC (1984), and recently MUSCHINSKI (2004), discuss the power

$$P_r = \frac{R}{2} \langle |I|^2 \rangle \quad (2.7)$$

of the backscattered pulse measured at the receiver output (here  $R$  is the receiver resistance) by means of Eq. (2.6), the traditional approach by TATARSKII (1961) is slightly different. TATARSKII (1961, chapter 4) considered the electric field vector associated with a plane wave travelling through a small test volume  $V$  and used Maxwell’s equations to find the field vector of the wave scattered into a particular direction  $\mathbf{m}$  (TATARSKII, 1961, p. 63, eq. 4.8). Then he derived the mean intensity of the scattered wave and derived an equation for the scattering cross-section increment  $d\sigma$  for the wave scattered from the scattering volume  $V$  into a solid-angle increment  $d\Omega$  in the direction  $\mathbf{m}$ :

$$d\sigma = 2\pi k_0^4 V \sin^2 \chi \Phi_{mm}(\mathbf{k}_0 - k_0 \mathbf{m}) d\Omega \quad (2.8)$$

(TATARSKII, 1961, p. 68, eq. 4.19), where  $k_0 = 2\pi/\lambda$  is the wave number of both the incident wave and the scattered wave,  $\chi$  is the angle between the electromagnetic field vector of the incident wave and the propagation direction  $\mathbf{m}$  of the scattered wave,  $\mathbf{k}_0$  is the wave vector

of the incident wave,  $\mathbf{m}$  is the wave vector of the scattered wave, and  $\Phi_{nm}(\mathbf{k})$  is the three-dimensional, spectral density of refractive-index variance at the wave vector  $\mathbf{k}$ . For backscatter, we have  $\chi = 90^\circ$  (the field vector is perpendicular to the propagation path) and  $\mathbf{k}_0 - k_0\mathbf{m} = 2\mathbf{k}_0$ . The magnitude of the “Bragg wave vector”  $2\mathbf{k}_0$  is usually referred to as the Bragg wave number,

$$k_B = 2k_0 = \frac{4\pi}{\lambda}. \quad (2.9)$$

If the refractive-index perturbations are statistically isotropic at a particular wave number  $k$ , and if  $k$  lies within the inertial subrange of the refractive-index turbulence, both of which are common, although not unchallenged assumptions for atmospheric refractive-index perturbations at wavelengths of 1 m or shorter (e.g., MUSCHINSKI and WODE, 1998; LUCE et al., 2001a; MUSCHINSKI and LENSCHOW, 2001; BALSLEY et al., 2003), then  $\Phi_{nm}(\mathbf{k})$  depends only on the magnitude  $k$  of the wave vector and is proportional to the refractive-index structure parameter  $C_n^2$ :

$$\Phi_{nm}(\mathbf{k}) = \frac{\Gamma(8/3) \sin(\pi/3)}{4\pi^2} C_n^2 k^{-11/3} = 0.0330 C_n^2 k^{-11/3} \quad (2.10)$$

(TATARSKII, 1961, p. 48, eq. 3.24).

It has become common practice to quantify the ratio between incident and backscattered intensity in terms of the volume reflectivity

$$\eta = \frac{1}{V} \frac{d\sigma_b}{d\Omega/4\pi}, \quad (2.11)$$

where  $d\sigma_b$  is the cross-section increment for backscatter, i.e.,  $\chi = 90^\circ$  and  $\mathbf{k}_0 - k_0\mathbf{m} = 2\mathbf{k}_0$ . Inserting (2.8) leads to

$$\eta = 8\pi^2 k_0^4 \Phi_{nm}(2\mathbf{k}_0). \quad (2.12)$$

If the volume  $V$  is filled with refractive-index turbulence that is isotropic at the Bragg wave number and homogeneous across the volume  $V$ , and if  $2k_0$  lies in the inertial subrange, then (2.10) is valid and one obtains

$$\eta = 0.379 C_n^2 \lambda^{-1/3}. \quad (2.13)$$

This relationship follows immediately from Tatarskii’s analysis, as just shown, but is usually credited to OTTERSTEN (1969) who, to the best of our knowledge, was the first to present the relationship between  $\eta$  and  $C_n^2$  in the form of Eq. (2.13).

The advantage of the DOVIAK and ZRNIC (1984) approach is that it avoids the concept of a local scattering cross section, which may cause problems if the refractive-index correlation lengths are not small compared to the Fresnel length. This was recently pointed out by TATARSKII (2003), who now strongly questions

his earlier approach. MUSCHINSKI (2004), however, found that both approaches, that is, the Fraunhofer approximation (TATARSKII, 1961) and the Fresnel approximation (DOVIAK and ZRNIC, 1984), lead to the same result, namely to Eq. (2.13), if the refractive-index perturbations are Bragg-isotropic, which in many cases is a valid assumption, in particular for UHF RWPs operating in the atmospheric boundary layer.

## 2.5 Combining radio-wave propagation theory with basic fluid dynamics: The relationship between Doppler shift and radial wind velocity

The main purpose of a radar wind profiler is to measure vertical profiles of the three components,  $u$ ,  $v$ , and  $w$ , of the wind vector. The standard procedure is the so-called Doppler beam swinging (DBS) technique, where the radial wind velocity,  $v_r$ , is measured in at least three non-coplanar beam directions, and  $u$ ,  $v$ , and  $w$  are retrieved from the  $v_r$  measurements by means of elementary trigonometric relationships. For a given beam direction,  $v_r$  is obtained through

$$\omega_D = -k_B v_r, \quad (2.14)$$

where

$$\omega_D = \frac{\int \phi(\omega) \omega d\omega}{\int \phi(\omega) d\omega} \quad (2.15)$$

is the Doppler shift. In the measurement example discussed in Section 2, the radar wavelength was 62 cm and the Doppler shift was  $-18$  Hz, such that  $v_r = +5.6$   $\text{m s}^{-1}$ . A negative Doppler shift and a positive  $v_r$  means that the air moves away from the radar.

For more than two decades, the  $v_r$ - $\omega_D$  relationship, (2.14), has been the key equation for operational RWP. Eq. (2.14) can be derived easily based on the assumption that the scattering volume is populated by point scatterers that are advected with the wind velocity. In the case of scatter from turbulence, however, which is the usual case for RWP applications, there are no point scatterers. Instead, the scattering volume is filled with a continuous refractive-index field that is random in time and space and is usually characterized by horizontal correlation lengths that are large compared to the size of the scattering volume and by correlation times that are long compared to the dwell time.

Although it is obvious that the point-scatterers assumption is invalid for most RWP applications, for more than two decades, the RWP community has taken the validity of (2.14) for granted. Doubts that (2.14) might be incomplete or erroneous have come from different sources. HOCKING et al. (1986) showed that Bragg-anisotropy, which is common for echoes observed with VHF radars at near-zenith directions and

is known as ‘‘VHF aspect sensitivity,’’ leads to erroneous radial wind velocities, and they suggested a correction formula. NASTROM and VAN ZANDT (1994) found that long-term averages of vertical velocities observed with vertically pointing VHF radars usually show a downward bias of a few centimeters per second, and they explained this bias with a negative covariance between vertical-velocity fluctuations and radar-reflectivity fluctuations resulting from upward-propagating gravity waves. MUSCHINSKI (1996) offered an alternative explanation: Bragg-anisotropic features associated with Kelvin-Helmholtz billows in the shear regions of upper-level jet streams lead to a downward bias in the lower shear region and an upward bias in the upper shear region. Recently, the upward bias hypothesized by MUSCHINSKI (1996) was observed by YAMAMOTO et al. (2003).

To the best of our knowledge, MUSCHINSKI (1998) was the first to use the basic equation for single scatter, (2.6), to investigate the validity of the traditional  $v_r$ - $\omega_D$  relationship (2.14) for the case of scatter from turbulent refractive-index perturbations advected by a turbulent wind field. He found that in general,  $\omega_D$  is the sum of three parts: first, the mean-wind contribution,  $-k_B v_r$ , which is the only term that appears in the traditional  $v_r$ - $\omega_D$  relationship (2.14); second, a term that is proportional to the Bragg-component of the spatial quadrature spectrum of radial-wind and refractive-index perturbations, a term that TATARSKII and MUSCHINSKI (2001) later called the ‘‘correlation velocity;’’ and a third term that is proportional to the covariance of  $v_r$  perturbations and  $\eta$  perturbations, or, in other words, proportional to the radial flux of clear-air radar reflectivity.

Recently, MUSCHINSKI (2004) expanded and generalized the earlier analysis (MUSCHINSKI, 1998) and found for the  $m$ th moment of the Doppler spectrum,  $M_{11}^{(m)}$ , the equation

$$M_{11}^{(m)} = \frac{1}{i^m} \iiint \iiint G_{11}(\mathbf{x}', \mathbf{x}'') R_{nn}^{(m)}(\mathbf{x}', \mathbf{x}'') d^3 x' d^3 x'', \quad (2.16)$$

where

$$R_{nn}^{(m)}(\mathbf{x}', \mathbf{x}'') = \left\langle n(\mathbf{x}') \frac{\partial^m}{\partial t^m} n(\mathbf{x}'') \right\rangle \quad (2.17)$$

is the two-point, cross-covariance function of the refractive index and of the  $m$ th local time derivative of the refractive index, and where

$$G_{11}(\mathbf{x}', \mathbf{x}'') = G_1^*(\mathbf{x}') G_1(\mathbf{x}'') \quad (2.18)$$

is a new instrument function.

MUSCHINSKI (2004) studied  $R_{nn}^{(1)}(\mathbf{x}', \mathbf{x}'')$  and  $R_{nn}^{(2)}(\mathbf{x}', \mathbf{x}'')$  based on simplifying assumptions like the random Taylor hypothesis. Much further work,

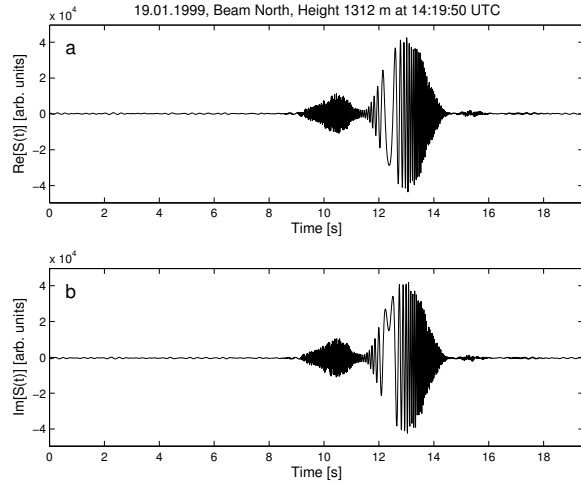


**Figure 5:** Time series of the in-phase (a) and quadrature (b) component of an RWP signal with severe aircraft echo contamination.

however, needs to be done to systematically investigate the functions  $R_{nn}^{(m)}(\mathbf{x}', \mathbf{x}'')$ , which would be the basis of a full understanding of the higher moments of RWP Doppler spectra.

## 2.6 Non-stationary clutter and time-frequency decomposition

Aircraft, birds, and moving objects on the ground may severely contaminate RWP signals. Often their echo intensity exceeds the clear-air echo intensity by several orders of magnitude, and their radial velocities may vary from centimeters per second to tens (birds, cars) or even hundreds of meters per second. An important feature of this type of clutter is that its Doppler frequency may change significantly during the dwell time. As we will see, these so-called transient or non-stationary signals can be resolved sufficiently well neither in time domain nor in frequency domain.

An example of a signal that is severely contaminated by an aircraft echo is given in Figure 5. The transient airplane clutter between  $t = 9$  s and  $t = 16$  s is much stronger than the clear-air echoes, which are not resolved in the figure. This contamination shows a typical variation in amplitude with distinct maxima and minima. This amplitude variation is a direct result of the antenna radiation pattern of the RWP. A calculated pattern for the Lindenberg 482-MHz RWP is shown in Figure 6. Assume that a hard target with constant radar reflectivity is moving through the RWP antenna beam. It will necessarily experience a varying illumination which in turn will lead to a varying echo amplitude. The observed amplitude modulation will therefore depend on the real radiation pattern of the antenna, the flight trajectory, and the speed of this target. A simple theoretical model for an airplane return was given by BOISSE et al. (1999).

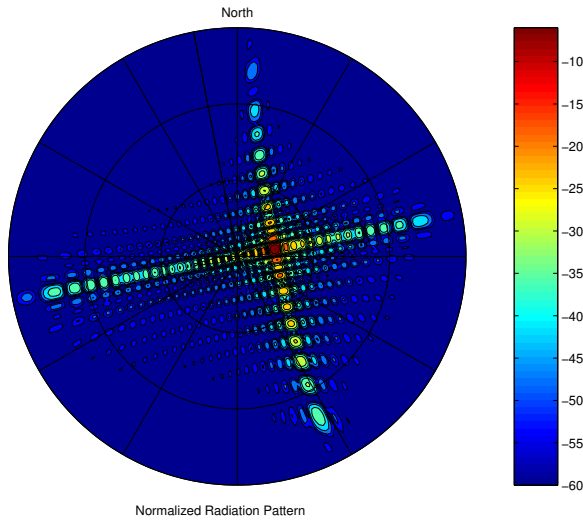


**Figure 6:** Ideal antenna radiation pattern of the east beam of the Lindenbergl 482 MHz RWP.

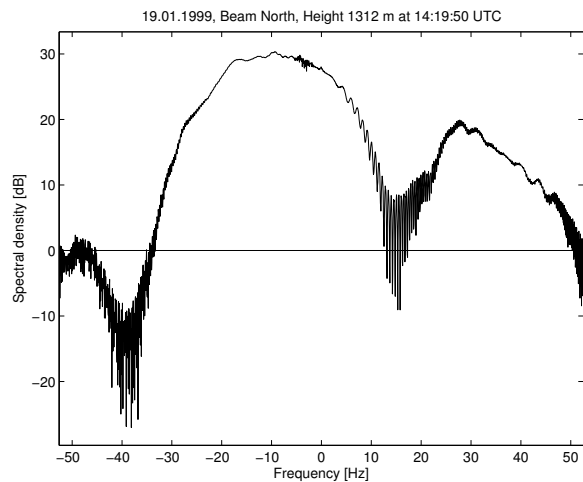


**Figure 7:** Frequency spectrum of the signal shown in Figure 5.

The frequency spectrum of the contaminated signal is depicted in Figure 5. Because of the transient nature of the aircraft echo, the clutter signal occupies a fairly wide frequency range, and it is nearly impossible to identify the clear-air component in the spectrum. The noise level at 0 dB computed with the algorithm by HILDEBRAND and SEKHON (1974) does not make much sense here, since noise is completely dominated by the airplane echo. It is obvious that neither the time series nor the spectrum is an adequate representation to characterize the properties of this signal.

Generally, time representation (sampled data) and frequency representation (Fourier transformed signal) are two alternative ways of looking at the same piece of information. The time representation offers the highest resolution in time, but there is no frequency resolu-

tion. That means two signal components can still be distinguished even if their energy is concentrated within a very short, but non-overlapping period of time, no matter what frequency information the two components carry. On the other hand, if two components overlap in time, they cannot be distinguished, even if their energy is concentrated at different frequencies. Also, it is difficult to read the desired frequency information from a pure time-domain representation.

Frequency representation possesses the highest possible frequency resolution, but there is no time resolution. For transient signals such as airplane echoes, neither representation is optimal, as we will see in the following example.

We construct a simple test signal consisting of two components: A (stationary) harmonic wave  $s_1(t)$  and a (non-stationary) damped linear chirp  $s_2(t)$  are added to yield the two-component signal  $s(t)$ :

$$\begin{aligned} s(t) &= s_1(t) + s_2(t) \\ &= \exp(2\pi i f_0 t) \\ &\quad + 100 \exp\left(-\frac{t^2}{2\sigma^2}\right) \exp\left(2\pi i \cdot \frac{1}{2} at^2\right), \end{aligned} \tag{2.19}$$

where we choose the constant frequency  $f_0 = 3$  Hz, the angular acceleration  $a = 0.6 \text{ Hz}\cdot\text{s}^{-1}$  and the damping factor  $\sigma = 5$  s. The signal  $s$  and its Fourier spectrum are shown in Figures 8 and 9, respectively. Since  $s_2$  exceeds  $s_1$  by two orders of magnitude,  $s_1$  is no longer visible in the time series plot. In the frequency spectrum,  $s_1$  is observed as a small kink at  $f_0 = 3$  Hz. The instantaneous frequency of an analytic signal  $s(t) = A(t) \exp[i\Phi(t)]$  is defined as  $f_{\text{inst}}(t) = \frac{1}{2\pi} \frac{d}{dt} [\Phi]$  (HLAWATSCH and BOUDREAU-BARTELS, 1992; BOASHASH, 1992; FLANDRIN, 1999). For the non-stationary component  $s_2$ , we obtain  $f_{\text{inst}}(t) = \frac{d}{dt} \left(\frac{1}{2} at^2\right) = at$ . Because the instantaneous frequency changes in time, the signal energy is spread over the whole axis in both time and frequency domain. In neither time, nor frequency representation,  $s_1$  and  $s_2$  can be separated easily.

A better way to facilitate the understanding of such signals is provided by so-called time-frequency (TF) representations. The most prominent TF representations are linear, like the short-time or windowed Fourier transform (WFT) or wavelet transforms.<sup>1</sup> Other TF representations are quadratic, such as the spectrogram, the scalogram or the Wigner-Ville distribution (COHEN, 1989; HLAWATSCH and BOUDREAU-BARTELS, 1992; FLANDRIN, 1999).

Time-frequency representations are yet another way of looking at a signal; they are a compromise between

<sup>1</sup>Wavelet transforms are usually referred to as a time-scale representation, where scale is the reciprocal of frequency.

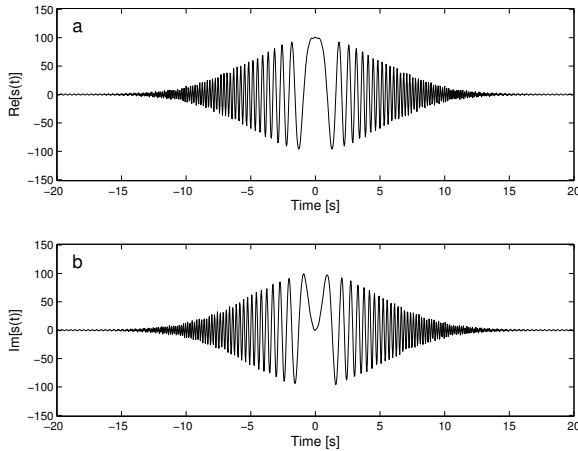


**Figure 8:** In-phase (a) and quadrature (b) component of test signal  $s$ .

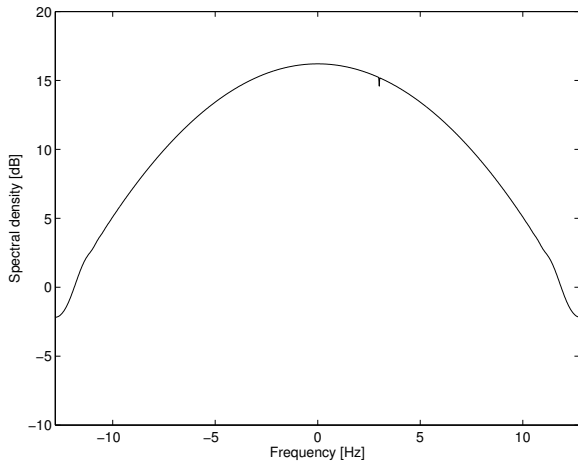


**Figure 9:** Frequency spectrum of the test signal  $s$ .

time and frequency representation. If properly chosen, linear TF representations contain exactly the same amount of information, and the original signal can be stably reconstructed. Here we will concentrate on the WFT having these properties. Other successful attempts using wavelet methods for filtering RWP signals have already been made (JORDAN et al., 1997; BOISSE et al., 1999; LEHMANN and TESCHKE, 2001; JUSTEN et al., 2004).

The WFT maps an univariate signal  $s(t)$  to a bivariate function  $F_s(t, f)$ . Time resolution can be traded for frequency resolution but both resolutions cannot be made arbitrarily high at the same time. The WFT using a Gaussian window function offers optimal time-frequency resolutions (GABOR, 1946; MALLAT, 1999). Thus, we will use this type of window.

Figure 10 shows a spectrogram of the signal  $s$  in (2.19). A spectrogram is defined as the squared absolute value of the WFT  $F_s(t, f)$ . This gives — similarly to

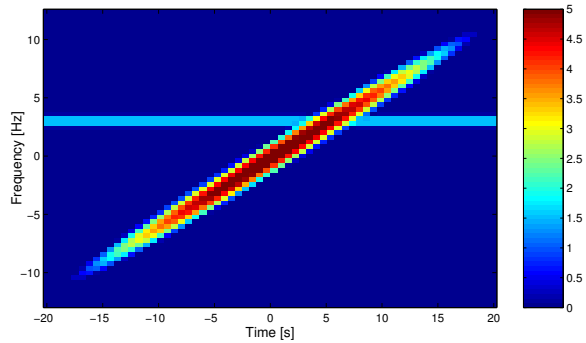


**Figure 10:** Spectrogram of the test signal  $s$ .

the Fourier spectrum — a measure of signal energy. The stationary part  $s_1$  appears as a horizontal line at  $f_0 = 3$  Hz. The non-stationary part  $s_2$  is visible as an inclined line with slope  $a = 0.6 \text{ Hz s}^{-1}$ . Note that the overlap of  $s_1$  and  $s_2$  is rather small. Thus, both parts can now be easily separated.

The airplane echo shown in the beginning of this Section has a structure similar to the transient signal  $s_2$ . Thus, we exemplarily show how it is possible to remove  $s_2$ , while at the same time keeping the stationary part  $s_1$ . Figure 11 schematically explains our method. For fixed  $\bar{f}$ , one "row"  $F_s(\cdot, \bar{f})$  shows a large peak at a time where the instantaneous frequency  $f_{\text{inst}}(t) = at$  of the transient component  $s_2$  meets  $\bar{f}$ . However, the stationary part  $s_1$  does not produce such a peak since it does not change frequency in time. When  $\bar{f}$  happens to match the frequency  $f_0$  of  $s_1$ , the overall level of  $F_s(\cdot, \bar{f})$  will be larger, but there will be no peak. Hence, by removing the peaks in every row of the WFT and setting the corresponding coefficients to zero, we completely remove the transient part. The stationary part is left almost unaffected. Only small parts of  $s_1$  are removed, namely, where  $s_1$  and  $s_2$  overlap. Note that for clarity, Figure 11 only shows the real part of the spectrogram. The actual filtering is carried out on the complex WFT.

A filtered signal can now be reconstructed from the filtered WFT. Figures 12 and 13 show the filtered signal and its Fourier spectrum. The filtered signal clearly resembles the sinusoidal wave  $s_1$  up to a certain neighborhood of  $t = f_0/a = 5$  s, where some parts have been accidentally removed. In the Fourier spectrum, we see a peak at  $f_0 = 3$  Hz. Nothing is left from the non-stationary component  $s_2$ .

We will now apply these ideas to the contaminated signal given in Figure 5. Figure 14 shows a spectrogram of this signal. Due to their stationary nature, ground clutter and clear-air signal appear as *horizontal* lines at 0 Hz and  $-4$  Hz, respectively. A strong airplane echo emerges as *diagonal* lines from  $t = 6$  s to  $t = 18$  s. The more pronounced falling diagonal is the actual airplane echo. Its slope is directly related to the *change* of radial velocity

of the airplane (BOISSE et al., 1999), which is significant in the measurement period. The crossing of different radar antenna side lobes results in an oscillatory amplitude behaviour. The falling diagonal is aliased at  $t = 9$  s and  $t = 16$  s.

The raising diagonal, which is an attenuated and mirrored version of the falling one, is an echo phantom (the so-called “mirror image”) resulting from imperfect quadrature of  $I$  and  $Q$  in the receiver (DOVIÁK and ZRNÍČ, 1993).

In Figures 15 to 17, the filtered spectrogram, the filtered signal and the filtered Fourier spectrum are presented. The strong airplane echo from  $t = 9$  s to  $t = 16$  s (compare Figure 5) has vanished. The clear-air signal, which could only be observed as a small oscillation at  $-4$  Hz in the unfiltered spectrum, now dominates the Fourier spectrum. A smaller ground-clutter peak has also been revealed.

It is especially remarkable that the method performs so well even though the signal-to-clutter ratio (computed from the original and filtered spectrum) is  $-32$  dB, which is a result of the TF representation’s ability to separate transient and stationary components. This is closely related to its time–frequency resolution, which is optimal for the WFT using a Gaussian window. Thus, this method is particularly suitable for intermittent clutter filtering.

Note that in contrast to intermittent clutter, both ground clutter and the clear-air signal are stationary. Therefore, it does not seem to make sense to address the problem of ground clutter filtering with time–frequency methods. Fourier methods seem to be more appropriate here.

### 3 Two-signal radar wind profiling

In the previous section, we described several aspects of a single signal measured with an RWP. Modern RWP, however, offers the possibility to sample the same scattering volume with different sampling functions at the same time. In this section, we consider the additional information that can be extracted from the *cross-covariance function* and the *cross-spectrum* of two signals,

$$I_1(t) = \iiint G_1(\mathbf{x}') n(\mathbf{x}', t) d\mathbf{x}' \quad (3.1)$$

and

$$I_2(t) = \iiint G_2(\mathbf{x}'') n(\mathbf{x}'', t) d\mathbf{x}'' \quad (3.2)$$

where  $G_1(\mathbf{x}')$  and  $G_2(\mathbf{x}'')$  are two different sampling functions that overlap in space in some well-defined and well-designed fashion. Before we discuss properties of and design criteria for the sampling functions in more detail, we consider the cross-covariance function

$$C_{12}(t, \tau) = \langle I_1^*(t) I_2(t + \tau) \rangle. \quad (3.3)$$

Here, the angular brackets stand for the ensemble average.

#### 3.1 Cross-covariance function and cross-spectrum of two RWP signals

In general,  $C_{12}(t, \tau)$  is a function of both time  $t$  and time lag  $\tau$ . For many RWP applications, however, it is a valid assumption that  $I_1(t)$  and  $I_2(t)$  are statistically stationary during the dwell time, such that  $C_{12}$  is a function only of  $\tau$ . Then we have

$$C_{12}(\tau) = \iiint \iiint G_{12}(\mathbf{x}', \mathbf{x}'') R_{nn}^{(0)}(\mathbf{x}', \mathbf{x}'', \tau) d^3x' d^3x'', \quad (3.4)$$

where

$$G_{12}(\mathbf{x}', \mathbf{x}'') = G_1^*(\mathbf{x}') G_2(\mathbf{x}'') \quad (3.5)$$

is the combined sampling function and

$$R_{nn}^{(0)}(\mathbf{x}', \mathbf{x}'', \tau) = \langle n(\mathbf{x}', t) n(\mathbf{x}'', t + \tau) \rangle \quad (3.6)$$

is the spatial autocovariance function of the refractive index.

In full analogy to the definition of the Doppler spectrum in the single-signal case, we now define the Doppler cross-spectrum for the two-signal case:

$$\phi_{12}(\omega) = \frac{1}{2\pi} \int C_{12}(\tau) \exp(-i\omega\tau) d\tau. \quad (3.7)$$

As in the single-signal case, the lowest spectral moments are of particular interest. The  $m$ th cross-spectral moment is

$$M_{12}^{(m)} = \int \phi_{12}(\omega) \omega^m d\omega. \quad (3.8)$$

According to the moments theorem – a derivation for complex-valued signals can be found in Appendix A of MUSCHINSKI (2004) –, the  $m$ th moment is (apart from the phase factor  $i^m$ ) equal to the  $m$ th  $\tau$ -derivatives of  $C_{12}(\tau)$  at zero time lag:

$$M_{12}^{(m)} = \frac{1}{i^m} \left. \frac{\partial^m}{\partial \tau^m} C_{12}(\tau) \right|_{\tau=0}. \quad (3.9)$$

It is straightforward (MUSCHINSKI, 2004) to express the spectral moments in terms of  $G_{12}(\mathbf{x}', \mathbf{x}'')$  and  $R_{nn}^{(m)}(\mathbf{x}', \mathbf{x}'')$ :

$$M_{12}^{(m)} = \frac{1}{i^m} \iiint \iiint G_{12}(\mathbf{x}', \mathbf{x}'') R_{nn}^{(m)}(\mathbf{x}', \mathbf{x}'') d\mathbf{x}' d\mathbf{x}'', \quad (3.10)$$

where  $R_{nn}^{(m)}(\mathbf{x}', \mathbf{x}'')$  is the spatial cross-covariance function of the refractive index and the  $m$ th local time derivative of the refractive index, as introduced in Section 2.5. Note that all spectral moments are unambiguously described by a *purely spatial* refractive-index statistic.

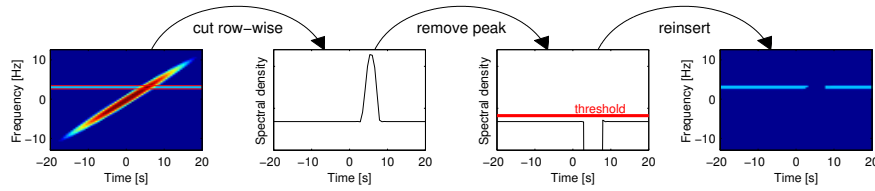


**Figure 11:** Filtering process. Transient signal components induce peaks in rows of the spectrogram (second from left). They are removed by a thresholding process (second from right), where the threshold is automatically selected from each row. The filtered spectrogram (right) or rather the filtered WFT is reconstructed to a filtered time series.

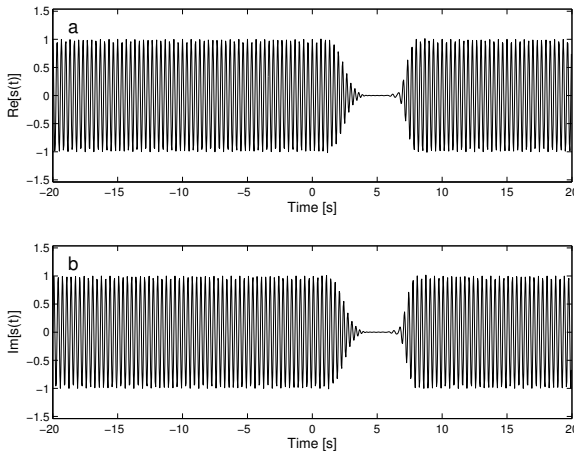


**Figure 12:** Filtered signal, reconstructed from the filtered WFT (see Figure 11).

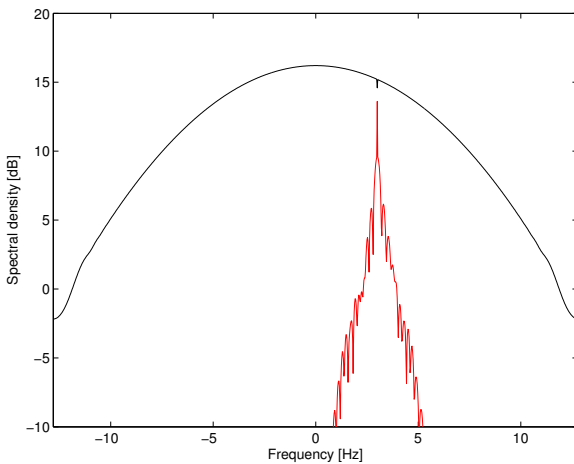


**Figure 13:** Fourier spectrum of the original signal  $s$  (black) and spectrum of the corresponding filtered signal (red).

### 3.2 Two-signal RWP techniques

The general equation (3.10) can now be applied to various families of instrument functions  $G_{12}(\mathbf{x}', \mathbf{x}'')$ . These families are associated with different “two-signal RWP techniques”. The different  $G_{12}(\mathbf{x}', \mathbf{x}'')$  families are distinguished by how the two sampling functions  $G_1(\mathbf{x}')$

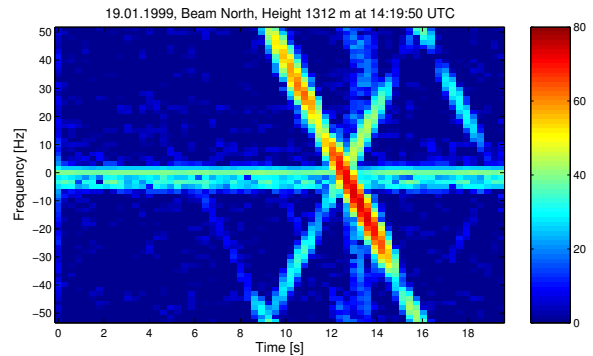


**Figure 14:** Spectrogram of the signal shown in Figure 5.

and  $G_2(\mathbf{x}'')$  differ from each other. The two techniques that so far have been used most often are the frequency-domain interferometry (FDI) and the spaced-antenna (SA) technique, which we describe first. Later, we discuss the outlook for using other possibilities to take advantage of two-signal RWP.

FDI was first implemented by KUDEKI and STITT (1987) at the Jicamarca VHF radar. The idea is to sample the same scattering volume simultaneously and phase-coherently with two (slightly) different Bragg wavelengths. This requires operating the radar with two different carrier frequencies,  $f_1$  and  $f_2$ . FDI enables one to retrieve two parameters that cannot be measured with single-signal RWP: the radial location of a (single) localized scatterer (or scattering layer) within the pulse volume and the radial extent, or thickness, of the scatterer or scattering layer. While the phase of the (complex) signal covariance  $C_{12}(\tau = 0)$  provides the location, the magnitude of  $C_{12}(\tau = 0)$  gives the thickness.

FDI has been successfully used to observe the structure and evolution of features whose height extent is small compared to the radar’s pulse length. CHILSON et al. (1997) were the first to use FDI to track upper-tropospheric Kelvin-Helmholtz billows with a height resolution of about twenty meters, although the pulse length, which defines the range resolution for single-signal RWP, was as large as 300 m. MUSCHINSKI et al. (1999) were the first to apply FDI for the observation of the slow downward motion of long-lived layers in the free troposphere. In general, the local temporal rate of

change of layer height is dominated by the horizontal advection of a tilted layer. But in a time-height window where the horizontal wind speed was very small, MUSCHINSKI et al. (1999) retrieved the same downward velocity of  $2 \text{ cm s}^{-1}$  from three independent sources: the temporal change of FDI-retrieved layer height, the single-signal Doppler shifts, and the vertical motion diagnosed with a regional weather forecasting model. The magnitude and sign of that small vertical velocity was consistent with the subsidence associated with the high-pressure area that characterized the lower troposphere above the radar site at the observation time. Both the CHILSON et al. (1997) study and the MUSCHINSKI et al. (1999) study were carried out in the Harz Mountains in Northern Germany, using the SOUSY VHF radar operated by the Max-Planck Institut für Aeronomie in Katlenburg-Lindau. (SOUSY stands for “Sounding System”.)

The SA technique takes advantage of the possibility to observe the backscattered echo simultaneously with different receiving antennas (e.g., DOVIK et al., 1996). For typical SA applications, the beam axes of the transmitting antenna and of the various receiving antennas are all vertical. Two signals  $I_1$  and  $I_2$  measured with receiving antennas R1 and R2 are highly correlated if the (horizontal) spacing between R1 and R2 is small. In the limit of zero spacing, R1 and R2 are identical, such that  $I_1 = I_2$ , and the problem reduces to the single-signal case. The correlation decreases rapidly with increasing spacing. There is an optimum spacing, for which the energy in the imaginary part of  $\phi_{12}(\omega)$ , i.e., in the quadrature spectrum, reaches a maximum. While the normalized first moment of the co-spectrum (i.e., the real part of  $\phi_{12}(\omega)$ ), provides the vertical velocity, the first normalized moment of the quadrature spectrum gives the “baseline wind,” i.e., the component of the wind velocity vector along the direction of the horizontal spacing vector between R1 and R2. According to the moments theorem, the first moment of the quadrature spectrum is (apart from the factor  $i$ ) identical to the slope of the imaginary part of  $C_{12}(\tau)$  at  $\tau = 0$ . It is not clear why practically all researchers using the SA technique retrieve the baseline winds from  $C_{12}(\tau)$  (e.g., LATITIS et al., 1995) and not from  $\phi_{12}(\omega)$ .

The SA technique has various advantages and disadvantages as compared to the widely used DBS technique. The two main advantages of the SA technique are the possibility to retrieve all three wind components from the same scattering volume, which makes SA less sensitive to errors induced by small-scale, horizontal inhomogeneity of the vertical wind (such inhomogeneity is known to severely affect DBS wind measurements; see, e.g., WEBER et al., 1992), and the lack of the need to use off-zenith beam directions. Disadvantages include the need to receive multiple signals simultaneously, the

smaller signal-to-noise ratio, and the higher vulnerability to fading ground clutter. No consensus has yet been reached in the RWP community as to whether the DBS or the SA technique is to be preferred for operational purposes.

Other, more exotic two-signal RWP techniques are conceivable: sampling the same scattering volume with two different pulse lengths and/or receiver bandwidths; sampling the same volume simultaneously with two slightly different beam directions; or sampling the same volume simultaneously with two different beamwidths. It seems that none of these possibilities has been thoroughly explored so far.

## 4 Multi-signal radar wind profiling

As a generalization of single-signal or two-signal wind profiling, meteorological information can be extracted from the covariance matrix or the cross-spectral moment matrix of multiple signals  $S_j$ ,  $j = 1, \dots, J$ , which characterize the same scattering volume during the same time. It is important that the  $J$  signals are sampled phase-coherently and with a sampling period that is short compared to the correlation time of the clear-air component. There are various radar parameters with respect to which these signals may be different from each other but still represent structure and dynamics in the same volume of air. These parameters include the carrier frequency, the location of the receiving antenna, the center of the range gate, and the pulse length.

### 4.1 Optimization of the sampling function

For a monostatic radar, the sampling function  $G(\mathbf{x})$  in the far field is given by

$$G(\mathbf{x}) = A(\mathbf{x}) \exp[-i\beta|\mathbf{r}_0 + \mathbf{x}|] \quad (4.1)$$

(DOVIK and ZRNIC, 1984; MUSCHINSKI, 2004), where  $A(\mathbf{x})$  is a three-dimensional amplitude weighting function that defines the sampling volume,  $\beta$  is the Bragg wavenumber,  $\mathbf{r}_0$  is the vector pointing from the center of the sampling volume to the antenna center, and  $\mathbf{x}$  is the location relative to the center of the sampling volume.

Now, assume that a set of  $J$  phase-coherent signals

$$I_j(t) = \iiint G_j(\mathbf{x}') n(\mathbf{x}', t) d^3x', \quad (4.2)$$

is available, where we assume that in general the  $G_j(\mathbf{x}')$  differ from each other only with respect to the Bragg wavenumber  $\beta_j$ , the three-dimensional envelope of the pulse, and the range:

$$G_j(\mathbf{x}') = A_j(\mathbf{x}') \exp[-i\beta_j|\mathbf{r}_j + \mathbf{x}'|]. \quad (4.3)$$

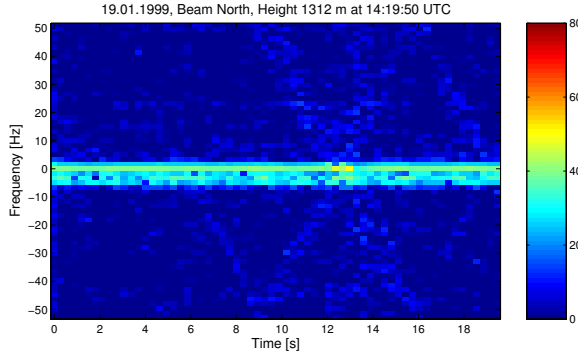


Figure 15: Spectrogram after removal of the aircraft clutter.

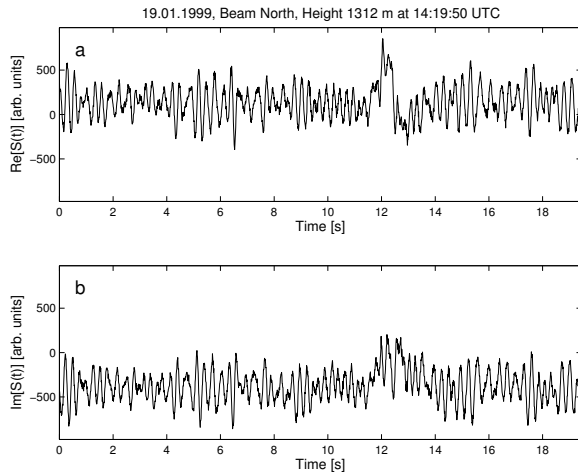


Figure 16: Signal, reconstructed from the filtered WFT (spectrogram shown in Figure 15).

For complex-valued weight coefficients  $w_j$  ( $j = 1, \dots, J$ ) we may consider the “synthesized” signal

$$I(t) = \sum_{j=1}^J w_j I_j(t), \quad (4.4)$$

which can be written in the same form as the integral for  $I_j(t)$ ,

$$I(t) = \iiint G(\mathbf{x}') n(\mathbf{x}', t) d^3x', \quad (4.5)$$

where

$$G(\mathbf{x}') = \sum_{j=1}^J w_j G_j(\mathbf{x}').$$

Here we assume that the refractive-index perturbations at a fixed location  $\mathbf{x}$  are statistically stationary with respect to time. Note that  $I(t)$  is of the same form as in the standard case, except that now the instrument function  $G(\mathbf{x}')$  can be some arbitrary function in the linear span of  $G_1, \dots, G_J$  because there are *a priori* no constraints with respect to the weighting vector  $w_j$ . Moreover, there

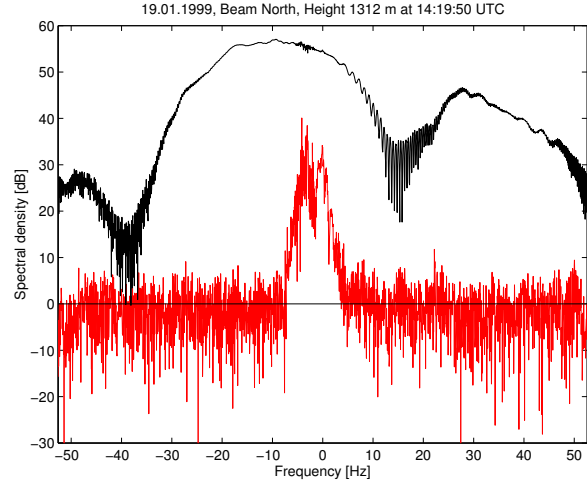


Figure 17: Fourier spectrum of the original RWP signal (black) shown in Figure 5 and spectrum of the corresponding filtered signal (red) from Figure 16.

is nothing that would keep one from choosing  $w_j$  differently for different locations  $\mathbf{x}$ . Then we have

$$I(\mathbf{x}, t) = \sum_{j=1}^J w_j(\mathbf{x}) \iiint G_j(\mathbf{x}') n(\mathbf{x}', t) d^3x'. \quad (4.6)$$

That is, based on the finite set of  $J$  signals  $I_j$  that characterize a given scattering volume, we are now in the position to synthesize an infinite set of new signals  $I(\mathbf{x}, t)$  by means of (4.6). Because  $w_j(\mathbf{x})$  can be freely chosen, there is no constraint for the spatial variability of  $I(\mathbf{x}, t)$  within the same scattering volume. The *general problem* is how to find the  $w_j(\mathbf{x})$  that allows us to retrieve meteorological information with *maximum accuracy*.

In order to attack this problem, we assume that the weight vector  $\mathbf{w}(\mathbf{x}) = (w_1(\mathbf{x}), \dots, w_J(\mathbf{x}))$  is complex valued; i.e.  $w_j(\mathbf{x}) = W_j(\mathbf{x}) \exp(i\varphi_j(\mathbf{x}))$ , such that  $W_j(\mathbf{x}) \in \mathbf{R}$  with  $\sum_{j=1}^J W_j(\mathbf{x}) = 1$  point-wise for all  $\mathbf{x}$ . The main constraint for the weighting vector follows from the assumption that at  $\mathbf{x}' = \mathbf{x}$ , the components  $w_j(\mathbf{x}) G_j(\mathbf{x})$  shall constructively interfere. Here,  $\mathbf{x}$  is the location “to be imaged.” This leads (modulo a factor  $2\pi$ ) to

$$\begin{aligned} \exp(i\varphi_j(\mathbf{x})) \exp[-i\beta_j|\mathbf{r}_j + \mathbf{x}|] &= 1, \\ \text{or equivalently } \varphi_j(\mathbf{x}) &= \beta_j|\mathbf{r}_j + \mathbf{x}| \end{aligned} \quad (4.7)$$

for  $j = 1, \dots, J$ . This results in the condition

$$\mathbf{e}^H(\mathbf{x}) \mathbf{w}(\mathbf{x}) = 1, \quad (4.8)$$

where  $\mathbf{e}^H(\mathbf{x}) := (\mathbf{e}^*(\mathbf{x}))^T = (\exp[i\beta_1|\mathbf{r}_1 + \mathbf{x}|], \dots, \exp[i\beta_J|\mathbf{r}_J + \mathbf{x}|])$  is sometimes referred to as the steering vector. The remaining task is to

determine, for any given  $\mathbf{x}$ , the optimum vector  $\mathbf{w}(\mathbf{x})$ . This is achieved by a “side-lobe minimization.” This requires that for a given  $\mathbf{x}$ , the signal variance

$$M_0(\mathbf{x}) \equiv \langle |I(\mathbf{x})|^2 \rangle \quad (4.9)$$

is to be minimized through variation of the  $\mathbf{w}(\mathbf{x})$ .  $M_0(\mathbf{x})$  can be expressed as follows

$$M_0(\mathbf{x}) = \mathbf{w}^H(\mathbf{x})\Psi\mathbf{w}(\mathbf{x}). \quad (4.10)$$

The entries of the signal covariance matrix  $\Psi$  are given by

$$(\Psi)_{jk} = \langle I_j^* I_k \rangle. \quad (4.11)$$

Combining the minimization of (4.9) and condition (4.8), we obtain the following optimization problem

$$\mathbf{w}^H(\mathbf{x})\Psi\mathbf{w}(\mathbf{x}) \rightarrow \min_{\mathbf{w}(\mathbf{x})}, \quad \mathbf{e}^H(\mathbf{x})\mathbf{w}(\mathbf{x}) = 1. \quad (4.12)$$

Since the problem is convex, there exists a minimizer which is given by

$$\mathbf{w}(\mathbf{x}) = \frac{\lambda}{2} \Psi^{-1} \mathbf{e}(\mathbf{x}) \quad (4.13)$$

for some Lagrangian parameter  $\lambda$ . For computational details we refer the reader to the abundant literature, e.g., JUNGNICHEL (1999). In order to fulfill the constraint  $\mathbf{e}^H(\mathbf{x})\mathbf{w}(\mathbf{x}) = 1$ , the parameter  $\lambda$  must satisfy

$$\lambda = \frac{2}{\mathbf{e}^H(\mathbf{x})\Psi^{-1}\mathbf{e}(\mathbf{x})} \quad (4.14)$$

and thus, combining (4.13) and (4.14), the optimal weight vector (and therewith the optimal  $G$ ) is of the form

$$\mathbf{w}(\mathbf{x}) = \frac{\Psi^{-1}\mathbf{e}(\mathbf{x})}{\mathbf{e}^H(\mathbf{x})\Psi^{-1}\mathbf{e}(\mathbf{x})}. \quad (4.15)$$

This is often referred to as the Capon-method.

#### 4.2 Range imaging and coherent radar imaging as examples of multi-signal RWP

Motivated by the success of frequency-domain interferometry (FDI) in resolving thin scattering layers, and based on reasoning similar to what we have described in Section 4.1, PALMER et al. (1999) introduced range imaging (RIM), the multi-signal counterpart of FDI, which is a two-signal RWP technique. The underlying assumption of FDI is that there is only one scattering layer in a given resolution volume. RIM does not require that assumption to be fulfilled.

The first RIM observations were obtained with the SOUSY VHF radar during a five-day-long demonstration experiment in May 1999 (CHILSON et al., 2001;

PALMER et al., 2001; MUSCHINSKI et al., 2001). Independently, on the Japanese MU radar LUCE et al. (2001b) implemented a technique that they called “frequency domain radar interferometric imaging” (FII). As explained in detail by MUSCHINSKI et al. (2001, p. 425), LUCE et al. (2001b) did not cycle fast enough through all frequencies and therefore could not fully exploit range-imaging capabilities. In other words, FII as implemented by LUCE et al. (2001b) is a hybrid of FDI and RIM.

The first RIM implementation on a UHF profiler was accomplished by CHILSON et al. (2003). Figure 18 shows the “RIM brightness,” from which one can retrieve local clear-air reflectivity, observed at a single range gate on the morning of April 10, 2001.

While the so-called spatial-interferometry technique (PFISTER, 1971; WOODMAN, 1971) is the angular counterpart of FDI, the so-called coherent radar imaging (CRI) technique is the angular counterpart of RIM. CRI was first used in the upper atmosphere for the observation of plasma irregularities (KUDEKI and SÜRÜCÜ, 1991). PALMER et al. (1998) were the first to use CRI in the lower atmosphere.

#### 4.3 Alternative perspectives by oversampling strategies

In Section 4.1, we have addressed the problem of how to find the optimum complex weights  $w_j(\mathbf{x})$  for a given location  $\mathbf{x}$  to be imaged. In this subsection, we outline a method to reconstruct the cross-covariance function  $\langle n^*(\mathbf{x}')n(\mathbf{x}'') \rangle$  and not only its Bragg component.

In order to illustrate the basic idea, let us consider instead of (4.1) the following family of sampling functions

$$G_{lmn}(\mathbf{x}) = \frac{1}{\sqrt{\sigma_l}} A \left( \frac{\mathbf{r}_n + \mathbf{x}}{\sigma_l} \right) \exp[-i\beta_m(\mathbf{r}_0 + \mathbf{r}_n + \mathbf{x})], \quad (4.16)$$

where  $A$  stands for an admissible window or so-called analyzing function (e.g. Gaussian),  $\mathbf{r}_n$  denotes the location,  $\beta_m$  the Bragg wavenumber, and  $\sigma_l$  (a dilation parameter) the pulse length. If one intends to reconstruct  $\langle n^*(\mathbf{x}')n(\mathbf{x}'') \rangle$ , one has to make use of the sample values

$$\langle I_{lmn}^* I_{l'm'n'} \rangle = \int \int G_{lmn}^*(\mathbf{x}') G_{l'm'n'}(\mathbf{x}'') \times \langle n^*(\mathbf{x}')n(\mathbf{x}'') \rangle d\mathbf{x}' d\mathbf{x}''. \quad (4.17)$$

The following observation illuminates the type of equation (4.17). For fixed  $\sigma_l$  (e.g.  $\sigma_l = 1$  for all  $l$ ) the integral transform is nothing more than the two-dimensional windowed Fourier transform evaluated at discrete points in the space–frequency domain, whereas for fixed  $\beta_m$  (4.17) results in the two-dimensional wavelet transform; for details we refer the reader to the very rich literature, e.g. DAUBECHIES (1992). For both situations there exists a well-developed theory on how to invert the integral equation. In the continuous framework (assume for

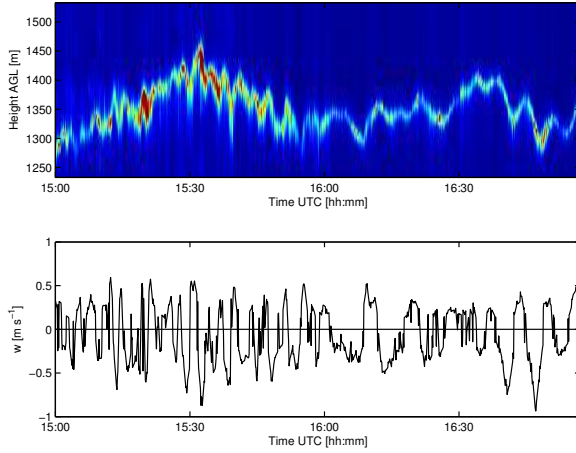


**Figure 18:** (a) Time-height cross section of “RIM brightness” retrieved from the first UHF RIM measurements. The data were collected on April 10, 2001, near Platteville, Colorado (CHILSON et al., 2003). (b) Doppler velocities retrieved from the same raw data.

a moment that the parameters  $\sigma$ ,  $\beta$ ,  $r$ ,  $\sigma'$ ,  $\beta'$ , and  $r'$  are continuously given) the inversion formula is in principle given by the adjoint integral operator; i.e.,

$$\langle n^*(\mathbf{x}')n(\mathbf{x}'') \rangle = \int \langle I_{\sigma\beta r}^* I_{\sigma'\beta'r'} \rangle \times G_{\sigma\beta r}^*(\mathbf{x}')G_{\sigma'\beta'r'}(\mathbf{x}'')d\mu(\sigma, \beta, r, \sigma', \beta', r') \quad (4.18)$$

Since our approach requires to deal with discrete parameter families  $(\sigma_l, \beta_m, \mathbf{r}_n, \sigma_{l'}, \beta_{m'}, \mathbf{r}_{n'})$ , we have to discretize this inversion formula in some adequate way. This leads directly to the so-called concept of frames (e.g., DUFFIN and SCHÄFER, 1952), i.e. to the discrete framework in which we are allowed to consider discrete families of parameters. The concept is well-understood for the Fourier as well as for the wavelet case; e.g., in the Fourier case the following family of functions

$$G_{l_0mn}(\mathbf{x}) = \frac{1}{\sqrt{2\pi}\sigma_{l_0}} \exp\left(-\frac{(n\tilde{\mathbf{r}} + \mathbf{x})^2}{2\sigma_{l_0}^2}\right) \times \exp\left[-im\tilde{\beta}(\mathbf{r}_0 + n\tilde{\mathbf{r}} + \mathbf{x})\right]_{(m,n) \in \mathcal{J}, \tilde{\beta}\tilde{\mathbf{r}} < 2\pi} \quad (4.19)$$

forms a frame, where  $\mathcal{J}$  denotes an adequate index set. A Fourier-reconstruction formula is then given by

$$\langle n^*(\mathbf{x}')n(\mathbf{x}'') \rangle = \sum_{\substack{(m,n) \in \mathcal{J} \\ (m',n') \in \mathcal{J}}} \langle I_{l_0mn}^* I_{l_0m'n'} \rangle \times \mathcal{D}(G_{l_0mn}^* G_{l_0m'n'}) (\mathbf{x}', \mathbf{x}'') \quad (4.20)$$

where the system  $\{\mathcal{D}(G_{l_0mn}^* G_{l_0m'n'})\}$  denotes the so-called dual frame which can be computed in some special situations exactly. In general, there exist several (linear as well as adaptive) schemes that approximate the

dual frame very well. A similar formula can be established for the wavelet transform. However, for certain technical/physical reasons, the pure Gabor or the pure wavelet case might be too restrictive for our approach. In order to allow more flexibility in constructing an adequate analyzing frame, we have to relax the restrictions made on  $\sigma_l$  or  $\beta_m$ . To this end, we consider the non-restricted family

$$\left\{ G_{\sigma_l \beta_m \mathbf{r}_n}^* G_{\sigma_{l'} \beta_{m'} \mathbf{r}_{n'}} \right\}_{(l,m,n,l',m',n') \in \mathcal{J}} \quad (4.21)$$

It is shown in DAHLKE et al. (2004a,b) that this family may form under certain assumptions on the sampling grid  $\mathcal{J}$  a so-called mixed Gabor–wavelet–frame. It was pointed out that one can identify reasonable parameter families such that an increase of the sampling density with respect to  $\{\sigma_l, \sigma_{l'}\}$  leads to a decrease of the redundancy with respect to  $\{\beta_m, \beta_{m'}\}$  and vice versa (what is of course of practical impact). We obtain the following reconstruction scheme

$$\langle n^*(\mathbf{x}')n(\mathbf{x}'') \rangle = \sum_{(n,m,l,n',m',l') \in \mathcal{J}} \langle I_{nmil}^* I_{n'm'l'} \rangle \times \mathcal{D}(G_{\sigma_n \beta_m \mathbf{r}_l}^* G_{\sigma_{n'} \beta_{m'} \mathbf{r}_{l'}}) (\mathbf{x}', \mathbf{x}'') \quad (4.22)$$

where  $\{\mathcal{D}(G_{\sigma_n \beta_m \mathbf{r}_l}^* G_{\sigma_{n'} \beta_{m'} \mathbf{r}_{l'}})\}_{(n,m,l,n',m',l') \in \mathcal{J}}$  stands again for the dual system. DAHLKE et al. (2004a,b) show how to construct or to approximate the dual frame function, or the so-called discrete reconstruction operator.

The whole concept of frame-based reconstruction schemes carries over to higher dimensions without essential changes. Moreover, the frame approach allows one to treat the reconstruction in a complete discrete setting, which is essential for fast numerical implementation. Note that the application of frame theory is strongly connected with incorporating oversampling (not only range oversampling). The main deficiency in the proposed method is that there might be a discrepancy between exact analytical inversion and the technical capabilities of radar devices. However, this results in the problem of identifying near-optimal parameter families, which requires of course a critical error analysis.

## 5 Summary and outlook

We have given a tutorial overview of concepts, problems, and solutions in advanced radar wind profiling (RWP). We have divided RWP into three categories: single-signal RWP, two-signal RWP, and multi-signal RWP.

Single-signal RWP, or traditional RWP, was pioneered thirty years ago (WOODMAN and GUILLÉN, 1974). Now it is a key technology for measuring winds and turbulence in the atmospheric boundary layer, the

free troposphere, and the lower stratosphere. The vast majority of radar wind profilers (RWPs) used for research and operational purposes are single-signal RWPs.

The standard technique to retrieve vertical profiles of the three-dimensional wind vector from single-signal RWPs is the Doppler beam-swinging (DBS) technique. The standard tool for the statistical analysis of signal time series is the periodogram, from which the first three moments of the clear-air spectrum are estimated. We have discussed the problems of separating the clear-air signal, clutter, and noise. Based on a measured signal that was severely contaminated by clutter from an aircraft, we have discussed the potential of time-frequency decomposition techniques to efficiently remove airborne clutter.

Two-signal and multi-signal RWP offer a wealth of additional options to overcome limitations inherent in traditional RWP. An overview of recent progress in the physical and mathematical concepts and techniques of two-signal and multi-signal RWP has been given.

Given the need to observe meteorological fields reliably with higher spatial and temporal resolution, to design and optimize observational networks and make them adaptive to ever-changing observational needs, radar wind profiling will remain a fertile area of interdisciplinary research and development in the decades to come.

## Acknowledgements

The authors thank Phil CHILSON, Jim JORDAN, Rich LATAITIS, and Bob PALMER for their helpful comments on earlier versions of this paper. Work on this paper begun when A. M. was with the University of Colorado at Boulder, Colorado and was affiliated with the NOAA Environmental Technology Laboratory. A. M.'s contribution was partially supported by the U. S. Army Research Office.

## References

- BALSLEY, B. B., M. L. JENSEN, R. G. FREHLICH, Y. MEILLIER, A. MUSCHINSKI, 2003: Extreme gradients in the nocturnal boundary layer: structure, evolution, and potential causes. – *J. Atmos. Sci.* **60**, 2496–2508.
- BARTH, M. F., R. B. CHADWICK, D. VAN DE KAMP, 1994: Data processing algorithms used by NOAA's wind profiler demonstration network. – *Ann. Geophysicae* **12**, 518–528.
- BATCHELOR, G. K., 1953: The theory of homogeneous turbulence. – Cambridge University Press, Cambridge.
- BOASHASH, B., 1992: Estimating and interpreting the instantaneous frequency of a signal - Part 1: Fundamentals. – *Proc. IEEE* **80**(4), 520–569.
- BOISSE, J.-C., V. KLAUS, J.-P. AUBAGNAC, 1999: A wavelet transform technique for removing airplane echos from ST radar signals. – *J. Atmos. Oceanic Technol.* **16**, 334–346.
- CHILSON, P. B., A. MUSCHINSKI, G. SCHMIDT, 1997: First observations of Kelvin-Helmholtz billows in an upper-level jet stream using VHF frequency domain interferometry. – *Radio Sci.* **32**, 1149–1160.
- CHILSON, P. B., R. D. PALMER, A. MUSCHINSKI, D. A. HOOPER, G. SCHMIDT, H. STEINHAGEN, 2001: SOMARE-99: A demonstrational field campaign for ultra-high resolution VHF atmospheric profiling using frequency diversity. – *Radio Sci.* **36**, 695–707.
- CHILSON, P. B., T.-Y. YU, R. G. STRAUCH, A. MUSCHINSKI, R. D. PALMER, 2003: Implementation and validation of range imaging on a UHF radar wind profiler. – *J. Atmos. Oceanic Technol.* **20**, 987–996.
- COHEN, L., 1989: Time-frequency distributions – a review. – *Proc. IEEE* **77**(7), 941–981.
- DAHLKE, S., G. STEIDL, G. TESCHKE, 2004a: Coorbit spaces and banach frames on homogeneous spaces with applications to analyzing functions on spheres. – *Adv. Comput. Math.* **21**(1–2), 147–180.
- , —, —, 2004b: Weighted coorbit spaces and banach frames on homogeneous spaces. – *J. Fourier Anal. Appl.* **10**(5), 507–539.
- DAUBECHIES, I., 1992: Ten Lectures on Wavelets. – SIAM, Philadelphia.
- DOVIK, R. J., D. S. ZRNIC, 1984: Reflection and scatter formula for anisotropically turbulent air. – *Radio Sci.* **19**, 325–336.
- , —, 1993: Doppler radar and weather observations, 2nd ed. – Academic Press, San Diego.
- DOVIK, R. J., R. J. LATAITIS, C. L. HOLLOWAY, 1996: Cross correlations and cross spectra for spaced antenna wind profilers – 1. Theoretical analysis. – *Radio Sci.* **31**, 157–180.
- DUFFIN, R. J., A. C. SCHÄFER, 1952: A class of nonharmonic Fourier series. – *Trans. Am. Math. Soc.* **72**, 341–366.
- FLANDRIN, P., 1999: Time-Frequency / Time-Scale Analysis. Wavelet Analysis and Its Applications. – Academic Press.
- GABOR, D., 1946: Theory of communication. – *J. Inst. Elec. Eng.* **93** (III), 429–457.
- GAGE, K. S., 1990: Radar observations of the free atmosphere: structure and dynamics. – In D. ATLAS (Ed.), *Radar in meteorology*, Amer. Meteor. Soc., Boston, 534–565.
- HILDEBRAND, P. H., R. S. SEKHON, 1974: Objective determination of the noise level in Doppler spectra. – *J. Appl. Meteor.* **13**, 808–811.
- HLAWATSCH, F., G. BOUDREAU-BARTELS, 1992: Linear and quadratic time-frequency signal representations. – *IEEE Sig. Proc. Magazine*, 21–67.
- HOCKING, W. K., R. RÜSTER, P. CZECHOWSKY, 1986: Absolute reflectivities and aspect sensitivities of VHF radio wave scatterers measured with the SOUSY radar. – *J. Atmos. Terr. Phys.* **48**, 131–144.
- JORDAN, J. R., R. J. LATAITIS, D. A. CARTER, 1997: Removing ground and intermittent clutter contamination from wind profiler signals using wavelet transforms. – *J. Atmos. Oceanic Technol.* **14**, 1280–1297.
- JUNGNICKEL, D. (Ed.), 1999: *Optimierungsmethoden*. – Springer, Berlin, Heidelberg, Germany.
- JUSTEN, L., G. TESCHKE, V. LEHMANN, 2004: Wavelet-

- based methods for clutter removal from radar wind profiler data. – In F. TRUCHETET (Ed.), *Wavelet Applications in Industrial Processing* Vol. 5266. The International Society for Optical Engineering, 157–168
- KOLMOGOROV, A. N., 1941: Local structure of turbulence in an incompressible fluid at very high Reynolds numbers. – *Dokl. Akad. Nauk SSSR* **30**, 299–303.
- KUDEKI, E., G. STITT, 1987: Frequency domain interferometry: a high resolution technique for studies of atmospheric turbulence. – *Geophys. Res. Lett.* **14**, 198–201.
- KUDEKI, E., F. SÜRÜCÜ, 1991: Radar interferometric imaging of field-aligned plasma irregularities in the equatorial electrojet. – *Geophys. Res. Lett.* **18**, 41–44.
- LATAITIS, R. J., S. F. CLIFFORD, C. L. HOLLOWAY, 1995: An alternative method for inferring winds from spaced-antenna radar measurements. – *Radio Sci.* **30**, 463–474.
- LEHMANN, V., G. TESCHKE, 2001: Wavelet based methods for improved wind profiler signal processing. – *Ann. Geophysicae* **19**, 825–836.
- LUCE, H., M. CROCHET, F. DALAUDIER, 2001a: Temperature sheets and aspect sensitive radar echoes. – *Ann. Geophysicae* **19**, 899–920.
- LUCE, H., M. YAMAMOTO, S. FUKAO, D. HELAL, M. CROCHET, 2001b: A frequency domain radar interferometric imaging (FII) technique based on high resolution methods. – *J. Atmos. Solar-Terr. Phys.* **63**, 201–214.
- MALLAT, S., 1999: *A Wavelet Tour Of Signal Processing*. – Academic Press.
- MUSCHINSKI, A., 1996: Possible effect of Kelvin-Helmholtz instability on VHF radar observations of the mean vertical wind. – *J. Appl. Meteor.* **35**, 2210–2217.
- , 1998: The first moments of the variance- and cross-spectra of standard and interferometric clear-air Doppler-radar signals. – NCAR Technical Note 441+STR, National Center for Atmospheric Research, Boulder, Colorado.
- , 2004: Local and global statistics of clear-air Doppler radar signals. – *Radio Sci.* **39**, RS1008, [Doi: 10.1029/2003RS002908](https://doi.org/10.1029/2003RS002908).
- MUSCHINSKI, A., D. H. LENSCHOW, 2001: Future directions for research on meter- and submeter-scale, atmospheric turbulence. – *Bull. Amer. Meteor. Soc.* **82**, 2831–2843.
- MUSCHINSKI, A., C. WODE, 1998: First in situ evidence for coexisting submeter temperature and humidity sheets in the lower free troposphere. – *J. Atmos. Sci.* **55**, 2893–2906.
- MUSCHINSKI, A., P. B. CHILSON, S. KERN, J. NIELINGER, G. SCHMIDT, T. PRENOSIL, 1999: First frequency-domain interferometry observations of large-scale vertical motion in the atmosphere. – *J. Atmos. Sci.* **56**, 1248–1258.
- MUSCHINSKI, A., P. B. CHILSON, R. D. PALMER, G. SCHMIDT, H. STEINHAGEN, 2001: Boundary-layer convection and diurnal variation of vertical-velocity characteristics in the free troposphere. – *Quart. J. Roy. Meteor. Soc.* **127**, 423–443.
- NASTROM, G. D., T. E. VAN ZANDT, 1994: Mean vertical motion seen by radar wind profilers. – *J. Appl. Meteor.* **33**, 984–995.
- OTTERSTEN, H. A., 1969: Radar backscattering from the turbulent clear atmosphere. – *Radio Sci.* **4**, 1251–1255.
- PALMER, R. D., S. GOPALAM, T.-Y. YU, S. FUKAO, 1998: Coherent radar imaging using Capon's method. – *Radio Sci.* **33**, 1585–1598.
- PALMER, R. D., T.-Y. YU, P. B. CHILSON, 1999: Range imaging using frequency diversity. – *Radio Sci.* **34**, 1485–1496.
- PALMER, R. D., P. B. CHILSON, A. MUSCHINSKI, G. SCHMIDT, T.-Y. YU, H. STEINHAGEN, 2001: SOMARE-99: Observations of tropospheric scattering layers using multiple-frequency range imaging. – *Radio Sci.* **36**, 681–693.
- PFISTER, W., 1971: The wave-like nature of inhomogeneities in the E-region. – *J. Atmos. Terr. Phys.* **33**, 999–1025.
- RÖTTGER, J., M. F. LARSEN, 1990: UHF/VHF radar techniques for atmospheric research and wind profiler applications. – In D. ATLAS (Ed.), *Radar in meteorology*, Amer. Meteor. Soc., Boston, 235–281.
- STRAUCH, R. G., D. A. MERRITT, K. P. MORAN, K. B. EARNSHAW, D. VAN DE KAMP, 1984: The Colorado wind profiling network. – *J. Atmos. Oceanic Technol.* **1**, 37–49.
- TATARSKII, V. I., 1961: *Wave propagation in a turbulent medium*. – McGraw-Hill, New York.
- , 2003: Theory of single scattering by random distributed scatterers. – *IEEE Trans. Ant. Prop.* **51**, 2806–2813.
- TATARSKII, V. I., A. MUSCHINSKI, 2001: The difference between Doppler velocity and real wind velocity in single scattering from refractive index fluctuations. – *Radio Sci.* **36**, 1405–1423.
- WEBER, B. L., D. B. WUERTZ, D. C. LAW, A. S. FRISCH, J. M. BROWN, 1992: Effects of small-scale vertical motion on radar measurements of wind and temperature profiles. – *J. Atmos. Oceanic Technol.* **9**, 193–209.
- WOODMAN, R. F., 1971: Inclination of the geomagnetic field measured by an incoherent scatter technique. – *J. Geophys. Res.* **76**, 178–184.
- WOODMAN, R. F., A. GUILLÉN, 1974: Radar observations of winds and turbulence in the stratosphere and mesosphere. – *J. Atmos. Sci.* **31**, 493–505.
- YAMAMOTO, M. K., F. FUJIWARA, T. HORINOCHI, H. HASHIGUCHI, S. FUKAO, 2003: Kelvin-Helmholtz instability around the tropical tropopause observed with the Equatorial Atmosphere Radar. – *Geophys. Res. Lett.* **30**, 1476, [Doi: 10.1029/2002GL016685](https://doi.org/10.1029/2002GL016685), Erratum: *Geophys. Res. Lett.* **30**, 1716, [Doi: 10.1029/2003GL017791](https://doi.org/10.1029/2003GL017791).



# Advanced intermittent clutter filtering for radar wind profiler: signal separation through a Gabor frame expansion and its statistics

V. Lehmann<sup>1</sup> and G. Teschke<sup>2</sup>

<sup>1</sup>Deutscher Wetterdienst, Meteorologisches Observatorium Lindenberg, 15848 Lindenberg, Germany

<sup>2</sup>Zuse-Institut Berlin, Takustr. 7, 14195 Berlin, Germany

Received: 18 July 2007 – Revised: 8 February 2008 – Accepted: 28 February 2008 – Published: 13 May 2008

**Abstract.** A new signal processing method is presented for the suppression of intermittent clutter echoes in radar wind profilers. This clutter type is a significant problem during the seasonal bird migration and often results in large discrepancies between profiler wind measurements and independent reference data. The technique presented makes use of a discrete Gabor frame expansion of the coherently averaged time series data in combination with a statistical filtering approach to exploit the different signal characteristics between signal and clutter. The rationale of this algorithm is outlined and the mathematical methods used are presented in due detail. A first test using data obtained with an operational 482 MHz wind profiler indicates that the method outperforms the previously used clutter suppression algorithm.

**Keywords.** Meteorology and atmospheric dynamics (Instruments and techniques) – Radio science (Remote sensing; Signal processing)

## 1 Introduction

Radar wind profilers (RWP) were developed from MST-Radars (Van Zandt, 2000) and have meanwhile become standard instruments for measuring wind velocities in the atmosphere. Overviews of the technical and scientific aspects of RWP including its signal processing have been provided, among others, by Gage (1990); Röttger and Larsen (1990); Doviak and Zrnic (1993) and Muschinski (2004). Especially the routine application by weather services and the assimilation of the data in Numerical Weather Prediction Models is an indicator for the degree of maturation that this technology has achieved, see e.g. Monna and Chadwick (1998); Bouttier (2001); Benjamin et al. (2004b); St-James and Laroche (2005); Ishihara et al. (2006). However, it is a matter of fact

that sometimes large and unacceptable differences are observed between the profiler data and independent reference measurements. In many cases these differences are clearly attributable to either clutter echoes or Radio Frequency interference. Spurious signals are often easily discernible in the Doppler spectrum by human experts, but not always adequately handled by the automatic processing. For that reason, research on improvements in wind profiler signal processing has remained a very active field over the last decade.

In this paper we deal with so-called intermittent clutter and propose a new filtering algorithm for the detection and suppression of these clutter signals in the profiler raw data. Of particular importance are echoes caused by migrating birds in spring and fall. It is well known that birds are effective targets for a wide range of radars from X-band to UHF (Vaughn, 1985; Bruderer, 1997a). In fact, most of the knowledge about migrating birds come from radar observations. That concerns in particular their flight behavior under the influence of environmental factors (Bruderer, 1997b). Radar ornithology is meanwhile a mature field and it is no surprise, that birds are also detected by the sensitive radar systems used for wind profiling. The susceptibility of wind profiler radar systems to bird echoes depends primarily on wavelength and antenna characteristics. It mostly affects L-band and UHF-systems, that is Boundary Layer profilers and Tropospheric profilers, as discussed in Wilczak et al. (1995). Intermittent clutter is an issue for the standard Doppler-beam swinging radars as well as for spaced antenna and imaging radar systems, where new mitigation techniques like adaptive beamforming have recently been proposed (Cheong et al., 2006; Chen et al., 2007). We mention in passing that other remote sensing instruments used in Meteorology are also affected by migrating birds (Mastrantonio et al., 1999; Gauthreaux and Belser, 1998; Gauthreaux et al., 1998; Zhang et al., 2005; Liu et al., 2005).

Intermittent clutter echoes caused by aircraft were already mentioned by Hogg et al. (1983), and a few years later it

*Correspondence to:* V. Lehmann  
(volker.lehmann@dwd.de)

became obvious that especially echoes from migrating birds can be a serious issue in wind profiling (Ecklund et al., 1990; Barth et al., 1994). If present, such spurious signals can cause a significant deterioration of the quality of the derived winds. To give an example, the investigation of low-level jets using RWP data is hampered by bird migration clutter (Stensrud, 1996). This makes it necessary to either use extensive quality control procedures to identify and skip contaminated data (Daniel et al., 1999; Song et al., 2005) or to limit the studies to periods where bird migration is negligible (Anderson and Arritt, 2001). Many other investigations using RWP data have mentioned the bird contamination problem, e.g. Ralph et al. (1998); Locatelli et al. (1998); Parker and Johnson (2000); Lundquist (2003); Nielsen-Gammon et al. (2007). While the need for an extensive manual data quality control and cleaning might be acceptable for research activities, it is surely not feasible in any operational setting. Nevertheless it is mandatory to avoid the assimilation of bird contaminated profiler wind data, as this can have significant effects on the quality of the forecasts (Semple, 2005). Due to the nature of the problem, a bird migration check at the operational center itself is not the best approach (Benjamin et al., 2004a). While current state-of-the-art profilers nowadays run more or less sophisticated algorithms on site to reduce bird contamination (Merritt, 1995; Jordan et al., 1997; Ishihara et al., 2006), practical experience supports the statement that the problem has not been fully resolved.

The problem of bird contamination has been well-known for more than a decade (Wilczak et al., 1995; Engelbart et al., 1998) and it still is a research topic in RWP signal processing. The first successful attempt to reduce bird contamination was made by Merritt (1995), who suggested a selective averaging method of the individual Doppler spectra based on a statistical criterion. The same method can also be applied off-line to averaged spectra, when data with higher resolution are not available (Pekour and Coulter, 1999). Weber (2005) used neural networks for a classification of contaminated single spectra, followed by a selective averaging. Other proposals have concentrated on modified peak detection in the Doppler spectrum to address spurious flier returns, among other clutter types (Griesser and Richner, 1998; Cornman et al., 1998; Morse et al., 2002; Weber et al., 2004). The disadvantage of all these methods is that the mitigation processing builds upon the Doppler spectra (either before or after spectral integration). Given the highly non-stationary characteristics of the intermittent clutter signal, it is necessary to deal with the problem before the Doppler spectrum is estimated, because Fourier methods are generally inadequate for nonstationary signals. In other words, the necessary nonlinear filtering has to be performed in the time domain. This approach was first suggested by Jordan et al. (1997) and further by Lehmann and Teschke (2001), who suggested wavelet decomposition and wavelet coefficient thresholding, to remove the clutter part of the signal. However, the a-priori unclear choice of the mother wavelet and – at least for the dyadic wavelet trans-

form – a suboptimal signal separation in the wavelet domain, especially near zero Doppler shift, makes an efficient separation of clutter and signal difficult.

Ideally one would like to have an intermittent clutter suppression algorithm that reduces the clutter part of the signal as best as possible, given the sampled data and that further quantifies its *degree of contamination* by providing some measure of clutter energy for quality control purposes. Furthermore, the algorithm must not degrade both data quality and availability in the no-clutter case, but it should perform as well as the proven standard processing methods. This requirement is more stringent than it may appear at first glance. In this paper, we propose a new signal-clutter separation method that attempts to meet these objectives. It is based on a redundant frame decomposition of the time series followed by the statistical filtering approach suggested by Merritt (1995).

The paper is organized as follows: Sect. 2 gives an overview of RWP signal characteristics and signal processing and identifies shortcomings of the currently used methods when intermittent clutter signals are present. Section 3 reviews basic results of the mathematical theory of frames, which deals with linear discrete signal representations. The goal is here to find a signal representation, that achieves optimal separation between the atmospheric and the clutter part of the signal. This is achieved by the discrete Gabor representation, which is discussed next. Section 4 focuses on a statistical approach to objectively identify the atmospheric signal component, based on well-justified statistical assumptions. A comparison of the new algorithm with the previously used signal processing techniques is shown in Sect. 5. The data used were obtained during routine operation of a 482 MHz wind profiler radar of the Deutscher Wetterdienst at Bayreuth, Germany in the fall of 2005. Finally, a summary and conclusions are given in Sect. 6.

## 2 RWP signal characteristics

### 2.1 General properties of the received signal

The relationship between the signal received by the radar and the scattering medium is the topic of radar instrument theory, which basically describes how atmospheric properties are mapped to the measurable function at the radar receiver output (Woodman, 1991; Muschinski, 2004). It is known that models for the scattering processes and the technical properties of the radar system must be considered here, which makes the task quite formidable. However, for the problem at hand it is not required to consider such theories in detail, because we are only interested in some rather general properties of the received signal, like statistical stationarity. For a pulsed RWP, the received signal at the antenna output has the following properties:

1. Continuous real-valued random voltage signal: Every measurable physical quantity is real. The randomness is the result of the random nature of the scattering process.
2. Intrinsically nonstationary: This is due to the impulsive character of the transmitted signal and the inhomogeneous vertical structure of the atmosphere.
3. Multi-component: Beside the ubiquitous noise, there may be signal contributions from several independent scattering processes, like Bragg scattering at fluctuations of the refractive index, Rayleigh scattering at precipitation and scattering at various clutter targets.
4. Narrowband: The signal is band-limited, with a maximum width that is largely determined by the bandwidth of the transmitted pulse.
5. Large dynamic range: The signal varies easily over many orders of magnitude, which is typical for all radar systems.

After a linear low-noise amplification, the first processing step is a (digital) quadrature demodulation of the analog band-limited signal. This leads to a complex baseband representation, where the signal is described through the time series of its in-phase (I) and quadrature-phase (Q) components. Property 1 is thus modified, because the signal has now become complex. Furthermore, uniform sampling for  $N$  fixed delay times (after pulse transmission, corresponding to  $N$  fixed ranges) at multiples of the radar inter-pulse period is then applied to generate  $N$  quasi-stationary sequences from the nonstationary signal. This stationarity assumption is usually valid for atmospheric scattering, ground clutter and noise, provided the scattering medium at a fixed height does not change its properties significantly over the length of the time series (Woodman, 1991). It is one of the basic assumptions of signal processing for atmospheric radars (Keeler and Passarelli, 1990). The process of generating the  $N$  sequences is called range-gate sampling and thereby, property 2 is modified. The remaining signal properties 3–5 are preserved for the  $N$  discrete data sequences, provided processing is linear. Finally, matched filtering of the band-limited signal is performed to achieve an optimal signal-to-noise ratio.

## 2.2 Classical signal model and its limitations

The classical RWP signal model assumption is that the demodulated discrete voltage sequence at the receiver output can be written as

$$\mathbf{S}[k] = \mathbf{I}[k]e^{i\omega k\Delta t} + \mathbf{N}[k], \quad (1)$$

where  $\mathbf{I}[k] \sim N(0, \sigma_{\mathbf{I}}^2)$  and  $\mathbf{N}[k] \sim N(0, \sigma_{\mathbf{N}}^2)$  are independent complex zero-mean Gaussian random vectors describing the atmospheric signal and the receiver noise, respectively (Zrnić, 1979),  $\Delta t$  is the sampling interval of the sequence

and  $\omega$  the mean Doppler frequency. Furthermore  $\mathbf{I}[k]$  is narrowband compared to the receiver bandwidth and  $|\omega| \leq \pi/\Delta t$  (Nyquist criterion). Because  $\mathbf{S}[k]$  is the result of the demodulation of a real valued zero-mean and stationary Gaussian random process, the resulting Gaussian complex random process is also wide-sense stationary and zero-mean. Furthermore, the sequence has a vanishing pseudo-covariance, that is we have  $\mathbf{E}(\mathbf{S}[k]\mathbf{S}[l])=0$ . Such a process is usually called proper, circular or phase-invariant (Neuser and Massey, 1993). We will use this property later in connection with a moments theorem for these processes (Reed, 1962).

Because  $\mathbf{S}[k]$  is Gaussian, it is completely characterized through its covariance matrix  $\mathbf{R}$  with entries

$$\begin{aligned} (\mathbf{R})_{k,l} &= \text{Cov}(\mathbf{S}[k], \mathbf{S}[l]) = \mathbf{E}(\mathbf{S}[k]\bar{\mathbf{S}}[l]) \\ &= \mathbf{E}(\mathbf{I}[k]\bar{\mathbf{I}}[l])e^{i\omega(k-l)\Delta t} + \mathbf{E}(\mathbf{N}[k]\bar{\mathbf{N}}[l]) \\ &= \sigma_{\mathbf{I}}^2 \varrho[k-l]e^{i\omega(k-l)\Delta t} + \sigma_{\mathbf{N}}^2 \delta_{k-l,0}, \end{aligned}$$

where  $\varrho$  is specified below. Furthermore, stationarity is assumed over typical dwell-times of  $\mathcal{O}(1 \text{ min})$ . While this is a classical assumption in radar signal processing (Zrnić, 1975, 1979; Woodman, 1985; Frehlich and Yadlowsky, 1994; Lottman and Frehlich, 1997), it is unknown for which maximal time series length this assumption can be made safely. We found that bird clutter signals are significantly nonstationary over typically used dwell times of about 30 s to 60 s. This is in sharp contrast to observed atmospheric signals, which exhibit a high degree of stationarity on that time scale, well in line with the classical assumptions.

Therefore we get the following expression for the autocovariance function

$$\text{ACov}(k) = \sigma_{\mathbf{I}}^2 \varrho[k]e^{i\omega k\Delta t} + \sigma_{\mathbf{N}}^2 \delta_{k,0} = \sigma^2 \rho[k], \quad (2)$$

where we set

$$\sigma^2 := \sigma_{\mathbf{I}}^2 + \sigma_{\mathbf{N}}^2 \quad \text{and} \quad \rho[k] := \frac{\sigma_{\mathbf{I}}^2 \varrho[k]e^{i\omega k\Delta t} + \sigma_{\mathbf{N}}^2 \delta_{k,0}}{\sigma_{\mathbf{I}}^2 + \sigma_{\mathbf{N}}^2}.$$

(The sequence  $\rho$  will be of importance when constructing adequate mean and variance estimators.) Finally, the autocorrelation function  $\varrho[k]$  is often assumed to follow a Gaussian correlation model, which corresponds to a Gaussian signal peak in the power spectrum. If the spectral width of the signal is  $w$ , then we have (Zrnić, 1979; Frehlich and Yadlowsky, 1994)

$$\varrho[k] = e^{-2\pi^2 w^2 k^2 \Delta t^2}. \quad (3)$$

Note that this Gaussian correlation model must not be confused with the characterization of the random process as Gaussian, which covers a much wider class of signals. The assertions are normally very well justified and therefore often used in simulations of the radar signal (Zrnić, 1975; Frehlich and Yadlowsky, 1994; Muschinski et al., 1999).

In reality, however, there is sometimes a third component contributing to the signal, namely clutter (Muschinski et al., 2005), so that the signal model must be written as:

$$\mathbf{S}[k] = \mathbf{I}[k]e^{i\omega k\Delta t} + \mathbf{N}[k] + \mathbf{C}[k]. \quad (4)$$

Clutter is the totality of undesired echoes and interfering signals, therefore it is impossible to generalize the properties of  $\mathbf{C}[k]$ . In the case of RWP, clutter includes in particular echoes from airborne objects such as aircraft and birds as well as returns from the ground. Interfering signals may be caused by other radio transmitters operating in the RWP receiver band. In the remainder of the paper, we restrict ourselves to intermittent clutter signals.

While the properties of the intermittent clutter component have not been systematically investigated, it is instructive to take a look at a few examples. Such have been presented by various authors: Wilczak et al. (1995) described the distinct characteristic of bird contaminated I and Q data when seen in an A-scope display, but the shown time series taken with a 924 MHz RWP is only 0.5 s long, which is too short to see its essential characteristics. Jordan et al. (1997) show an example of a 30 s long time series taken with a 915 MHz RWP during bird migration, which exhibits a variation in the envelope of the signal due to modulation of signal amplitude by the antenna beam pattern. Another example of intermittent clutter caused by airplanes and a simple theoretical model is given by Boisse et al. (1999). The most distinct feature here is also the time-dependent amplitude of the signal. A 19 s time series of a 482 MHz RWP containing an airplane echo is discussed in Muschinski et al. (2005).

In the fall of 2005, time series data of the coherently integrated I/Q signal of the RWP at Bayreuth, Germany were saved in the wind low mode to get a unique dataset for the investigation of bird migration. For 13 October, it was subjectively judged that the data showed a maximum of bird echoes. We have therefore selected this day for demonstration of the proposed algorithm. One particular dwell is shown in Fig. 3. The time series has a length of about 35 s and its nonstationarity is striking.

When data containing intermittent clutter components are compared to both clear air and ground clutter signals (see Muschinski et al., 2005, for an example), it is very obvious, that the main difference is the transient character of the intermittent clutter signal component. Following Friedlander and Porat (1989), we define a transient signal as a signal whose duration is short to the observation interval, in our case the dwell time. Such a behavior clearly reflects a nonstationarity of the underlying scattering process. It is not the sinusoidal signature that makes the difference, as a sufficiently strong clear air signal also exhibits a sinusoidal nature (see Figs. 1 and 2 in Muschinski et al., 2005) – the most distinct property of intermittent clutter is its nonstationarity.

### 2.3 Consequences for signal processing

Signal processing can be regarded as the art of extracting the maximum amount of information from a given measurement. This obviously means that the general properties of the signal determine the optimal mathematical processing methods. A stationary Gaussian stochastic process is without loss of information described by its time-independent second-order properties, that is the autocovariance function or, equivalently, the power spectrum. This assumption holds when Eq. (1) is valid, and the classical way to process RWP data is then based on a non-parametric estimation of the power spectrum using a discrete Fourier transform of the (usually coherently integrated) raw signal over the dwell-time. The power spectrum is commonly called the Doppler spectrum. Its first three moments are estimated after the noise contribution to the spectrum has been subtracted, to describe the basic properties of the atmospheric signal (Woodman, 1985). However, we have seen that the clutter contribution can be highly nonstationary. If the signal  $\mathbf{S}[k]$  contains nonstationary components, then the Doppler spectrum is no longer an adequate representation of the stochastic process because information regarding time dependency is already lost. So it cannot be expected that a successful intermittent clutter filtering strategy can be developed based on the Doppler spectrum. Therefore it is tempting to try methods that were developed in the framework of nonstationary signal processing. A necessary condition is obviously a separation of  $\mathbf{C}[k]$  from the stationary components  $\mathbf{I}[k]e^{i\omega k\Delta t} + \mathbf{N}[k]$ . To achieve this, we look for a representation of the signal in which we are able to discriminate between stationary and nonstationary signal components. This is the goal put forward in Wilczak et al. (1995): *Clearly, a superior technique would be one in which the bird signal and atmospheric signal could be differentiated from each other and processed independently.*

So far we have considered either a pure time representation of the signal, namely its discrete time series, or its complex Fourier transform as a pure frequency representation. Both are not optimal for transient phenomena, although they are complete representations of the same information. Therefore we look for an intermediate representation that aims at the joint time-frequency structure of the signal, so it needs to depend on both time and frequency. This is the topic of the next section. If we are able to separate stationary and nonstationary signal components in such a representation, then we might be able to suppress the nonstationary clutter part while leaving the stationary signal component essentially intact.

### 3 Signal representation via Gabor frame expansions

#### 3.1 The windowed Fourier transform and the time-frequency plane

Let us consider continuous signals first, although in practice we are always given a discretized signal. A quite natural way to analyze a continuous signal simultaneously in time and frequency is provided by the windowed Fourier transform (WFT), see Gabor (1946); Daubechies (1992); Kaiser (1994); Mallat (1999). It is essentially an extension of the well-known Fourier transform, where time localization is achieved by a pre-windowing of the signal with a normalized window function  $h \in \mathbb{L}^2(\mathbf{R})$ . For any given function  $S \in \mathbb{L}^2(\mathbf{R})$ , the WFT is defined as

$$V_h S(\tau, \omega) = \int_{-\infty}^{+\infty} S(t)h(t - \tau)e^{-i\omega t} dt . \quad (5)$$

The operator  $V_h$  maps isometrically between  $\mathbb{L}^2(\mathbf{R})$  and  $\mathbb{L}^2(\mathbf{R}^2)$ , that is a one-dimensional function/signal is with no loss of energy transformed via the WFT into a two-dimensional function depending on both time  $\tau$  and frequency  $\omega$ . The  $(\tau, \omega)$ -plane is called the time-frequency (TF) plane or briefly the phase space. This representation was suggested by Gabor (1946) to illustrate that *both time and frequency are legitimate references for describing a signal*. The squared modulus of  $V_h S$  is called the spectrogram, denoted by

$$P_h S(\tau, \omega) = |V_h S(\tau, \omega)|^2 , \quad (6)$$

and provides a measure for the energy of the signal in the time-frequency neighborhood of the point  $(\tau, \omega)$  and thus insight about the time-frequency structure of  $S$ . However, due to Heisenberg's uncertainty relation, there is no arbitrary resolution in time and frequency simultaneously, i.e. a point-wise frequency description in time domain and a point-wise time description in frequency domain is impossible. Formally, one considers in the uncertainty context for some centralized signal  $h$  with  $\|h\|=1$ , time and frequency variances

$$\sigma_t^2 = \int_{-\infty}^{+\infty} t^2 |h(t)|^2 dt \quad \sigma_\omega^2 = \frac{1}{2\pi} \int_{-\infty}^{+\infty} \omega^2 |\hat{h}(\omega)|^2 d\omega \quad (7)$$

for which the Heisenberg uncertainty relation yields

$$\sigma_t \cdot \sigma_\omega \geq \frac{1}{2} . \quad (8)$$

It can be shown, that equality in Eq. (8) is achieved when  $h$  is a translated, modulated or scaled version of the Gaussian function (equality means achieving optimal resolution in the time-frequency plane). Their time-frequency spread is visualized through a rectangle with widths  $\sigma_t$  and  $\sigma_\omega$  in the TF-plane, this is called a Heisenberg box – see Fig. 1. This optimality result shall be used later on, when elaborating a

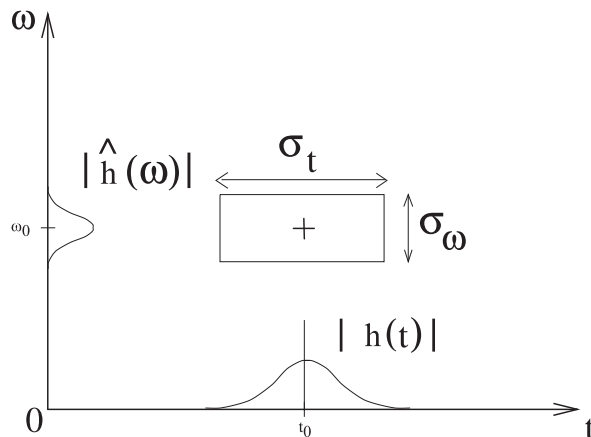


**Fig. 1.** Schematic representation of the time-frequency plane and the Heisenberg-box (resolution) of the window function  $h_{\tau, \omega}(t)$ , centered at time  $\tau=t_0$  and frequency  $\omega=\omega_0$ .

discrete version of Eq. (5). Since the WFT is an isometry, the inversion of  $V_h$  can be performed by its adjoint,

$$\begin{aligned} \langle S, S \rangle_{\mathbb{L}^2(\mathbf{R})} &= \|S\|_{\mathbb{L}^2(\mathbf{R})}^2 = \|V_h S\|_{\mathbb{L}^2(\mathbf{R}^2)}^2 \\ &= \langle V_h S, V_h S \rangle_{\mathbb{L}^2(\mathbf{R}^2)} = \langle V_h^* V_h S, S \rangle_{\mathbb{L}^2(\mathbf{R})} \end{aligned}$$

and therefore

$$S(t) = V_h^* V_h S(t) = \frac{1}{2\pi} \iint_{\mathbf{R}^2} V_h S(\tau, \omega) h(t - \tau) e^{i\omega t} d\omega d\tau . \quad (9)$$

Hence, in the continuous setting we still have signal analysis, transform Eq. (5), and signal synthesis, transform Eq. (9), in some straightforward way available and therefore time-frequency signal filtering can be performed in three simple steps (see e.g. Hlawatsch and Boudreaux-Bartels, 1992):

1. Analysis: Computation of the WFT using Eq. (5).
2. Modification of the WFT (e.g. time-dependent filtering).
3. Synthesis: Reconstruction of the modified signal using Eq. (9).

#### 3.2 From windowed Fourier transform to Gabor frame expansions

For discrete signals, continuous transforms (5) and (9) are not suitable and would create very redundant representations of the signal. A first adjustment can be achieved when Eqs. (5) and (9) are approximated by discrete sums. Discretizing Eq. (9) means taking only values of the WFT at some discrete lattice in phase space. As it was pointed out, e.g. in Daubechies (1992), the sampling density in phase space

plays a significant role for the existence and stability of a reconstruction formula, i.e. of a discrete version of Eq. (9).

Assume we are given some discrete subset  $\Lambda$  (to be specified below) of the TF-plane, then a naive discrete version of the inversion formula (9) would be

$$S(t) \stackrel{?}{\approx} \sum_{(m,k) \in \Lambda} V_h S(mT, k\Omega) h_{m,k}(t) \quad (10)$$

with

$$h_{m,k}(t) = h(t - mT) e^{ik\Omega t},$$

where the parameter  $T$  controls the discrete linear shift  $mT$  along the time axis and  $\Omega$  the sampling shift  $k\Omega$  in the frequency domain. In order to verify whether Eq. (10) indeed exhibits a reconstruction formula, we first observe that for a family of elementary signals or so-called atoms  $\{h_{m,k}\}_{(m,k) \in \Lambda}$  that is complete in  $\mathbb{L}^2(\mathbf{R})$  any  $S \in \mathbb{L}^2(\mathbf{R})$  can be represented by a linear expansion of the form

$$S(t) = \sum_{(m,k) \in \Lambda} a_{m,k} h_{m,k}(t). \quad (11)$$

But only in very specific cases, e.g. when  $\{h_{m,k}\}_{(m,k) \in \Lambda}$  forms an orthonormal basis,

$$a_{m,k} = \langle S, h_{m,k} \rangle = V_h S(mT, k\Omega)$$

and then Eq. (10) would indeed be an equality,

$$S(t) = \sum_{(m,k) \in \Lambda} \langle S, h_{m,k} \rangle h_{m,k}(t).$$

In general, this is not the case, i.e. we only have

$$S(t) \neq \sum_{(m,k) \in \Lambda} \langle S, h_{m,k} \rangle h_{m,k}(t) = F^* F S(t),$$

where the operator  $F^* F$  and its properties are briefly discussed in Appendix A. For a detailed analysis and discussion on this subject we refer the interested reader to, e.g., Daubechies (1992). To reconstruct  $S$  (i.e. to invert  $F^* F$ ), special properties on  $\Lambda$  and on the analyzing atoms (the dual functions to  $h$ ) are required. In what follows, we shall focus on the practically relevant biorthogonal case, in which the construction of the analyzing atoms becomes simple and, moreover, numerically stable. To this end, suppose there is some auxiliary family  $g_{m,k}(t) = g(t - mT) e^{ik\Omega t}$  (yet unknown) available that serves as a reservoir of analyzing atoms used to compute the Gabor coefficients  $a_{m,k}$  via Eq. (5),

$$a_{m,k} = \langle S, g_{m,k} \rangle = V_g S(mT, k\Omega) = \int S(t') \bar{g}_{m,k}(t') dt'. \quad (12)$$

This approach was originally proposed by Bastiaans (1980). Inserting now Eq. (12) into Eq. (11) yields

$$\begin{aligned} S(t) &= \sum_{(m,k) \in \Lambda} \int S(t') \bar{g}_{m,k}(t') dt' h_{m,k}(t) \\ &= \int S(t') \left( \sum_{(m,k) \in \Lambda} \bar{g}_{m,k}(t') h_{m,k}(t) \right) dt'. \end{aligned}$$

Equality in the latter equation is assured as long as

$$\sum_{m,k} \bar{g}_{m,k}(t') h_{m,k}(t) = \delta(t - t'). \quad (13)$$

Condition (13) is called the *biorthogonality relation* and restricts the choice of  $g$  in dependence on the preassigned function  $h$ . The particular choice of the window function  $h$  (e.g. its variance  $\sigma_h$ ), the time shift  $T$  and the frequency shift  $\Omega$  directly controls the existence, uniqueness, convergence properties and the numerical stability of the Gabor expansion (11), which exists for arbitrary signals  $S(t)$  only if  $\Omega T \leq 2\pi$ ; this is a frame theoretical result, see Daubechies (1990); Mallat (1999). The physical meaning of this inequality is nothing but the Nyquist sampling criterion and represents the sampling density.  $\Omega T = 2\pi$  is called critical sampling. This was Gabor's original suggestion, as he was aiming at elementary signals *conveying exactly one datum or one "quantum of information"*. In other words, there was no interest in any redundancy.

Gabor (1946) called the sampling density an *information diagram*. In his attempt to derive a theory of communication, each area represents one elementary quantum of information which Gabor proposed to call a *logon*. Although conceptually simple and appealing, the Gabor expansion at minimal sampling density in the TF-plane ( $\Omega T = 2\pi$ ) has no nice mathematical structure. In particular, it does not form a basis with the basis functions localized in time and frequency. A relaxation of the equality  $\Omega T = 2\pi$  is therefore required and generates a crucial degree of freedom in the Gabor expansion, this at the expense of oversampling and a possible non-uniqueness. For  $\Omega T > 2\pi$  the stability of the expansion is lost.

### 3.3 Gabor frame expansions for discretely sampled signals

So far we have discretized Eq. (9) resulting in the Gabor frame expansion (11) for  $S \in \mathbb{L}^2(\mathbf{R})$ . But when it comes to real applications, only finitely many discretely sampled values of  $S$  are available; namely  $\mathbf{S}[n] = S(n\Delta t)$ ,  $n = 0, \dots, N-1$ . Therefore it becomes necessary to develop a fully discrete concept for evaluating the Gabor coefficients (12). Moreover, the discrete subset  $\Lambda$  in Eq. (11) is in general infinite and hence also not suitable for a numerical implementation. The sum needs to be appropriately truncated and, in addition, a discrete version of the dual function  $g$  needs to be derived.

We now illustrate how to proceed for discrete data  $\mathbf{S}$ . More details can be found in the original paper by Wexler and Raz (1990) and Appendix B. Assume we are given some discrete and finite time (periodic) signal  $\tilde{\mathbf{S}}$  with sampling points  $n=0, \dots, N-1$ , that is  $\tilde{\mathbf{S}}[n]=\tilde{\mathbf{S}}[n+N]$ . We therefore have to periodize the analysis and synthesis windows as well,

$$\tilde{\mathbf{h}}[n] = \sum_l \mathbf{h}[n + lN], \quad \tilde{\mathbf{g}}[n] = \sum_l \mathbf{g}[n + lN].$$

Slightly abusing the notation, we omit the tilde denoting periodic (finite) functions in the following. The signal  $\mathbf{S}$  can be discretely represented by

$$\mathbf{S}[n] = \sum_{m=0}^{M-1} \sum_{k=0}^{K-1} a_{m,k} \mathbf{h}_{m,k}[n], \quad (14)$$

whereas the Gabor coefficients can be derived from

$$a_{m,k} = \sum_{n=0}^{N-1} \mathbf{S}[n] \tilde{\mathbf{g}}_{m,k}[n]. \quad (15)$$

Introducing integers  $\Delta M$  and  $\Delta K$  and the toral component  $W_N = \exp[2\pi i/N]$ , the discrete analysis and synthesis windows can be rewritten as

$$\mathbf{h}_{m,k}[n] = \mathbf{h}[n - m\Delta M] W_N^{nk\Delta K},$$

$$\mathbf{g}_{m,k}[n] = \mathbf{g}[n - m\Delta M] W_N^{nk\Delta K}.$$

As can be seen,  $\Delta M$  denotes the time and  $\Delta K$  the frequency step size. They correspond to  $T$  and  $\Omega$ . In our setting they are constrained by  $\Delta M \cdot M = \Delta K \cdot K = N$ . The reconstruction formula becomes

$$\begin{aligned} \mathbf{S}[j] &= \sum_{m=0}^{M-1} \sum_{k=0}^{K-1} a_{m,k} \mathbf{h}_{m,k}[j] \\ &= \sum_{l=0}^{N-1} \mathbf{S}[l] \sum_{m=0}^{M-1} \sum_{k=0}^{K-1} \tilde{\mathbf{g}}_{m,k}[l] \mathbf{h}_{m,k}[j], \end{aligned}$$

where we have assumed that the following discrete version of biorthogonality relation (13) for the sequences  $\mathbf{h}$  and  $\mathbf{g}$  is fulfilled,

$$\sum_{m=0}^{M-1} \sum_{k=0}^{K-1} \tilde{\mathbf{g}}_{m,k}[l] \mathbf{h}_{m,k}[j] = \delta_{l,j}.$$

It can be shown (for a proof see Appendix B) that the biorthogonality relation is satisfied if

$$\sum_{j=0}^{N-1} \mathbf{h}[j + qK] W_N^{-jpM} \tilde{\mathbf{g}}[j] = \frac{N}{MK} \delta_{p,0} \delta_{q,0} \quad (16)$$

for  $0 \leq p \leq \Delta M - 1$  and  $0 \leq q \leq \Delta K - 1$ . System (16) can be rewritten in matrix form: Let  $\mathbf{v} = (N/(MK), 0, \dots, 0)^T$  be a vector of length  $\Delta M \Delta K$  and  $\mathbf{g} = (g[0], \dots, g[N-1])$

the vector representing the discretely sampled dual frame, and let  $\mathbf{A}$  be the matrix of size  $\Delta M \Delta K \times N$  with entries  $\mathbf{A}_{(p,q),j} = \tilde{\mathbf{h}}(j+qK) W_N^{jpM}$ , then the dual frame atom  $\mathbf{g}$  is the solution of the linear system

$$\mathbf{A} \mathbf{g} = \mathbf{v}. \quad (17)$$

For oversampling  $\Delta M \Delta K < N$ , system (17) is underdetermined, and the solution is no longer unique and therefore there is a variety of possible dual frame atoms  $\mathbf{g}$ .

### 3.4 On the choice of the analysis and synthesis atom and the TF-plane lattice

As we have seen, there is a high degree of freedom when constructing a frame representation of some signal  $\mathbf{S}$ . In particular,

- i) the choice of the synthesis window  $\mathbf{h}$
- ii) the choice of the time-frequency sampling grid  $\Lambda$ , i.e. the choice of  $\Delta M$  and  $\Delta K$ , which specifies the redundancy/non-redundancy and therewith the non-uniqueness/uniqueness of the Gabor frame expansion (14)
- iii) the choice of  $\mathbf{g}$  in case of  $\Delta M \Delta K < N$ , i.e. in the oversampling situation, one may add further desirable constraints on the solution  $\mathbf{g}$  of system (17), e.g. minimum energy-norm.

These three aspects shall now be discussed:

At i): Any absolute and square integrable function  $\mathbf{h}$  is appropriate. However, as mentioned above, Heisenberg's uncertainty relation (8) requires for optimal time-frequency resolution a Gaussian function. Therefore, we choose

$$h(t) = \pi^{-1/4} \sigma_h^{-1/2} e^{-t^2/(2\sigma_h^2)}, \quad \text{such that } \|h\| = 1, \quad (18)$$

where the scaling parameter  $\sigma_h$  (determined below) shall allow either a better resolution in time or in frequency. As we shall see in iii), the time-frequency localization properties of synthesis function  $h$  carry over to analysis function  $g$ .

At ii): The most important parameters that control the sampling density in the TF-plane are  $\Delta K$  and  $\Delta M$ . Together with the specification  $\sigma_h$  they fully determine (up to non-canonical choices of  $g$ ) the discrete Gabor representation of some given function. In principle, the only requirement is  $\Delta K \Delta M \leq N$ . But because of Heisenberg's principle, too dense sampling (high redundancy) of the TF-plane is not worth the trouble. More precisely, let  $\Delta t$  denote the sampling size of  $\mathbf{S}$ , i.e.  $\mathbf{S}[n] = S(n\Delta t)$ , with total period of  $\mathbf{S}$  of  $N\Delta t = T_d$  (often referred to as the dwell time). Then, in the classical FFT context, the frequencies

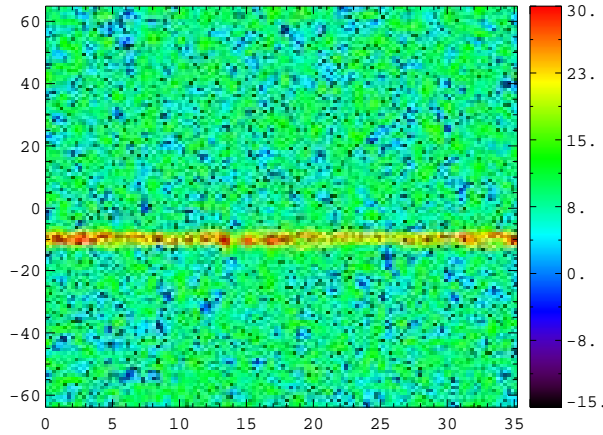


**Fig. 2.** Gabor phase space representation of a simulated RWP signal containing only noise and an atmospheric component. The x-axis shows time (in seconds) and the y-axis frequency (in Hz). Color contours (logarithmic scaling in dB) denote the power of the Gabor coefficients.

are due to Nyquist's law automatically spaced with resolution  $1/T_d$  within  $[-1/2\Delta t, 1/2\Delta t]$ . Through the flexibility of the Gabor representation we may individually set up the time and frequency spacing. Let us consider to this end the Heisenberg box size, i.e. the time and frequency variances (Eq. 7), which take for our particular  $h$  the form  $\sigma_t^2 = \sigma_h^2/2$  and  $\sigma_\omega^2 = (2\sigma_h^2)^{-1}$ . If we restrict the spacing of the TF-plane to this box size (essentially smaller would produce an overlapping of the boxes), i.e. setting  $\Delta\tau = \Delta M \Delta t = \sigma_t^2$  and  $\Delta\omega = \Delta K/T_d = \sigma_\omega^2$ , Heisenberg's uncertainty principle (Eq. 8) and the solvability of Eq. (17) yields

$$N \geq \Delta M \Delta K \geq \frac{1}{4} N. \quad (19)$$

The right inequality in Eq. (19) represents an upper sampling bound, which prevents an unnecessary Heisenberg box overlapping. If now an application requires a time resolution  $\Delta\tau$  in the Gabor representation, we immediately obtain in the context of Heisenberg's uncertainty principle the optimal scaling factor for the synthesis (and therewith for the analysis) atom,

$$\sigma_h^2 = 2\Delta\tau,$$

and a suggestion for the sampling density in time and frequency,

$$\Delta M = \lfloor \Delta\tau / \Delta t \rfloor, \quad \frac{N}{\Delta M} \geq \Delta K \geq \frac{N}{4\Delta M}.$$

At iii): In the oversampling situation ( $\Delta M \Delta K < N$ ), the non-uniqueness can be used to add desirable constraints to the solution, for example minimum energy. This was discussed

in greater detail in Qian and Chen (1993) and Qian et al. (1992): Since  $\mathbf{A}$  is underdetermined, we may rewrite Eq. (17) by applying the QR decomposition to its transposed form as

$$(\mathbf{R}^T | 0) \mathbf{Q}^T \mathbf{g} = (\mathbf{R}^T | 0) \begin{pmatrix} \mathbf{x} \\ \mathbf{y} \end{pmatrix} = \mathbf{v}$$

and thus  $\mathbf{x} = (\mathbf{R}^T)^{-1} \mathbf{v}$ . Because  $\mathbf{Q}\mathbf{Q}^T = \text{Id}$ , it follows

$$\mathbf{g} = \mathbf{Q} \begin{pmatrix} \mathbf{x} \\ \mathbf{y} \end{pmatrix} = (\mathbf{Q}_x | \mathbf{Q}_y) \begin{pmatrix} \mathbf{x} \\ \mathbf{y} \end{pmatrix} = \mathbf{Q}_x \mathbf{x} + \mathbf{Q}_y \mathbf{y}.$$

Since  $\mathbf{h}$  is in the range  $(\mathbf{Q}_x)$  and because  $\text{range}(\mathbf{Q}_x) \perp \text{range}(\mathbf{Q}_y)$ , one has  $\mathbf{Q}_y^T \mathbf{h} = \mathbf{0}$  (which is of interest below). Moreover, we observe that the analysis window  $\mathbf{g}$  is the sum of two orthogonal vectors with  $\|\mathbf{g}\|^2 = \|\mathbf{x}\|^2 + \|\mathbf{y}\|^2$ . Due to Eq. (17),  $\mathbf{Q}_x \mathbf{x} = \mathbf{Q}_x (\mathbf{R}^T)^{-1} \mathbf{v}$ , but  $\mathbf{Q}_y \mathbf{y}$  may depend on other constraints. When searching for the minimum norm solution, we simply set  $\|\mathbf{Q}_y \mathbf{y}\|^2 = \|\mathbf{y}\|^2 = 0$  and obtain

$$\mathbf{g} = \mathbf{Q}_x \mathbf{x} = \mathbf{Q}_x (\mathbf{R}^T)^{-1} \mathbf{v} = \mathbf{g}_{\min}$$

which is nothing than  $\mathbf{g}_{\min} = \mathbf{A}^T (\mathbf{A}\mathbf{A}^T)^{-1} \mathbf{v}$ . However, for a meaningful interpretation of the Gabor expansion, we would prefer an analysis window  $\mathbf{g}$  that is locally concentrated in the TF-plane. The design of such a function  $\mathbf{g}$  when the synthesis function  $\mathbf{h}$  as well as  $\Delta K$  and  $\Delta M$  are given is a nontrivial problem, which was addressed in Qian and Chen (1993) and Qian et al. (1992). The problem can be formulated as follows: Given an optimally concentrated function  $\mathbf{h}$  (e.g. the preassigned synthesis function), find its biorthogonal function  $\mathbf{g}$  whose shape best approximates time and frequency shifted versions of  $\mathbf{h}$ , i.e. minimize

$$E(\mathbf{g}, a, b) = \left\| \frac{\mathbf{g}}{\|\mathbf{g}\|} - \mathbf{h}_{a,b} \right\|^2 = 2 \left( 1 - \frac{1}{\|\mathbf{g}\|} \Re \langle \mathbf{g}, \mathbf{h}_{a,b} \rangle \right),$$

while  $\mathbf{A}\mathbf{g} = \mathbf{v}$ . For fixed  $a$  and  $b$ , the optimal vector  $\mathbf{y}$  in the representation for  $\mathbf{g}$  ( $\mathbf{x}$  is still fixed through the biorthogonality relation) is given by

$$\mathbf{y} = \frac{\|\mathbf{x}\|^2}{\Re \langle \mathbf{Q}_x \mathbf{x}, \mathbf{h}_{a,b} \rangle} \mathbf{Q}_y^T \mathbf{h}_{a,b}.$$

Choosing  $\mathbf{h}_{a,b} = \mathbf{h}$  yields  $\mathbf{Q}_y^T \mathbf{h}_{a,b} = \mathbf{0}$  (see above) and thus  $\mathbf{y} = \mathbf{0}$  and consequently,  $\mathbf{g} = \mathbf{g}_{\min}$ , i.e. the shape of  $\mathbf{g}_{\min}$  best approximates the shape of  $\mathbf{h}$ . Therefore, the TF-plane localization properties of  $\mathbf{h}$  carry over to  $\mathbf{g}$  in this case. But note that in principle any function  $\mathbf{h}_{a,b}$  is allowed and thus there is a large variety of possible analysis atoms  $\mathbf{g}$ .

### 3.5 Gabor representation of two examples

To illustrate the signal separation property of the discrete Gabor expansion for a single dwell, we consider two examples.

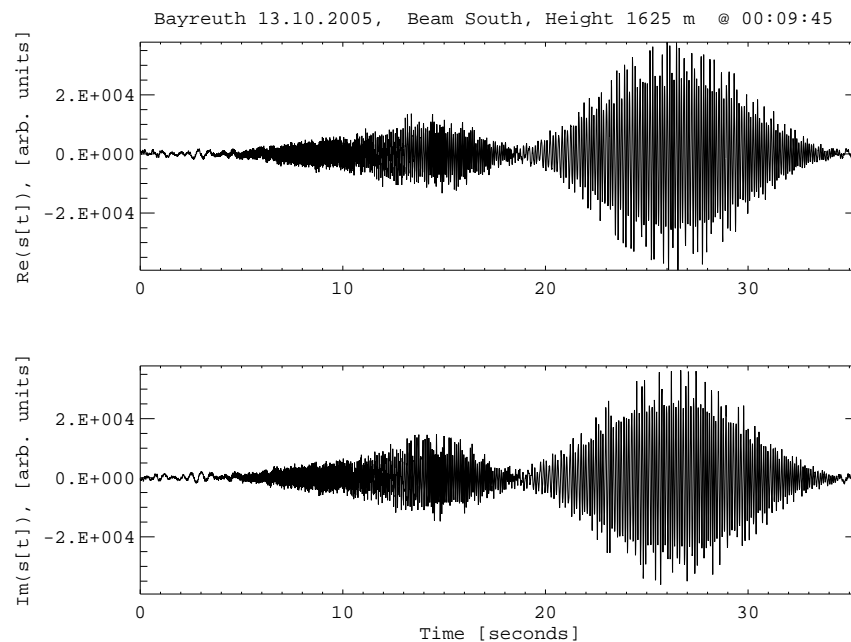


**Fig. 3.** Time series of the in-phase (upper plot) and quadrature (lower plot) component of the baseband signal measured with the 482-MHz RWP at Bayreuth, Germany, at 00:09:45 UTC on 13 October 2005 (south beam, range gate 9). The complex time series contains 4608 samples. Each sample is the coherent sum of 94 echoes from subsequent pulses.

The method of Zrnić (1975) was first used to simulate a signal in line with the classical signal model, which contains only noise and a stationary atmospheric component. In the frequency domain, the atmospheric signal peak is assumed to be a Gaussian centered at  $f_d = \omega/2\pi = -10.9 \text{ s}^{-1}$  and with a spectral width of  $w = 0.9 \text{ s}^{-1}$ . The discrete spectrogram of this signal is shown in Fig. 2. The atmospheric signal component is represented as a horizontal line (stationarity) centered at the prescribed Doppler frequency. Noise is spread over the complete TF plane.

Now let's take a look at measured time series data containing an additional intermittent clutter component. This dataset is further discussed in Sect. 5. The original I/Q data is shown in Fig. 3. Clearly, this time series is not stationary but contains transient components due to migrating birds. Assuming that a time resolution of  $\mathcal{O}(1\text{s})$  is sufficient to resolve these transients, we select a time resolution of about 0.5 s for the Gabor expansion. This corresponds to a frequency resolution of about 2 Hz. An appropriate sampling density in the TF-plane is achieved with  $\Delta M = 64$  and  $\Delta K = 64$ . Setting  $M = 128$  and  $K = 128$ , we get an oversampling factor of 3.5; the optimal scaling is given by  $\sigma_h^2 \approx 1$ . In contrast to the simulated case, the spectrogram of the measured signal shown in Fig. 4 shows additional nonstationary signal components, which are a typical signature of contamination by intermittent clutter. Taking a look at the pure time representation

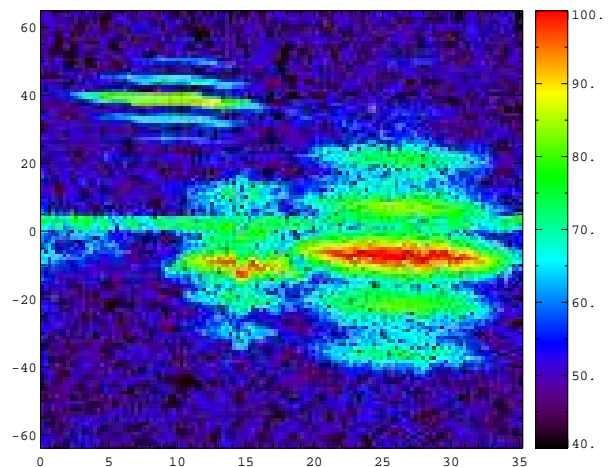


**Fig. 4.** Same representation as in Fig. 2, but for the data shown in Fig. 3. The three transient signal components are clearly separated from the stationary atmospheric signal component.

of the signal it is difficult to identify the separate transients, which show up as maxima of the envelope of the I/Q signal. However, Fig. 4 shows the same signal, but now its Gabor phase-space representation. This clearly provides a far better

picture of the signal transients, even if the spectrogram shows only the modulus of the Gabor coefficients (the Gabor coefficients itself are complex). Visible are three distinct transitory bird-events. Two of them overlap in time and can therefore not easily be distinguished in the time representation. All bird signals are much stronger in amplitude than the atmospheric signal of interest. The latter can be seen as a line at quasi-constant frequency, centered at about 3 Hz. By comparing Fig. 2 with the real data shown in Fig. 4, the goal of the filtering process becomes evident.

#### 4 Filtering through the statistics of Gabor frame coefficients

##### 4.1 Motivation for the statistical approach

With the tool of the Gabor representation at hand, the next step is to derive an appropriate filtering strategy for removal of the transient clutter signals. Our intention is to use the available a-priori knowledge about the signal components (atmosphere, noise, clutter) to construct an objective decision process aiming at a proper signal component separation.

It is well-justified that both the atmospheric and the noise signal component are stationary Gaussian random processes. The atmospheric signal has a bounded spectral width much smaller than Nyquist interval, whereas noise is white and spread over the full TF plane. Not much is known in contrast about intermittent clutter, only the non-property that this signal component is nonstationary over typical dwell-times. We make use of this a-priori information to derive a filter that has a pass-characteristics for realizations of wide-sense stationary random processes and a stop-characteristics for all non-stationary processes. That is, signals looking like the simulated example shown in Fig. 2 should not be affected by the filtering process. The goal is thus to derive an objective procedure, which modifies the Gabor phase space representation of signals in such a way, that stationary Gaussian signal components are preserved.

One can imagine several strategies for implementing such a filter. For instance, this could be based on image processing techniques or a fuzzy-logic approach similar to the one used by Cornman et al. (1998). We follow a simpler statistical approach, which has first been used by Merritt (1995) for the same problem, where it is applied to the temporal sequence of Doppler spectral coefficients at fixed frequency bins. The goal is to construct a similar test, but this time in Gabor phase space. We therefore need to analyze the statistical properties of the Gabor coefficients with respect to the different signal components, in order to distinguish between clear air and clutter return. This immediately leads to the question of how the properties of Gaussian stationary processes are mapped to the Gabor coefficients  $a_{m,k}$  or  $|a_{m,k}|^2$ . This problem is discussed in the next paragraph.

##### 4.2 Mean and variance estimator for Gabor spectrogram coefficients

Since we aim at constructing a statistical test (see the next section below) which is based on the expectation and the variance of the individual Gabor spectrogram coefficients  $|a_{m,k}|^2$ , we need to define adequate estimators for the expectation and the variance based on our observations (given through  $\mathbf{S}$ ).

First, to simplify the notation, we introduce  $a_\lambda$  as a shorthand notation of  $a_{m,k}$ , i.e. in what follows we set  $\lambda=(m, k)$ . Then, the Gabor spectrogram coefficients take the form

$$|a_\lambda|^2 = \sum_{n=0}^{N-1} \mathbf{S}[n] \mathbf{g}_\lambda[n] \sum_{l=0}^{N-1} \bar{\mathbf{S}}[l] \bar{\mathbf{g}}_\lambda[l].$$

As mentioned in the previous section, we assume that the data sequence  $\mathbf{S}$  satisfies for all  $n=0, \dots, N-1$ ,

$$\mathbf{E}\mathbf{S}[n] = 0 \quad \text{and} \quad \mathbf{E}\mathbf{S}[n] \bar{\mathbf{S}}[n+l] = \sigma^2 \rho[l].$$

With these two assumptions, the expectation and the covariance of the Gabor spectrogram coefficients are given by

$$\mathbf{E}|a_\lambda|^2 = \sigma^2 \langle \rho * \mathbf{g}_\lambda, \mathbf{g}_\lambda \rangle,$$

$$\text{Cov}(|a_\lambda|^2, |a_\eta|^2) = \sigma^4 |\langle \rho * \mathbf{g}_\lambda, \mathbf{g}_\eta \rangle|^2,$$

which is shown in Appendix C (Lemma 3 and Lemma 4). The “\*”-symbol stands here for the discrete convolution. The latter two formulas show the influence of the dependency of  $\mathbf{S}$  and the redundancy of the Gabor frame expansion. In case  $\mathbf{S}$  would be i.i.d. (i.e.  $\rho[l] = \delta_{l,0}$ ), it follows

$$\mathbf{E}|a_\lambda|^2 = \sigma^2 \quad \text{and} \quad \text{Cov}(|a_\lambda|^2, |a_\eta|^2) = \sigma^4 |\langle \mathbf{g}_\lambda, \mathbf{g}_\eta \rangle|^2.$$

If, moreover,  $\{\mathbf{g}_\lambda\}_{\lambda \in \Lambda}$  forms an orthonormal system, the covariance matrix becomes diagonal; i.e. as long as we deal with a redundant frame, the Gabor spectrum is always correlated with a range of dependency described by the decay of the Gramian matrix of  $\{\mathbf{g}_\lambda\}_{\lambda \in \Lambda}$  (up to the convolution with  $\rho$ ). The essential observation for our purpose is

$$\text{Var}|a_\lambda|^2 = \sigma^4 |\langle \rho * \mathbf{g}_\lambda, \mathbf{g}_\lambda \rangle|^2 = (\mathbf{E}|a_\lambda|^2)^2.$$

Consequently,

$$\frac{(\mathbf{E}|a_\lambda|^2)^2}{\text{Var}|a_\lambda|^2} = 1, \quad (20)$$

which holds true for independent as well as dependent samples  $\mathbf{S}[n]$  that follow a distribution which is determined by its moments. As property (20) constrains only the first two moments, it may hold true for a much richer class of distributions (in particular, it holds true for normally distributed random variables).

In order to construct a statistical test that verifies property (20), we have to find optimal estimators for  $\mathbf{E}|a_\lambda|^2$  and

$\text{Var}|a_\lambda|^2$  that are based on a finite number of observations. To this end, we introduce an index subset  $\Omega_\lambda \subset \Lambda$  containing  $\lambda$  and  $L-1$  further different indices  $\eta$ , i.e.  $|\Omega_\lambda|=L$ . As an estimator for  $\mathbb{E}|a_\lambda|^2 = \sigma^2 \langle \rho * \mathbf{g}_\lambda, \mathbf{g}_\lambda \rangle$ , which is based on  $L$  neighboring observation variables, we define

$$\hat{E}(\Omega_\lambda) := \frac{1}{C_{\Omega_\lambda}} \sum_{\eta \in \Omega_\lambda} |a_\eta|^2, \tag{21}$$

where the constant is given by

$$C_{\Omega_\lambda} = \sum_{\eta \in \Omega_\lambda} \frac{\langle \rho * \mathbf{g}_\eta, \mathbf{g}_\eta \rangle}{\langle \rho * \mathbf{g}_\lambda, \mathbf{g}_\lambda \rangle} > 1.$$

For i.i.d. samples  $\mathbf{S}[n]$ , the correcting multiplier in estimator (21) reduces to  $C_{\Omega_\lambda} = |\Omega_\lambda| = L$ , and therefore Eq. (21) is then nothing but the well-known mean estimator,

$$\hat{E}(\Omega_\lambda) = \frac{1}{L} \sum_{\eta \in \Omega_\lambda} |a_\eta|^2.$$

Assuming there exists some small  $\varepsilon > 0$  with

$$\sum_{\eta', \eta \in \Omega_\lambda} |\langle \rho * \mathbf{g}_{\eta'}, \mathbf{g}_\eta \rangle|^2 \leq C_{\Omega_\lambda}^{2-\varepsilon},$$

Lemmas 5 and 6 (see Appendix C) verify that Eq. (21) is a consistent estimator for  $\mathbb{E}|a_\lambda|^2$ , i.e.

$$\lim_{L \rightarrow \infty} \mathbb{E}|\hat{E}(\Omega_\lambda) - \mathbb{E}|a_\lambda|^2|^2 = \lim_{L \rightarrow \infty} (\text{Var}(\hat{E}(\Omega_\lambda)) + (\mathbb{E}|a_\lambda|^2 - \mathbb{E}(\hat{E}(\Omega_\lambda)))^2) = 0.$$

By the same reasoning, we define an estimator for variance,

$$\hat{V}(\Omega_\lambda) := C \sum_{\eta \in \Omega_\lambda} (|a_\eta|^2 - \hat{E}(\Omega_\lambda))^2, \tag{22}$$

where the constant is defined by

$$C^{-1} := 2 \sum_{\eta \in \Omega_\lambda} \frac{c_\eta^2}{c_\lambda^2} + (L - 2C_{\Omega_\lambda}) \left( 1 + \frac{1}{(\sum_\eta c_\eta)^2} \sum_{\xi, \alpha \in \Omega_\lambda} c_{\xi, \alpha}^2 \right). \tag{23}$$

Similar as before, it is shown (see Lemma 7 in Appendix C) that estimator (22) is unbiased (and certainly consistent, but the proof is omitted). Switching to the i.i.d. case yields

$$\begin{aligned} C^{-1} &= 2L + (L - 2L) \left( 1 + \frac{1}{L^2} \sum_{\xi, \alpha \in \Omega_\lambda} c_{\xi, \alpha}^2 \right) \\ &= L - \frac{1}{L} \sum_{\xi, \alpha \in \Omega_\lambda} |\langle \mathbf{g}_\xi, \mathbf{g}_\alpha \rangle|^2 \end{aligned}$$

and therefore Eq. (22) simplifies to

$$\hat{V}(\Omega_\lambda) = \frac{L}{L^2 - \sum_{\xi, \alpha \in \Omega_\lambda} |\langle \mathbf{g}_\xi, \mathbf{g}_\alpha \rangle|^2} \sum_{\eta \in \Omega_\lambda} (|a_\eta|^2 - \hat{E}(\Omega_\lambda))^2,$$

which can be easily seen with the help of formula (C1). If, moreover,  $\{\mathbf{g}_\lambda\}$  forms an orthonormal basis, we end up with the classical variance estimator

$$\hat{V}(\Omega_\lambda) = \frac{1}{L-1} \sum_{\eta \in \Omega_\lambda} (|a_\eta|^2 - \hat{E}(\Omega_\lambda))^2.$$

### 4.3 A statistical test performing signal identification

After having established estimators  $\hat{E}(\Omega_\lambda)$  and  $\hat{V}(\Omega_\lambda)$ , we aim now for the construction of a test that identifies Gabor coefficients associated with intermittent clutter returns. Typically, an atmospheric return is stationary and assumed to follow a Gaussian distribution, i.e. a test on the first two moments of the signal will give us some indication if this is true.

The basic idea goes back to Merritt (1995), who statistically tested a sequence of single (non-averaged) Doppler spectra in to order decide whether a particular Fourier power spectrum coefficient was due to a Gaussian or non-Gaussian signal. For this, he used the classical test of Hildebrand and Sekhon (1974) in a modified way. Following this approach, we consider the squared modulus of the Gabor phase space coefficients,  $|a_{m,k}|^2$ . Because we are interested in stationary signal components, we consider the sequence  $|a_{m,k}|^2$  for fixed frequency bins, i.e. we just pick individual rows and let only the time index change. For a fixed frequency index  $k$ , we have to test the elements  $|a_{m,k}|^2$  to be of stationary Gaussian type. Typically, we assume the observed sequence  $|a_{m,k}|^2$  to be possibly affected by non-stationary intermittent clutter. Then, we will get  $\hat{E}(\Omega_\lambda)^2 / \hat{V}(\Omega_\lambda) < 1$ . We also make use of the fact that intermittent clutter signals are almost always stronger than the (clear air) atmospheric return.

To identify intermittent clutter practically, we proceed as follows: in a first step, define the index set representing the  $k$ -th row, which we denote by  $\Omega_k = \{(m, k) : m=0, \dots, M-1\}$ , and sort for each  $k$  the sequence  $\{|a_{m,k}|^2\}_{(m,k) \in \Omega_k}$  in decreasing order. That is, we derive the order statistic of  $\{|a_{m,k}|^2\}_{(m,k) \in \Omega_k}$  which we denote by  $\{[a]_{m,k}|^2\}_{(m,k) \in \Omega_k}$  ( $[ \cdot ]$  stands for the order statistic map). Therefore, we have  $[a]_{m,k}|^2 \geq [a]_{m+1,k}|^2$  for all  $(m, k) \in \Omega_k$ . For  $l=0, \dots, M-1$ , we define subsets  $\Omega_k(l) = \{(m, k) : m=l, \dots, M-1\}$ . The largest coefficients are stepwise discarded, which has the goal of eliminating the clutter signal component. Using the quantities  $\hat{E}(\Omega_k(l))$  and  $\hat{V}(\Omega_k(l))$  of the subset, the test statistics  $\vartheta$  is computed for  $l=0, \dots, M-1$  as long as

$$\vartheta(|[a]_{l,k}|^2) := \frac{(\hat{E}(\Omega_k(l)))^2}{\hat{V}(\Omega_k(l))} < 1$$

holds. The largest coefficient of the first subset for which the test (positive for clutter) is not satisfied (a clutter-free subset) is then taken as a threshold for a frequency-dependent identification of the clutter component.

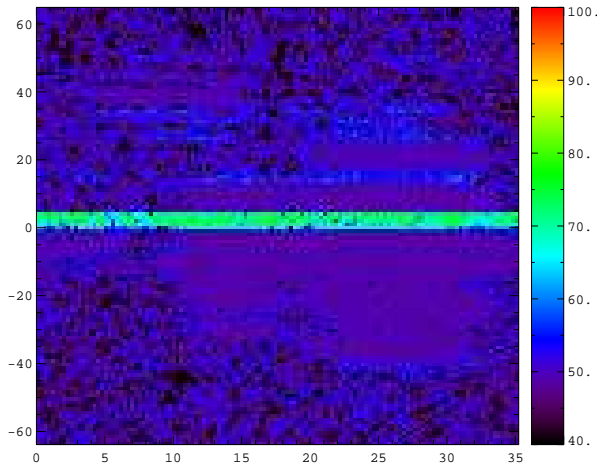


**Fig. 5.** Same as in Fig. 4, but after filtering. For the transient signal components, the Gabor coefficients were replaced by estimated thresholds for the stationary signal contribution at the given frequency.

#### 4.4 Signal separation through Gabor coefficient thresholding

All coefficients  $|a_{m,k}|^2$  greater than the threshold determined in the last section are regarded as clutter. One problem exists, if the subset  $\Omega_k(l)$  becomes too small in this iterative process. Then the statistical estimate will become unstable and the estimation of a local threshold is no longer meaningful. This should not happen if the dwell time is sufficiently long, but it is not always known how long the dwell time must be for various types of intermittent clutter. Further investigations are needed to clarify this question. However, it might nevertheless be attempted to clean data sets regardless of the dwell time used. In such cases it can happen that some nonstationary components have a duration on the order of the dwell time. Then it can be useful to replace the local threshold with a non frequency-dependent global threshold, which could be derived from stable estimates of local thresholds at other frequencies  $k$ . Such a global threshold should be constructed in such a way, that it reflects the noise level in the Gabor representation. For instance, it could be estimated by averaging over a certain number of the smallest local thresholds. This method, however, has a risk of clipping also the atmospheric (clear-air) signal component.

Leaving this problem aside, we can formulate the filtering procedure as follows: A coefficient  $|[a]_{l,k}|^2$  for which  $\vartheta(|[a]_{l,k}|^2) \geq 1$  holds is associated with clear air return. Based on the test, we introduce a clutter index set as

$$\Omega_k^c := \{(m, k) : \vartheta(|[a]_{m,k}|^2) < 1, m = 0, \dots, M-1\}$$

The coefficients  $a_{m,k} \in \Omega_k^c$  are finally set to  $t_k e^{i \arg a_{m,k}}$ , where

$t_k$  is the average value of the remaining coefficients,

$$t_k = \frac{1}{|\Omega_k \setminus \Omega_k^c|} \sum_{(m,k) \in \Omega_k \setminus \Omega_k^c} |a_{m,k}|.$$

The *main result* of this paper – the nonlinear filtering – is now formulated in the following:

*Let  $\mathbf{S}$  be the given RWP signal. Based on our model assumptions, the filtered component is given by*

$$\Phi(\mathbf{S})[n] = \sum_{k=0}^{K-1} \left\{ \sum_{(m,k) \in \Omega_k \setminus \Omega_k^c} a_{m,k} \mathbf{h}_{m,k}[n] + \sum_{(m,k) \in \Omega_k^c} t_k e^{i \arg a_{m,k}} \mathbf{h}_{m,k}[n] \right\}.$$

Finally, we discuss a practical aspect of the filtering method: The evaluation of the clutter index set  $\Omega_k^c$  requires the computation of the modified variance estimator. However, the computational overhead involved in calculating the modified variance estimator is obviously greater than in the case of the classical variance estimator. Our experience has shown that the variance estimates obtained with the two methods usually do not differ much. It may therefore be appropriate to use the classical variance estimator, if a saving of processing power is necessary for a real time implementation of the algorithm. This is left for a future study.

## 5 A real example: comparison with classical processing

### 5.1 Data set

Now let us illustrate the performance of the proposed filtering algorithm by applying it to RWP data obtained with the 482 MHz wind profiler at Bayreuth, Germany on 13 October 2005. This radar is one of three operational systems that the Deutscher Wetterdienst currently uses in its aerological network. The technical characteristics are summarized in Table 1. More details and an overview of the standard signal processing steps are given in Lehmann et al. (2003). For wind measurements, the system is running in a four-beam Doppler beam swinging configuration using two different pulse widths of 1667 ns (low mode) and 3333 ns (high mode). The averaging time for wind measurement is 26 min, another 4 min are used for RASS measurements of the virtual temperature. For the investigation of bird migration we consider only low mode data. The relevant sampling parameters are given in Table 2. Of interest are further the resolution of the time series  $\Delta t = 0.007708$  s, the number of data samples  $N = 4608$  and the total length or dwell time  $T_d = N \Delta t = 35.518464$  s.

During the bird migration season in October of 2005, full time series data of the coherently integrated demodulated receiver voltage signal were saved in the wind low mode.

**Table 1.** Technical parameters of the 482 MHz RWP/RASS at Bayreuth/Germany.

Center frequency	482.0078 MHz
Peak (Average) power	16 (2.4) kW
Pulse modulation	Amplitude (B/W) Phase (pulse compression)
Pulse widths (vert. resolution)	1.7 $\mu$ s (250 m) 2.2 $\mu$ s (330 m) 3.3 $\mu$ s (500 m) 4.4 $\mu$ s (660 m)
Antenna type	Phased array of 180 CoCo antennas
Antenna aperture (area)	142 m <sup>2</sup> (12.4×11.5 m)
On-axis gain above isotropic	$\geq$ 34 dBi
One-way half power (3 dB) beamwidth	$\leq$ 3
Oblique beam zenith distance	15.2
RX type	Heterodyne (IF 60 MHz), Digital IF
LNA noise figure	$\leq$ 0.6 dB
A/D conversion	14 bit (@ max 66 MHz)
Pulse compression	Bi-phase, complementary, max 32 bit
System sensitivity	$\leq$ -154 dBm
Vertical measuring range	16 km (wind), 4 km (virt. temp.)

Both wind and spectral data were manually reviewed to identify days with significant bird migration. It is well known, that a human expert can easily detect bird migration events by searching for typical patterns in the wind measurements (northeasterly directions in fall, discontinuities at sunrise and sunset), which are additionally accompanied by irregular and wide, sometimes multiple peaks in the Doppler spectra. In contrast to most clutter-free situations, those peaks often exhibit a poor time and range gate continuity. Time-height plots of the estimated moments (power, radial velocity and spectral width) are helpful to get a quick overview of potentially interesting cases, and a closer look into the time series data then typically confirms the conjecture of bird migration. Particular significant bird migration was noted on 13 October and we therefore selected this day as a test case for the new bird mitigation algorithm. A significant fraction of this data was contaminated with bird returns; the effect is best seen in Fig. 10. Here, the winds have been computed without any intermittent clutter removal algorithm.

The consensus method is normally not able to suppress the effect of the bird echoes because of their frequent occurrence. The operationally used intermittent clutter removal algorithm (ICRA), a particular implementation of the statistical averaging method proposed by Merritt (1995), could only alleviate the problem, see Fig. 11. Also, the operational quality control (Weber-Wuertz continuity check, not shown) was only able to flag a small percentage of the contaminated data, because the erroneous wind data exhibited the typical intrinsic consistency.

## 5.2 Processing details and results

A software was developed for reading and writing of the profiler time series data using the proprietary binary data format. This made it easy to process the data using the Gabor filter and to save them again in the original file format. The reprocessed data could therefore be seamlessly integrated in the off-line version of the operational wind profiler software, to compare the performance of the different algorithms.

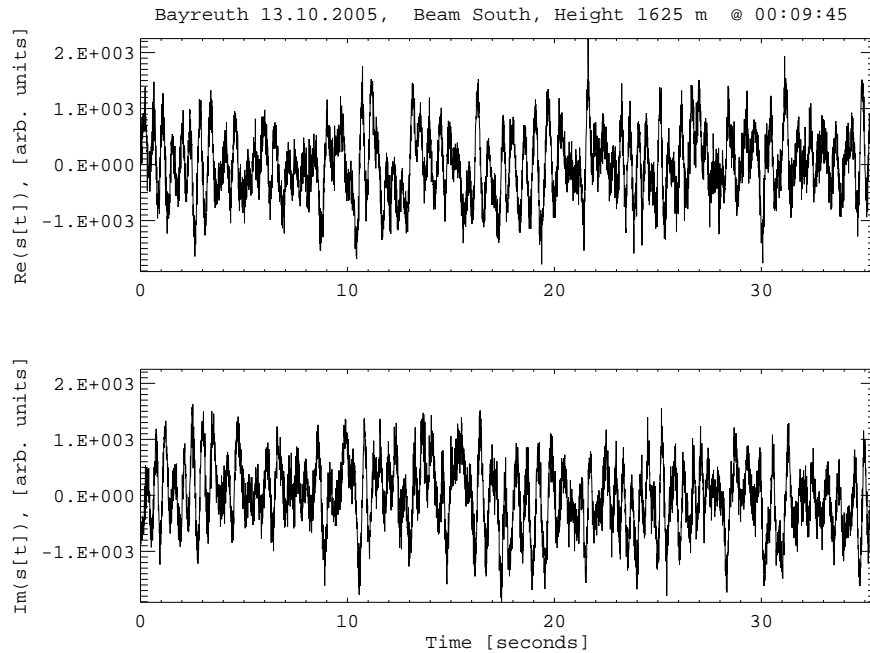


**Fig. 6.** Same as in Fig. 3, but for the cleaned signal obtained from the filtered Gabor representation shown in Fig. 5.

**Table 2.** TX and RX sampling parameters in routine operation.

	Wind Low-Mode
Inter Pulse Period	82 $\mu$ s
Pulse Width	1.7 $\mu$ s
Tx Duty	2.07%
# of code bits	1 (phase flip)
Pulse Peak Power (PEP)	16 kW
Spacing (on RX)	1.0 $\mu$ s
# of Gates	50
First Gate	8.6 $\mu$ s

As an example, we consider again the measurement taken in the south beam of the profiler at range gate 9 (1.6 km height a.g.l.), with a start time of the dwell at 00:09:45 UTC. This time series was already discussed in Sect. 3. As described in Sect. 4, local (constant frequency) thresholds were estimated to separate the clutter part of the signal from the stationary components atmosphere and noise. During processing of the complete dataset it was revealed that the dwell time of about 35 s was apparently rather short to guarantee that every observed intermittent clutter signal exhibits a clear transient behavior. Sometimes the duration of the clutter signal component was on the order of the dwell time instead. If this is the case, then the estimation of the local threshold may become unstable and signal separation can partly fail with the

result that clutter energy leaks through the filter. One way to remedy this problem is to replace local thresholds with a global threshold as described above. For the example data, this was done if more than 30 percent of the Gabor coefficients at a particular frequency were classified as clutter. The global threshold was then computed as the median over 15 percent of the smallest local thresholds, to get an estimate for the noise level. Another way to handle this situation would be to either flag this range gate as suspect or to replace the data with random white noise. Further research is needed to learn more about typical intermittent clutter characteristics and to optimize both the data sampling and the performance of the filter. The method described in this paper should be a useful tool for such investigations.

Application of the filtering strategy yields a filtered Gabor phase-space representation, which is shown in Fig. 5. Here, the moduli of the coefficients  $a_{m,k}$  representing the transient (bird) contributions have been replaced by an estimation of the stationary signal component at that frequency (either noise or atmospheric signal). The reconstructed I/Q time series after back-transformation from the Gabor phase space domain is presented in Fig. 6. The nonstationary signal components have been suppressed and also the amplitude has been significantly reduced. It is easy to measure the reduction of total power by computing the difference in variance between the unfiltered and the filtered data, to get an information about how much clutter energy was removed by the filter.

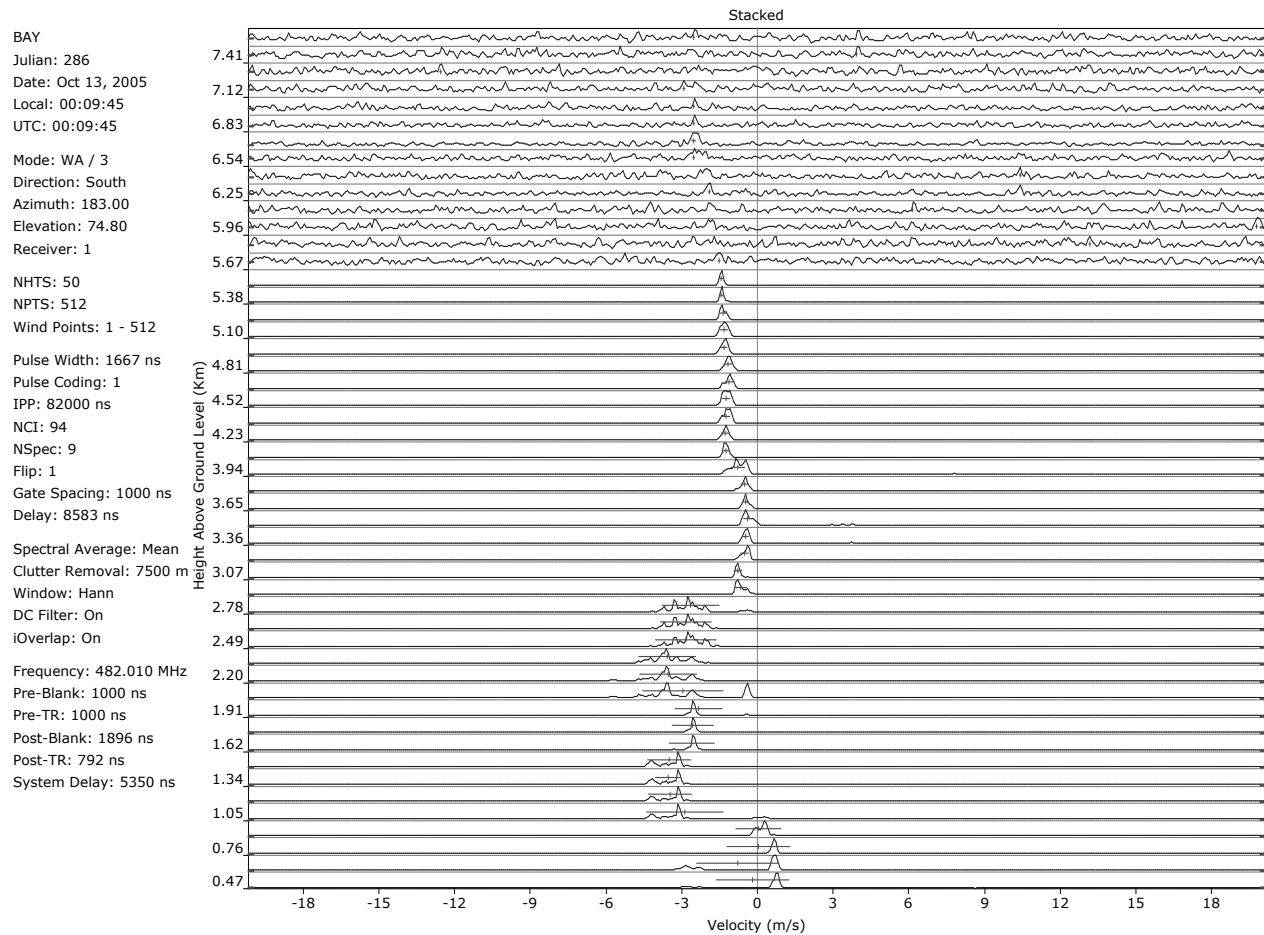


**Fig. 7.** Stacked plot of Doppler spectra for all low mode range gates, obtained through standard processing without any bird mitigation algorithm. Data were measured with the 482-MHz RWP at Bayreuth, Germany, at 00:09:45 UTC on 13 October 2005 (south beam). The estimated first and second moments are symbolized as a cross, where the vertical line shows the first moment (mean Doppler speed) and the horizontal line denotes spectral width. Massive bird contamination can be seen in the range gates below 3.0 km height.

Gabor filtering was performed for the complete dataset and the resulting bird-cleaned time series data were used for reprocessing of the whole day. This was compared with two additional processing methods: Method 1 used no intermittent clutter filtering algorithm, whereas method 2 used the routinely employed Intermittent Clutter Algorithm (ICRA), an implementation of the Statistical Averaging Method (SAM) originally proposed by Merritt (1995). The results for all range gates for the dwell taken at 00:09:45 UTC (stacked Doppler spectra) are shown in Figs. 7 (no filtering), 8 (ICRA filtering) and 9 (Gabor filtering). Without filtering, the lowest 17 range gates show spurious peaks and also large spectral widths due to the transient bird echoes. Note especially the discontinuity in height of the location of the estimated signal peak (derived Doppler velocity). With ICRA processing, the effect of the birds has been drastically re-

duced, but there are still range gates which show spurious peaks. This indicates that ICRA was unable to reduce the clutter energy completely. Figure 9 shows the processing results of the newly suggested filtering algorithm. The spurious remnants of the bird clutter are almost completely gone, although range gates 15 and 16 (2.49 and 2.64 km height agl) show apparently some bird clutter energy leaking through. This is also reflected in the somewhat larger spectral width at these heights. However, the spectral peak is now continuous across all heights and the spectral width estimates are mostly unaffected by the clutter.

Finally, the horizontal wind vector data derived through the three different processing methods are shown in Figs. 10 (no clutter filtering), 11 (ICRA processing) and 12 (Gabor filtering), respectively. The color coding is due to the wind speed (magnitude of the horizontal wind vector). Obviously,

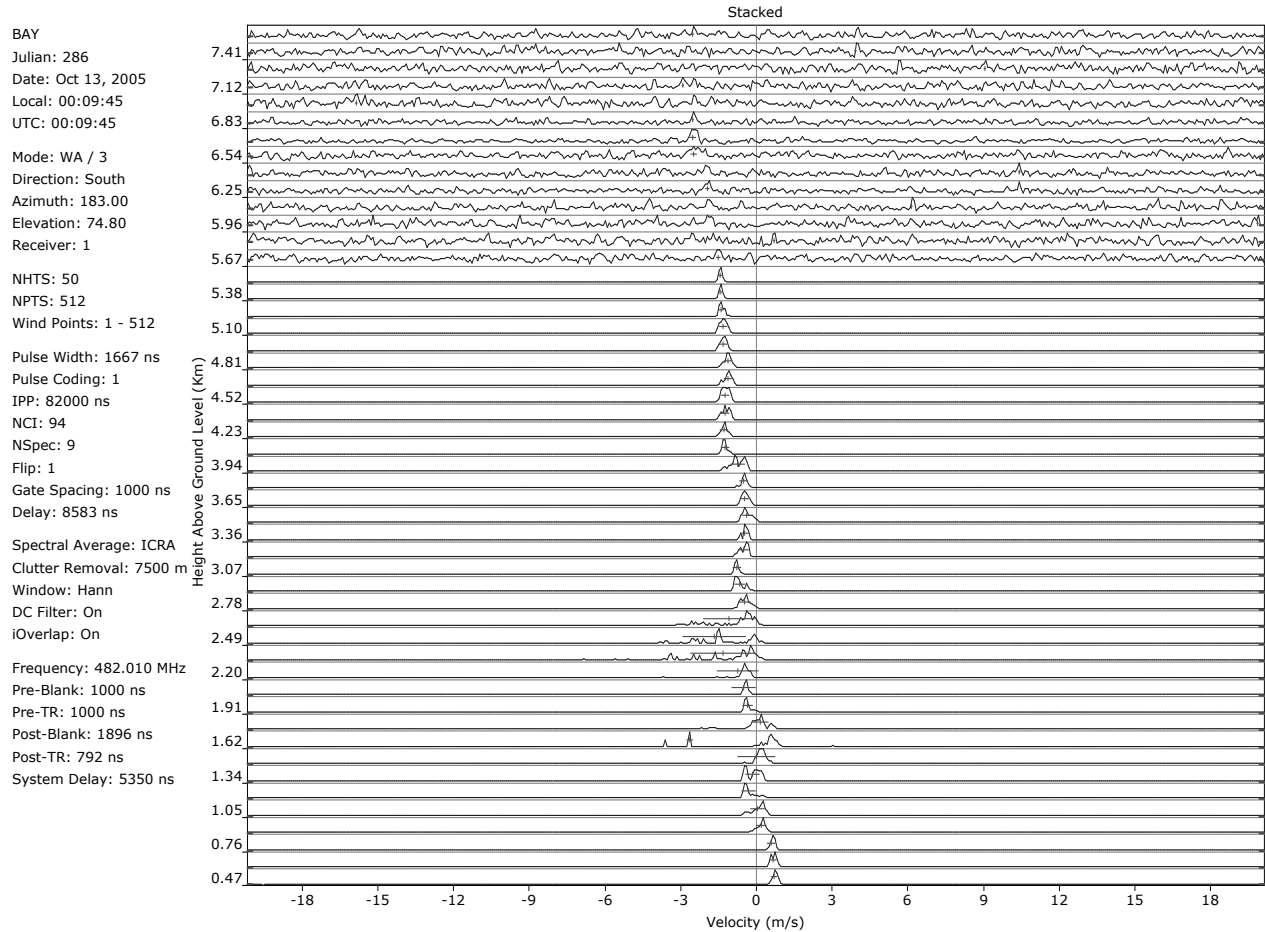


**Fig. 8.** Same as in Fig. 7, but Doppler spectra were estimated using the operational bird-mitigation algorithm ICRA. Bird contamination below 3.0 km height is reduced compared to Fig. 7, but still significant.

the clutter contamination has been drastically reduced by the new algorithm.

## 6 Conclusions

We have dealt with wind profiler signals obtained during bird migration and shown, how the signals can be decomposed into a time-frequency representation. A Gabor frame representation was used for a time-frequency analysis of the data and turned out to be a good method for signal-clutter separation. Previous attempts for intermittent clutter filtering have made use of the wavelet transform (WT) and its discrete versions (Jordan et al., 1997; Boisse et al., 1999; Lehmann and Teschke, 2001), so it is interesting to briefly discuss the difference between the dyadic wavelet and the Gabor approach, and to point out why we favor the Gabor method in comparison. The dyadic WT is another way of analyzing nonstationary signals. The difference lies in the tiling of the TF-plane

by the elementary signals (or time-frequency atoms). In the Gabor (WFT) approach, the tiling is uniform with fixed resolution. This is in contrast to the wavelet approach, where the tiling is generally variable. For example, an orthonormal wavelet basis decomposes the frequency axis in dyadic intervals whose sizes grow exponentially. In other words, the frequency resolution gets worse the more the time resolution is improved. This is wanted if the signals under investigation have high-frequency components of short duration embedded within low-frequency components of slow temporal variation. For the RWP signals however, we found no evidence for such a behavior. The intermittent clutter components occur at nearly all frequencies within the typical Nyquist range, with no obvious difference in temporal characteristics. In particular, they can occur close to zero frequency where the temporal resolution of the WT is the worst. Especially in this case, the WT seems not to be ideal for resolving the transient nature of the intermittent clutter.

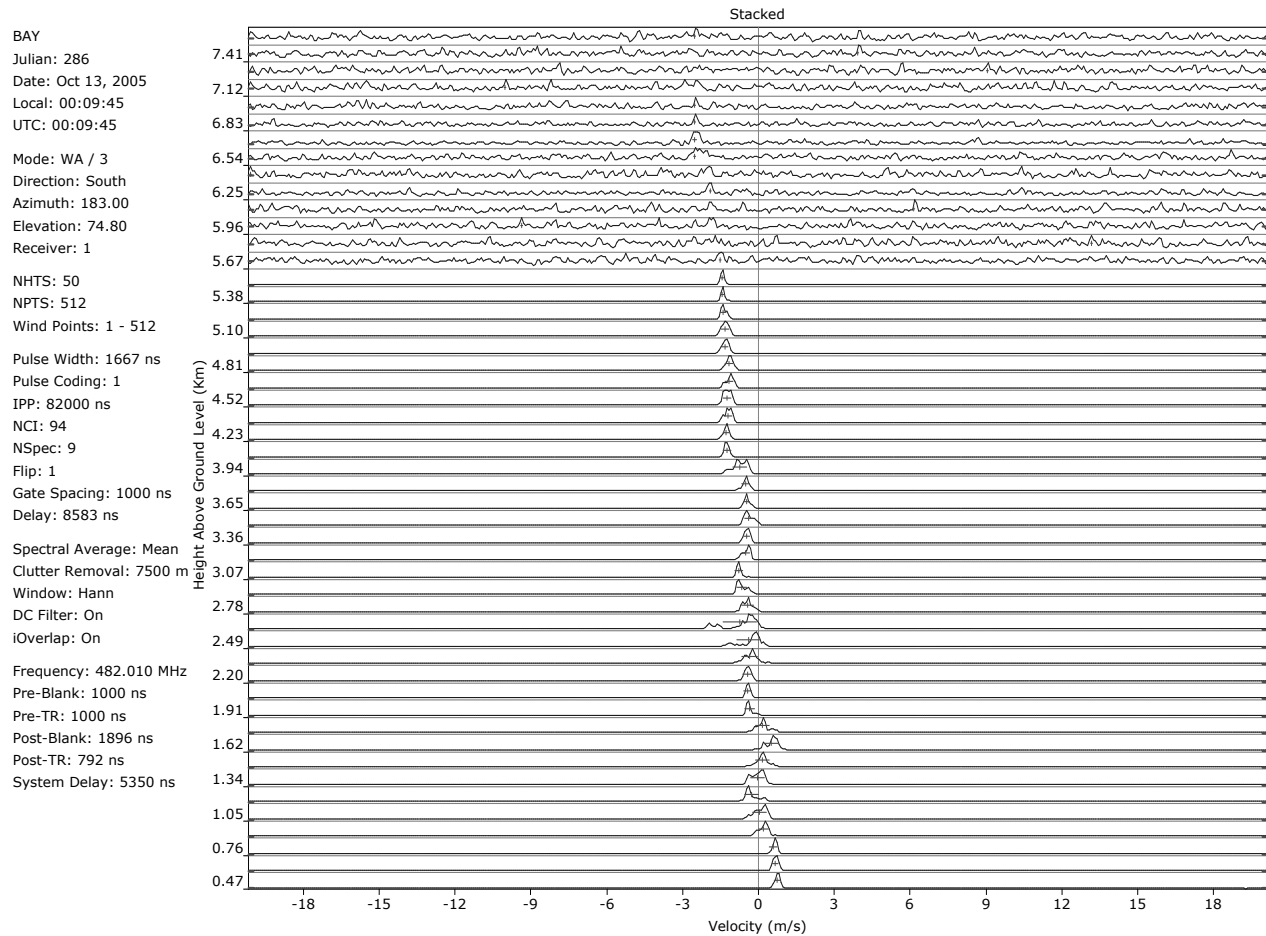


**Fig. 9.** Same as in Fig. 7, but Doppler spectra were estimated after statistical Gabor filtering of the original time series. Only minor remnants of bird contamination can be seen in range gates 15 and 16 (at 2.5 and 2.6 km height).

Examples of clutter signals in both representations shown by Justen and Lehmann (2003) illustrate this quite clearly. So the argument which is often used against the WFT, namely its constant time-frequency resolution, turns out to be advantageous. Additionally, the Gabor expansion using a Gaussian window achieves the best possible time-frequency resolution by reaching the lower limit of the Heisenberg uncertainty constraint.

To identify the clutter contribution to the signal, we make use of the a-priori information that the atmospheric signal component of interest can be adequately modelled as a stationary, proper complex Gaussian random process. Using this assumption, a test statistic is constructed to serve as a criterion for the discrimination between stationary and non-stationary signal components. This follows the approach first suggested by Merritt (1995). However, in case of the redundant Gabor transform it turns out, that the variance estimator

has to be modified to guarantee its unbiasedness and consistency. Proofs for the necessary modifications are given in detail.

Finally, the algorithm has been applied to a dataset obtained with a 482 MHz wind profiler during bird migration. It could be demonstrated that the performance of the new algorithm was superior to the performance of the operationally used intermittent clutter reduction algorithm, without obvious negative side effects. Application of the algorithm has shown, that sampling settings of the wind profiler play an important role in the clutter mitigation capabilities of the algorithm. This is not unexpected, since both the sampling period and the dwell time determine the resolution of the Doppler spectrum and obviously also the resolution of any time-frequency representation. Furthermore, longer dwell times may ease the identification of transient clutter signals and the stable estimation of the thresholds for noise and the

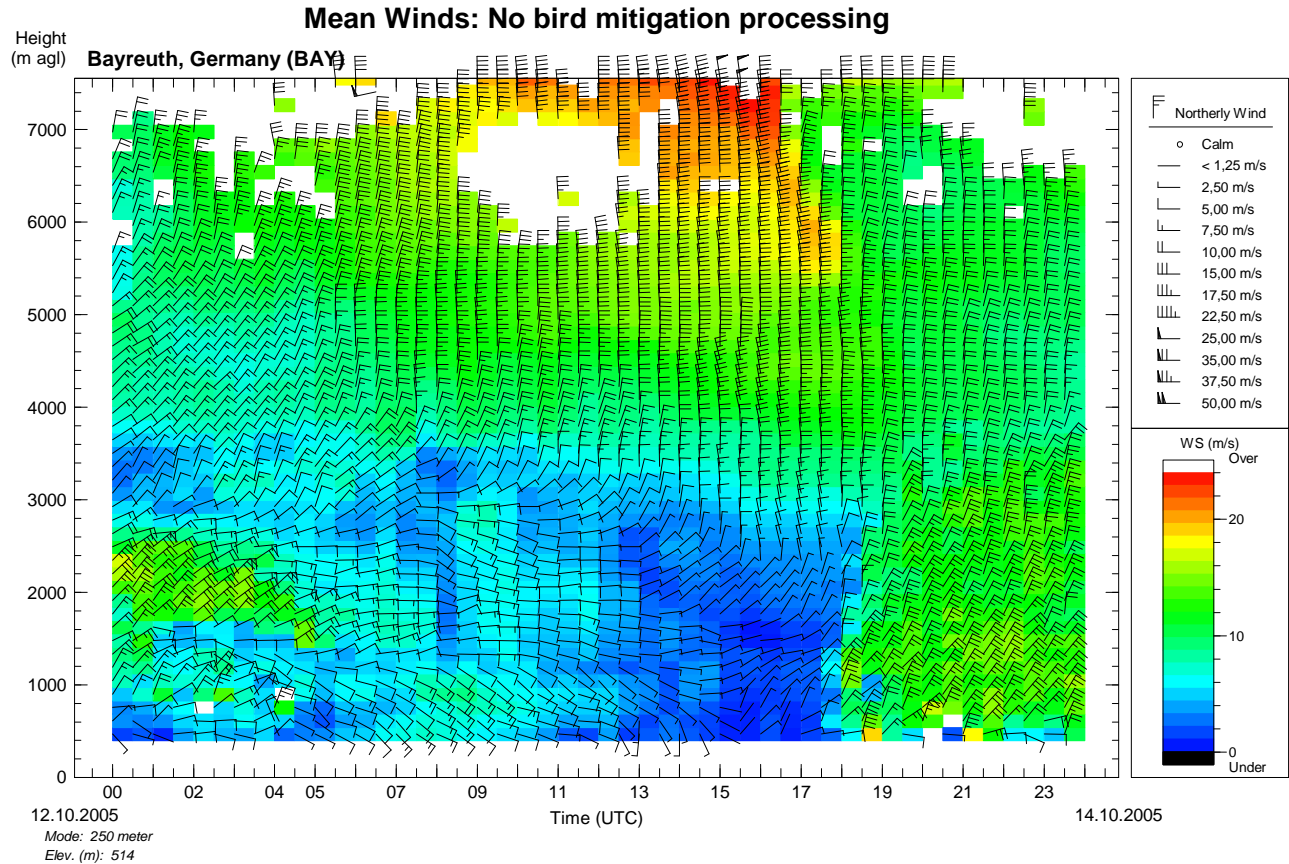


**Fig. 10.** Wind barb plot of horizontal winds measured in the low mode at Bayreuth on 13 October 2005. The x-axis shows time and the y-axis denotes height. Data have been color coded by wind speed. The signal processing was using no bird mitigation algorithm. Relatively strong northeasterly winds below about 3.5 km indicate strong bird migration, this can be seen between 00:00 and 05:00 UTC at heights around 1000 m and above 1600 m and especially after 18 UTC from the lowest gate to about 3500 m.

stationary atmospheric component. This is especially important for cases where atmospheric and clutter signal overlap in frequency.

Future work is suggested for a better quantitative characterization of intermittent clutter signals during dense bird migration. This should allow to optimize both sampling and processing settings for operational wind profiler systems. A long-term evaluation of the new algorithm would be useful to determine its limits and to estimate the performance improvements of the new methods, in comparison with previously used algorithms. This would be facilitated by an online-implementation of the method and a means to compare the profiler wind measurement with independent data, e.g. radiosonde measurements.

## Appendix A

### Frame theory

We briefly review some basic facts on frames using the abstract notation of functional analysis, but the reader is advised to consult the comprehensive literature for details (Heil and Walnut, 1989; Daubechies, 1990; Carmona et al., 1998; Mallat, 1999; Christensen, 2001).

The frame theory generalizes the concept of bases in Hilbert spaces (even in more general spaces). Let  $H$  be some Hilbert space (e.g. the space of function of finite energy denoted with  $\mathbb{L}^2(\mathbf{R})$  to which our signal  $S(t)$  normally belongs to), the pair of parenthesis  $\langle \cdot, \cdot \rangle$  the associated inner product and  $\|\cdot\|_H^2 = \langle \cdot, \cdot \rangle$  the induced norm. A frame  $\{h_\lambda : \lambda \in \Lambda\}$  in  $H$  is a system of functions for which there exist constants  $0 < A \leq B < \infty$  such that for all  $s \in H$

$$A\|S\|_H^2 \leq \sum_{\lambda \in \Lambda} |\langle S, h_\lambda \rangle|^2 \leq B\|S\|_H^2. \quad (\text{A1})$$

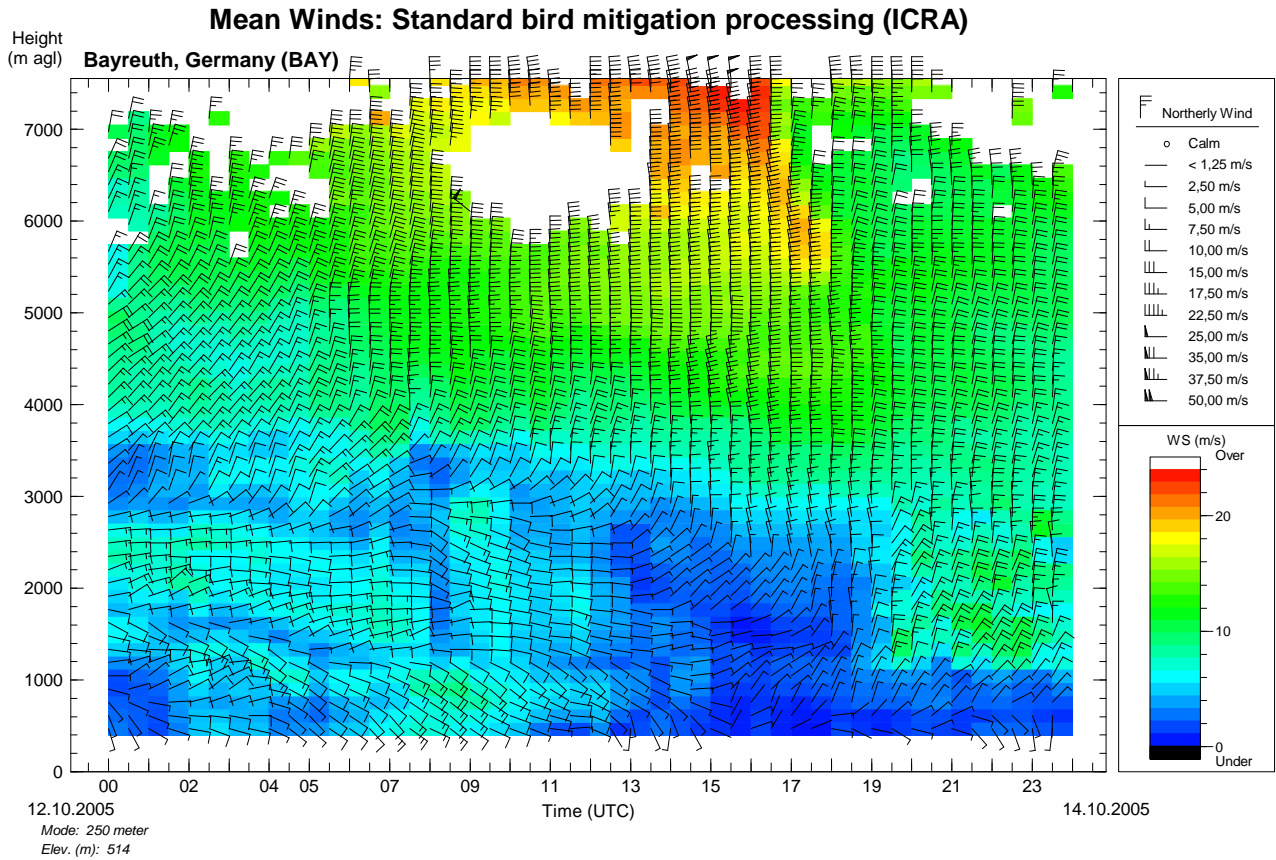


**Fig. 11.** Same as in Fig. 10. The signal processing was using the standard ICRA algorithm. Bird contamination has been reduced compared to Fig. 10, but is still significant after 19:00 UTC. A few other northeasterly wind barbs around 02:00 UTC are affected by intermittent clutter echoes.

The map,  $F : H \rightarrow \ell_2$ , defined via  $F : f \mapsto \{\langle f, h_\lambda \rangle\}$  is usually referred to as the frame operator (analysis operator). So the signal is characterized by inner products with the frame. To answer the question of how  $f$  can again be synthesized from the inner products  $\{\langle f, h_\lambda \rangle\}$ , we consider the adjoint frame operator given by  $F^*c = \sum_{\lambda \in \Lambda} c_\lambda h_\lambda$ . This allows us to write

$$F^*Ff = \sum_{\lambda \in \Lambda} \langle f, h_\lambda \rangle h_\lambda. \tag{A2}$$

If  $F^*F$  equals the identity  $\text{Id}$ ,  $F^*$  performs a perfect reconstruction. This is the case when  $\{h_\lambda\}$  forms an orthonormal basis. However, in general one has to apply  $(F^*F)^{-1}$  to Eq. (A2). This is possible since the inverse exists and is bounded because of Eq. (A1),

$$A \cdot \text{Id} \leq F^*F \leq B \cdot \text{Id}$$

and thus

$$B^{-1} \cdot \text{Id} \leq (F^*F)^{-1} \leq A^{-1} \cdot \text{Id}.$$

Since  $(F^*F)^{-1}$  is self-adjoint and denoting  $(F^*F)^{-1}h_\lambda = g_\lambda$ , one consequently has

$$\begin{aligned} \sum_{\lambda \in \Lambda} \langle S, g_\lambda \rangle h_\lambda &= F^*F(F^*F)^{-1}S = S \\ &= (F^*F)^{-1}F^*FS = \sum_{\lambda \in \Lambda} \langle S, h_\lambda \rangle g_\lambda. \end{aligned} \tag{A3}$$

In frame lore,  $g_\lambda$  is referred to as the canonical dual frame with respect to  $h_\lambda$ .

In general,  $(F^*F)^{-1}$  cannot be explicitly computed but must be approximated by an iterative approach. However, the situation can be essentially relaxed when assuming that the frames  $\{h_\lambda\}$  and  $\{g_\lambda\}$  form not a primal-dual, but a bi-orthogonal frame pair, i.e.  $\langle h_\lambda, g_\eta \rangle = \delta_{\lambda,\eta}$ . If  $\tilde{F}$  denotes the frame operator with respect to  $g_\lambda$ , then  $\tilde{F} = F(F^*F)^{-1}$  and one may write  $(\langle h_\lambda, g_\eta \rangle)_{\lambda,\eta \in \Lambda} = \tilde{F}F^*$ , which is diagonal. Therefore,  $\tilde{F}$  is an analysis and  $F^*$  a synthesis operator yielding perfect reconstruction (and vice versa, i.e. exchanging the roles of  $\tilde{F}$  and  $F^*$ ). If now the bi-orthogonality relation

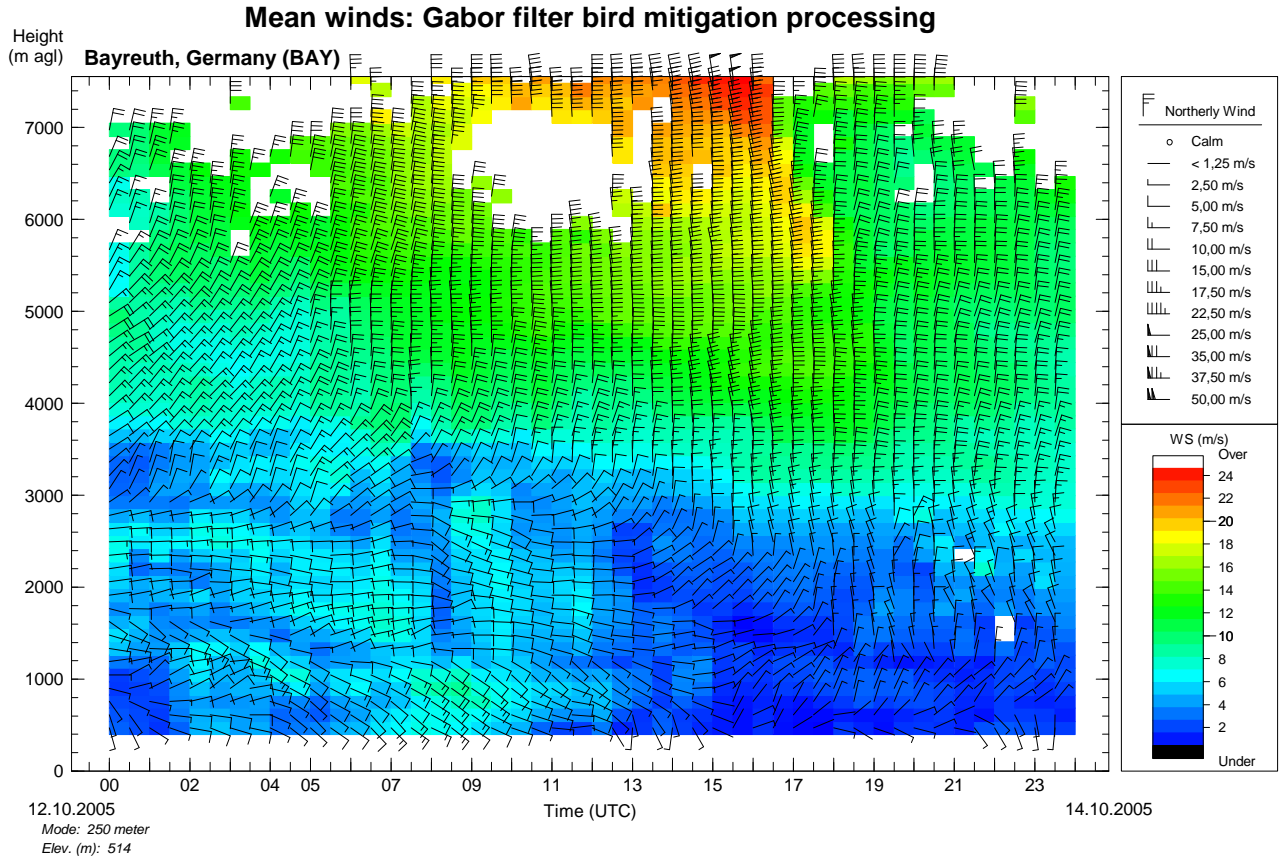


**Fig. 12.** Same as in Fig. 10. The signal processing was using the new Gabor filter algorithm. Bird contamination has again been reduced compared to Fig. 11. There are no indications of bird migration between 00:00 and 05:00 UTC, and only a few obvious outliers and missing data after 19:00 UTC.

yields a way to derive  $g_\lambda$ , the inverse of  $F^*F$  needs not to be computed.

**Appendix B**

**Biorthogonal discrete Gabor frame expansion**

The following lemma can be retraced to its original form in Wexler and Raz (1990), it gives an explicit proof of the biorthogonality relation.

**Lemma 1** Assume the relation

$$\sum_{j=0}^{N-1} \bar{\mathbf{g}}[j] \mathbf{h}[j + qK] W^{-jpM} = N/(MK) \delta_{p,0} \delta_{q,0} \quad (\text{B1})$$

is fulfilled for  $0 \leq p \leq \Delta M - 1$  and  $0 \leq q \leq \Delta K - 1$ . Then the

biorthogonality relation

$$\sum_{m=0}^{M-1} \sum_{k=0}^{K-1} \bar{\mathbf{g}}_{m,k}[l] \mathbf{h}_{m,k}[j] = \delta_{l,j}$$

holds true.

*Proof.* This assertion can be shown directly. Let

$$f(l, j) := \sum_{m=0}^{M-1} \sum_{k=0}^{K-1} \bar{\mathbf{g}}_{m,k}[l] \mathbf{h}_{m,k}[j],$$

then

$$f(l, j) = \sum_{m=0}^{M-1} \bar{\mathbf{g}}[l - m\Delta M] \mathbf{h}[j - m\Delta M] \sum_{k=0}^{K-1} W^{k(j-l)\Delta K}.$$

We still have,

$$\sum_{k=0}^{K-1} W^{k(j-l)\Delta K} = \sum_{k=0}^{K-1} e^{i2\pi k(j-l)/K} = \begin{cases} K, & \text{if } (j-l)/K \in \mathbb{Z} \\ 0, & \text{else} \end{cases}.$$

Since  $(j-l)/K \in \mathbb{Z}$  means there exists some  $q \in \mathbb{Z}$  such that  $q=(j-l)/K$  or  $j-l-qK=0$ , we may consequently write (by the Poisson Summation Formula and the made assumption)

$$\begin{aligned} f(l, j) &= \sum_{m=0}^{M-1} \bar{\mathbf{g}}[l - m\Delta M] \mathbf{h}[j - m\Delta M] K \sum_q \delta_{j-l-qK,0} \\ &= K \sum_q \delta_{j-l-qK,0} \sum_{m=0}^{M-1} \bar{\mathbf{g}}[l - m\Delta M] \mathbf{h}[l + qK - m\Delta M] \\ &= K \sum_q \delta_{j-l-qK,0} \times \\ &\quad \Delta M^{-1} \sum_{p=0}^{\Delta M-1} \left( \sum_{j'=0}^{N-1} \bar{\mathbf{g}}[j'] \mathbf{h}[j' + qK] W^{-j'pM} \right) W^{lpM} \\ &= K \sum_q \delta_{j-l-qK,0} M/N \sum_{p=0}^{\Delta M-1} N/(MK) \delta_{p,0} \delta_{q,0} W^{lpM} \\ &= \delta_{j,l}. \end{aligned}$$

□

### Appendix C

#### Statistical properties of the Gabor coefficients

**Lemma 2** Let  $\mathbf{S}$  be given and assume  $\mathbf{E}\mathbf{S}[n]=0$  for all  $n=0, \dots, N-1$  and that  $a_\lambda$  is as defined in Eq. (15). Then  $\mathbf{E}a_\lambda=0$ .

*Proof.* By definition,  $a_\lambda = \sum_{n=0}^{N-1} \mathbf{S}[n] \mathbf{g}_\lambda[n]$ . Therefore,  $\mathbf{E}a_\lambda = \sum_{n=0}^{N-1} \mathbf{E}\mathbf{S}[n] \mathbf{g}_\lambda[n] = 0$ . □

**Lemma 3** Let  $\mathbf{S}$  be given and assume  $\mathbf{E}\mathbf{S}[n]=0$  for all  $n=0, \dots, N-1$  and that  $a_\lambda$  is as defined in Eq. (15). Moreover, assume a range of dependency of neighboring samples of  $\mathbf{S}$  which is characterized by the auto-covariance function  $\rho$  of  $\mathbf{S}$ , i.e.  $\mathbf{E}(\mathbf{S}[n] \bar{\mathbf{S}}[n+l]) = \sigma^2 \rho[l]$ . Then

$$\text{Cov}(a_\lambda, a_\eta) = \sigma^2 \langle \rho * \mathbf{g}_\lambda, \mathbf{g}_\eta \rangle,$$

where “\*” denotes the discrete convolution.

The latter lemma states that the Gabor coefficients  $a_\lambda$  turn into dependent random variables (even when  $\rho$  is a delta sequence, i.e. for independent samples of  $\mathbf{S}$ ). The range of dependency is determined by the sampling density in

the time-frequency space and the range of dependency of  $\mathbf{S}$ . In case  $\mathbf{S}$  is a sequence of i.i.d. random variables, the dependency of  $a_\lambda$  is fully characterized by the reproducing kernel  $\langle \mathbf{g}_\lambda, \mathbf{g}_\eta \rangle$ .

*Proof.* By Lemma 2,  $\text{Cov}(a_\lambda, a_\eta) = \mathbf{E}(a_\lambda \bar{a}_\eta)$ . Therefore,

$$\begin{aligned} \text{Cov}(a_\lambda, a_\eta) &= \mathbf{E} \left( \sum_{n=0}^{N-1} \mathbf{S}[n] \mathbf{g}_\lambda[n], \sum_{l=0}^{N-1} \bar{\mathbf{S}}[l] \bar{\mathbf{g}}[l] \right) \\ &= \sum_{n=0}^{N-1} \sum_{l=0}^{N-1} \mathbf{E}(\mathbf{S}[n] \bar{\mathbf{S}}[l]) \mathbf{g}_\lambda[n] \bar{\mathbf{g}}_\eta[l] \\ &= \sigma^2 \sum_{n=0}^{N-1} \sum_{l=0}^{N-1} \rho[l-n] \mathbf{g}_\lambda[n] \bar{\mathbf{g}}_\eta[l] \\ &= \sigma^2 \sum_{l=0}^{N-1} (\rho * \mathbf{g}_\lambda)[l] \bar{\mathbf{g}}_\eta[l] = \sigma^2 \langle \rho * \mathbf{g}_\lambda, \mathbf{g}_\eta \rangle. \end{aligned}$$

□

A special case of Lemma 3 is  $\mathbf{E}|a_\lambda|^2 = \sigma^2 \langle \rho * \mathbf{g}_\lambda, \mathbf{g}_\lambda \rangle$ .

**Lemma 4** Make the same assumptions as in Lemma 3. Then

$$\text{Cov}(|a_\lambda|^2, |a_\eta|^2) = \sigma^4 |\langle \rho * \mathbf{g}_\lambda, \mathbf{g}_\eta \rangle|^2.$$

*Proof.* First, note that for proper Gaussian complex random variables  $\mathbf{S}[k]$  with  $\mathbf{E}\mathbf{S}[k]=0$  and  $\text{Cov}(\mathbf{S}[k] \bar{\mathbf{S}}[l]) = \mathbf{E}(\mathbf{S}[k] \bar{\mathbf{S}}[l]) = \sigma^2 \rho(l-k)$  we have (Reed, 1962)

$$\begin{aligned} &\mathbf{E}(\mathbf{S}[k] \bar{\mathbf{S}}[l] \mathbf{S}[n] \bar{\mathbf{S}}[m]) \\ &= \mathbf{E}(\mathbf{S}[k] \bar{\mathbf{S}}[l]) \mathbf{E}(\mathbf{S}[n] \bar{\mathbf{S}}[m]) + \mathbf{E}(\mathbf{S}[k] \bar{\mathbf{S}}[m]) \mathbf{E}(\bar{\mathbf{S}}[l] \mathbf{S}[n]) \\ &= \sigma^4 (\rho[l-k] \rho[m-n] + \rho[m-k] \bar{\rho}[n-l]). \end{aligned}$$

With the help of Lemma 3 (special case),

$$\text{Cov}(|a_\lambda|^2, |a_\eta|^2) = \mathbf{E}(|a_\lambda|^2 |a_\eta|^2) - \sigma^4 \langle \rho * \mathbf{g}_\lambda, \mathbf{g}_\lambda \rangle \langle \rho * \mathbf{g}_\eta, \mathbf{g}_\eta \rangle$$

and thus it remains to derive  $E(|a_\lambda|^2|a_\eta|^2)$ . Using the moment theorem of Reed (1962), we have,

$$\begin{aligned} E(|a_\lambda|^2|a_\eta|^2) &= \left( \sum_{k=0}^{N-1} \mathbf{S}[k] \mathbf{g}_\lambda[k] \sum_{l=0}^{N-1} \bar{\mathbf{S}}[l] \bar{\mathbf{g}}_\lambda[l] \times \right. \\ &\quad \left. \sum_{n=0}^{N-1} \mathbf{S}[n] \mathbf{g}_\eta[n] \sum_{m=0}^{N-1} \bar{\mathbf{S}}[m] \bar{\mathbf{g}}_\eta[m] \right) \\ &= \sum_{k,l,n,m=0}^{N-1} E(\mathbf{S}[k] \bar{\mathbf{S}}[l] \mathbf{S}[n] \bar{\mathbf{S}}[m]) \mathbf{g}_\lambda[k] \bar{\mathbf{g}}_\lambda[l] \mathbf{g}_\eta[n] \bar{\mathbf{g}}_\eta[m] \\ &= \sigma^4 \sum_{k,l,n,m=0}^{N-1} (\rho[l-k] \rho[m-n] + \rho[m-k] \bar{\rho}[n-l]) \times \\ &\quad \mathbf{g}_\lambda[k] \bar{\mathbf{g}}_\lambda[l] \mathbf{g}_\eta[n] \bar{\mathbf{g}}_\eta[m] \\ &= \sigma^4 \left( \sum_{l,m=0}^{N-1} \bar{\mathbf{g}}_\lambda[l] \bar{\mathbf{g}}_\eta[m] \left\{ \sum_{k=0}^{N-1} \rho[l-k] \mathbf{g}_\lambda[k] \right\} \times \right. \\ &\quad \left. \left\{ \sum_{n=0}^{N-1} \rho[m-n] \mathbf{g}_\eta[n] \right\} + \sum_{m,n=0}^{N-1} \mathbf{g}_\eta[n] \bar{\mathbf{g}}_\eta[m] \left\{ \sum_{k=0}^{N-1} \rho[m-k] \mathbf{g}_\lambda[k] \right\} \times \right. \\ &\quad \left. \left\{ \sum_{l=0}^{N-1} \bar{\rho}[n-l] \bar{\mathbf{g}}_\lambda[l] \right\} \right) \\ &= \sigma^4 \left( \sum_{l,m=0}^{N-1} \bar{\mathbf{g}}_\lambda[l] \bar{\mathbf{g}}_\eta[m] (\rho * \mathbf{g}_\lambda)[l] (\rho * \mathbf{g}_\eta)[m] + \right. \\ &\quad \left. \sum_{m,n=0}^{N-1} \mathbf{g}_\eta[n] \bar{\mathbf{g}}_\eta[m] (\rho * \mathbf{g}_\lambda)[m] (\bar{\rho} * \bar{\mathbf{g}}_\lambda)[n] \right) \\ &= \sigma^4 \left( \langle \rho * \mathbf{g}_\lambda, \mathbf{g}_\lambda \rangle \langle \rho * \mathbf{g}_\eta, \mathbf{g}_\eta \rangle + |\langle \rho * \mathbf{g}_\lambda, \mathbf{g}_\eta \rangle|^2 \right), \end{aligned}$$

and consequently,

$$\text{Cov}(|a_\lambda|^2, |a_\eta|^2) = \sigma^4 |\langle \rho * \mathbf{g}_\lambda, \mathbf{g}_\eta \rangle|^2.$$

□

After having verified the basic properties of the Gabor power coefficients, we prove that estimator (21) is consistent and that estimator (22) is unbiased (The proof of consistency is omitted, because this requires the computation of the 8th-mixed moment).

**Lemma 5** *The estimator  $\hat{E}(\Omega_\lambda)$  unbiased, i.e. it holds  $E\hat{E}(\Omega_\lambda) = \sigma^2 \langle \rho * \mathbf{g}_\lambda, \mathbf{g}_\lambda \rangle$ .*

*Proof.* This follows by the definition of  $C_{\Omega_\lambda}$  and Lemma 3,

$$\begin{aligned} E\hat{E}(\Omega_\lambda) &= \frac{1}{C_{\Omega_\lambda}} \sum_{\eta \in \Omega_\lambda} E|a_\eta|^2 \\ &= \frac{1}{C_{\Omega_\lambda}} \sum_{\eta \in \Omega_\lambda} \sigma^2 \langle \rho * \mathbf{g}_\eta, \mathbf{g}_\eta \rangle = \sigma^2 \langle \rho * \mathbf{g}_\lambda, \mathbf{g}_\lambda \rangle. \end{aligned}$$

**Lemma 6** *Assume, for the dual frame  $\{\mathbf{g}_\lambda : \lambda \in \Lambda\}$  there exists some  $\varepsilon > 0$  such that the condition*

$$\sum_{\eta', \eta \in \Omega_\lambda} |\langle \rho * \mathbf{g}_{\eta'}, \mathbf{g}_\eta \rangle|^2 \leq C_{\Omega_\lambda}^{2-\varepsilon}$$

*is fulfilled. Then the estimator  $\hat{E}(\Omega_\lambda)$  satisfies*

$$\text{Var}(\hat{E}(\Lambda)) \leq \sigma^4 C_{\Omega_\lambda}^{-\varepsilon}$$

*and is therefore consistent.*

*Proof.* Similar as in the proof of Lemma 4 we directly obtain

$$\begin{aligned} \text{Var}(\hat{E}(\Omega_\lambda)) &= E(\hat{E}(\Omega_\lambda))^2 - \sigma^4 |\langle \rho * \mathbf{g}_\lambda, \mathbf{g}_\lambda \rangle|^2 \\ &= \frac{1}{C_{\Omega_\lambda}^2} \sum_{\eta', \eta \in \Omega_\lambda} E(|a_{\eta'}|^2 |a_\eta|^2) - \sigma^4 |\langle \rho * \mathbf{g}_\lambda, \mathbf{g}_\lambda \rangle|^2 \\ &= \frac{\sigma^4}{C_{\Omega_\lambda}^2} \left( \sum_{\eta', \eta \in \Omega_\lambda} \left\{ \langle \rho * \mathbf{g}_{\eta'}, \mathbf{g}_{\eta'} \rangle \langle \rho * \mathbf{g}_\eta, \mathbf{g}_\eta \rangle + \right. \right. \\ &\quad \left. \left. |\langle \rho * \mathbf{g}_{\eta'}, \mathbf{g}_\eta \rangle|^2 \right\} - C_{\Omega_\lambda}^2 |\langle \rho * \mathbf{g}_\lambda, \mathbf{g}_\lambda \rangle|^2 \right) \\ &= \frac{\sigma^4}{C_{\Omega_\lambda}^2} \sum_{\eta', \eta \in \Omega_\lambda} |\langle \rho * \mathbf{g}_{\eta'}, \mathbf{g}_\eta \rangle|^2 \leq \sigma^4 C_{\Omega_\lambda}^{-\varepsilon}. \end{aligned}$$

□

**Lemma 7** *The estimator  $\hat{V}(\Lambda)$  is unbiased, i.e. it holds  $E\hat{V}(\Omega_\lambda) = \sigma^4 |\langle \rho * \mathbf{g}_\lambda, \mathbf{g}_\lambda \rangle|^2$ .*

*Proof.* With similar arguments as in the proof of Lemma 4 and with the shorthand notations

$$c_\lambda := \langle \rho * \mathbf{g}_\lambda, \mathbf{g}_\lambda \rangle \text{ and } c_{\lambda, \eta} := \langle \rho * \mathbf{g}_\lambda, \mathbf{g}_\eta \rangle$$

we have the following expressions

$$\begin{aligned} E|a_\eta|^4 &= \sigma^4 (c_\eta^2 + c_\eta^2) = 2\sigma^4 c_\eta^2, \\ E(|a_\eta|^2 \hat{E}(\Omega_\lambda)) &= \frac{\sigma^4}{C_{\Omega_\lambda}} \sum_{\xi \in \Omega_\lambda} (c_\eta c_\xi + c_{\eta, \xi}^2), \\ E(\hat{E}(\Omega_\lambda))^2 &= \frac{\sigma^4}{C_{\Omega_\lambda}^2} \sum_{\xi, \alpha \in \Omega_\lambda} (c_\alpha c_\xi + c_{\xi, \alpha}^2). \end{aligned}$$

Therefore with  $L=|\Omega_\lambda|$  and the definition of  $C$  in Eq. (23),

$$\begin{aligned}
\mathbb{E} \hat{V}(\Omega_\lambda) &= C \sum_{\eta \in \Omega_\lambda} \mathbb{E}(|a_\eta|^2 - \hat{E}(\Omega_\lambda))^2 \\
&= C \sum_{\eta \in \Omega_\lambda} \left\{ \mathbb{E}|a_\eta|^4 - 2 \mathbb{E}(|a_\eta|^2 \hat{E}(\Omega_\lambda)) + \mathbb{E}(\hat{E}(\Omega_\lambda))^2 \right\} \\
&= \sigma^4 C \sum_{\eta \in \Omega_\lambda} \left\{ 2c_\eta^2 - \frac{2}{C\Omega_\lambda} \sum_{\xi \in \Omega_\lambda} (c_\eta c_\xi + c_{\eta,\xi}^2) + \right. \\
&\quad \left. \frac{1}{C^2\Omega_\lambda} \sum_{\xi,\alpha \in \Omega_\lambda} (c_\alpha c_\xi + c_{\xi,\alpha}^2) \right\} \\
&= \sigma^4 C \sum_{\eta \in \Omega_\lambda} \left\{ 2c_\eta(c_\eta - c_\lambda) - \frac{2}{C\Omega_\lambda} \sum_{\xi \in \Omega_\lambda} c_{\eta,\xi}^2 + \right. \\
&\quad \left. c_\lambda^2 + \frac{1}{C^2\Omega_\lambda} \sum_{\xi,\alpha \in \Omega_\lambda} c_{\xi,\alpha}^2 \right\} \\
&= \sigma^4 C \left\{ 2 \sum_{\eta \in \Omega_\lambda} c_\eta(c_\eta - c_\lambda) + Lc_\lambda^2 + \right. \\
&\quad \left. \frac{L - 2C\Omega_\lambda}{C^2\Omega_\lambda} \sum_{\xi,\alpha \in \Omega_\lambda} c_{\xi,\alpha}^2 \right\} \\
&= \sigma^4 c_\lambda^2 C \left\{ 2 \sum_{\eta \in \Omega_\lambda} \frac{c_\eta^2}{c_\lambda^2} + \right. \\
&\quad \left. (L - 2C\Omega_\lambda) \left( 1 + \frac{1}{(\sum_{\eta} c_\eta)^2} \sum_{\xi,\alpha \in \Omega_\lambda} c_{\xi,\alpha}^2 \right) \right\} \\
&= \sigma^4 c_\lambda^2 .
\end{aligned}$$

□

*Acknowledgements.* The critical review provided by two anonymous reviewers helped to improve the manuscript and is greatly appreciated.

Topical Editor F. D'Andrea thanks A. Muschinski and another anonymous referee for their help in evaluating this paper.

## References

- Anderson, C. J. and Arritt, R. W.: Representation of Summertime Low-Level Jets in the Central United States by the NCEP-NCAR Reanalysis, *J. Climate*, 14, 234–247, 2001.
- Barth, M., Chadwick, R., and van de Kamp, D.: Data Processing Algorithms Used by NOAA's Wind Profiler Demonstration Network, *Ann. Geophys.*, 12, 518–528, 1994, <http://www.ann-geophys.net/12/518/1994/>.
- Bastiaans, M.: Gabor's expansion of a signal into Gaussian elementary signals, *P. IEEE*, 68, 538–539, 1980.
- Benjamin, S. G., Devenyi, D., Weygandt, S. S., Brundage, K. J., Brown, J. M., Grell, G. A., Kim, D., Schwartz, B. E., Smirnova, T. G., Smith, T. L., and Manikin, G. S.: An Hourly Assimilation-Forecast Cycle: The RUC, *Mon. Weather Rev.*, 132, 495–518, 2004a.

- Benjamin, S. G., Schwartz, B. E., Szoke, E. J., and Koch, S. E.: The value of wind profiler data in U.S. weather forecasting, *B. Am. Meteorol. Soc.*, pp. 1871–1886, 2004b.
- Boisse, J.-C., Klaus, V., and Aubagnac, J.-P.: A Wavelet Transform Technique for Removing Airplane Echos from ST Radar Signals, *J. Atmos. Ocean. Tech.*, 16, 334–346, 1999.
- Bouttier, F.: The use of profiler data at ECMWF, *Meteorol. Z.*, 10, 497–510, 2001.
- Bruderer, B.: The Study of Bird Migration by Radar Part 1: The Technical Basis, *Naturwissenschaften*, 84, 1–8, 1997a.
- Bruderer, B.: The Study of Bird Migration by Radar Part 2: Major Achievements, *Naturwissenschaften*, 84, 45–54, 1997b.
- Carmona, R., Hwang, W.-L., and Torresani, B.: *Practical Time-Frequency Analysis*, Academic Press, 1998.
- Chen, M.-Y., Yu, T.-Y., Chu, Y.-H., Brown, W. O., and Cohn, S. A.: Application of Capon technique to mitigate bird contamination on a spaced antenna wind profiler, *Radio Sci.*, 42, RS6005, doi:10.1029/2006RS003604, 2007.
- Cheong, B., Hoffman, M., Palmer, R., Frasier, S. J., and Lopez-Dekker, F.: Phased-Array Design for Biological Clutter Rejection: Simulation and Experimental Validation, *J. Atmos. Ocean. Tech.*, 23, 585–598, 2006.
- Christensen, O.: Frames, Riesz Bases and Discrete Gabor/Wavelet Expansions, *B. Am. Math. Soc.*, 38, 273–291, 2001.
- Comman, L. B., Goodrich, R. K., Morse, C. S., and Ecklund, W. L.: A Fuzzy Logic Method for Improved Moment Estimation from Doppler Spectra, *J. Atmos. Ocean. Tech.*, 15, 1287–1305, 1998.
- Daniel, C. J., Arritt, R. W., and Anderson, C. J.: Accuracy of 404-MHz Radar Profilers for Detection of Low-Level Jets over the Central United States, *J. Appl. Meteorol.*, 38, 1391–1396, 1999.
- Daubechies, I.: *The Wavelet Transform, Time-Frequency Localization and Signal Analysis*, *IEEE T. Inform. Theory*, 36, 961–1005, 1990.
- Daubechies, I.: *Ten Lectures on Wavelets*, SIAM, Philadelphia, 1992.
- Doviak, R. J. and Zrnic, D. S.: *Doppler Radar and Weather Observations*, Academic Press, 1993.
- Ecklund, W., Carter, D., Balsley, B., Currier, P., Green, J., Weber, B., and Gage, K.: Field tests of a lower tropospheric wind profiler, *Radio Sci.*, 25, 899–906, 1990.
- Engelbart, D., Górsdorf, U., and Ruhe, W.: Effects and Observation of Migrating Birds on a Boundary-Layer Windprofiler in Eastern Germany, *Meteorol. Z.*, NF 7, 280–287, 1998.
- Frehlich, R. and Yadlowsky, M.: Performance of Mean-Frequency Estimators for Doppler Radar and Lidar, *J. Atmos. Ocean. Tech.*, 11, 1217–1230, 1994.
- Friedlander, B. and Porat, B.: Detection of Transient Signals by the Gabor Representation, *IEEE T. Acoust. Speech.*, ASSP-37, 169–180, 1989.
- Gabor, D.: Theory of communication, *J. IEE (London)*, 93, 429–457, 1946.
- Gage, K. S.: Radar observations of the free atmosphere: Structure and dynamics, in: *Radar in Meteorology*, edited by: Atlas, D., pp. 534–565, Amer. Meteor. Soc., Boston, 1990.
- Gauthreaux, S. A. and Belser, C. G.: Displays of Bird Movements on the WSR-88D: Patterns and Quantification, *Weather Forecast.*, 13, 453–464, 1998.
- Gauthreaux, S. A., Mizrahi, D. S., and Belser, C. G.: Bird Migration and Bias of WSR-88D Wind Estimates, *Weather Forecast.*, 13,

- 465–481, 1998.
- Griesser, T. and Richner, H.: Multiple peak processing algorithm for identification of atmospheric signals in Doppler radar wind profiler spectra, *Meteorol. Z.*, N.F.7, 292–302, 1998.
- Heil, C. E. and Walnut, D. F.: Continuous and Discrete Wavelet Transforms, *SIAM Rev.*, 31, 628–666, 1989.
- Hildebrand, P. H. and Sekhon, R.: Objective Determination of the Noise Level in Doppler Spectra, *J. Appl. Meteorol.*, 13, 808–811, 1974.
- Hlawatsch, F. and Boudreaux-Bartels, G.: Linear and Quadratic Time-Frequency Signal Representations, *IEEE Signal Proc. Mag.*, pp. 21–67, 1992.
- Hogg, D., Decker, M., Guiraud, F., Earnshaw, K., Merritt, D., Moran, K., Sweezy, W., Strauch, R., Westwater, E., and Little, C.: An Automatic Profiler of the Temperature, Wind and Humidity in the Troposphere, *J. Clim. Appl. Meteorol.*, 22, 807–831, 1983.
- Ishihara, M., Kato, Y., Abo, T., Kobayashi, K., and Izumikawa, Y.: Characteristics and Performance of the Operational Wind Profiler Network of the Japan Meteorological Agency, *J. Meteorol. Soc. Jpn.*, 84, 1085–1096, 2006.
- Jordan, J. R., Lataitis, R. J., and Carter, D. A.: Removing Ground and Intermittent Clutter Contamination from Wind Profiler Signals Using Wavelet Transforms, *J. Atmos. Ocean. Tech.*, 14, 1280–1297, 1997.
- Justen, L. and Lehmann, V.: Radar wind profiler signal processing using redundant windowed Fourier and wavelet transforms, in: 6th International Conference on Tropospheric Profiling – Extended Abstracts, 2003.
- Kaiser, G.: A Friendly Guide to Wavelets, Birkhäuser, Basel, 1994.
- Keeler, R. J. and Passarelli, R. E.: Signal Processing for Atmospheric Radars, in: *Radar in Meteorology*, edited by: Atlas, D., chap. 20a, pp. 199–229, American Meteorological Society, Boston, 1990.
- Lehmann, V. and Teschke, G.: Wavelet Based Methods for Improved Wind Profiler Signal Processing, *Ann. Geophys.*, 19, 825–836, 2001, <http://www.ann-geophys.net/19/825/2001/>.
- Lehmann, V., Dibbern, J., Görsdorf, U., Neuschaefer, J. W., and Steinhagen, H.: The new operational UHF Wind Profiler Radars of the Deutscher Wetterdienst, in: 6th International Conference on Tropospheric Profiling – Extended Abstracts, 2003.
- Liu, S., Xu, Q., and Zhang, P.: Identifying Doppler Velocity Contamination Caused by Migrating Birds. Part II: Bayes Identification and Probability Tests, *J. Atmos. Ocean. Tech.*, 22, 1114–1121, 2005.
- Locatelli, J. D., Stoelinga, M. T., Hobbs, P. V., and Johnson, J.: Structure and Evolution of an Undular Bore on the High Plains and Its Effects on Migrating Birds, *B. Am. Meteorol. Soc.*, 79, 1043–1060, 1998.
- Lottman, B. and Frehlich, R.: Evaluation of Doppler radar velocity estimators, *Radio Sci.*, 32, 677–686, 1997.
- Lundquist, J. K.: Intermittent and Elliptical Inertial Oscillations in the Atmospheric Boundary Layer, *J. Atmos. Sci.*, 60, 2661–2673, 2003.
- Mallat, S.: A Wavelet Tour of Signal Processing, Academic Press, 1999.
- Mastrantonio, G., Naithani, J., Anderson, P., Argenti, S., and Pentenko, I.: Quantitative Analysis and Interpretation of Dot Echoes Observed with a Doppler Sodar, *J. Atmos. Ocean. Tech.*, 16, 1928–1940, 1999.
- Merritt, D. A.: A Statistical Averaging Method for Wind Profiler Doppler Spectra, *J. Atmos. Ocean. Tech.*, 12, 985–995, 1995.
- Monna, W. A. and Chadwick, R. B.: Remote-Sensing of Upper-Air Winds for Weather Forecasting: Wind-Profiler Radar, *B. World Meteorol. Organ.*, 47, 124–132, 1998.
- Morse, C. S., Goodrich, R. K., and Cornman, L. B.: The NIMA Method for Improved Moment Estimation from Doppler Spectra, *J. Atmos. Ocean. Tech.*, 19, 274–295, 2002.
- Muschinski, A.: Local and Global Statistics of Clear-Air Doppler Radar Signals, *Radio Sci.*, 39, doi:10.1029/2003RS002908, 2004.
- Muschinski, A., Sullivan, P. P., Wuertz, D. B., Hill, R. J., Cohn, S. A., Lenschow, D. H., and Doviak, R. J.: First Synthesis of Wind-Profiler Signals on the Basis of Large-Eddy Simulation Data, *Radio Sci.*, 34, 1437–1459, 1999.
- Muschinski, A., Lehmann, V., Justen, L., and Teschke, G.: Advanced Radar Wind Profiling, *Meteorol. Z.*, 14, 609–626, 2005.
- Neeser, F. D. and Massey, J. L.: Proper Complex Random Processes with Applications to Information Theory, *IEEE T. Inform. Theory*, 39, 1293–1302, 1993.
- Nielsen-Gammon, J. W., McNider, R. T., Angevine, W. M., White, A. B., and Knupp, K.: Mesoscale model performance with assimilation of wind profiler data: Sensitivity to assimilation parameters and network configuration, *J. Geophys. Res.*, 112, D09119, doi:10.1029/2006JD007633, 2007.
- Parker, M. D. and Johnson, R. H.: Organizational Modes of Midlatitude Mesoscale Convective Systems, *Mon. Weather Rev.*, 128, 3413–3436, 2000.
- Pekour, M. and Coulter, R.: A Technique for Removing the Effect of Migrating Birds in 915-MHz Wind Profiler Data, *J. Atmos. Ocean. Tech.*, 16, 1941–1948, 1999.
- Qian, S. and Chen, D.: Discrete Gabor Transform, *IEEE T. Signal Process.*, 41, 2429–2438, 1993.
- Qian, S., Chen, K., and Li, S.: Optimal biorthogonal functions for finite discrete-time Gabor expansion, *Signal Process.*, 27, 177–185, 1992.
- Ralph, F. M., Armi, L., Bane, J. M., Dorman, C., Neff, W. D., Neiman, P. J., Nuss, W., and Persson, P. O. G.: Observations and Analysis of the 10–11 June 1994 Coastally Trapped Disturbance, *Mon. Weather Rev.*, 126, 2435–2465, 1998.
- Reed, I. S.: On a Moment Theorem for Complex Gaussian Processes, *IRE T. Inform. Theory*, IT-8, 194–195, 1962.
- Röttger, J. and Larsen, M.: UHF/VHF Radar Techniques for Atmospheric Research and Wind Profiler Applications, in: *Radar in Meteorology*, chap. 21a, pp. 235–281, American Meteorological Society, Boston, 1990.
- Seiple, A.: Forecast Error Investigation 12th October 2003: Assimilation of Contaminated Wind Profiler Data into the Global Model (Forecasting Research Technical Report No. 465), Tech. rep., UK Met Office, 2005.
- Song, J., Liao, K., Coulter, R. L., and Lesht, B. M.: Climatology of the Low-Level Jet at the Southern Great Plains Atmospheric Boundary Layer Experiments Site, *J. Appl. Meteorol.*, 44, 1593–1606, 2005.
- St-James, J. S. and Laroche, S.: Assimilation of Wind Profiler data in the Canadian Meteorological Centre's Analysis System, *J. Atmos. Ocean. Tech.*, 22, 1181–1194, 2005.

- Stensrud, D. J.: Importance of Low-Level Jets to Climate: A Review, *J. Climate*, 9, 1698–1711, 1996.
- Van Zandt, T.: A Brief History of the Development of Wind Profiling or MST Radars, *Ann. Geophys.*, 18, 740–749, 2000, <http://www.ann-geophys.net/18/740/2000/>.
- Vaughn, C. R.: Birds and Insects as Radar Targets: A Review, *P. IEEE*, 73, 205–227, 1985.
- Weber, B., Welsh, D., Merritt, D., Wuertz, D., Wolfe, D., and Wilfong, T.: A new paradigm for Doppler radar wind profiler signal processing, Tech. Rep. OAR ETL-306, NOAA – Environmental Technology Laboratory, 2004.
- Weber, H. C.: Classification of contaminated data from wind profiler measurements by Neural Networks, Ph.D. thesis, Swiss Federal Institute of Technology Zürich, 2005.
- Wexler, J. and Raz, S.: Discrete Gabor Expansions, *Signal Process.*, 21, 207–220, 1990.
- Wilczak, J., Strauch, R., Ralph, F., Weber, B., Merritt, D., Jordan, J., Wolfe, D., Lewis, L., Wuertz, D., Gaynor, J., McLaughlin, S., Rogers, R., Riddle, A., and Dye, T.: Contamination of Wind Profiler Data by Migrating Birds: Characteristics of Corrupted Data and Potential Solutions, *J. Atmos. Ocean. Tech.*, 12, 449–467, 1995.
- Woodman, R. F.: Spectral moment estimation in MST radars, *Radio Sci.*, 20, 1185–1195, 1985.
- Woodman, R. F.: A General Statistical Instrument Theory of Atmospheric and Ionospheric Radars, *J. Geophys. Res.*, 96, 7911–7928, 1991.
- Zhang, P., Liu, S., and Xu, Q.: Identifying Doppler Velocity Contamination Caused by Migrating Birds. Part I: Feature Extraction and Quantification, *J. Atmos. Ocean. Tech.*, 22, 1105–1113, 2005.
- Zrnić, D. S.: Simulation of Weatherlike Doppler Spectra and Signals, *J. Appl. Meteorol.*, 14, 619–620, 1975.
- Zrnić, D. S.: Estimation of Spectral Moments for Weather Echoes, *IEEE T. Geosci. Elect.*, GE-17, 113–128, 1979.



# Optimal Gabor frame expansion based intermittent clutter filtering method for radar wind profiler

VOLKER LEHMANN \*

*Deutscher Wetterdienst, Meteorologisches Observatorium Lindenberg*

## ABSTRACT

Intermittent clutter signals are frequently observed by radar wind profilers during the seasonal bird migration. A novel statistical filtering algorithm based on a simultaneous time-frequency analysis of the profilers raw data was recently proposed to address shortcomings of existing methods. The foundation of this method is a Gabor frame expansion of the I/Q-time series of the demodulated receiver voltage. In this paper, two objective criteria are suggested to obtain an optimal set-up for the discrete Gabor frame expansion from the multitude of possibilities: First, the choice of near-tight frames for a predefined maximum redundancy and second, the requirement that the analyzing bandwidth of the used Gaussian window function should provide a simultaneously sparse representation of both atmospheric signal components and intermittent clutter. The question of optimal sampling settings, especially dwell time, for a maximum reduction of bird interference is also discussed. Using data obtained during intense bird migration events it is shown that a combination of filtering and quality control of the result is required to prevent the occurrence of significant systematic and correlated errors in the final wind measurement.

## 1. Introduction

Radar wind profilers (RWP) have become standard instruments for measuring wind velocities in the atmosphere. Its data are used in a variety of applications, ranging from numerical weather forecasting (Monna and Chadwick 1998; Bouttier 2001; Benjamin et al. 2004a; St-James and Laroche 2005; Ishihara et al. 2006), air-quality monitoring (Cros et al. 2004; Dabberdt et al. 2004; White et al. 2006) to numerous research activities and field campaigns (Fukao 2007). Reviews of the theoretical foundations of RWP have been given by Röttger and Larsen (1990); Woodman (1991); Gage and Gossard (2003); Muschinski (2004). While further work is still necessary for a full theoretical understanding of the measurements, there are also a number of difficulties outside of the scope of existing instrument theory, which need to be dealt with in practice. The most prominent issue here is certainly the clutter problem (Muschinski et al. 2005).

For UHF and L-band profiler systems, intermittent clutter echoes from birds during their seasonal migration in spring and fall are particularly troublesome. At the peak of the seasonal migration, large and unacceptable differences are observed between the profiler measurements and independent reference data. The errors incurred tend to be correlated in height and time, which is a serious problem in the data assimilation of numerical weather prediction models where observation errors are typically assumed to

be uncorrelated (Stewart et al. 2008). The assimilation of such erroneous data, if not detected and excised, has a negative impact on the quality of the forecasts (Semple 2005; Cardinali 2009).

The problem is known for many years (Ecklund et al. 1990; Barth et al. 1994; Wilczak et al. 1995, 1996; Engelbart et al. 1998; Richner and Kretzschmar 2001; Benjamin et al. 2004b), even though the clear effects of bird clutter on the measurements are apparently not always well understood by data users (Tanaka et al. 2007). Research on improvements in intermittent clutter filtering for wind profiler has therefore continued over the last decade. For a summary of previous work on this issue, see e.g. Wilczak et al. (1995); Lehmann and Teschke (2008).

The increase of available processing power at the sites over the last decade meanwhile allows the application of rather sophisticated detection and filtering algorithms to the raw data of the measurement, that is the time series of the demodulated (and to some extent coherently averaged) receiver voltage. Recently, Lehmann and Teschke (2008) have suggested a time-frequency analysis based approach using a Gabor frame decomposition of the raw data, followed by a simple statistical classification and filtering. The latter is based on the standard RWP signal model assumption that both the atmospheric echo and the receiver noise can be described as independent complex zero-mean Gaussian random vectors (Zrnić 1975, 1979; Wood-

man 1985; Lottman and Frehlich 1997). In the following, this will be called the Gabor filtering algorithm for brevity. Time-frequency analysis generally provides considerable insight into the properties of the raw data at a level that goes beyond the widely-used Doppler spectrum; this is of interest for all signals whose power spectra vary in time. In this paper, however, we will largely focus on the problem of the filtering of intermittent clutter signals.

Single comparisons using data from different profiler systems have shown that Gabor filtering performs better than other available methods (Merritt 1995; Jordan et al. 1997), assuming of course that the used software implementations were correct. However, especially during periods of strong bird migration one can still find cases where even the Gabor algorithm fails to remove all clutter energy. The reason for this is caused by clutter signal components, which have a time duration on the order of the dwell time. This problem was mentioned in Lehmann and Teschke (2008) and two areas for improvements were identified: 1) optimization of the data sampling and 2) optimization of the filter performance. These two points will be discussed in the following.

The paper is organized as follows: Section 2 reviews briefly the Gabor filtering algorithm. In section 3, strategies for an optimal adaption of the discrete Gabor frame expansion parameters are discussed. This includes the selection of the discretization lattice and the bandwidth of the analyzing Gaussian window function. The first point is more technical and aims at obtaining a nearly tight discrete frame for a given data length (dwell time) and window bandwidth, which is advantageous for a well-localized time-frequency representation. The second builds upon the idea of finding an optimally sparse representation for both atmospheric and clutter signal component in the transformed (time-frequency) signal space. This is more difficult, because the properties of the clutter signals are not very well known. In this context, the problem of selecting an optimal dwell time is also discussed. In the fourth section, a proposal is made for an addition quality control step after the filtering process. This is based on available a-priori information of the desired atmospheric signal component. The goal is here to identify cases where the filtering fails due to a breakdown of assumptions. Case studies illustrate the approaches discussed before. Finally, conclusions are given in Section 5.

## 2. The Gabor filtering algorithm

### a. Gabor frame expansion

The discrete Gabor frame expansion is briefly reviewed in the following, further details can be found in Wexler and Raz (1990); Qian and Chen (1993); Lehmann and Teschke (2008). The general concept of frames is introduced in Appendix A. Let  $\mathbf{S}$  be a discrete and finite time signal with

sampling points  $n = 0, \dots, N - 1$ , that is  $S[n] = S(n\Delta T)$ . The signal is assumed to be  $N$ -periodic, that is  $S[n] = S[n + qN]$ ,  $\forall q \in \mathbb{Z}$ . In the context of finite dimensional signal spaces, the general concept of Gabor frame expansion leads to the discrete Gabor transform (DGT), which can be described using linear algebra and implemented on a computer (Feichtinger et al. 2007; Christensen 2008). The signal  $\mathbf{S}$  will therefore be regarded as an element of the linear vector space  $\mathbb{C}^N$ .

The Gabor frame expansion can be interpreted as a discretized version of the continuous windowed Fourier transform, where the time-frequency plane (Gabor phase space) is sampled at finitely many points of a discrete lattice  $\Lambda$  (Daubechies 1990; Gröchenig 2001). Here, we consider only regular rectangular grids, although other variants are possible (Prinz 1996). The lattice is described by the integer parameters  $\Delta M, \Delta K$ , which must be divisors of  $N$ .

If the set of vectors of translated and modulated windows  $\mathbf{h}$

$$h_{m,k}[n] = h[n - m\Delta M]e^{\frac{2\pi i n k \Delta K}{N}} \quad (1)$$

with  $m = 0, \dots, M - 1$ ,  $M = N/\Delta M$  and  $k = 0, \dots, K - 1$ ,  $K = N/\Delta K$  fully spans the vector space  $\mathbb{C}^N$ , then we say that the discrete Gabor family (sometimes also called a Gabor triple)

$$\mathcal{G}(\mathbf{h}, \Delta M, \Delta K) := \{\mathbf{h}_{m,k}, \forall m, k\}$$

is a frame for  $\mathbb{C}^N$ .  $\Delta M$  denotes the time and  $\Delta K$  the frequency step size. The number of elements of the discrete Gabor family is

$$M \cdot K = \frac{N}{\Delta M} \frac{N}{\Delta K} = \frac{N}{\Delta M \Delta K} N := rN$$

where  $r$  is called the redundancy factor of the frame,  $M$  and  $K$  are also called dual lattice constants. It is clear from dimensional reasoning that  $\mathcal{G}(\mathbf{h}, \Delta M, \Delta K)$  cannot be a frame for  $\mathbb{C}^N$  if  $r < 1$ , so  $r \geq 1$  is always required. This puts another constraint on the lattice parameters  $\Delta M, \Delta K$  for a given signal length  $N$ . In the following, only the oversampling case  $r > 1$  is considered, for the critically sampled case is of no practical importance because of the bad localization properties of the dual window due to the Balian-Low obstruction theorem (Mallat 1999).

The discrete Gabor expansion of the signal  $\mathbf{S}$  (synthesis equation) can be written as

$$S[n] = \sum_{m=0}^{M-1} \sum_{k=0}^{K-1} a_{m,k} h_{m,k}[n], \quad (2)$$

where the Gabor coefficients are obtained through an inner product of the signal vector with the  $MK$  dual frame vectors  $\mathbf{g}_{m,k}$  (analysis equation):

$$a_{m,k} = \sum_{n=0}^{N-1} S[n] \bar{g}_{m,k}[n] . \quad (3)$$

The overbar denotes complex conjugation. Both relations are mappings between the transformed signal space, that is the vector space of Gabor coefficients  $\mathbb{C}^{M \times K}$  and the signal space  $\mathbb{C}^N$ . The pair of equations (2) and (3) is also called DGT. Inserting the analysis equation (3) in the synthesis equation (2), one gets

$$\begin{aligned} S[j] &= \sum_{m=0}^{M-1} \sum_{k=0}^{K-1} a_{m,k} h_{m,k}[j] \\ &= \sum_{l=0}^{N-1} S[l] \sum_{m=0}^{M-1} \sum_{k=0}^{K-1} \bar{g}_{m,k}[l] h_{m,k}[j] , \end{aligned}$$

One sees immediately that the signal  $\mathbf{S}$  is recovered if

$$\sum_{m=0}^{M-1} \sum_{k=0}^{K-1} \bar{g}_{m,k}[l] h_{m,k}[j] = \delta_{l,j} . \quad (4)$$

This is a discrete biorthogonality relation for the sequences  $\mathbf{h}$  and  $\mathbf{g}$ . It can be shown (Wexler and Raz 1990; Lehmann and Teschke 2008) that this condition is satisfied if the dual frame sequence  $\mathbf{g}$  fulfills the Wexler-Raz relation

$$\sum_{j=0}^{N-1} h[j + qK] e^{-2\pi i \frac{j p M}{N}} \bar{g}[j] = \frac{N}{MK} \delta_{p,0} \delta_{q,0} \quad (5)$$

for  $0 \leq p \leq \Delta M - 1$  and  $0 \leq q \leq \Delta K - 1$ . System (5) can be rewritten in matrix form: Let  $\mathbf{v} = (N/(MK), 0, \dots, 0)^T$  be a vector of length  $\Delta M \Delta K$  and  $\mathbf{g} = (g[0], \dots, g[N-1])$  the vector representing the discretely sampled dual frame, and let  $\mathbf{A} \in \mathbb{C}^{\Delta M \Delta K \times N}$  a matrix with entries

$$\mathbf{A}_{(p,q),j} = \bar{h}(j + qK) e^{2\pi i \frac{j p M}{N}} ,$$

then the dual frame atom  $\mathbf{g}$  is the solution of the linear system

$$\mathbf{A} \mathbf{g} = \mathbf{v} . \quad (6)$$

The Wexler-Raz relation provides a necessary and sufficient condition for the dual window (Prinz 1996). Due to the restriction to the oversampling case  $r > 1$ ,  $\Delta M \Delta K < N$ . As a consequence, the linear system (6) is under-determined and the solution is no longer unique. Equations (5) and (6) thus determine only a set of all possible dual windows

$$\Gamma_g := \{ \gamma_j, \quad \mathbf{A} \gamma_j = \mathbf{v}, \quad \forall j \} .$$

It can be shown (Prinz 1996) that  $\Gamma_g$  is an affine vector space and it remains to select one dual for concrete computations. A particular solution is the canonical dual with

minimum norm  $\|\mathbf{g}\|$  for which  $\|\mathbf{g}\| < \|\gamma_j\|$ , which is provided by the pseudoinverse of  $\mathbf{A}$  (Qian and Chen 1993, Appendix A):

$$\mathbf{g} = \mathbf{A}^T (\mathbf{A} \mathbf{A}^T)^{-1} \mathbf{v}$$

It has the property of being as close as possible to the primal window  $\mathbf{h}$  (Qian et al. 1992; Lehmann and Teschke 2008) which is desirable for a good localization in time-frequency analysis. Therefore, it will always be used in the following.

The window  $\mathbf{h}$  is selected as a discrete Gaussian, for it provides the best possible localization in time and frequency that is possible due to the Heisenberg uncertainty relation (Lehmann and Teschke 2008). In the discrete Gabor frame expansion it is necessary to periodize this window (Wexler and Raz 1990, Appendix D) so

$$h[n] = \sum_l e^{-\frac{2\pi s}{N}(n+lN)^2}, l \in \mathbb{Z} \quad (7)$$

This window is normalized to assure  $\|\mathbf{h}\| = 1$ . The width of this window controls the actual time-frequency resolution of the DGT, it is determined through the parameter  $s$ .

#### b. Statistical signal classification

The classical RWP signal model assumption is that RWP raw signal at the receiver output can be written as

$$S[k] = I[k] e^{i\omega k \Delta T} + N[k] . \quad (8)$$

$\mathbf{S}$  is the result of the demodulation of two independent real valued zero-mean and stationary Gaussian random processes, which leads  $I[k]$  and  $N[k]$  to be independent complex (circularly) stationary Gaussian random vectors with zero mean, describing the atmospheric signal and the receiver noise respectively (Zrnić 1979; Neeser and Massey 1993). The sequence has a vanishing pseudo-covariance and is therefore called proper, that is  $\mathbf{E}(S[k] S[l]) = 0$ , the sampling interval is  $\Delta T$  and  $\omega$  denotes the mean Doppler frequency. Because  $S[k]$  is Gaussian, it is completely characterized through its covariance matrix  $\mathbf{R}$  with entries

$$\begin{aligned} (\mathbf{R})_{k,l} &= \text{Cov}(S[k], S[l]) = \mathbf{E}(S[k] \bar{S}[l]) \\ &= \mathbf{E}(I[k] \bar{I}[l]) e^{i\omega(k-l)\Delta T} + \mathbf{E}(N[k] \bar{N}[l]) \\ &= \sigma_{\mathbf{I}}^2 \varrho[k-l] e^{i\omega(k-l)\Delta T} + \sigma_{\mathbf{N}}^2 \delta_{k-l,0}, \end{aligned}$$

where stationarity has been assumed in the last step. The autocorrelation function  $\varrho[k]$  is often assumed to follow a Gaussian correlation model, which is equivalent to a Gaussian signal peak in the power spectrum. If the spectral width of the signal is  $w$ , then (Zrnić 1979; Frehlich and Yadlowsky 1994)

$$\varrho[k] = e^{-2\pi^2 \omega^2 k^2 \Delta T^2} . \quad (9)$$

For identification of non-stationary (intermittent) clutter components, a statistical test based on the expectation and the variance of the individual Gabor spectrogram coefficients  $|a_{m,k}|^2$  is constructed. With the shorthand notation  $\lambda = (m, k)$ , the Gabor spectrogram coefficients  $a_\lambda := a_{m,k}$  take the form

$$|a_\lambda|^2 = \sum_{n=0}^{N-1} S[n] g_\lambda[n] \sum_{l=0}^{N-1} \bar{S}[l] \bar{g}_\lambda[l] .$$

Assuming that the data sequence  $\mathbf{S}$  satisfies for all  $n = 0, \dots, N-1$ ,

$$\mathbb{E}(S[n]) = 0 \quad \text{and} \quad \mathbb{E}(S[n] \bar{S}[n+l]) = \sigma^2 \rho[l] ,$$

the expectation and the covariance of the Gabor spectrogram coefficients are given by

$$\mathbb{E}(|a_\lambda|^2) = \sigma^2 \langle \rho * \mathbf{g}_\lambda, \mathbf{g}_\lambda \rangle ,$$

$$\text{Cov}(|a_\lambda|^2, |a_\eta|^2) = \sigma^4 |\langle \rho * \mathbf{g}_\lambda, \mathbf{g}_\eta \rangle|^2 .$$

The ‘\*’-symbol stands here for the discrete convolution. Note that the formulas show both the influence of the dependency of  $\mathbf{S}$  and the redundancy of the Gabor frame expansion. The essential observation is that

$$\text{Var}(|a_\lambda|^2) = \sigma^4 |\langle \rho * \mathbf{g}_\lambda, \mathbf{g}_\lambda \rangle|^2 = (\mathbb{E}|a_\lambda|^2)^2 ,$$

so obviously

$$\frac{(\mathbb{E}|a_\lambda|^2)^2}{\text{Var}|a_\lambda|^2} = 1 , \quad (10)$$

for independent as well as dependent samples  $S[n]$ , provided the assumption of a stationary Gaussian random process is correct. This may hold true for a much richer class of distributions, but it surely is true for normally distributed random variables.

For a statistical test that verifies property (10), unbiased and consistent estimators for  $\mathbb{E}(|a_\lambda|^2)$  and  $\text{Var}(|a_\lambda|^2)$  based on a finite number of observations have to be constructed. The technical details are given in Lehmann and Teschke (2008).

Typically, an atmospheric return is considered to be stationary and Gaussian. A test on the first two moments of the signal will give an indication if this is true. This idea goes back to Merritt (1995). Quite similar, the clutter identification is based on a test of the squared modulus of the Gabor phase space coefficients,  $|a_{m,k}|^2$ . Because the filter should have pass characteristic for all stationary signal components, the sequence  $|a_{m,k}|^2$  is considered for fixed frequency bins. Typically, the sequence  $|a_{m,k}|^2$  can

be affected by non-stationary (intermittent) clutter. In this case,  $\hat{E}(\Omega_\lambda)^2 / \hat{V}(\Omega_\lambda) < 1$ .

Intermittent clutter signals are almost always stronger than the (clear air) atmospheric return so a removal of the clutter part of the signal can be achieved by discarding the largest coefficients in a stepwise fashion until

$$\vartheta(|[a]_{l,k}|^2) := \frac{(\hat{E}(\Omega_k(l)))^2}{\hat{V}(\Omega_k(l))} < 1$$

holds for the test statistics. The largest coefficient of the subset for which the test (positive for clutter) is not satisfied (a clutter-free subset) is then taken as a threshold for a frequency-dependent identification of the clutter component. The filtered signal can thus be written as

$$\Phi(\mathbf{S})[n] = \sum_{k=0}^{K-1} \left\{ \sum_{(m,k) \in \Omega_k \setminus \Omega_k^c} a_{m,k} h_{m,k}[n] + \sum_{(m,k) \in \Omega_k^c} t_k e^{i \arg a_{m,k}} h_{m,k}[n] \right\} ,$$

where the Gabor coefficients which have been classified as clutter affected are now replaced by the frequency-dependent threshold  $t_k$ .

### 3. Optimality considerations

The set-up of the DGT for a concrete case is not uniquely determined because a selection has to be made for both the lattice parameters  $\Delta M, \Delta K$  and the width parameter  $s$  of the primal window. Furthermore, the length  $N$  of the signal depends on the dwell time  $T_d$ . It is not a-priori clear how these parameters should be chosen in an optimal way, to obtain the best possible results with the Gabor filter. This will be discussed in the following.

#### a. Discretization lattice parameters

For a given discrete signal  $\mathbf{S}$  of length  $N$  and a discrete Gaussian primal window with fixed parameter  $s$  and the selection of the canonical dual window (pseudo-inverse solution of the Wexler-Raz system), the only freedom is in the definition of the time and frequency step size or discretization lattice  $\Lambda$ . In principle, the only constraint are  $r > 1$  and  $\Delta M, \Delta K$  must be divisors of  $N$ . In Lehmann and Teschke (2008) it was argued that an upper bound for the redundancy might be useful as well, to prevent an *unnecessary Heisenberg box overlapping* for the sake of saving computational costs. Indeed, it is possible to define a useful and problem oriented constraint that allows an optimization of the DGT. This is shown in the following.

The number of possible Gabor systems  $\mathcal{G}(\mathbf{h}, \Delta M, \Delta K)$  is obviously finite for fixed  $N$  and  $s$ . It is therefore possible to use the constraint

$$E(\mathbf{g}, \mathbf{h}) = \left\| \frac{\mathbf{g}}{\|\mathbf{g}\|} - \mathbf{h} \right\|^2 \rightarrow \min. \quad (11)$$

for selecting the canonical Gabor system  $\mathcal{G}(\mathbf{h}, \Delta M, \Delta K; \mathbf{g})$  that provides this minimum globally, that is over all possible lattices. This assures that the analysis (or dual) window  $\mathbf{g}$  is as close to  $\mathbf{h}$  as possible. Note that for a given discretization lattice  $\Lambda$  and a pre-defined window width  $s$ , this is locally already the case due to the choice of the canonical dual. The primal window  $\mathbf{h}$  was selected as Gaussian, due to its superior time-frequency localization properties (i.e. it minimizes the Heisenberg uncertainty). It is very useful to preserve these properties for the dual as well, because then

$$g[n] \approx \alpha h[n], \quad (12)$$

with  $\alpha = \|\mathbf{g}\|$ . This can be achieved with near-tight frames. Daubechies (1991) has given the following relation between primal and dual window

$$\mathbf{g} = \frac{2}{A+B} \mathbf{h} + \mathcal{O}\left(\frac{B}{A} - 1\right), \quad (13)$$

where  $A$  and  $B$  are the frame bounds, see also equation (A8). By definition,  $A \approx B$  for a near tight frame, so equation (12) is indeed approximately valid and the redundancy of the frame is  $(A+B)/2$  for normalized frame vectors (Daubechies 1992; Mallat 1999). Then, the analysis equation (3) can be approximately written as

$$a_{m,k} \approx \alpha \sum_{n=0}^{N-1} S[n] \bar{h}_{m,k}[n], \quad (14)$$

which leads to an orthogonal-like DGT (Qian and Chen 1993):

$$S[n] \approx \alpha \sum_{m=0}^{M-1} \sum_{k=0}^{K-1} \left( \sum_{j=0}^{N-1} S[j] \bar{h}_{m,k}[j] \right) h_{m,k}[n]. \quad (15)$$

Here,  $a_{m,k}$  would indeed be a measure for the similarity between the signal  $\mathbf{S}$  and "the basis"  $\mathbf{h}_{m,k}$ . This optimization can be considered as an attempt to generate a near-tight frame (Qian and Chen 1999). To reduce the computational load of this approach it is useful to require  $r \leq r_{max}$ . This limits the number of possible canonical Gabor systems to be tested for finding the lattice parameters  $\Delta M, \Delta K$  that minimize equation (11). For  $N = 8192, s = 1, r_{max} = 8$  and the useful restriction  $2 \leq \Delta M, \Delta K \leq N/2$  there are 30 different pairs  $(\Delta M, \Delta K)$  which generate admissible discrete Gabor systems  $\mathcal{G}(\mathbf{h}, \Delta M, \Delta K; \mathbf{g})$ . The optimal pair is then easily found to be  $\Delta M = \Delta K = 256$ . Note that this is a case of integer oversampling, that is  $\Delta M \Delta K$

is also a divisor of  $N$ . For  $N = 4608$ , the number of possible lattice parameter pairs is 199; it is greater because of non-integer oversampling. In this case,  $\Delta M = \Delta K = 192$  is optimal. In general, the optimal pair tends to have maximum redundancy, that is  $r = r_{max}$ , although not always.

For illustration of both an optimal and a non-optimal selection of the lattice parameters  $M$  and  $K$ , consider example data obtained with the operational RWP at Bayreuth on March 29, 2008 during spring migration. Figure 1 shows the time-series of the demodulated receiver voltage for the East Beam low mode at the range gate centered at 1191 m agl. A strong intermittent signal can be seen in the middle of the series. The corresponding Gabor spectrogram (squared modulus of the DGT) is shown in Figure 2. The DGT was computed using optimal lattice parameters  $M = 128, K = 256$  obtained through the selection process described above, with a prescribed maximum redundancy of 4. The window bandwidth parameter  $s$  was selected as 0.5. Primal and dual window function are plotted in Figure 3. The similarity in shape of both windows is obvious. The difference in absolute values reflects the redundancy of the frame: The higher the redundancy, the greater is the difference in absolute values between primal and dual window, see equation (13).

For a non-optimal choice of  $M = 512, K = 64$  (all other parameters being equal), the dual window is no longer similar to the primal (Gaussian) window, as shown in Figure 5. It has become oscillatory and, compared to the primal window, it is not very well localized in time. As a consequence, the spectrogram becomes blurred and the strong transient is smeared in time. While the essential features of the signal are still visible, it is obvious that the selection of the optimal lattice parameters is much better adapted to the problem of separating signal and clutter.

#### b. Analyzing window bandwidth - sparse representations

From a physical point of view, the most important parameter of the DGT is the joint time-frequency resolution controlled by the parameterized width  $s$  of the primal window. Wexler and Raz (1990) have suggested to characterize the time resolution more directly through an effective width parameter defined as

$$T_1 = \|\mathbf{h}\|/h_{max},$$

where  $h_{max}$  is the maximum value of  $\mathbf{h}$ . One could also choose the essential support of the primal window as a measure of time resolution (Gröchenig 2001), but any exact number is only a matter of definition.

Intuitively it is clear that the time resolution must be "high enough" (the window "short enough") to resolve the transient clutter echoes. On the other hand, the (ideal) atmospheric signal is very well described by the Gaussian correlation model (9), so the signal has a finite spectral width

w. A good representation of such a signal therefore imposes also a lower limit on the spectral resolution in the time-frequency plane. For a coarser frequency resolution, the atmospheric signal would be stretched along the frequency axis. More Gabor coefficients would be needed to describe it and the chance of having an overlap of atmospheric signal and clutter in phase space would be greater.

As an example, consider again the data shown in Figure 1. The effects of a short primal window (high time resolution) with  $s = 10.0$  corresponding to  $T_1 = 0.15s$  is clearly visible in Figure 7. Remarkable is the appearance of a modulation signature in the clutter transient. It is known that such signatures can be caused by the wing-beat of birds (Bruderer 1997; Zaugg et al. 2008), so this observation detail raises the confidence that the clutter signal is indeed caused by a bird. Another spectrogram was computed using a longer primal window (low time resolution) with the parameters  $s = 0.01$  corresponding to  $T_1 = 4.6s$ , see Figure 6. While the wing-beat signature of the bird echo can no longer be seen due to the coarse time resolution, the better frequency resolution makes it easier to detect the clear air atmospheric signal near a frequency of  $f_d = -2s^{-1}$ .

Apparently, the resolution in time and frequency has to be balanced carefully for an optimal simultaneous representation of both atmospheric signal and clutter. The filtering quality will obviously depend on how well a separation between the two signal components can be achieved. If  $\Omega \subseteq \Lambda$  denotes the subset of the lattice points that is influenced by the signal, the ideal case would be a clear separation by a non-overlapping partition of  $\Omega$  into the subsets  $\Omega^s, \Omega^c$ , describing atmospheric signal and clutter components respectively, so that

$$\begin{aligned}\Omega^c \cup \Omega^s &= \Omega \\ \Omega^c \cap \Omega^s &= \emptyset.\end{aligned}$$

This ideal case of a perfect signal-clutter separation can of course only approximately be realized. However this approach leads to the idea of striving for a Gabor representation where both atmospheric signal and clutter are described with only a few coefficients  $a_{m,k}$ . This is called a *sparse representation* (Allen and Mills 2004; Mallat 2009).

Typically, sparse representations are constructed with a dictionary of elementary signals or atoms, see Chen et al. (2001). For the given problem, however, only the Gabor frame representation is considered because it appears to be quite well adapted to the observed signals and also allows the construction of a reasonably fast computational algorithm. In particular, it is obviously an efficient way to describe both a stationary Gaussian signal and also non-stationary components whose variations in time are bounded. Assuming that the signal can be written as the sum of the independent signal components atmospheric

echo and intermittent clutter, i.e.  $\mathbf{S} = \mathbf{I} + \mathbf{C}$ , the goal is to find a Gabor frame representation where

$$S[n] = \sum_{(m,k) \in \Lambda \setminus \Omega_c} a_{m,k} h_{m,k}[n] + \sum_{(m,k) \in \Omega_c} a_{m,k} h_{m,k}[n].$$

An optimal representation requires that both the atmospheric signal set as well as the clutter component signal set are as small as possible, that is the number of non-zero Gabor coefficients  $a_{m,k}$  should be as small as possible (sparse), to minimize the chance for overlap. In contrast, a dense representation of decomposition coefficients would make signal classification and thus separation harder (Allen and Mills 2004).

The sparsity of a signal representation can be measured in a variety of ways (Hurley and Rickard 2008). The traditional way is simply to count the number of non-zero coefficients in the series expansion. However, this is inappropriate in the presence of noise: Infinitesimal small values would be treated in the same way as large and significant values are. Therefore, a slightly modified measure is used

$$\ell_\epsilon^0 := \#a_{m,k}, |a_{m,k}| > \epsilon,$$

where the number of all Gabor coefficients greater than a threshold  $\epsilon$  is counted. The threshold is selected sufficiently large to avoid the counting of noise coefficients, because the interest is solely in the representation of both the atmospheric and the clutter component of the signal. Note that no sparse representation can be found for noise. The difference between the amplitude of the observed 482 Mhz wind profiler signals at heights below 4 km and noise is typically larger than one order of magnitude, so the precise selection of this threshold is not critical. The value is chosen to be one order of magnitude (10 dB) larger than the median value of the smallest 25 percent of the  $M \cdot K$  Gabor coefficients  $a_{m,k}$ , which is taken as an estimate for the noise level.

For the example shown in Figures 2, 6 and 7, the  $\ell_\epsilon^0$  sparsity is estimated as 0.227 ( $s=10$ ), 0.212 ( $s=0.5$ ) and 0.271 ( $s=0.01$ ). Smaller values indicate a better adapted signal representation. This figure of merit needs to be determined in a statistical sense over a longer data set, to be of practical use (provided it is not attempted to find the optimal value for every single case, which is computationally prohibitive at present). To get an estimate about the average sparsity over a ten to fifteen minute long measurement period, the parameter was calculated for two data sets obtained with the 482 MHz wind profiler radar at Bayreuth (Lehmann et al. 2003):

- i. Dec 31, 2008, 01:00 - 01:17: Clear-air signal and noise, but no clutter

- ii. Mar 29, 2008, 23:46 - 23:54: Bird echoes during nocturnal migration in spring, clear-air and noise

The two data sets were manually reviewed: The first set contains indeed no intermittent clutter returns (e.g. airplanes) in a cloud-free winter night, while the second set exhibits plenty of bird echoes confined to the lowest 25 range gates (heights below 4 km AGL) during a nocturnal spring migration peak. The average value of the  $\ell_\epsilon^0$  sparsity has been calculated for a primal window parameter range from  $s = 2^{-8}$  to  $s = 2^5$  in dyadic steps. The result is shown in Figures 8 for the clear-air data set and 9 for the clutter data set. For the clear-air data,  $\ell_\epsilon^0$  is constant for small width parameters  $s$  (long windows with high frequency resolutions) until about  $s = 2^{-5}$  and increases then monotonically for larger values. This is an indication that the Doppler spectrum provides a sparse representation for a stationary signals as long as the spectral peak is sufficiently resolved. Due to the finite spectral width of the clear-air signal, sparsity is not improved by a higher spectral resolution. On the other hand, a reduction of frequency resolution due to an improved time resolution reduces sparsity, because the clear-air signal is stretched over more Gabor coefficients along the frequency axis. In contrast to this simple relation, the sparsity for the clutter case has a pronounced maximum for  $s = 2^{-1}$ . This indicates the optimal time-frequency resolution for the clutter signal: If the primal window width is accordingly selected, the DGT will achieve the optimally sparse representation.

### c. Sampling settings: Dwell time

The most important sampling parameters for estimating a Doppler spectrum are the time discretization step  $\Delta T$  and the length of the time series  $T_d$ . Assuming a sufficiently large setting of the Nyquist frequency, the selection of dwell time  $T_d$  has to be carefully considered in radar data acquisition.  $T_d$  is defined differently in the literature, see e.g. Strauch et al. (1984); Lottman and Frehlich (1997). Here, we follow Muschinski (2004) and define the dwell time as the total observation time (or the length  $N$  of the time series) that is used for the non-parametric estimation of a Doppler spectrum. This definition includes any spectral (or incoherent) integration and is similar to Lottman and Frehlich (1997), with the exception that signal processing time is ignored for simplicity.

Obviously, the dwell time should be as short as possible to get a high time resolution of the measurement. It is known that meaningful and valid measurement of the Doppler shift can be obtained with dwell times of 1 s, as discussed in Muschinski (2004). For example, the Turbulent Eddy Profiler (Mead et al. 1998), uses typical dwell times (selected after the measurement) from about 2 to 8 s. On the other hand, a better spectral resolution is only achieved with longer dwell times, this is due to the Heisen-

berg uncertainty relation (Mallat 1999). In the presence of noise, longer observation times are required to reduce the statistical uncertainty of the estimation (Woodman and Guillen 1974; Zrnić 1979; Woodman 1985) and to improve the detectability of weak signals (Gage and Balsley 1978). In most wind profiling applications, dwell times typically range from about 15 s (Böhme et al. 2004) to more than 100 s (Merceret 2000), with values of around 30 s being typical.

Choosing the dwell time thus essentially balances time and frequency resolution as well as signal detectability and moment estimation accuracy; it is obviously largely depending on the signal-to-noise ratio of the signal and the desired frequency resolution. Often, the problem is only mentioned in passing: An upper-limit for the dwell time is typically formulated by the requirement that the contribution of dwell time to the estimated spectral width (due to intra-dwell frequency changes) should be negligible (Gage and Balsley 1978; Strauch et al. 1984; Gossard et al. 1998; White et al. 1999). For a lower limit, it is stated that the spectral resolution must be high enough to adequately sample the spectral shape of the atmospheric signal peak (Woodman 1985; Wilfong et al. 1999). More generally, it could be stated that the resolution should be high enough to resolve all relevant stationary signal peaks (including clutter and RFI) in the Doppler spectrum. It thus appears that an a-priori estimation of the optimal dwell time is not possible, for both the true spectral shape of the atmospheric signal and the possible deviations from its stationarity are unknown. Furthermore, signal characteristics will differ with respect to the underlying scattering process. A simultaneous time-frequency analysis of the radar signal has apparently the potential to further investigate this problem.

For intermittent clutter due to migrating birds, Merritt (1995) has suggested a third condition for the selection of  $T_d$ : *The radar must dwell on each antenna beam long enough to allow moving objects sufficient time for their signals to change Doppler bins, angular position, and/or range gates. Therefore, a conservative approach would be to use the largest possible radar dwell time.* In other words,  $T_d$  must be sufficiently long so that the clutter signal component can be regarded as non-stationary. The motivation for this statement stems from considerations of the signal properties resulting from a single flier, moving with a constant horizontal speed over an idealized wind profiler. Assuming that the horizontal speed of a bird is  $\mathcal{O}(10\text{ms}^{-1})$  (Bruderer and Boldt 2001), then a typical (one-way, half-power) beamwidth of  $3^\circ$  corresponds to a lateral width of the beam from about 50 m at a height of 1 km to a about 250 m at a height of 5 km. This means that the crossing time of a single bird through the main scattering volume is  $\mathcal{O}(10\text{ s})$ . Of course, scattering also occurs when the bird flies through the sidelobes of the radar which could then

extend this time by about an order of magnitude.

A long enough dwell time would therefore allow to observe a change of the spectral characteristics of the single clutter target in time. The actual time–frequency picture of such a signal can look quite complicated though, as it is depending on the antenna radiation pattern, the flight trajectory and additional echo modulation by the target. Furthermore, a strong signal might lead to receiver saturation and associated nonlinear effects. However, the observed contamination features in the spectrogram confirm this general assumption. The duration of such features ranges between a few seconds and a minute.

A dwell time of about two minutes should therefore suffice to resolve transient clutter features in time–frequency space. In fact, Merritt (1995) states that *Observations to date ... demonstrate that radar contamination from migrating birds is effectively reduced using somewhat longer dwells (1-2 min) than have been traditionally used (20-30 s)*. For the spring migration season 2009, the Lindenberg 482 Mhz wind profiler (Steinhagen et al. 1998) was therefore configured to use a rather long dwell time of 147 s, the complete sampling parameters are given in Table 1.

It turned out, however, that using a longer dwell time is no panacea for improving the efficiency of the Gabor filtering algorithm. During dense migration, it is unfortunately the rule rather than the exception that a larger number of birds is crossing the radar scattering volume during the dwell. An example is shown in Figure 10. The corresponding Gabor spectrogram (Fig. 11) clearly shows the individual transients. Obviously, the dwell contains no contiguous time interval of more than a second without strong bird echoes. In this particular case it can be conjectured from the range gates above and below (not shown) that the true atmospheric signal should be located at a frequency of about 3 Hz for reasons of vertical wind profile continuity. However, there is no evidence of such signal in Figure 11 at all, it is obviously completely covered by the clutter component. Consequently, it can not be expected that any filtering algorithm is able to retrieve it. Indeed, the filtered Gabor spectrogram (Figure 12) shows that although the strong transients have been eradicated, the estimated signal intensity in the frequency range from about -30 to + 45 Hz is still way to high to allow for an identification of the weaker atmospheric signal. From a signal analysis point of view it remains questionable if such situations can be remedied at all. An improvement over this situation can probably only be achieved by hardware measures leading to a reduction of the size of the radar scattering volume (narrower beam, lower sidelobes and shorter pulses). Such an approach could reduce the number of observed transients per dwell, thus raising the chance for a separability of the atmospheric return.

#### 4. Quality control of the filtering

##### a. An indicator of nonstationarity

It was shown in the previous section, that the Gabor filtering is not always able to completely remove the bird contamination during dense bird migration. This makes it necessary to think about an additional quality control step. Filtering fails in cases where either the number of intermittent clutter transients is very high or where the dwell time is short compared to the duration of the transients. Fortunately, the algorithm can provide an indication about the non-stationarity of the signal which is not easily available otherwise. As detailed in Lehmann and Teschke (2008), the Hildebrand-Sekhon test is performed for the sorted Gabor coefficients  $|[a]_{(m,k)}|^2$  for all frequency indices  $k = 0, \dots, K - 1$ . For each frequency index  $k$ , the test identifies an index subset that is assumed to be free of intermittent clutter:

$$\Omega_k^c := \{(m, k) : \vartheta(|[a]_{m,k}|^2) > 1, \forall m\}$$

For fixed  $k$ , this condition will be fulfilled for  $m = m_c, \dots, M - 1$ .  $m_c$  is the time index of the largest clutter-free Gabor spectrogram coefficient. For each range gate, one thus obtains a vector  $\mathbf{m}_c = [m_c(0), m_c(1), \dots, m_c(K - 1)]^T$  of such indices. Information about the degree of non-stationary contamination is then simply obtained through the normalized quantity

$$\beta = \frac{\max(\mathbf{m}_c)}{M}.$$

The parameter  $\beta$  tends to be very small for stationary signals. On the other hand,  $\beta \rightarrow 1$  is an indication that the statistical test was not fulfilled for the majority of Gabor spectrogram coefficients at one or more frequency index  $k$ . Thus the non-stationary signal components have a duration that approaches the length of the dwell time. This is a well known failure condition for the Hildebrand-Sekhon test: In the usual application of noise level estimation in a Doppler spectrum, a similar situation occurs when the signal has a spectral width comparable to the full Nyquist range, see e.g. Figure 7 in Muschinski et al. (2005). The parameter  $\beta$  can therefore be used together with additional a-priori information about reasonable atmospheric signals to obtain an estimate about the quality of the filtering.

##### b. A-priori information about atmospheric signals

Equation (9) is usually a good model for the autocorrelation function of atmospheric signals, it also implies that the Doppler spectrum is Gaussian. This assumption is indeed valid for many observed signals (Woodman 1985), and therefore moments of higher order than two are usually not estimated in profiler signal processing. In contrast, bird contamination leads to signal peaks which deviate significantly from the Gaussianity assumption (Wilczak et al.

1995; Kretzschmar et al. 2003). A test of the deviation from Gaussianity thus can give additional information about the origin of the particular signal peak.

Out of the three moments that are typically estimated from the Doppler spectrum by single peak-picking algorithms (see Appendix B), the spectral width  $M_2$  contains the most promising information for the identification of intermittent clutter. In general, the spectral width of RWP signals is depending on

- spatio-temporal structure of wind and refractive index field for clear-air (Bragg) scattering
- size and velocity distribution of scattering particles for Rayleigh scattering
- geometry (size) of the radar sampling volume (determined by antenna radiation pattern, pulse and receiver filter characteristics)
- characteristics of the spectral estimator (e.g. particular window function for reducing the bias of the power spectrum)
- dwell time for non-stationary signals

There is still a considerable debate in the literature about the correct way of separating the individual effects, especially with regard to estimation of the eddy dissipation rate (Fang and Doviak 2008; Jacoby-Koaly et al. 2002; White et al. 1999; Gossard et al. 1998; Hocking 1996; Cohn 1995; Hocking 1983, 1985). Muschinski (2004) has derived a general formulation for clear-air scattering and provided an expression for the spectral width based on the statistics of both the velocity and refractive index field as well as on the radar sampling characteristics. However, simplifying assumptions have to be made for the interpretation of this equation and much remains to be learned for a full understanding (Muschinski et al. 2005). Somewhat surprisingly, statistical information of the Doppler spectrum moments seems to be restricted to either smaller data sets or case studies (Williams et al. 1995; Ralph et al. 1995; White et al. 1996). However, it has to be kept in mind that those quantities depend on the characteristics of the radar sampling function, which makes direct comparisons between different instruments somewhat difficult.

### *c. Combining spectral width with the nonstationarity indicator*

The bird detection algorithm which is operationally used in the NOAA wind profiler network uses a spectral width based thresholding (1 m/s) with considerable success (van de Kamp 1996). However, a large spectral width is not per se an indication for intermittent clutter: Rayleigh scattering due to precipitation is also known to generate wide signal peaks in Doppler spectra, depending on the actual drop-size distribution (Wakasugi et al. 1986; Ralph et al.

1995; Williams et al. 1995; McDonald et al. 2004; Testik and Barros 2007). This suggests a combination of spectral width thresholding with the nonstationarity indicator  $\beta$ : A large value of the spectral width is considered to be indicative of bird clutter if and only if the Gabor filtering step has indicated a high degree of non-stationarity, that is if  $\beta$  is above a certain threshold. Through this combination, signal peaks with large spectral widths in the Doppler spectrum are not discarded in general.

As an example of this approach, results from a single case are presented. Of course, the picture will become more complete after more cases have been investigated. To get the idea of the degree of clutter contamination, the winds are first processed using a standard method without any attempt of clutter filtering, see Figure 13. From the wind arrow plot, it is obvious that bird clutter has affected the height ranges below 5 km, with an artificial local wind maximum in a height band extending from about 1000 m to 3000 m.

Ideally, the wind measurements of the profiler would be compared with an independent reference having nearly the same vertical and temporal resolution, for example a Doppler wind lidar (Cohn and Goodrich 2002)). Such data is unfortunately not available for Bayreuth. Even though the nearest Radiosonde station is only about 50 km away, it would only provide one or two measurements during the time of bird migration (e.g. at 18 and 00 UTC) and therefore very likely miss the maximum. The penury of upper-air measurements at these scales has therefore lead to the increased use of comparisons with model data, to estimate the quality of a wind profiler (Steinhagen et al. 1994; Panagi et al. 2001; Hooper et al. 2008). A very short range model forecast of DWD's COSMO-EU model (Steppler et al. 2003; Schättler et al. 2002-2008) is therefore taken as a reference. COSMO-EU is a non-hydrostatic numerical weather prediction model with a grid size of  $\Delta x = 7$  km and 40 vertical layers. Although the model uses the Bayreuth wind profiler through a nudging approach, it can be assumed that a + 08...11 h free forecast is independent from the profiler data measured after model initialization. The model is only used to get some qualitative information about the "true" wind field and its extremes. Figure 17 shows the COSMO-EU wind forecast for Bayreuth plotted on exactly the same height and time scale as the profiler measurements. Model wind profiles were only available at a hourly interval. The vertical resolution of the model wind profiles is coarser than the corresponding resolution of the wind profiler. Although there are differences between model and measurement, as expected, it is nevertheless obvious that the model shows no local wind maximum below 5 km height in the time range of interest.

A comparison of the winds obtained without intermittent clutter filtering (Figure 13) with the results from the

operational intermittent clutter reduction algorithm ICRA (Figure 14) shows that the effects of the birds have been greatly reduced. However, the wind speed maxima below about 3000 m are still due to residual clutter. The Gabor filtering (Figure 15) processing has further reduced the clutter effects, which is an indication that the algorithm performs better than operational processing. But also here, artificial wind speed maxima are still visible in the last three profiles. The issue becomes very obvious when the Doppler spectra (not shown) are inspected.

Finally, the results from Gabor filtering with the spectral width based quality control step is shown in Figure 16. The width threshold was set to  $2 \text{ ms}^{-1}$  and  $\beta$  was selected as 0.5. The additional QC has resulted in a rejection of data where the Gabor filtering was not successful due to a breakdown of its assumptions. Comparing this plot with Figure 13 indicates that the data from the height band with the strongest clutter echoes were removed. Artificial wind speed values due bird clutter are no longer obvious, but this comes of course at the expense of a decrease in data availability.

## 5. Conclusions and further work

The discrete Gabor frame expansion was presented as a method to analyze wind profiler raw data simultaneously in time and frequency. This allows a separation of stationary atmospheric signals (clear-air or continuous precipitation) and non-stationary (intermittent) clutter signals. A statistical method can then be employed to achieve an objective filtering of the intermittent signal components from the data.

The filtering results can be optimized by a judicious selection of the discrete Gabor frame expansion parameters in order to achieve the best possible separation in Gabor phase space between the atmospheric signal component and the intermittent clutter component. This can be realized by first selecting a discretization lattice (constants  $\Delta M, \Delta K$  and maximum oversampling ratio  $r$ ) in such a way, that the resulting discrete frame is near-tight, with the dual window function having an almost identical shape compared to the primal Gaussian window. In this case, both the analysis and the synthesis window have superior localization properties in the time-frequency plane. Second, the analysis bandwidth of the Gaussian window must be adapted to the data for obtaining a simultaneous sparse representation of both the atmospheric signal and clutter. For the test data set it turned out that a maximally-sparse representation could be achieved for a time resolution  $T1$  of the primal window of about 0.5 s, which appears to be quite reasonable for typical intermittent echoes. Both optimizations improve the separation of signal components and thus make the filtering step more efficient. Comparisons with other intermittent clutter filtering methods show

a consistent superiority of the Gabor filtering approach.

However, there appears to be a critical bird density beyond which the clutter filtering fails and a retrieval of the clear-air atmospheric echo signals seems not to be possible. Such cases were observed during dense migration events. An additional quality-control step has therefore been added to flag the Doppler moments in case of a breakdown of the assumptions inherent in the Gabor filter. This makes it possible to avoid the calculation of clutter-contaminated winds. A possible way out of this dilemma is obviously a reduction of the size of the radar scattering volume, to reduce the number of bird transients per time interval in the time series data. However, this would require to have larger antennas (more narrow antenna beam and lower sidelobes) and greater system bandwidths (shorter pulse durations). Both measures are difficult to realize due to existing radio frequency allocation constraints and radar hardware costs.

A comprehensive objective evaluation of the algorithm performance should be the next step before the Gabor filtering method can be introduced into operational radar wind profiler systems. This requires high resolution reference data, ideally from other measurement systems like Doppler-Lidar (Grund et al. 2001; Shen et al. 2008; Pearson et al. 2009) or as a second alternative, independent wind analysis and forecast data from current state-of-the-art NWP-models.

### *Acknowledgments.*

The author wishes to express his appreciation to Prof. Dr. Gerd Teschke, who was essential for developing the mathematical algorithm and for getting him acquainted with frames. Further thanks go to Raisa Lehtinen, for asking the right questions during the implementation of the method in the online software of the Vaisala wind profiler. Part of this work was supported by the European COST action ES-0702 *European Ground-Based Observations of Essential Variables for Climate and Operational Meteorology*.

The author also benefitted from numerous discussions with many colleagues working on wind profiler radars over the last decade, in particular Prof. Dr. Andreas Muschinski, Drs. Lutz Justen, Earl E. Gossard, Richard G. Strauch, Bob L. Weber, James R. Jordan and John W. Neuschaefer. Special thanks go to Prof. Dr. Thomas Foken, who convinced me to finish this work, for his continuous support during the project.

## APPENDIX A

### **Linear signal decompositions: Bases and Frames**

To put the Gabor frame expansion into wider context, a brief overview of linear signal decompositions is given in

the following. For details, the reader is advised to consult the textbooks Daubechies (1992); Mallat (1999); Allen and Mills (2004); Christensen (2008).

Assuming that a signal  $\mathbf{f}$  is element of a separable Hilbert space  $\mathcal{H}$  (e.g. the space of functions of finite energy denoted with  $\mathbb{L}^2(\mathbb{R})$  to which our signal  $\mathbf{f}$  normally belongs to), with norm  $\|\cdot\|$  and inner product  $\langle \cdot, \cdot \rangle$ , a series

$$\mathbf{f} = \sum_i a_i \mathbf{b}_i \quad i \in \mathbb{Z}, \{a_i\} \in \mathbb{C}, \{\mathbf{b}_i\} \in \mathcal{H} \quad (\text{A1})$$

is called a decomposition of  $\mathbf{f}$  into *atoms* or *elementary building blocks*. Of course  $\overline{\text{span}\{\mathbf{b}_i\}} = \mathcal{H}$  is required. Depending on the particular system of atoms  $\{\mathbf{b}_i\}$ , the set of expansion coefficients  $\{a_i\}$  does sometimes provide a simpler and more concise description of intrinsic signal properties. A change of  $\{\mathbf{b}_i\}$  will obviously lead to a different perspective on the same data. If only a few of the coefficients  $\{a_i\}$  have significant absolute values (e.g. greater than zero), then the system  $\{\mathbf{b}_i\}$  is well-adapted to  $\mathbf{f}$ . This is called a *sparse representation*, it provides the most compact signal description and makes it easier to extract useful information from  $\mathbf{f}$ , for the properties of the system  $\{\mathbf{b}_i\}$  are known (Chen et al. 2001).

A well-known concept is to use an orthonormal basis  $\{\mathbf{e}_i\}$ , then

$$\mathbf{f} = \sum_i \langle \mathbf{f}, \mathbf{e}_i \rangle \mathbf{e}_i \quad (\text{A2})$$

and the (unique) coefficients  $\{a_i\}$  can easily be calculated as inner products. In this case, energy conservation is expressed with the completeness (Plancherel) relation

$$\|\mathbf{f}\|^2 = \sum_i |\langle \mathbf{f}, \mathbf{e}_i \rangle|^2. \quad (\text{A3})$$

However, the quest for finding a well-adapted basis is not always successful, because of the very stringent requirements for the basis elements (e.g. linear independence). A more flexible, but also exact and robust generalization is provided by frames. This comes at the expense that the expansion coefficients will no longer be unique in general.

A frame is a countable family of elements  $\{\mathbf{h}_k\} \in \mathcal{H}$  if there exist constants  $0 < A \leq B < +\infty$  (called frame bounds) such that  $\forall \mathbf{f} \in \mathcal{H}$

$$A\|\mathbf{f}\|_{\mathcal{H}}^2 \leq \sum_k |\langle \mathbf{f}, \mathbf{h}_k \rangle|^2 \leq B\|\mathbf{f}\|_{\mathcal{H}}^2. \quad (\text{A4})$$

This is sometimes called a *pseudo-Plancherel theorem* (Heil and Walnut 1989). If  $A = B$  then the frame is called tight and if  $A \approx B$  then the frame is called near-tight or snug (Daubechies 1991). The lower bound guarantees the completeness of the frame: Only the null element is orthogonal to all elements in  $\mathcal{H}$  because  $\sum_k |\langle \mathbf{f}, \mathbf{h}_k \rangle|^2 = 0$

implies  $\|\mathbf{f}\| = 0$ , so  $\overline{\text{span}\{\mathbf{h}_k\}} = \mathcal{H}$ . The upper bound makes sure that the linear analysis or coefficient operator  $T$

$$T : \mathcal{H} \rightarrow \mathcal{R}(T) \subseteq \ell_2, \quad T : \mathbf{f} \mapsto \{\langle \mathbf{f}, \mathbf{h}_k \rangle\} \quad (\text{A5})$$

is bounded with  $\|T\|^2 \leq B$ . This operator maps functions (vectors) to sequences and thus describes the signal through inner products with the frame elements. The frame condition (A4) is necessary and sufficient to guarantee that  $T$  is invertible on its image  $\mathcal{R}(T)$  and to assure that the reconstruction series defined by the synthesis operator  $T^*$  is well defined (Mallat 1999).  $T^*$  is the adjoint of  $T$  and reconstructs the signal by mapping from sequences (numbers) to functions (vectors):

$$T^* : \ell_2 \rightarrow \mathcal{H} \quad T^*\{c_k\} = \sum_k c_k \mathbf{h}_k. \quad (\text{A6})$$

The composition of  $T$  and  $T^*$  yields the frame operator  $S$  (note that sometimes  $T$  is called frame operator), which maps functions (vectors) to functions (vectors):

$$S : \mathcal{H} \rightarrow \mathcal{H} \quad S\{\mathbf{f}\} = T^*T\{\mathbf{f}\} = \sum_k \langle \mathbf{f}, \mathbf{h}_k \rangle \mathbf{h}_k. \quad (\text{A7})$$

$S$  is a linear, self-adjoint, bounded and strictly positive operator due to the frame condition (A4), which can be rewritten in operator form as  $A \cdot \mathbf{1} \leq S \leq B \cdot \mathbf{1}$ . It is therefore invertible and its inverse is bounded (Daubechies 1992).

The system  $\{\mathbf{g}_k\} = \{S^{-1}\mathbf{h}_k\}$  is called the canonical dual, it is obtained by applying the inverse frame operator  $S^{-1}$  to the frame elements  $\{\mathbf{h}_k\}$ .  $\{\mathbf{g}_k\}$  is also a frame with lower bound  $B^{-1}$  and upper bound  $A^{-1}$ .

Applying the inverse frame operator to (A7), any  $\mathbf{f} \in \mathcal{H}$  can be written as unconditionally norm-convergent series (convergence does not depend on the order of the elements in the series):

$$\begin{aligned} \mathbf{f} = S^{-1}S\mathbf{f} &= \sum_k \langle \mathbf{f}, \mathbf{h}_k \rangle S^{-1}\mathbf{h}_k \\ &= \sum_k \langle \mathbf{f}, \mathbf{h}_k \rangle \mathbf{g}_k. \\ \mathbf{f} = SS^{-1}\mathbf{f} &= \sum_k \langle S^{-1}\mathbf{f}, \mathbf{h}_k \rangle \mathbf{h}_k \\ &= \sum_k \langle \mathbf{f}, S^{-1}\mathbf{h}_k \rangle \mathbf{h}_k \\ &= \sum_k \langle \mathbf{f}, \mathbf{g}_k \rangle \mathbf{h}_k. \end{aligned}$$

The frame thus allows a decomposition as well as a reconstruction of the signal and the coefficients can be

computed through inner products with the dual frame elements. Note that the coefficients are in general not unique, for the frame may contain dependent elements so that  $\mathbf{d} = \sum_k c_k \mathbf{h}_k = 0$  is possible. Then

$$\begin{aligned} \mathbf{f} &= \sum_k \langle \mathbf{f}, \mathbf{g}_k \rangle \mathbf{h}_k + \mathbf{d} \\ &= \sum_k (\langle \mathbf{f}, \mathbf{g}_k \rangle + c_k) \mathbf{h}_k \end{aligned}$$

For tight frames  $A \cdot \mathbb{1} = S$ , so that  $S^{-1} = A^{-1} \mathbb{1}$ , therefore  $\mathbf{f} = S^{-1} \mathbf{S} \mathbf{f} = A^{-1} \sum_k \langle \mathbf{f}, \mathbf{h}_k \rangle \mathbf{h}_k$ . If the frame is only near-tight, then  $S \approx 0.5(A + B) \mathbb{1}$  and

$$\mathbf{f} = \frac{2}{A+B} \sum_k \langle \mathbf{f}, \mathbf{h}_k \rangle \mathbf{h}_k + R\mathbf{f} \approx \frac{2}{A+B} \sum_k \langle \mathbf{f}, \mathbf{h}_k \rangle \mathbf{h}_k \quad (\text{A8})$$

The inverse frame operator  $(S)^{-1}$  is often approximated using an iterative approach. There are, however, specific frames where the problem of determining  $(S)^{-1}$  is considerably simpler. Among them are Gabor frames, which are generated by translating and modulating of a single window function, see equation (1). Several explicit constructions of Gabor frames are known, one is provided by the Wexler-Raz biorthogonality condition (Wexler and Raz 1990; Janssen 1995; Daubechies et al. 1995), which reduces the problem of finding the dual frame to the solution of a linear system e.g. equation (5). A recent review of Gabor frames is given in Heil (2007), finite-dimensional Gabor systems are treated e.g. in Strohmer (1998).

## APPENDIX B

### Standard wind profiler signal processing

The standard wind profiler signal processing is briefly summarized here, details can be found in Woodman (1985); Tsuda (1989); Röttger and Larsen (1990). After demodulation and range gating, the receiver signal  $\mathbf{S}$  at one particular range gate forms a discrete complex time series for  $k = 0, \dots, N_{ci} \cdot N_p \cdot N_s - 1$  (The length of the time series is written as a product of three integers for later convenience):

$$S[k] = S_I[k] + iS_Q[k]. \quad (\text{B1})$$

The sampling time  $\Delta T$  depends on the inter-pulse period. Considering only one range gate, the next step is a simple preprocessing method called coherent integration:

$$S^{ci}[m] = \frac{1}{N_{ci}} \sum_{n=0}^{N_{ci}-1} S[m \cdot N_{ci} + n]. \quad (\text{B2})$$

This is essentially a digital filter operation followed by decimation to a length of  $N_p \cdot N_s$  (Farley 1985), whereby the sampling interval is increased to  $N_{ci} \Delta T$ . Its frequency response is referred to as comb-filtering (Schmidt et al. 1979). To estimate the Doppler spectrum, the nonparametric Periodogram method using a simple window sequence  $\mathbf{w}$  (e.g. Hanning) is used. Additionally, spectral or incoherent averaging is applied (Strauch et al. 1984; Tsuda 1989) to reduce the variance of the estimate. This is *Welch's overlapped segment averaging (WOSA) estimator* (Welch 1967; Percival and Walden 1993). For  $N_s$  segments of length  $N_p$  without overlapping of the blocks,  $N_s$  single spectrum estimates are obtained as

$$P[l, k] = \frac{1}{N_p} \left| \sum_{m=0}^{N_p-1} w[m] S^{ci}[l \cdot N_p + m] e^{-i \frac{2\pi k m}{N_p}} \right|^2 \quad (\text{B3})$$

$$P[k] = \frac{1}{N_s} \sum_{l=0}^{N_s-1} P[l, k] \quad (\text{B4})$$

The dwell time for the estimation of a Doppler spectrum is  $T_d = N_s \cdot N_p \cdot N_{ci} \Delta T$ . To discriminate between electronic noise and echo signals, a mean noise level  $P_N$  is objectively estimated using the method of Hildebrand and Sekhon (1974). Next, the signal peak caused by the atmospheric return is selected. A simple but well-established method is used which always selects the maximum energy peak (Strauch et al. 1984; May and Strauch 1989), this is called a single peak algorithm. For multiple peak spectra more complicated methods have been proposed (Riddle and Angevine 1991; Griesser 1998; Cornman et al. 1998; Morse et al. 2002; Weber et al. 2004).

The first three moments of the Doppler spectrum are: Echo power  $M_0$ , Doppler velocity  $M_1$  and spectral variance  $M_2$ , they are calculated for frequency bins where  $P[k] > P_N$ , that is between lower and upper signal bounds  $k_1$  and  $k_2$ :

$$M_0 = \sum_{k=k_1}^{k_2} (P[k] - P_N) \quad (\text{B5})$$

$$M_1 = \frac{1}{M_0} \sum_{k=k_1}^{k_2} k (P[k] - P_N) \quad (\text{B6})$$

$$M_2 = \frac{1}{M_0} \sum_{k=k_1}^{k_2} (k - M_1)^2 (P[k] - P_N). \quad (\text{B7})$$

Note that there are differences in the definitions of the spectral width. Here, the convention used in Carter et al. (1995) is used, where spectral width is defined as  $\sigma_v = 2\sqrt{M_2}$ .

## REFERENCES

- Allen, R. L. and D. W. Mills, 2004: *Signal Analysis: Time, Frequency, Scale and Structure*. IEEE Press and Wiley-Interscience.
- Barth, M., R. Chadwick, and D. van de Kamp, 1994: Data processing algorithms used by NOAA's wind profiler demonstration network. *Ann. Geophys.*, **12**, 518–528.
- Benjamin, S. G., B. E. Schwartz, E. J. Szoke, and S. E. Koch, 2004a: The value of wind profiler data in U.S. weather forecasting. *Bull. Amer. Meteor. Soc.*, 1871–1886.
- Benjamin, S. G., et al., 2004b: An hourly assimilation - forecast cycle: The RUC. *Mon. Wea. Rev.*, **132**, 495–518.
- Böhme, T., T. Hauf, and V. Lehmann, 2004: Investigation of short -period gravity waves with the Lindenberg 482 MHz tropospheric wind profiler. *Quart. J. Roy. Meteor. Soc.*, **130**, 2933–2952.
- Bouttier, F., 2001: The use of profiler data at ECMWF. *Meteor. Z.*, **10** (6), 497–510.
- Bruderer, B., 1997: The study of bird migration by radar part 1: The technical basis. *Naturwissenschaften*, **84**, 1–8.
- Bruderer, B. and A. Boldt, 2001: Flight characteristics of birds: I. radar measurements of speed. *Ibis*, **143**, 178–204.
- Cardinali, C., 2009: Monitoring the observation impact on the short-range forecast. *Quart. J. Roy. Meteor. Soc.*, **135**, 239–250.
- Carter, D., K.S.Gage, W.L.Ecklund, W.M.Angevine, P.E.Johnston, A.C.Riddle, J.Wilson, and C.R.Williams, 1995: Developments in UHF lower tropospheric wind profiling at NOAA's Aeronomy Laboratory. *Radio Sci.*, **30** (4), 977–1001.
- Chen, S. S., D. L. Donoho, and M. A. Saunders, 2001: Atomic decomposition by basis pursuit. *SIAM Rev.*, **43**, 129–150.
- Christensen, O., 2008: *Frames and Bases. An Introductory Course*. Applied and Numerical Harmonic Analysis, Birkhäuser.
- Cohn, S. A., 1995: Radar measurements of turbulent eddy dissipation rate in the troposphere: A comparison of techniques. *J. Atmos. Oceanic Technol.*, **12**, 85–95.
- Cohn, S. A. and R. K. Goodrich, 2002: Radar wind profiler radial velocity: A comparison with Doppler lidar. *J. Appl. Meteor.*, **41**, 1277–1282.
- Cornman, L. B., R. K. Goodrich, C. S. Morse, and W. L. Ecklund, 1998: A fuzzy logic method for improved moment estimation from Doppler spectra. *J. Atmos. Oceanic Technol.*, **15** (6), 1287–1305.
- Cros, B., et al., 2004: The ESCOMPTE program: an overview. *Atmos. Res.*, **69**, 241–279.
- Dabberdt, W. F., G. Frederick, R. Hardesty, W.-C. Lee, and K. Underwood, 2004: Advances in meteorological instrumentation for air quality and emergency response. *Meteor. Atmos. Phys.*, **87**, 57–88.
- Daubechies, I., 1990: The wavelet transform, time-frequency localization and signal analysis. *IEEE T. Inform. Theory*, **36** (5), 961–1005.
- Daubechies, I., 1991: *Advances in Spectrum Analysis and Array Processing*, chap. The Wavelet Transform: A Method for Time-Frequency Localization, 366–417. Prentice Hall.
- Daubechies, I., 1992: *Ten Lectures on Wavelets*. SIAM, Philadelphia.
- Daubechies, I., H. J. Landau, and Z. Landau, 1995: Gabor time-frequency lattices and the Wexler-Raz identity. *J. Fourier Anal. Appl.*, **1**, 437–478.
- Ecklund, W., D. Carter, B. Balsley, P. Currier, J. Green, B. Weber, and K. Gage, 1990: Field tests of a lower tropospheric wind profiler. *Radio Sci.*, **25** (5), 899–906.
- Engelbart, D., U. Görzdorf, and W. Ruhe, 1998: Effects and observation of migrating birds on a Boundary-Layer Windprofiler in Eastern Germany. *Meteor. Z.*, **NF 7**, 280–287.
- Fang, M. and R. J. Doviak, 2008: Coupled contributions in the Doppler radar spectrum width equation. *J. Atmos. Oceanic Technol.*, **25**, 2245–2258.
- Farley, D., 1985: On-line data processing techniques for MST radars. *Radio Sci.*, **20** (6), 1177–1184.
- Feichtinger, H. G., F. Luef, and T. Werther, 2007: A guided tour from linear algebra to the foundations of Gabor analysis. *Gabor and Wavelet Frames*, Word Scientific Publisher Company, Lecture Note Series.
- Frehlich, R. and M. Yadlowsky, 1994: Performance of mean-frequency estimators for Doppler radar and lidar. *J. Atmos. Oceanic Technol.*, **11**, 1217–1230.
- Fukao, S., 2007: Recent advances in atmospheric radar study. *J. Meteor. Soc. Japan*, **85B**, 215–239.

- Gage, K. and B. Balsley, 1978: Doppler radar probing of the clear atmosphere. *Bull. Amer. Meteor. Soc.*, **59** (9), 1074–1093.
- Gage, K. S. and E. E. Gossard, 2003: Recent developments in observation, model, and understanding atmospheric turbulence and waves. *Radar and Atmospheric Science: A Collection of Essays in Honor of David Atlas*, R. M. Wakimoto and R. Srivastava, Eds., Am. Meteorol. Soc., 139–174.
- Gossard, E., D. Wolfe, K. Moran, R. Paulus, K. Anderson, and L. Rodgers, 1998: Measurement of clear-air gradients and turbulence properties with radar wind profilers. *J. Atmos. Oceanic Technol.*, **15**, 321–342.
- Griesser, T., 1998: Multipeakanalyse von Dopplerspektren aus Windprofiler-Radar-Messungen. Ph.D. thesis, Eidgenössische Technische Hochschule Zürich.
- Gröchenig, K., 2001: *Foundations of Time-Frequency Analysis*. Birkhäuser.
- Grund, C. J., R. M. Banta, J. L. George, J. N. Howell, M. J. Post, R. A. Richter, and A. M. Weickmann, 2001: High-resolution Doppler Lidar for Boundary Layer and cloud research. *J. Atmos. Oceanic Technol.*, **18**, 376–393.
- Heil, C. E., 2007: History and evolution of the density theorem for Gabor frames. *J. Fourier Anal. Appl.*, **13**, 113–166.
- Heil, C. E. and D. F. Walnut, 1989: Continuous and discrete wavelet transforms. *SIAM Rev.*, **31** (4), 628–666.
- Hildebrand, P. H. and R. Sekhon, 1974: Objective determination of the noise level in Doppler spectra. *J. Appl. Meteor.*, **13**, 808–811.
- Hocking, W. K., 1983: On the extraction of atmospheric turbulence parameters from radar backscatter doppler spectra - i. theory. *J. Atmos. Terr. Phys.*, **45** (2/3), 89–102.
- Hocking, W. K., 1985: Measurement of turbulent energy dissipation rates in the middle atmosphere by radar techniques: A review. *Radio Sci.*, **20** (6), 1403–1422.
- Hocking, W. K., 1996: An assessment of the capabilities and limitations of radars in measurements of upper atmosphere turbulence. *Adv. Space Res.*, **17**, (11)37–(11)47.
- Hooper, D. A., J. Nash, T. Oakley, and M. Turp, 2008: Validation of a new signal processing scheme for the MST radar at Aberystwyth. *Ann. Geophys.*, **26**, 3253–3268.
- Hurley, N. and S. Rickard, 2008: Comparing measures of sparsity. *arXiv:0811.4706v1*, 1.
- Ishihara, M., Y. Kato, T. Abo, K. Kobayashi, and Y. Izumikawa, 2006: Characteristics and performance of the operational wind profiler network of the Japan Meteorological Agency. *J. Meteor. Soc. Japan*, **84** (6), 1085–1096.
- Jacoby-Koaly, S., B. Campistron, S. Bernard, B. Benech, F. Ardhun-Girard, J. Dessens, E. Dupont, and B. Carissimo, 2002: Turbulent dissipation rate in the Boundary Layer via UHF wind profiler Doppler spectral width measurements. *Bound.-Layer Meteor.*, **103**, 361–389.
- Janssen, A. J. E. M., 1995: Duality and biorthogonality for Weyl-Heisenberg frames. *J. Fourier Anal. Appl.*, **1**, 403–436.
- Jordan, J. R., R. J. Lataitis, and D. A. Carter, 1997: Removing ground and intermittent clutter contamination from wind profiler signals using wavelet transforms. *J. Atmos. Oceanic Technol.*, **14**, 1280–1297.
- Kretzschmar, R., N. B. Karayiannis, and H. Richner, 2003: Removal of bird-contaminated wind profiler data based on neural networks. *Pattern Recognit.*, **36**, 2699–2712.
- Lehmann, V., J. Dibbern, U. Gørsdorf, J. W. Neuschaefer, and H. Steinhagen, 2003: The new operational UHF wind profiler radars of the Deutscher Wetterdienst. *6th International Conference on Tropospheric Profiling - Extended Abstracts*.
- Lehmann, V. and G. Teschke, 2008: Advanced Intermittent Clutter Filtering for Radar Wind Profiler: Signal Separation through a Gabor Frame Expansion and its Statistics. *Ann. Geophys.*, **26**, 759–783.
- Lottman, B. and R. Frehlich, 1997: Evaluation of Doppler radar velocity estimators. *Radio Sci.*, **32** (2), 677–686.
- Mallat, S., 1999: *A Wavelet Tour of Signal Processing*. Academic Press.
- Mallat, S., 2009: *A Wavelet Tour of Signal Processing - the Sparse Way*. Academic Press.
- May, P. T. and R. G. Strauch, 1989: An examination of wind profiler signal processing algorithms. *J. Atmos. Oceanic Technol.*, **6**, 731–735.
- McDonald, A. J., T. K. Carey-Smith, D. A. Hooper, G. J. Fraser, and B. P. Lublow, 2004: The effect of precipitation on wind-profiler clear air returns. *Ann. Geophys.*, **22**, 3959–3970.
- Mead, J. B., G. Hopcraft, S. J. Frasier, B. D. Pollard, C. D. Cherry, D. H. Schaubert, and R. E. McIntosh, 1998: A volume-imaging radar wind profiler for atmospheric boundary layer turbulence studies. *J. Atmos. Oceanic Technol.*, **15**, 849–859.

- Merceret, F. J., 2000: The coherence time of midtropospheric wind features as a function of vertical scale from 300 m to 2 km. *J. Appl. Meteor.*, **39**, 2409–2420.
- Merritt, D. A., 1995: A statistical averaging method for wind profiler Doppler spectra. *J. Atmos. Oceanic Technol.*, **12** (5), 985–995.
- Monna, W. A. and R. B. Chadwick, 1998: Remote-sensing of upper-air winds for weather forecasting: Wind-profiler radar. *B. World Meteorol. Organ.*, **47** (2), 124–132.
- Morse, C. S., R. K. Goodrich, and L. B. Cornman, 2002: The NIMA method for improved moment estimation from Doppler spectra. *J. Atmos. Oceanic Technol.*, **19**, 274–295.
- Muschinski, A., 2004: Local and global statistics of clear-air Doppler radar signals. *Radio Sci.*, **39** (RS1008), doi:10.1029/2003RS002908.
- Muschinski, A., V. Lehmann, L. Justen, and G. Teschke, 2005: Advanced radar wind profiling. *Meteor. Z.*, **14** (5), 609–626.
- Neuser, F. D. and J. L. Massey, 1993: Proper complex random processes with applications to information theory. *IEEE T. Inform. Theory*, **39** (4), 1293–1302.
- Panagi, P., E. Dicks, G. Hamer, and J. Nash, 2001: Preliminary results of the routine comparison of wind profiler data with The Meteorological Office Unified Model vertical wind profiles. *Phys. Chem. Earth (B)*, **26**, 187–191.
- Pearson, G., F. Davies, and C. Collier, 2009: An analysis of the performance of the UFAM pulsed Doppler Lidar for observing the Boundary Layer. *J. Atmos. Oceanic Technol.*, **26**, 240–250.
- Percival, D. B. and A. T. Walden, 1993: *Spectral Analysis for Physical Applications*. Cambridge University Press.
- Prinz, P., 1996: Theory and algorithms for discrete 1-dimensional gabor frames. M.S. thesis, Univ. Vienna.
- Qian, S. and D. Chen, 1993: Discrete Gabor transform. *IEEE T. Signal Proces.*, **41** (7), 2429–2438.
- Qian, S. and D. Chen, 1999: Joint time-frequency analysis. *IEEE Signal Process. Mag.*, **16**, 52–67.
- Qian, S., K. Chen, and S. Li, 1992: Optimal biorthogonal functions for finite discrete-time Gabor expansion. *Signal Process.*, **27**, 177–185.
- Ralph, F. M., P. J. Neiman, D. W. van de Kamp, and D. C. Law, 1995: Using spectral moment data from NOAA’s 404-MHz radar wind profilers to observe precipitation. *Bull. Amer. Meteor. Soc.*, **76** (10), 1717–1739.
- Richner, H. and R. Kretzschmar, 2001: Bird identification on 1290-MHz wind profiler data applying neural networks and neurofuzzy systems. *Phys. Chem. Earth (B)*, **26**, 181–185.
- Riddle, A. and W. Angevine, 1991: Ground clutter removal from profiler spectra. *Proceedings of the Fifth Workshop on Technical and Scientific Aspects of MST Radar*, B. Edwards, Ed., SCOSTEP Secretariat, University of Illinois, 1406 W. Green Street, Urbana, IL 61801, USA, Scientific Committee on Solar Terrestrial Physics (SCOSTEP), 418–420.
- Röttger, J. and M. Larsen, 1990: UHF/VHF radar techniques for atmospheric research and wind profiler applications. *Radar in Meteorology*, American Meteorological Society, Boston, chap. 21a, 235–281.
- Schättler, U., G. Doms, and C. Schraff, 2002–2008: A description of the nonhydrostatic regional COSMO-model. Tech. rep., Deutscher Wetterdienst.
- Schmidt, G., R. Rüster, and P. Czechowsky, 1979: Complementary code and digital filtering for detection of weak VHF radar signals from the Mesosphere. *IEEE Trans. Geosci. Electron.*, **GE-17** (4), 154–161.
- Simple, A., 2005: Forecast error investigation 12th October 2003: Assimilation of contaminated wind profiler data into the global model (Forecasting Research Technical Report No. 465). Tech. rep., UK Met Office.
- Shen, F., H. Cha, D. Sun, D. Kim, and S. O. Kwon, 2008: Low tropospheric wind measurements with Mie Doppler Lidar. *Optical Rev.*, **15**, 204–209.
- St-James, J. S. and S. Laroche, 2005: Assimilation of wind profiler data in the Canadian Meteorological Centre’s analysis system. *J. Atmos. Oceanic Technol.*, **22**, 1181–1194.
- Steinhagen, H., J. Dibbern, D. Engelbart, U. Görsdorf, V. Lehmann, J. Neisser, and J. W. Neuschaefer, 1998: Performance of the first European 482 MHz wind profiler radar with RASS under operational conditions. *Meteor. Z.*, **N.F.7**, 248–261.
- Steinhagen, H., et al., 1994: Field campaign for the comparison of SOUSY radar wind measurements with rawinsonde and model data. *Ann. Geophys.*, **12**, 746–764.
- Stappeler, J., G. Doms, U. Schättler, H. Bitzer, A. Gassmann, U. Damrath, and G. Gregoric, 2003: Meso-gamma scale forecasts using the nonhydrostatic model LM. *Meteor. Atmos. Phys.*, **82**, 75–96.
- Stewart, L., S. Dance, and N. Nichols, 2008: Correlated observation errors in data assimilation. *Int. J. Num. Meth. Fluid.*, **56**, doi: 10.1002/fld.1636, 1521–1527.

- Strauch, R. G., D. A. Merritt, K. P. Moran, K. B. Earnshaw, and D. van de Kamp, 1984: The Colorado wind profiling network. *J. Atmos. Oceanic Technol.*, **1**, 37–49.
- Strohmer, T., 1998: Numerical algorithms for discrete Gabor expansions. *Gabor Analysis and Algorithms: Theory and Applications*, H. Feichtinger and T. Strohmer, Eds., Birkhäuser.
- Tanaka, H., et al., 2007: Surface flux and atmospheric boundary layer observations from the laps project over the middle stream of the Huaihe river basin in China. *Hydrol. Processes*, **21**, 1997–2008.
- Testik, F. Y. and A. P. Barros, 2007: Toward elucidating the microstructure of warm rainfall: a survey. *Rev. Geophys.*, **RG2003**, 2005RG000182, 1–21.
- Tsuda, T., 1989: *Middle Atmosphere Program - Handbook for MAP*, Vol. 30, chap. Data Acquisition and Processing, 151–183. ICSU Scientific Committee on Solar-Terrestrial Physics (SCOSTEP), ISAR 24.-28. November 1988, Kyoto.
- van de Kamp, D., 1996: A new algorithm to identify errors caused by migrating birds in profiler winds. Tech. Rep. SR/SSD 96-36, NOAA Forecasting Systems Laboratory.
- Wakasugi, K., A. Mizutani, M. Matsuo, S. Fukao, and S. Kato, 1986: A direct method for deriving drop-size distribution and vertical air velocities from VHF Doppler radar spectra. *J. Atmos. Oceanic Technol.*, **3**, 623–629.
- Weber, B., D. Welsh, D. Merritt, D. Wuertz, D. Wolfe, and T. Wilfong, 2004: A new paradigm for Doppler radar wind profiler signal processing. Tech. Rep. OAR ETL-306, NOAA - Environmental Technology Laboratory.
- Welch, P. D., 1967: The use of fast Fourier transform for the estimation of power spectra: A method based on time averaging over short, modified periodograms. *IEEE Trans. Audio Electroacoustics*, **AU-15**, 70–73.
- Wexler, J. and S. Raz, 1990: Discrete Gabor expansions. *Signal Process.*, **21**, 207–220.
- White, A., R. Lataitis, and R. Lawrence, 1999: Space and time filtering of remotely sensed velocity turbulence. *J. Atmos. Oceanic Technol.*, **16**, 1967–1972.
- White, A. B., C. W. Fairall, A. S. Frisch, B. W. Orr, and J. B. Snider, 1996: Recent radar measurements of turbulence and microphysical parameters in marine boundary layer clouds. *Atmos. Res.*, **40**, 177–221.
- White, A. B., et al., 2006: A wind profiler trajectory tool for air quality transport applications. *J. Geophys. Res.*, **111**, doi:10.1029/2006JD007475.
- Wilczak, J., E. Gossard, W. Neff, and W. Eberhard, 1996: Ground-based remote sensing of the atmospheric boundary layer: 25 years of progress. *Bound.-Layer Meteor.*, **78**, 321–349.
- Wilczak, J., et al., 1995: Contamination of wind profiler data by migrating birds: Characteristics of corrupted data and potential solutions. *J. Atmos. Oceanic Technol.*, **12** (3), 449–467.
- Wilfong, T. L., D. A. Merritt, R. J. Lataitis, B. L. Weber, D. B. Wuertz, and R. G. Strauch, 1999: Optimal generation of radar wind profiler spectra. *J. Atmos. Oceanic Technol.*, **16**, 723–733.
- Williams, C. R., W. L. Ecklund, and K. S. Gage, 1995: Classification of precipitating clouds in the tropics using 915-MHz wind profilers. *J. Atmos. Oceanic Technol.*, **12**, 996–1012.
- Woodman, R. F., 1985: Spectral moment estimation in MST radars. *Radio Sci.*, **20**, 1185–1195.
- Woodman, R. F., 1991: A general statistical instrument theory of atmospheric and ionospheric radars. *J. Geophys. Res.*, **96** (A5), 7911–7928.
- Woodman, R. F. and A. Guillen, 1974: Radar observation of winds and turbulence in the stratosphere and mesosphere. *J. Atmos. Sci.*, 493–505.
- Zaugg, S., G. Saporta, E. van Loon, H. Schmaljohann, and F. Liechti, 2008: Automatic identification of bird targets with radar via patterns produced by wing flapping. *J. R. Soc. Interface*, doi:10.1098/rsif.2007.1349, 1–13.
- Zrnić, D. S., 1975: Simulation of weatherlike Doppler spectra and signals. *J. Appl. Meteor.*, **14**, 619–620.
- Zrnić, D. S., 1979: Estimation of spectral moments for weather echoes. *IEEE T. Geosci. Elect.*, **GE-17** (4), 113–128.

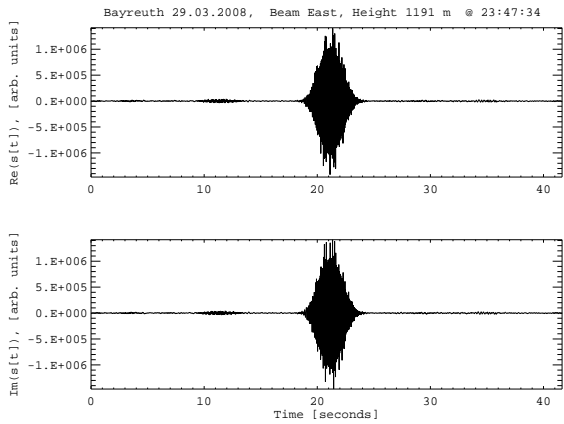


FIG. 1. Demodulated receiver signal of the 482 MHz wind profiler at Bayreuth, obtained during bird migration on March 29, 2008. The total length of the time series is 41.65 s.

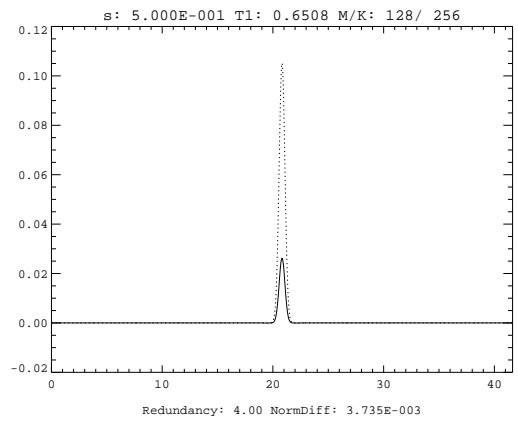


FIG. 3. Primal window function  $\mathbf{h}$  (dotted) and dual window function  $\mathbf{g}$  (solid) used for calculation of the DGT in Fig. 2. Note that beside the different norm due to the redundancy of the DGT, the shape of the functions is nearly identical.

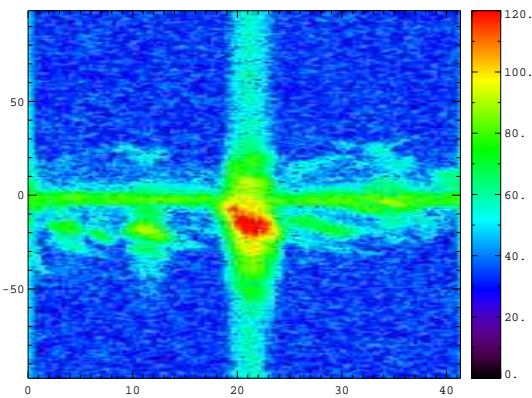


FIG. 2. Time-Frequency analysis (Gabor spectrogram) of the signal shown in Fig 1. The x-axis shows time (in seconds) and the y-axis frequency (in Hz). Color contours (logarithmic scaling in dB) denote signal power. The DGT has been computed using optimal lattice parameters  $M$  and  $K$ . The sparsity of the spectrogram is 0.212

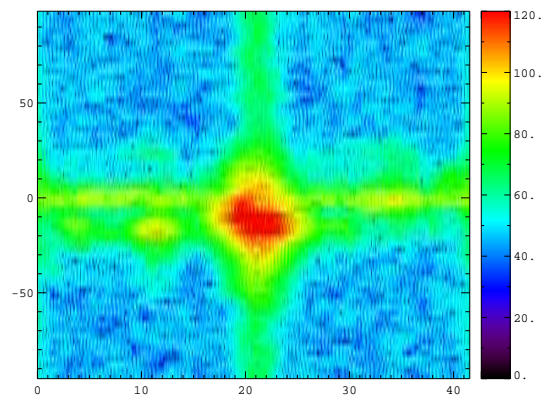


FIG. 4. Same as in Fig. 2, but for non-optimal lattice parameters  $M$  and  $K$ .

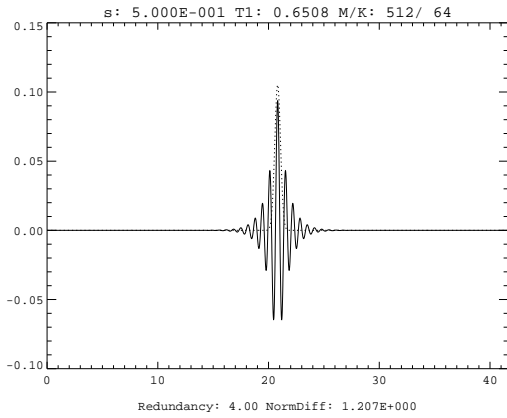


FIG. 5. Same as in Fig. 3, but for non-optimal lattice parameters  $M$  and  $K$  used in Fig. 4. Due to the choice of the sub-optimal lattice parameters, the dual window function is no longer well localized.

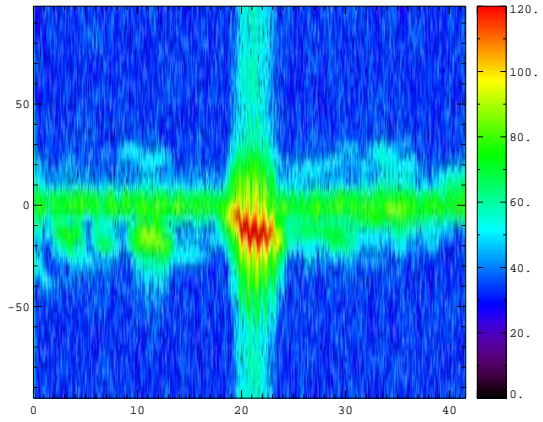


FIG. 7. Same as in Fig. 11, but for a primal window with width parameter 10.0, corresponding to a resolution of  $T_1 = 0.15$  s. The  $\ell_\epsilon^0$  sparsity measure of the spectrogram is 0.227.

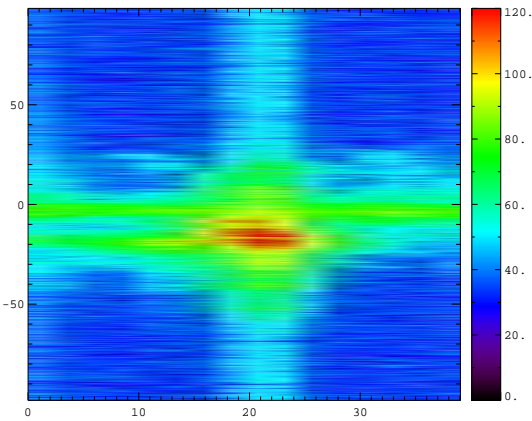


FIG. 6. Same as in Fig. 11, but for a primal window with width parameter 0.01, corresponding to a resolution of  $T_1 = 4.6$  s. The  $\ell_\epsilon^0$  sparsity measure of the spectrogram is 0.271.

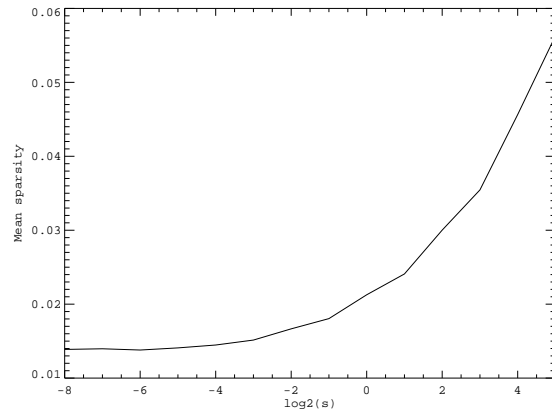


FIG. 8. Mean  $\ell_\epsilon^0$  sparsity measure of the Gabor representation of the lowest 25 range gates for a data set obtained on Dec 31, 2008 between 01:00 - 01:17 UTC, as a function of the primal window width  $s$  (note the logarithmic scaling). This data set has been manually reviewed to assure that it contains only clear air echoes.

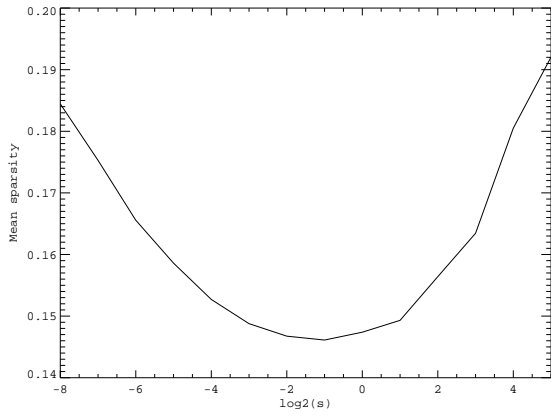


FIG. 9. Same as in Fig. 8, but for a data set obtained on Mar 29, 2008 between 23:46 - 23:54 UTC during intense bird migration in spring.

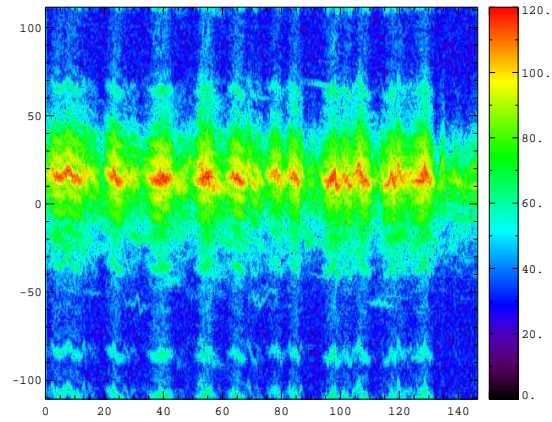


FIG. 11. Same as in Fig. 2, but for the signal shown in Fig 10. The primal window width parameter is 2.0 which corresponds to a resolution of  $T_1 = 0.57$  s and the  $\ell_\epsilon^0$  sparsity measure of the spectrogram is 0.402.

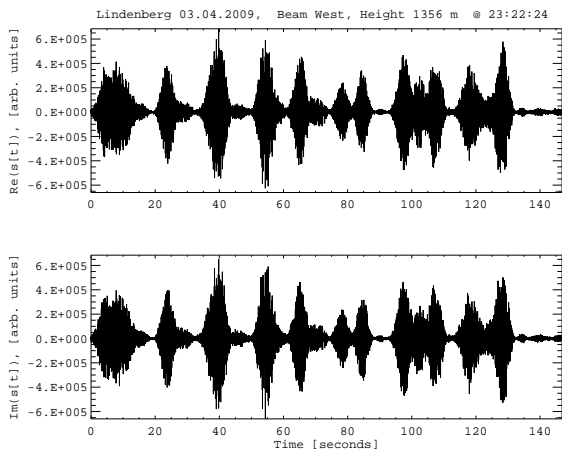


FIG. 10. Demodulated receiver signal of the 482 MHz wind profiler at Lindenberg, obtained during dense bird migration on April 03, 2009. The total length of the time series is 146.87 s.

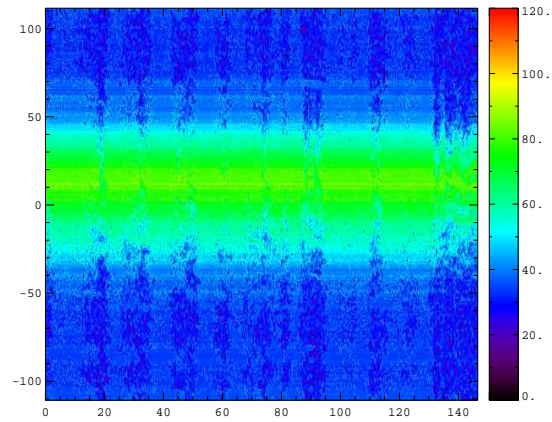


FIG. 12. As in Fig 11, but for the filtered Gabor spectrogram.

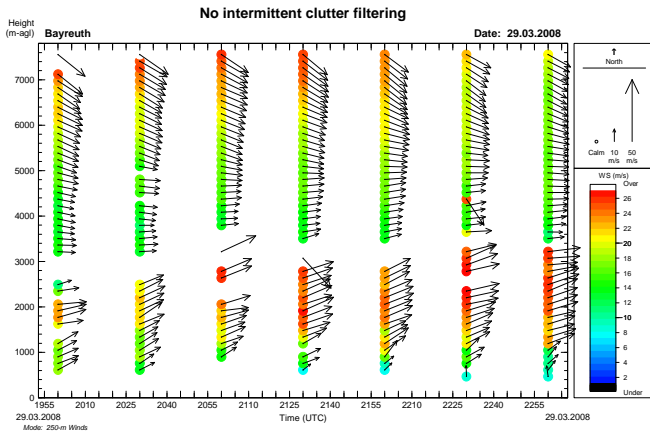


FIG. 13. Arrow plot of horizontal winds measured in the low mode at Bayreuth on March 29, 2008. For clarity, only the time from 20:00 - 23:00 UTC is shown. The x-axis shows time and the y-axis denotes height (agl). Data have been color coded by wind speed. The signal processing was using no intermittent clutter filtering algorithm at all, the results are only shown for a better identification of the clutter affected height range. Note that bird clutter only affects the height ranges below 5 km, with a maximum in a band from about 1000 m to 3000 m.

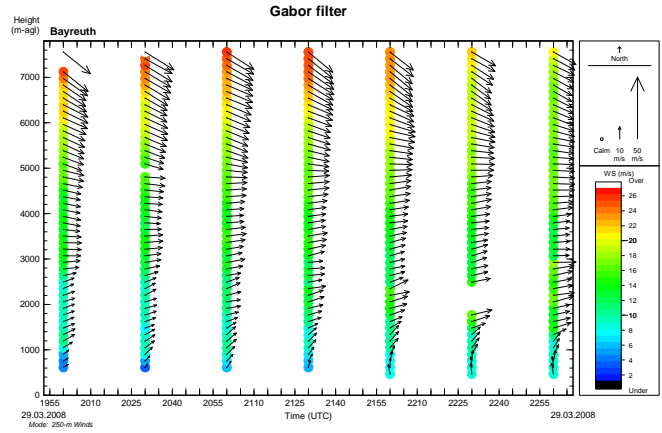


FIG. 15. Same as in Figure 13, but for Gabor filtering processing. The effects of the birds are further reduced in comparison with Fig. 14, which is an indication that the algorithm performs better than standard operational processing. However, there are still artificial wind speed maxima due bird clutter - this can especially be seen in the last three profiles.

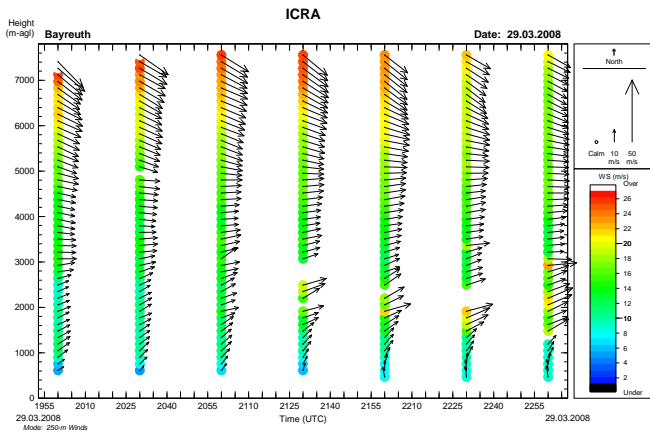


FIG. 14. Same as in Fig. 13, but for standard processing using the operational intermittent clutter reduction algorithm ICRA. The effects of the birds have been reduced, but the wind speed maxima in the heights below about 3000 m are still due to the birds.

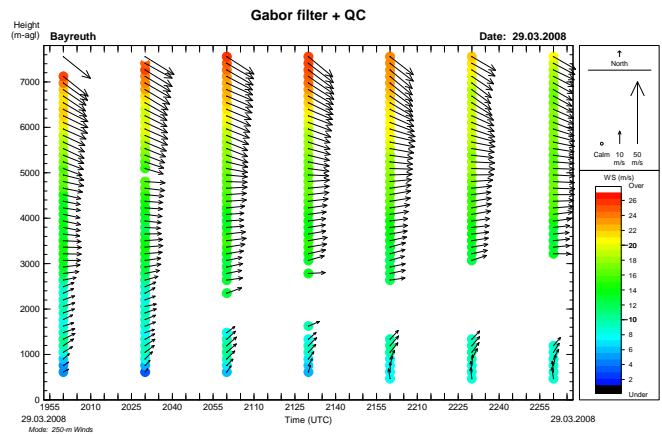


FIG. 16. Same as in Fig. 13, but for Gabor filtering and additional quality control of the filtering result. The QC results in a rejection of data where the Gabor filtering was not successful due to a breakdown of its assumptions. Comparing this plot with Fig. 13 indicates that the data from the height band with the strongest clutter echoes were removed. Artificial wind speed values due bird clutter are no longer obvious.

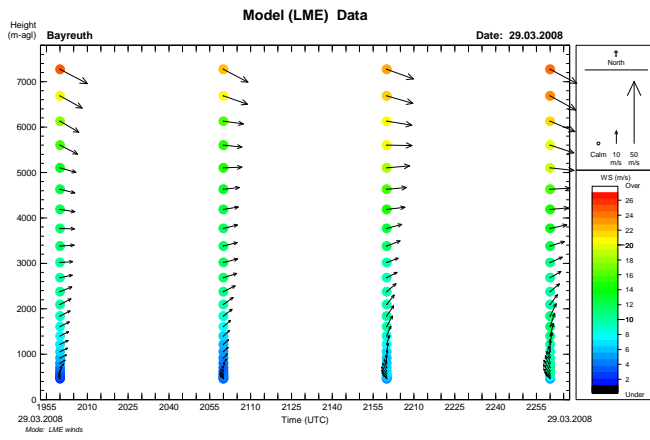


FIG. 17. Arrow plot of horizontal winds forecasted by the 12 UTC run of DWD's COSMO-EU (LME) model for the grid point Bayreuth on March 29, 2008, for the time and height range shown in the previous plots. Data are color coded by wind speed. Model wind profiles were only available at a hourly interval. Note also, that the vertical resolution of the model wind profiles is coarser than the corresponding resolution of the wind profiler. Although there are differences between model and measurement, as expected, it is nevertheless obvious that the model shows no local wind maximum below 5 km height.

TABLE 1. Radar parameters in routine operation

	Bayreuth (29.03.2008)	Lindenberg (03.04.2009)
Inter Pulse Period	82 $\mu s$	83 $\mu s$
Pulse Width	1.7 $\mu s$	1.7 $\mu s$
$N_{ci}$	62	54
$N$ (# of FFT bins)	512	1024
$N_{sp}$	16	32
Gate spacing (on RX)	1.00 $\mu s$	1.17 $\mu s$
# of Gates	50	57
First Gate	3.2 $\mu s$	3.5 $\mu s$

## **Erklärung**

Hiermit erkläre ich, dass ich die Arbeit selbständig verfasst und keine anderen als die von mir angegebenen Quellen und Hilfsmittel benutzt habe.

Ferner erkläre ich, dass ich nicht anderweitig mit oder ohne Erfolg versucht habe, diese Dissertation einzureichen. Ich habe keine gleichartige Doktorprüfung an einer anderen Hochschule endgültig nicht bestanden.

Bayreuth, den